INFORMATION TO USERS

This reproduction was made from a copy of a document sent to us for microfilming. While the most advanced technology has been used to photograph and reproduce this document, the quality of the reproduction is heavily dependent upon the quality of the material submitted.

The following explanation of techniques is provided to help clarify markings or notations which may appear on this reproduction.

1. The sign or "target" for pages apparently lacking from the document photographed is "Missing Page(s)". If it was possible to obtain the missing page(s) or section, they are spliced into the film along with adjacent pages. This may have necessitated cutting through an image and duplicating adjacent pages to assure complete continuity.

2. When an image on the film is obliterated with a round black mark, it is an indication of either blurred copy because of movement during exposure, duplicate copy, or copyrighted materials that should not have been filmed. For blurred pages, a good image of the page can be found in the adjacent frame. If copyrighted materials were deleted, a target note will appear listing the pages in the adjacent frame.

3. When a map, drawing or chart, etc., is part of the material being photographed, a definite method of "sectioning" the material has been followed. It is customary to begin filming at the upper left hand corner of a large sheet and to continue from left to right in equal sections with small overlaps. If necessary, sectioning is continued again — beginning below the first row and continuing on until complete.

4. For illustrations that cannot be satisfactorily reproduced by xerographic means, photographic prints can be purchased at additional cost and inserted into your xerographic copy. These prints are available upon request from the Dissertations Customer Services Department.

5. Some pages in any document may have indistinct print. In all cases the best available copy has been filmed.

University Microfilms International
300 N. Zeeb Road
Ann Arbor, MI 48106

8502918

Rathkopf, James Arden

FINITE ELEMENT RESPONSE MATRIX METHOD FOR THE SOLUTION OF THE TRANSPORT EQUATION

The University of Michigan PH.D. 1984

University Microfilms International 300 N. Zeeb Road, Ann Arbor, MI 48106

FINITE ELEMENT RESPONSE MATRIX METHOD FOR THE SOLUTION OF THE TRANSPORT EQUATION

by
James Arden Rathkopf

A dissertation submitted in partial fulfillment
of the requirements for the degree of
Doctor of Philosophy
(Nuclear Engineering)
in The University of Michigan
1984

Doctoral Committee:

Associate Professor William R. Martin, Chairman
Professor James J. Duderstadt
Professor John C. Lee
Professor Wei H. Yang

RULES REGARDING THE USE OF

MICROFILMED DISSERTATIONS

Microfilmed or bound copies of doctoral dissertations submitted to The University of Michigan and made available through University Microfilms International or The University of Michigan are open for inspection, but they are to be used only with due regard for the rights of the author. Extensive copying of the dissertation or publication of material in excess of standard copyright limits, whether or not the dissertation has been copyrighted, must have been approved by the author as well as by the Dean of the Graduate School. Proper credit must be given to the author if any material from the dissertation is used in subsequent written or published work.

ACKNOWLEDGEMENTS

I thank my thesis committee chairman, Dr. William R. Martin, for his advise, assistance, and friendship. I am also grateful to Drs. James J. Duderstadt, John C. Lee, and Wei H. Yang for serving on my committee.

I appreciate the effort of the Department of Nuclear Engineering in providing financial support during the course of this research. Funding was provided by the Vectorized Monte Carlo Project supported by Lawrence Livermore National Laboratory (LLNL), by the Horace H. Rackham School of Graduate Studies Pre-Doctoral Fellowship, and other sources.

I extend special thanks to the members of the Theoretical Physics Division (now Computational Physics Division) of LLNL for their support and the opportunity to spend two summers working with them--the second summer on this research.

Finally, Marcia T. Saunders deserves a word of thanks for her excellent typing skills and accommodating schedule.

TABLE OF CONTENTS

ACKNOWLEDGEMENTS ii

LIST OF FIGURES v

LIST OF TABLES ix

CHAPTER

I. INTRODUCTION 1

II. GENERAL MULTIDIMENSIONAL DERIVATION OF THE METHOD 16

The First-Order Neutron Transport Equation 17
The Response Kernel Equations 19
The Response Matrix Equations 22
The Weak Transport Equation 28
The Galerkin Approximation 31
Response Matrix Derivation 34
Iterative Solution Scheme 44
Special Case: Identical Local and Global Mesh 54

III. APPLICATION TO SPECIFIC GEOMETRIES 62

Application of the Method in One Dimension 62
Application of the Method in Two Dimensions 70

IV. COMPUTER IMPLEMENTATION 85

Computer Implementation in One Dimension . 85
Finite Element Basis Function Construction 85
Finite Element Matrix Calculation . . . 96
Response Matrix Generation 104
Iterative Solution Method 115

Computer Implementation in Two Dimensions 122
Finite Element Basis Function Construction 122
Finite Element Matrix Calculation . . . 126
Response Matrix Generation 129
Iterative Solution Method 138

V. COMPUTATIONAL TESTING 151

Computer Code Organization 152

One-Dimensional Numerical Experimentation 154

Reed's Problem 154
NSE 71 Problem 172
Lattice Problem 176
One-Dimensional Eigenvalue Problem . . . 180
Computational Considerations 183
Summary 189

Two-Dimensional Numerical Experimentation 189
Ray Effect Problem 190
Computational Considerations 222
Summary 230

VI. SUMMARY 231

REFERENCES 238

LIST OF FIGURES

Figure

2-1. Iterative solution scheme with external source. 52

2-2. Iterative solution scheme with fission source. 55

3-1. Physical domain of one-dimensional slab geometry. 63

3-2. Division of one-dimensional spatial domain. . 66

3-3. Analytical domain for one-dimensional region ℓ. 68

3-4. Two-dimensional spatial domain. 73

3-5. Division of two-dimensional spatial domain. . 74

3-6. Two-dimensional angular coordinate system. . 75

3-7. Side numbering convention in two dimensions. 76

3-8. Incoming boundary angular and spatial two-dimensional domain. 78

3-9. Volume and surface support points in two dimensions. 83

4-1. One-dimensional linear basis function. . . . 87

4-2. One-dimensional quadratic basis functions. . 89

4-3. Two-dimensional linear basis function. . . . 92

4-4. Two-dimensional quadratic basis functions. . 93

4-5. Arrangement of one-dimensional linear basis functions in angle. 97

4-6. Volume one-dimensional phase-space support points. 98

4-7. Linear basis functions on the standard interval. 101

4-8. Block structure of $\underline{\underline{A}}_{\ell}$ in one dimension. . . . 103

4-9. Volume and surface one-dimensional phase-space support points. 106

4-10. Local and global one-dimensional spatial basis functions. 111

4-11. Volume two-dimensional phase-space support points. 124

4-12. Two-dimensional surface support points. . . . 130

4-13. Two-dimensional spatial volume support point numbering system. 132

4-14. Two-dimensional spatial surface support point numbering system. 133

4-15. Two-dimensional sweep schemes. 150

5-1. Computer codes used to generate response matrices for region ℓ. 153

5-2. Use of global solution computer codes. . . . 155

5-3. Reed's Problem. 156

5-4. Reed's Problem: Monte Carlo benchmark. . . . 158

5-5. Reed's Problem: FTRAN and response matrix (mesh size = 0.25cm) 160

5-6. Reed's Problem: response matrix (mesh size = 0.5 and 0.25 cm) 163

5-7. Reed's Problem: coarse mesh (1.0 cm). . . . 165

5-8. Reed's Problem: fine mesh (0.25 cm). 168

5-9. Reed's Problem: quadratic vs. linear (no projection) 170

5-10. Reed's Problem: quadratic vs. linear (with local/global projection) 171

5-11. NSE 71 Problem. 173

5-12. NSE 71 Problem: scalar flux. 174

5-13. NSE 71 Problem: scalar flux (scale reduced). 175

5-14. Lattice Problem. 177

5-15. Lattice Problem: homogeneous regions. . . . 178

5-16. Lattice Problem: heterogeneous regions. . . 181

5-17. Number of iterations vs. relaxation parameter (Reed's Problem--5/5/cm) 186

5-18. Ray Effect Problem. 191

5-19. Ray Effect Problem (c=1/3)--scalar flux along side 2: 8x8-3344 vs. 4x4-5544 (local=global). 195

5-20. Ray Effect Problem (c=1/3)--scalar flux along side 2: 8x8-3344 vs. 6x6-3344 (local=global). 196

5-21. Ray Effect Problem (c=1/3)--scalar flux along side 2: 4x4-4444 vs. 6x6-3344 (local=global). 197

5-22. Ray Effect Problem (c=1/3)--scalar flux along side 2: 8x8-3344 vs. 4x4-3344 (local=global). 198

5-23. Ray Effect Problem (c=1/3)--scalar flux along side 2: 8x8-3344 vs. 2x2-3344 (local=global). 199

5-24. Ray Effect Problem (c=1/3)--scalar flux along side 2: FTRAN2-9944 vs. 4x4-3344. 201

5-25. Ray Effect Problem (c=1/3)--scalar flux along side 2: FTRAN2-9944 vs. FTRAN2-7744. . . . 202

5-26. Two-dimensional angular mesh. 203

5-27. Ray Effect Problem (c=1/3)--scalar flux along side 2, 6x6 angular mesh: FTRAN2 vs. response matrix method. 204

5-28. Ray Effect Problem (c=1/3)--scalar flux along side 2: local-global projection in angle (configuration = 6x6). 206

5-29. Ray Effect Problem (c=1/3)--scalar flux along side 2: local-global projection in angle (configuration = 4x4). 208

5-30. Ray Effect Problem (c=1/3)--scalar flux along side 2: FTRAN2 results. 209

5-31. Ray Effect Problem (c=1/3)--scalar flux along side 2: local-global projection in space. 211

5-32. Ray Effect Problem (c=1/3)--scalar flux along side 2: 4x4-5544 vs. 4x4-3344. 212

5-33. Ray Effect Problem (c=1/3)--scalar flux along side 2: 2x6-7344 vs. 6x6-3344. 215

5-34. Ray Effect Problem (c=1/3)--scalar flux along side 2: projection in space from 7 point fine mesh (x-direction). 216

5-35. Ray Effect Problem (c=1/3)--scalar flux along side 2: 2x6-7344/3344 vs. 2x2-3344. . . . 217

5-36. Ray Effect Problem (c=1/3)--scalar flux along side 2: 6x2-3744 vs. 2x6-7344. 218

5-37. Ray Effect Problem (c=1/3)--scalar flux along side 2: projection in space from 7 point fine mesh (y-direction). 219

5-38. Ray Effect Problem (c=2/3)--scalar flux along side 2: 8x8-3344 vs. 6x6-3344. 220

5-39. Ray Effect Problem (c=2/3)--scalar flux along side 2: 8x8-3344 vs. 4x4-3344. 221

5-40. Number of iterations vs. relaxation parameter (Ray Effect Problem, c=1/3). 226

5-41. Number of iterations vs. relaxation parameter (Ray Effect Problem, c=2/3). 227

LIST OF TABLES

Table

2-1. Summary of Response Matrix Definitions . . . 59

3-1. Boundary Domains in Two Dimensions 77

4-1. One-Dimensional Projection Matrices and their Inner Products 113

4-2. Two-Dimensional Projection Matrices and their Inner Products 136

5-1. Errors in Scalar Flux for Reed's Problem . . 161

5-2. Errors in Scalar Flux for Coarse Mesh Reed's Problem: Constant Global Mesh 164

5-3. Errors in Scalar Flux for Fine Mesh Reed's Problem 167

5-4. Errors in Scalar Flux for Reed's Problem: Quadratic vs. Linear Basis Functions . . . 169

5-5. Lattice Problem Scalar Fluxes 179

5-6. One-Dimensional Eigenvalues 182

5-7. One-Dimensional Response Matrix Generation Costs 184

5-8. Computational Costs to Solve Reed's Problem . 188

5-9. Errors in Scalar Flux of Ray Effect Problem (c=1/3): Local=Global 194

5-10. Errors in Scalar Flux of Ray Effect Problem (c=1/3): Effect of Fine Angular Mesh . . . 207

5-11. Errors in Scalar Flux of Ray Effect Problem (c=1/3): Effect of Spatial Projection . . 213

5-12. Two-Dimensional Storage Requirements 223

5-13. Two-Dimensional Response Matrix Generation Costs 224

5-14. Computational Costs to Solve Ray Effect Problem (c=1/3) 228

5-15. Comparison of Computational Cost: FTRAN2 vs. Response Matrix Method 229

CHAPTER I

INTRODUCTION

In order to safely and economically design and operate nuclear power plants, the neutron density distribution in the reactor core, as well as many other parameters, must be known very accurately. The workhorses of the core design industry are computer codes based on neutron diffusion theory, an approximation to the essentially exact transport theory. The neutron transport equation has almost always been used to find the distribution of neutrons in physical configurations ill-suited for the diffusion approximation; those with highly heterogeneous regions, such as localized sources, strong absorbers, or voids--features which tend to nullify the basic premise of diffusion theory that scattering tends to force the neutron density to be isotropic. Transport codes have therefore been used almost to the exclusion of all other types for the study of reactor shields, control rods and various thermonuclear applications. With the increasing sophistication of reactor cores, however, the need for transport calculations in this application is on the upswing.

The most popular transport methods are the deterministic discrete ordinates method and the probabilistic Monte

Carlo method. The discrete ordinates or S_N method provides a simple, effective, but potentially expensive means of solution. Even in one dimension, the mesh spacing of the spatial discretization must be a fraction of the mean free path of the neutron to provide point-to-point coupling. Finer angular discretization requires correspondingly smaller spatial mesh spacing. The ray effect that plagues the S_N method in two-dimensional geometries necessitates either a very fine angular mesh or elegant ray effect mitigation tricks; both increase computational costs.

A basic feature of the Monte Carlo method is its ability to represent any geometry exactly. Unfortunately, many neutron histories must be traced in order to reduce the statistical deviation to an acceptable value. Monte Carlo is usually reserved for only the most stringent transport problems or to benchmark other methods, although recent advances in the application of high-speed vector processors to Monte Carlo has resulted in its more efficient use in certain applications.

The two methods described above provide accurate solutions to the transport equation but at a severe penalty in computational effort. This effort can be reduced greatly if either (1) the mesh spacing in a deterministic calculation can be decreased resulting in a coarse mesh, or (2) the solutions for several small regions can be combined to provide a solution for the entire system. With larger

problems being analyzed the need for increased efficiency is all the more obvious.

The purpose of this work is to develop a transport theory method that uses both of these ideas for reducing computational costs. This method is based on the philosophies of the response matrix method and the formalisms of a finite element method. In the remainder of this chapter, both of these techniques are discussed together with some related concepts.

The response matrix method and the closely related interface current method are techniques used to solve the neutron transport or diffusion equation by dividing a large spatial domain into smaller regions, arriving at a solution on each region, and coupling these regional solutions in some manner to obtain a global description of the neutron flux distribution on the large volume. In general, the regional solutions found by the response matrix method are expressed as matrices which represent the probabilities of transmission and reflection of incoming neutrons after any number of collisions in the region. These collisions may result in absorption, scattering, or even fission. An element of a matrix, R_{ij}, gives the probability of a neutron entering the region with state 'j' causing a neutron of state 'i' to leave the region. A state may be any discretized characteristic of a neutron distribution, be it energy, angle, or position along the boundary. The transmission and reflection matrices generated in the interface

current technique, on the other hand, are first-flight probabilities for the region. As noted in a review of the methods by Leonard [Leo76], the interface current method can be reduced to the response matrix method under certain conditions.

Early application of the response matrix method to the one-dimensional transport equation used matrices that were calculated analytically. Matrices for thick regions were generated using clever doubling and adding relations from matrices of thin regions. These, in turn, were found from simple exponential attenuation rules [Fil73] or by use of invariant imbedding [Pfe69]. Invariant imbedding theory [Win62], an alternative to the conventional Boltzmann equation, is a natural candidate for use with the response matrix method because it is derived by examining the external behavior, or response, of a system to incoming neutrons as its size is varied. Response matrices of the transfer matrix method [Aro67] are found by analytical solution of the transport equation via an eigenvalue method.

Doubling and adding rules can also be used to calculate response matrices representing the solution of the diffusion equation. Thin slab probabilities can be found, for example, by iterative use of adding relations themselves [Shi63a] or by direct analytical solution of the diffusion approximation [Aok65].

Once response matrices have been calculated for each region, the global solution proceeds by iterating on the

interface currents or fluxes by applying the following matrix equations in succession:

$$\underline{J}_{out}^{(n)} = \underline{\underline{R}}\, \underline{J}_{in}^{(n-1)} + \underline{J}_{out}^{ext} \tag{1.1}$$

$$\underline{J}_{in}^{(n)} = \underline{\underline{H}}\, \underline{J}_{out}^{(n)} \tag{1.2}$$

where $\underline{\underline{R}}$ is a concatenation of all regional response matrices, $\underline{\underline{H}}$ is a coupling matrix, $\underline{J}_{out}^{ext}$ is the discretized outgoing interface current due to a fixed source, and $\underline{J}_{in}^{(n)}$ and $\underline{J}_{out}^{(n)}$ are, respectively, the discretized incoming and outgoing interface currents or fluxes for iteration n. The eigenvalue or multiplication constant, k, of a multiplying medium is determined from the ratio of interface currents or fluxes from two consecutive iterations

$$k^{(n)} = k^{(n-1)} \frac{\P \underline{J}_{in}^{(n)} \P}{\P \underline{J}_{in}^{(n-1)} \P} \tag{1.3}$$

where $\P \underline{J} \P$ is a summation norm. Because the response matrices of a multiplying medium themselves depend on the eigenvalue of the entire system, they must be recalculated as updated eigenvalues are found. For the analytical methods mentioned above, this is only a slight inconvenience. It is more difficult for the modern numerical methods we turn to next.

Modern response matrix methods of solution of the multidimensional neutron transport equation utilize various means of generating the response matrices themselves. These include the collision probability method, current matching, discrete ordinates, and Monte Carlo [Saj81,Pry73,Lew77]. Different approximations are introduced to discretize the spatial and angular dependence of the flux. Saji, et al. [Saj81] divide the interface into many small segments and assume a flat spatial distribution on each segment. In the interior of the region, a high-order expansion of the flux distribution in space is used. The angular dependence is approximated by a first-order Legendre expansion in each half-space (DP_1). Pryor and Graves [Pry73] assume the same spatial dependence on the interface, but only a flat distribution in the region interior. A DP_0 angular expansion is used. The dependence of the response matrices on the multiplication constant is eliminated by expanding the response matrices themselves in a series in terms of 1/k where the coefficients can be thought of as the response matrix for succeeding generations of neutrons. Weiss [Wei77] has reported two other methods of handling this dependence: expressing the k-dependence of the response matrix analytically; or, calculating response matrices for several values of the multiplication constant and then interpolating as k is recalculated.

The formulation of the interface current method eliminates the dependence of the pre-calculated probability

matrices on the multiplication constant. The interface current method is a simplification of the classical collision probability method. Instead of allowing interaction between all spatial regions, only neighboring regions are coupled through their interfaces. This reduces the dense coupling of variables that plagues the collision probability method but results in some loss of accuracy and theoretical rigor [Lew77]. As mentioned earlier, this method is characterized by transmission and escape probabilities of particles to or from the interfaces without suffering any collisions. This results in two two-matrix equations: the first gives the outgoing interface angular flux, $\underline{\phi}_{out}$, in terms of the uncollided contributions from the incoming interface flux, $\underline{\phi}_{in}$, and in terms of the volumetric source, $\underline{S}$, which includes scattering and fission

$$\underline{\phi}_{out} = \underline{\underline{R}}^{FF}_{S\leftarrow S}\ \underline{\phi}_{in} + \underline{\underline{R}}^{FF}_{S\leftarrow V}\ \underline{S} \tag{1.4}$$

the second equation gives the volumetric flux, $\underline{\phi}_{v}$, due to the uncollided contribution from the same quantities

$$\underline{\phi}_{v} = \underline{\underline{M}}^{FF}_{V\leftarrow S}\ \underline{\phi}_{in} + \underline{\underline{M}}^{FF}_{V\leftarrow V}\ \underline{S} \tag{1.5}$$

where the superscript 'FF' denotes first-flight matrices. The global solution proceeds by means of an inner-outer iteration process. Interface fluxes are found in the inner iteration (labeled 'n')

$$\underline{\phi}_{out}^{(n)} = \underline{\underline{R}}_{S\leftarrow S}^{FF}\, \underline{\phi}_{in}^{(n-1)} + \underline{\underline{R}}_{S\leftarrow V}^{FF}\, \underline{S}^{(m-1)} \tag{1.6}$$

$$\underline{\phi}_{in}^{(n)} = \underline{\underline{H}}\, \underline{\phi}_{out}^{(n)} \tag{1.7}$$

After convergence, the volumetric source and multiplication constant are found in an outer iteration step (labeled 'm')

$$\underline{\phi}_{v}^{(m)} = \underline{\underline{M}}_{V\leftarrow S}^{FF}\underline{\phi}_{in}^{(n)} + \underline{\underline{M}}_{V\leftarrow V}^{FF}\underline{S}^{(m)} \tag{1.8}$$

$$\underline{S}^{(m)} = \frac{1}{k^{(m-1)}}\, \underline{\underline{F}}\, \underline{\phi}_{v}^{(m)} \tag{1.9}$$

$$k^{(m)} = k^{(m-1)} \frac{\P \underline{S}^{(m)} \P}{\P \underline{S}^{(m-1)} \P} \tag{1.10}$$

where $\underline{\underline{F}}$ is a matrix giving the fission and scattering source as a function of the volumetric flux. The inner-outer iteration procedure is repeated until the volumetric source and multiplication constant have converged.

The matrices for the method are almost always derived from the integral transport equation [Dud79]. The interface current method, it follows, shares with integral transport methods the difficulty of treatment of anisotropic scattering: with greater orders of anisotropy more balance equations must be solved and a correspondingly larger number of probabilities must be pre-calculated. For example, in a general geometry, linear anisotropic scattering necessitates

the solution of four integral transport equations: one for the scalar flux and three for the first moments. The many applications of the interface current method vary primarily in their means of discretizing angle and space on the interfaces and interiors of the regions in order to provide adequate accuracy while keeping the computational effort to a minimum. If the order of approximation is too low, an effect known as refraction occurs [Leo76] where, in a non-scattering medium, the highly anisotropic nature of the flux distribution may be reduced, resulting in reflection rather than transmission through a region. The approximations used include various combinations of spatial treatments: constant or linearly varying flux on the interface or in the interior. Jonsson, et al. [Jon75] approximate the spatial dependence by means of a Fourier expansion and the angular dependence by spherical harmonics, although only DP_0 has been used. Chen, et al. [Che71] allow the angular flux to be linearly anisotropic; Mueller and Wagner [Mue72] consider only isotropic flux; and Sanchez [San77] uses a DP_1 approximation. A method that successfully reduces the refraction effect has been developed by Anderson and Honeck [And73]. The angular flux is approximated by a P_1 expansion about a direction that is determined on the basis of the neutron flow. A directed anisotropic flux distribution can be better approximated with this method if the expansion direction is chosen correctly.

A method simialr to the interface current method has been developed for diffusion theory by Lawrence and Dorning [Law80a]. In this method, a multidimensional problem is reduced to two coupled one-dimensional problems by integrating over the transverse directions. Green's functions are used to relate volumetric (nodal) and interface fluxes. This method has also been applied to the transport equation by the same authors [Law80b]. The flux distribution in the interior is expanded in terms of one-dimensional Legendre polynomials, the flux is assumed flat on the interface, and the discrete ordinates method is used to approximate the angular dependence.

The method described in this work uses the phase-space finite element method as the method of solution of the neutron transport equation on each region. Finite elements are therefore the device of discretization of space and angle. Several methods have been developed based on the second-order, even-parity form of the transport equation [Mil73a,Mil73b] which has some advantages over the conventional first-order form. The second-order form is self-adjoint, permitting use of a variational approach and iterative solution schemes. The even-parity flux that is found using this equation is always positive and only half of the angular domain need be analyzed. The treatment of anisotropic scattering, however, is prohibitively awkward. The first-order form, in contrast, can be formulated only through the Galerkin method. Moreover, the structure of the

resulting matrix precludes use of iterative solution methods. Anisotropic scattering can be treated simply, however, and, because the first-order form is the conventional formulation of the transport equation, it is well understood and the angular flux has the usual interpretation. The present method uses the first-order form exclusively.

The phase-space finite element method has been applied to both the one-dimensional and two-dimensional first-order transport equations [Mar77,Yeh78]. In one dimension, the method is competitive with the discrete ordinates method. The two-dimensional implementation is much less efficient than the two-dimensional discrete ordinates method because direct solution of large matrices is necessary. In order to increase computational efficiency, a segmented solution method [Lor79,Mar81] has been devised. Like the response matrix method, the volume is divided into segments and a global solution is found by converging on the interface fluxes. In contrast to the response matrix method, the interior fluxes must be found at each iteration. Instead of individual escape and transmission matrices for each segment, the contribution of each segment to the large finite element matrix is calculated. No efficiency is gained for the one-dimensional case but significant improvements are found in two dimensions.

The second-order, even-parity finite element method has been cast in a form similar to the response matrix method

known as the constrained finite element method [Bri77]. In its one-dimensional implementation, the spatial domain is divided into regions and the even-parity angular flux is constrained to be independent of angle at region interfaces. This constraint is equivalent to a P_1 approximation (cosine current) because odd moments in angle vanish in the even-parity formulation. In fact, as the region size is decreased, the method mimics a P_1 method. The two-dimensional method [Bri80] is similar to the one-dimensional case. Again, at the interface, the angular dependence is restricted to be independent of angle and thus isotropic. Furthermore, the spatial dependence of this "scalar" flux is constrained so that the flux can vary linearly between coarse nodal points on the interface. The even-parity angular flux varies linearly between points on a fine spatial and angular grid in the interior of the region; on the interface of the region, the flux is described on a coarse spatial grid and coarse angular (only one value specifies the flux shape in angle) grid. A response matrix method was developed for the second-order finite element method by forcing the incoming and outgoing angular fluxes to be independent of angle, in contrast to the constrained finite element method where the flux over the entire angular domain is constrained to be independent of angle. This method was found to be inferior to the constrained finite element method because such a requirement can only be approximated by the second-order, even-parity transport equation which

cannot reproduce odd moments of angular flux. The method was therefore abandoned after one-dimensional testing.

The finite element response matrix method (FERM) for the solution of the diffusion equation [Nak83] incorporates some of the features of the interface current scheme, the classical response matrix method, and the constrained finite element method. Like the interface current method, a system of two equations each with two matrices is used as part of inner-outer iteration procedure to obtain a global solution

$$\underline{J}_{out} = \underline{\underline{R}}^{D}_{S \leftarrow S} \, \underline{J}_{in} + \underline{\underline{R}}^{D}_{S \leftarrow V} \, \underline{S} \tag{1.11}$$

$$\underline{\phi}_{v} = \underline{\underline{M}}^{D}_{V \leftarrow S} \, \underline{J}_{in} + \underline{\underline{M}}^{D}_{V \leftarrow V} \, \underline{S} \tag{1.12}$$

$$\underline{S} = \frac{1}{k} \, \underline{\underline{F}} \, \underline{\phi}_{v} \tag{1.13}$$

where $\underline{J}_{out}$ and $\underline{J}_{in}$ are the outgoing and incoming partial currents, respectively, $\underline{\phi}_{v}$ is the volumetric scalar flux, and 'D' denotes diffusion theory. The matrices represent transmission and reflection after any number of scattering collisions and can be thought of as diffusion escape probabilities, in contrast to the first-flight escape probabilities of the interface current method. The matrices, then, can be considered response matrices in the classical sense with one exception: the fission source is treated separately. A novel local-global mesh structure, an

elaboration of that of the constrained finite element method, is used by FERM. The solution of the diffusion equation is first found by application of the finite element method on a fine mesh on the interior and boundaries of each region. This solution is then projected onto a coarse mesh and incorporated into the four response matrices. The global solution is expressed on the coarse mesh, making FERM a method suitable for large scale, coarse mesh calculations of reactor cores.

The diffusion theory FERM serves as the inspiration for the transport theory method of this work. In it a set of four response matrices are found that represent transport escape probabilities after any number of scattering events. Angular fluxes, rather than partial currents, are found by means of an inner-outer iteration procedure using the following equations:

$$\underline{\phi}_{+} = \underline{\underline{R}}_{S \leftarrow S} \underline{\phi}^{S}_{in} + \underline{\underline{R}}_{S \leftarrow V} \underline{S}^{V} \tag{1.14}$$

$$\underline{\phi}^{V} = \underline{\underline{M}}_{V \leftarrow S} \underline{\phi}^{S}_{in} + \underline{\underline{M}}_{V \leftarrow V} \underline{S}^{V} \tag{1.15}$$

In the following chapter, the method is developed for a general multidimensional geometry. The method of projection from a fine mesh to a coarse mesh and the iteration solution procedure is discussed. The application of the method to one- and two-dimensional geometries are discussed in detail in the third chapter. In subsequent chapters, the one- and

two-dimensional implementation and its testing are described, including a discussion of the method's accuracy and efficiency.

CHAPTER II

GENERAL MULTIDIMENSIONAL DERIVATION OF THE METHOD

In this chapter, the response matrix method is developed for a general multidimensional geometry. After introducing the first-order transport equation and response kernel equations, general response matrix equations are developed following the steps outlined by Nakata [Nak83]. The weak form of the transport equation is then derived. By application of the Galerkin phase-space finite element technique, a matrix approximation to the weak form is found. This derivation of the Galerkin method follows closely that of Ukai [Uka72] and Martin [Mar77]. The response matrices are found by projecting the solution of this matrix equation onto coarse meshes on the surface and interior of the region again using the method developed by Nakata for the diffusion approximation. Finally, iterative schemes for the global solution are described for two classes of problems: fixed source problems and multiplying medium problems.

The First-Order Neutron Transport Equation

The spatial domain $\mathcal{R}$, over which a spatial and angular distribution of neutrons is sought, is divided into L distinct regions such that

$$\mathcal{R} = \bigcup_{\ell=1}^{L} \mathcal{R}_\ell$$

and

$$\mathcal{R}_\ell \cap \mathcal{R}_m = 0 \quad \text{if } \ell \neq m$$

where $\mathcal{R}_\ell$ is the spatial domain of region ℓ.

Consider the first-order neutron transport equation for a single region ℓ

$$\underline{\Omega}\cdot\underline{\nabla}\phi(\underline{r},\underline{\Omega}) + \Sigma_t(\underline{r})\phi(\underline{r},\underline{\Omega}) = \int_{4\pi} d\underline{\Omega}'\Sigma_s(\underline{r},\underline{\Omega}'\cdot\underline{\Omega})\phi(\underline{r},\underline{\Omega}') + S(\underline{r},\underline{\Omega}) \tag{2.1}$$

subject to a specified incoming boundary condition

$$\phi(\underline{r},\underline{\Omega}) = \phi_{in,\ell}(\underline{r},\underline{\Omega}) \text{ on } \Gamma_\ell^- \tag{2.2}$$

where $\phi(\underline{r},\underline{\Omega})$ - angular flux

$\Sigma_t(\underline{r})$ - total cross section

$\Sigma_s(\underline{r},\underline{\Omega}'\cdot\underline{\Omega})$ - differential scattering cross section

Γ_ℓ^- - incoming boundary

The volumetric source, $S(\underline{r},\underline{\Omega})$, may represent a fission source

$$S(\underline{r},\underline{\Omega}) = \frac{1}{k}\frac{\nu\Sigma_f(\underline{r})}{4\pi}\int_{4\pi} d\underline{\Omega}'\,\phi(\underline{r},\underline{\Omega}') \tag{2.3}$$

where $\Sigma_f(\underline{r})$ - fission cross section

ν - average number of neutrons released per fission

k - multiplication constant or eigenvalue

or an external, specified source of neutrons

$$S(\underline{r},\underline{\Omega}) = S_{ex}(\underline{r},\underline{\Omega}) \tag{2.4}$$

or a combination of both (if the medium is sub-critical).

For convenience the following additional notation is introduced:

4π = angular domain

V = phase-space: $\mathcal{R}x4\pi$

V_ℓ = phase-space of region ℓ: $\mathcal{R}_\ell x4\pi$

∂R_ℓ = boundary of region ℓ

$\underline{n}_\ell$ = unit outward normal to ∂R_ℓ

Γ_ℓ = $\partial R_\ell \times 4\pi$

Γ_ℓ^+ = outgoing boundary:
all $(\underline{r},\underline{\Omega}) \in \Gamma_\ell$ for $\underline{n}_\ell \cdot \underline{\Omega} > 0$

Γ_ℓ^- = incoming boundary:
all $(\underline{r},\underline{\Omega}) \in \Gamma_\ell$ for $\underline{n}_\ell \cdot \underline{\Omega} < 0$

The Response Kernel Equations

Because the transport equation is linear, an expression giving the outgoing angular flux, that is

$$\phi_{\ell+}(\underline{r},\underline{\Omega}) = \phi(\underline{r},\underline{\Omega}) \qquad \text{for } (\underline{r},\underline{\Omega}) \in \Gamma_\ell^+ \tag{2.5}$$

can be written in terms of the specified quantities $\phi_{in,\ell}(\underline{r},\underline{\Omega})$ and $S(\underline{r},\underline{\Omega})$,

$$\begin{aligned}\phi_{\ell+}(\underline{r},\underline{\Omega}) = {} & \int_{\Gamma_\ell^-} ds' d\underline{\Omega}' \, |\underline{n}_\ell \cdot \underline{\Omega}'| R_S^\ell(\underline{r}',\underline{\Omega}' \to \underline{r},\underline{\Omega}) \phi_{in,\ell}(\underline{r}',\underline{\Omega}') \\ & + \int_{V_\ell} d\underline{r}' d\underline{\Omega}' R_V^\ell(\underline{r}',\underline{\Omega}' \to \underline{r},\underline{\Omega}) S(\underline{r}',\underline{\Omega}') \\ & \qquad \text{for } (\underline{r},\underline{\Omega}) \in \Gamma_\ell^+ \end{aligned} \tag{2.6}$$

where

$R_S^{\ell}(\underline{r}',\underline{\Omega}'\rightarrow\underline{r},\underline{\Omega})$ = response kernel for outgoing angular flux due to the transport of the neutrons entering region ℓ

$R_V^{\ell}(\underline{r}',\underline{\Omega}'\rightarrow\underline{r},\underline{\Omega})$ = response kernel for outgoing angular flux due to the transport of the neutrons produced within $\mathcal{R}_{\ell}$.

In the conventional response matrix formulation $\phi_{\ell+}(\underline{r},\underline{\Omega})$ is written,

$$\phi_{\ell+}(\underline{r},\underline{\Omega}) = \int_{\Gamma_{\ell}^-} ds'd\underline{\Omega}' |\underline{n}_{\ell}\cdot\underline{\Omega}'| R^{\ell}(\underline{r}',\underline{\Omega}'\rightarrow\underline{r},\underline{\Omega})\phi_{in,\ell}(\underline{r}',\underline{\Omega}') + \phi_{\ell+}^{ext}(\underline{r},\underline{\Omega}) \qquad \text{for } (\underline{r},\underline{\Omega})\epsilon\Gamma_{\ell}^+ \tag{2.7}$$

where

$R^{\ell}(\underline{r}',\underline{\Omega}'\rightarrow\underline{r},\underline{\Omega})$ = response kernel for outgoing angular flux due to an arbitrary incoming flux

$\phi_{\ell+}^{ext}$ = outgoing angular flux due to fixed source within $\mathcal{R}_{\ell}$.

The primary difference between the two kernels R_S^{ℓ} and R^{ℓ} is that the latter represents the **total** contribution of the incoming flux to the outgoing flux through streaming, redirection through scattering, and, perhaps most significantly, generation of secondary neutrons by means of fission. The kernel R_S^{ℓ}, on the other hand, allows transport

from surface to surface by all these processes **except** fission (and downscatter, in the case of a multi-group formulation). In a multiplying medium, then, R^{ℓ} is dependent on the multiplication constant, but R_S^{ℓ} is not.

Because the fission source is included in $S(\underline{r},\underline{\Omega})$ and not in R_S^{ℓ} an ancillary equation must be used to find the angular flux in the interior of $\mathcal{R}_{\ell}$, which in turn gives the fission contribution to $S(\underline{r},\underline{\Omega})$:

$$\phi(\underline{r},\underline{\Omega}) = \int_{\Gamma_{\ell}^-} ds' d\underline{\Omega}' |\underline{n}_{\ell}\cdot\underline{\Omega}'| M_S^{\ell}(\underline{r}',\underline{\Omega}'\rightarrow\underline{r},\underline{\Omega})\phi_{in,\ell}(\underline{r}',\underline{\Omega}') + \int_{V_{\ell}} d\underline{r}' d\underline{\Omega}' M_V^{\ell}(\underline{r}',\underline{\Omega}'\rightarrow\underline{r},\underline{\Omega})S(\underline{r}',\underline{\Omega}') \quad \text{for } (\underline{r},\underline{\Omega})\epsilon V_{\ell} \tag{2.8}$$

The Response Matrix Equations

The equations presented in the previous section provide a means of solution of the transport equation. But, in order to solve them on a computer some method of discretizing these equations must be chosen. The choice here is to approximate the functions of interest--$\phi_{\ell+}(\underline{r},\underline{\Omega})$, $S(\underline{r},\underline{\Omega})$, $\phi_{in,\ell}(\underline{r},\underline{\Omega})$, and $\phi(\underline{r},\underline{\Omega})$--as series expansions in terms of polynomials. The particular polynomials chosen are finite element basis functions which span subsets of two spaces of functions--one that exists only on the region interfaces and problem boundary, and the other on the interior of all regions. The two sets of functions are called the global surface basis functions and the global volume basis functions. The details of the construction of the finite element basis functions are left until the discussion of the formulation of the method in specific geometries, i.e., one and two spatial dimensions, in Chapter III. As will be discussed, the elements are piecewise continuous polynomial functions defined on a mesh that discretizes both the configuration space and the angular space.

The fluxes defined on the interface of region ℓ are expanded in terms of the global surface basis functions,

$$\begin{aligned}\phi_{in,\ell}(\underline{r},\underline{\Omega}) &\simeq \sum_{i=1}^{M_S} \Psi_{S_i}(\underline{r},\underline{\Omega})\ \phi^S_{in,\ell_i} \\ &\simeq \underline{\Psi}_S^T\ \underline{\phi}^S_{in,\ell}\end{aligned} \tag{2.9}$$

$$\phi_{\ell+}(\underline{r},\underline{\Omega}) \simeq \underline{\Psi}_S^T \, \underline{\phi}^S_{\ell+} \tag{2.10}$$

where 'T' indicates transpose,

$$\underline{\Psi}_S = \text{col}\,(\Psi_{S_1}, \Psi_{S_2}, \ldots, \Psi_{S_{M_S}})$$

$$\underline{\phi}^S_{\text{in},\ell} = \text{col}(\phi^S_{\text{in},\ell_1}, \phi^S_{\text{in},\ell_2}, \ldots, \phi^S_{\text{in},\ell_{M_S}})$$

$$\underline{\phi}^S_{\ell+} = \text{col}(\phi^S_{\ell+_1}, \phi^S_{\ell+_2}, \ldots, \phi^S_{\ell+_{M_S}})$$

and

$$\Psi_{S_i}(\underline{r},\underline{\Omega}),\ i = 1, 2, \ldots, M_S$$

are the basis functions of the M_S-dimensional global surface function space, $S^{h^S} \subset H^S$, where

$$H^S = \{\Psi_S(\underline{r},\underline{\Omega}) \mid (\underline{r},\underline{\Omega}) \in \bigcup_{\ell=1}^{L} \Gamma_\ell,\ \langle\Psi_S,\Psi_S\rangle_+ + \langle\Psi_S,\Psi_S\rangle_- < \infty\}$$

and

$$\langle \Phi,\Psi\rangle_{\pm} = \text{global surface inner product}$$

$$\equiv \sum_{\ell=1}^{L} \langle \Phi,\Psi\rangle_{\pm\ell}$$

$$\langle \Phi,\Psi\rangle_{\pm\ell} = \text{local surface inner product}$$

$$\equiv \int_{\Gamma_\ell^{\pm}} ds d\underline{\Omega} |\underline{\dot{n}}_\ell \cdot \underline{\Omega}| \Phi(\underline{r},\underline{\Omega})\Psi(\underline{r},\underline{\Omega})$$

The value h^S characterizes the spacing of the support points of the global surface basis functions.

Similarly, the quantities defined on the region interiors are expressed in terms of the global volume basis functions:

$$S(\underline{r},\underline{\Omega}) \simeq \sum_{i=1}^{M} \Psi_i(\underline{r},\underline{\Omega})\ S^V_{\ell i} \simeq \underline{\Psi}^T\ \underline{S}^V_\ell \tag{2.11}$$

$$\phi(\underline{r},\underline{\Omega}) \simeq \underline{\Psi}^T\ \underline{\phi}^V_\ell \tag{2.12}$$

In this case, the M-dimensional global volume function space S^{h^V} is a subspace of H_E, where

$$H_E = \{\Psi(\underline{r},\underline{\Omega}) \mid (\underline{r},\underline{\Omega})\epsilon V,\ (\Psi,\Psi) + (|\underline{\nabla}\Psi|,|\underline{\nabla}\Psi|) < \infty\}$$

and

$$(\Phi,\Psi) = \text{global volume inner product}$$

$$\equiv \sum_{\ell=1}^{L} (\Phi,\Psi)_\ell$$

$$(\Phi,\Psi)_\ell = \text{local volume inner product}$$

$$\equiv \int_{V_\ell} d\underline{r}\, d\underline{\Omega}\, \Phi(\underline{r},\underline{\Omega})\Psi(\underline{r},\underline{\Omega})$$

The space S^{h^V} is spanned by

$$\Psi(\underline{r},\underline{\Omega}),\ i = 1,\ 2,\ \ldots,\ M$$

The reasons for the restriction on the surface and volume inner products will become clear in the ensuing manipulation.

Substituting these approximations into Eq. (2.2),

$$\sum_{k=1}^{M_S} \Psi_{S_k} \phi_{\ell+S_k} =$$

$$\sum_{i=1}^{M_S} \phi^S_{\text{in},\ell_i} \int_{\Gamma_\ell^-} ds'\, d\underline{\Omega}'\, |\underline{n}_\ell \cdot \underline{\Omega}'|\, R_S^\ell(\underline{r}',\underline{\Omega}' \to \underline{r},\underline{\Omega}) \Psi_{S_i}(\underline{r}',\underline{\Omega}') \qquad (2.13)$$

$$+ \sum_{i=1}^{M} S^V_{\ell_i} \int_{V_\ell} d\underline{r}'\, d\underline{\Omega}'\, R_V^\ell(\underline{r}',\underline{\Omega}' \to \underline{r},\underline{\Omega}) \Psi_i(\underline{r}',\underline{\Omega}')$$

$$\text{for } (\underline{r},\underline{\Omega}) \in \Gamma_\ell^+$$

multiplying by $\Psi_{S_j}(\underline{r},\underline{\Omega})$ and $|\underline{n}_\ell \cdot \underline{\Omega}|$, and integrating over the outgoing surface, $(\underline{r},\underline{\Omega}) \epsilon \Gamma_\ell^+$, yields a discrete form for Eq. (2.2):

$$\underline{\phi}_{\ell+}^S = \underline{\underline{R}}_{S \leftarrow S}^{\ell} \underline{\phi}_{in,\ell}^S + \underline{\underline{R}}_{S \leftarrow V}^{\ell} \underline{S}_\ell^V \tag{2.14}$$

The exact definitions of the response matrices $\underline{\underline{R}}_{S \leftarrow S}^{\ell}$ and $\underline{\underline{R}}_{S \leftarrow V}^{\ell}$ will be presented later in this chapter.

The supplementary equation giving the interior flux (Eq. (2.8)) can be discretized as well by substituting the appropriate series approximation, multiplying by $\Psi_j(\underline{r},\underline{\Omega})$, and integrating over the interior, $(\underline{r},\underline{\Omega}) \epsilon V_\ell$:

$$\underline{\phi}_\ell^V = \underline{\underline{M}}_{V \leftarrow S}^{\ell} \underline{\phi}_{in,\ell}^S + \underline{\underline{M}}_{V \leftarrow V}^{\ell} \underline{S}_\ell^V \tag{2.15}$$

By combining the four response matrices found for each region into four global matrices and introducing an interface coupling operator ($\underline{\underline{H}}$) and a fission source operator ($\underline{F}$), a system of equations is formed which gives the global distribution of neutrons:

$$
\begin{aligned}
\underline{\phi}_{+}^{S} &= \underline{\underline{R}}_{S\leftarrow S}\underline{\phi}_{in}^{S} + \underline{\underline{R}}_{S\leftarrow V}\underline{S}^{V} \\
\underline{\phi}_{in}^{S} &= \underline{\underline{H}}\ \underline{\phi}_{+}^{S} \\
\underline{\phi}^{V} &= \underline{\underline{M}}_{V\leftarrow S}\underline{\phi}_{in}^{S} + \underline{\underline{M}}_{V\leftarrow V}\underline{S}^{V} \\
\underline{S}^{V} &= \frac{1}{k^{(m)}}\ \underline{\underline{F}}\ \underline{\phi}^{V(m)}
\end{aligned}
\tag{2.16}
$$

Because these equations are solved iteratively, the efficiency of the solution method is strongly dependent on the dimension of the finite element function spaces. If the dimensions are reduced--which implies the mesh spacings are increased--the computational requirements decrease. Hence, the global mesh size determines the computational efficiency of the global iterative solution scheme.

Implicit in the preceeding derivation is the assumption that the kernels--R_S^{ℓ}, R_V^{ℓ}, M_S^{ℓ}, and M_V^{ℓ}--are known. They are, of course, not magically known but must be calculated by some means. The method selected for this work is the finite element method of solution of the weak form of the first-order neutron transport equation. The following two sections give the derivation of this weak form and its solution method. The details of the response matrix derivation are presented in the third section.

The Weak Transport Equation

The weak form of the transport equation is found by multiplying Eq. (2.1) by an arbitrary test function $\psi_\ell(\underline{r},\underline{\Omega})$ and integrating over the phase-space V_ℓ

$$\int_{V_\ell} d\underline{r}d\underline{\Omega}\ \underline{\Omega}\cdot\underline{\nabla}\phi(\underline{r},\underline{\Omega})\psi_\ell(\underline{r},\underline{\Omega}) + \int_{V_\ell} d\underline{r}d\underline{\Omega}\Sigma_t(\underline{r})\phi(\underline{r},\underline{\Omega})\ \psi_\ell(\underline{r},\underline{\Omega}) = \int_{V_\ell} d\underline{r}d\underline{\Omega}\psi_\ell(\underline{r},\underline{\Omega})\ \int_{4\pi} d\underline{\Omega}'\Sigma(\underline{r},\underline{\Omega}'\cdot\underline{\Omega})\phi(\underline{r},\underline{\Omega}') + \int_{V_\ell} d\underline{r}d\underline{\Omega}S(\underline{r},\underline{\Omega})\psi_\ell(\underline{r},\underline{\Omega}) \tag{2.17}$$

This test function is required to be a member of the set of test functions contained in the space H_E^ℓ:

$$H_E^\ell = \{\psi_\ell(\underline{r},\underline{\Omega}) \mid (\underline{r},\underline{\Omega})\epsilon V_\ell,\ (\psi_\ell,\psi_\ell)_\ell + (|\underline{\nabla}\psi_\ell|,|\underline{\nabla}\psi_\ell|)_\ell < \infty\}$$

or, stated simply, the test function and its gradient must be square integrable. The streaming term can be integrated by parts resulting in two surface terms and the transfer of the divergence operator from the angular flux to the test function:

$$\int_{V_\ell} \int d\underline{r} d\underline{\Omega}\ \underline{\Omega}\cdot\underline{\nabla}\phi(\underline{r},\underline{\Omega})\ \psi_\ell(\underline{r},\underline{\Omega}) =$$

$$- \int_{V_\ell} \int d\underline{r} d\underline{\Omega}\ \phi(\underline{r},\underline{\Omega})\underline{\Omega}\cdot\underline{\nabla}\psi_\ell(\underline{r},\underline{\Omega})$$

$$+ \int_{\Gamma_\ell^+} ds d\underline{\Omega} |\underline{n}_\ell\cdot\underline{\Omega}| \phi(\underline{r},\underline{\Omega})\psi_\ell(\underline{r},\underline{\Omega}) \qquad (2.18)$$

$$- \int_{\Gamma_\ell^-} ds d\underline{\Omega} |\underline{n}_\ell\cdot\underline{\Omega}| \phi(\underline{r},\underline{\Omega})\psi_\ell(\underline{r},\underline{\Omega})$$

The integral equation is written

$$-(\phi,\underline{\Omega}\cdot\underline{\nabla}\psi_\ell)_\ell + \langle\phi,\psi_\ell\rangle_{+\ell}$$

$$- \langle\phi,\psi_\ell\rangle_{-\ell} + (\Sigma_t\phi,\psi_\ell)_\ell = \qquad (2.19)$$

$$(K_{scat}\phi,\psi_\ell)_\ell + (S,\psi_\ell)_\ell$$

with the introduction of the following simplifying notation:

K_{scat} = scattering operator, defined

$$K_{scat}\phi(\underline{r},\underline{\Omega}) \equiv \int_{4\pi} d\underline{\Omega}' \Sigma_s(\underline{r},\underline{\Omega}'\cdot\underline{\Omega})\phi(\underline{r},\underline{\Omega}')$$

The specified incoming boundary condition, Eq. (2.2), replaces the angular flux in the incoming surface term and this term together with the other known term, the volumetric source, is moved to the right side:

$$-(\phi,\underline{\Omega}\cdot\underline{\nabla}\psi_\ell)_\ell + \langle\phi,\psi_\ell\rangle_{+\ell}$$

$$- (K_{scat}\phi,\psi_\ell)_\ell + (\Sigma_t\phi,\psi_\ell)_\ell = \tag{2.20}$$

$$\langle\phi_{in,\ell},\psi_\ell\rangle_{-\ell} + (S,\psi_\ell)_\ell$$

or, introducing the bilinear functional a_ℓ:

$$a_\ell(\psi_{\ell i},\psi_{\ell j}) =$$

$$- (\psi_{\ell i},\underline{\Omega}\cdot\underline{\nabla}\psi_{\ell j})_\ell + \langle\psi_{\ell i},\psi_{\ell j}\rangle_{+\ell} \tag{2.21}$$

$$- (K_{scat}\psi_{\ell i},\psi_{\ell j})_\ell + (\Sigma_t\psi_{\ell i},\psi_{\ell j})_\ell$$

Hence,

$$a_\ell(\phi,\psi_\ell) = \langle\phi_{in,\ell},\psi_\ell\rangle_{-\ell} + (S,\psi_\ell)_\ell \tag{2.22}$$

Thus, the weak form of the Eq. (2.1) is

Find $\phi(\underline{r},\underline{\Omega})\epsilon H_E^\ell$, such that for all $\psi_\ell(\underline{r},\underline{\Omega})\epsilon H_E^\ell$

$$a_\ell(\phi,\psi_\ell) = \langle\phi_{in,\ell},\psi_\ell\rangle_{-\ell} + (S,\psi_\ell)_\ell \tag{2.23}$$

Ukai has shown Eqs. (2.23) and (2.1) to be equivalent. This equivalence depends on the critical assumption that all test functions in H_E^ℓ are used in the solution procedure. Because these test functions number infinity, this solution method is beyond the abilities of even the most sophisticated supercomputer. By application of the Galerkin finite element approximation to Eq. (2.23), however, only a finite

number of test functions must be tried. This approximation, while permitting a solution, negates the exact equivalence of Eqs. (2.23) and (2.1); the solution is only approximate.

The Galerkin Approximation

Recall that the response matrices that were described earlier and will result from the current manipulations were expressed in terms of global basis functions. The larger the mesh size of the global support points, the more efficient the global iteration procedure. To solve the transport equation on the local region requires close spacing of the local mesh, however. The Galerkin approximation is formulated in terms of local basis functions on a relatively fine mesh. The resulting matrix solution is projected from the local mesh to the global mesh as described in the next section on the generation of the response matrices themselves.

An N-dimensional subspace, $S^{h^\ell} \subset H_E^\ell$, is chosen with basis functions

$$\psi_{\ell i}(\underline{r},\underline{\Omega}),\ i = 1,\ 2,\ \ldots,\ N$$

which are referred to as local basis functions, where the parameter h^ℓ describes the spacing of the mesh on region ℓ. The finite element approximation to the weak form (Eq. (2.23)) is

Find $\phi(\underline{r},\underline{\Omega})\epsilon S^{h^\ell}$, such that for all $\psi_{\ell j}(\underline{r},\underline{\Omega})\epsilon S^{h^\ell}$

$$a_\ell(\phi,\psi_{\ell j}) = \langle\phi_{in,\ell},\psi_{\ell j}\rangle_{-\ell} + (S,\psi_{\ell j})_\ell \qquad (2.24)$$

The angular flux, the unknown quantity, can be expressed as an expansion in terms of the basis functions because S^{h^ℓ} is finite dimensioned and $\phi(\underline{r},\underline{\Omega})\epsilon S^{h^\ell}$,

$$\phi(\underline{r},\underline{\Omega}) \simeq \sum_{i=1}^{N} \psi_{\ell i}(\underline{r},\underline{\Omega})\phi_{\ell i} = \underline{\psi}_\ell^T \underline{\phi}_\ell \qquad (2.25)$$

where

$$\underline{\psi}_\ell = \text{col}\ (\psi_{\ell 1},\ \psi_{\ell 2},\ \ldots,\ \psi_{\ell N})$$

$$\underline{\phi}_\ell = \text{col}\ (\phi_{\ell 1},\ \phi_{\ell 2},\ \ldots,\ \phi_{\ell N})$$

and T denotes transpose. Substituting the expansion into left side of Eq. (2.24)

$$\sum_{i=1}^{N} \phi_{\ell i} a_\ell(\psi_{\ell i},\psi_{\ell j}) = \langle\phi_{in,\ell},\psi_{\ell j}\rangle_{-\ell} + (S,\psi_{\ell j})_\ell \qquad (2.26)$$

and introducing some more notation

$$A_{\ell_{ji}} = a_\ell(\psi_{\ell i},\psi_{\ell j})$$

$$= -(\psi_{\ell i},\underline{\Omega}\cdot\underline{\nabla}\psi_{\ell j})_\ell + \langle\psi_{\ell i},\psi_{\ell j}\rangle_{+\ell}$$

$$- (K_{scat}\psi_{\ell i},\psi_{\ell j})_\ell + (\Sigma_t\psi_{\ell i},\psi_{\ell j})_\ell$$

$$\underline{\underline{A}}_\ell = \{A_{\ell_{ji}}\} \quad (N \times N \text{ matrix})$$

$$\phi_{in,\ell_j} = \langle\phi_{in,\ell},\psi_{\ell j}\rangle_{-\ell} \tag{2.27}$$

$$\underline{\Phi}_{in,\ell} = col(\phi_{in,\ell_1}, \phi_{in,\ell_2}, \ldots, \phi_{in,\ell_N})$$

$$S_{\ell_j} = (S,\psi_{\ell j})_\ell$$

$$\underline{S}_\ell = col(S_{\ell_1}, S_{\ell_2}, \ldots, S_{\ell_N})$$

results in the matrix equation

$$\underline{\underline{A}}_\ell\underline{\Phi}_\ell = \underline{\Phi}_{in,\ell} + \underline{S}_\ell \tag{2.28}$$

It is easy to demonstrate that $\underline{\underline{A}}_\ell$ is nonsingular and hence invertible. Note that the matrix $\underline{\underline{A}}_\ell$ includes no provision for a reflecting boundary condition. The boundary conditions for the global problem, i.e., on $\partial\mathcal{R}$, are treated

during the iterative global solution procedure described below.

Response Matrix Derivation

By inverting the finite element matrix for region ℓ

$$\underline{\Phi}_\ell = \underline{\underline{A}}_\ell^{-1} \underline{\Phi}_{in,\ell} + \underline{\underline{A}}_\ell^{-1} \underline{S}_\ell \tag{2.29}$$

an expression is found that relates the angular flux on the interior of region ℓ, which is expressed in terms of the local basis functions, to the incoming angular flux vector and the volumetric source vector. The incoming angular flux vector is defined as the surface inner product of the incoming flux with the local basis functions. Similarly, the volumetric source vector is defined as the volume inner product of the volumetric source and the local basis functions.

The local basis functions used thus far in the derivation are defined on a fine phase-space mesh on the interior of the region (V_ℓ). The fine mesh is necessary to achieve a suitably accurate solution. However, as mentioned previously, a coarser mesh--the global mesh introduced earlier--is desired to improve the efficiency of the response matrix iteration procedure used to find the global solution, i.e., the neutron distribution over the entire phase-space, V. Both of these objectives can be met by projecting the fine mesh, local solution onto the coarse global mesh.

Recall from Eq. (2.11) that the volumetric source distribution, $S(\underline{r},\underline{\Omega})$, can be expanded in terms of the global volume basis functions, and substituted into the expression defining S_{ℓ_j}

$$\begin{aligned} S_{\ell_j} &= (S,\psi_{\ell j})_\ell \\ &= \sum_{i=1}^{M} S^V_{\ell_i} \, (\Psi_i,\psi_{\ell j})_\ell \\ &= \sum_{i=1}^{M} (\underline{\underline{T}}_{\ell,V})_{ji} \, S^V_{\ell_i} \end{aligned} \tag{2.30}$$

or

$$\underline{S}_\ell = \underline{\underline{T}}_{\ell,V} \, \underline{S}^V_\ell \tag{2.31}$$

defining $\underline{\underline{T}}_{\ell,V}$ to simplify the expression. The superscript 'V' indicates global volume expansion coefficients. The mass matrix $\underline{\underline{T}}_{\ell,V}$ can be thought of as a means of projecting the expansion approximation from one set of basis functions to another, in this case from the global volume space to the local volume space.

Since the specified incoming flux, $\phi_{in,\ell}(\underline{r},\underline{\Omega})$, is defined only on the incoming boundary, Γ^-_ℓ, it can be expanded as before in terms of the set of global incoming surface basis functions, $\underline{\Psi}_S$:

$$\phi_{in,\ell}(\underline{r},\underline{\Omega}) \simeq \underline{\Psi}_S^T \underline{\phi}^S_{in,\ell} \tag{2.32}$$

Substitution of the expansion into the definition for ϕ_{in,ℓ_j}

$$\begin{aligned}\phi_{in,\ell_j} &= \langle \phi_{in,\ell}, \psi_{\ell j} \rangle_{-\ell} \\ &= \sum_i \phi^S_{in,\ell_i} \langle \Psi_{S_i}, \psi_{\ell_j} \rangle_{-\ell} \\ &= \sum_i (\underline{\underline{T}}_{\ell,S})_{ji} \phi^S_{in,\ell_i}\end{aligned} \tag{2.32}$$

results in a relationship between the local incoming flux vector and the global incoming flux vector:

$$\underline{\phi}_{in,\ell} = \underline{\underline{T}}_{\ell,S} \underline{\phi}^S_{in,\ell} \tag{2.33}$$

The superscript 'S' indicates global surface expansion coefficients. Substituting Eqs. (2.31) and (2.33) into Eq. (2.29) results in an expression

$$\underline{\phi}_\ell = \underline{\underline{A}}_\ell^{-1} \underline{\underline{T}}_{\ell,S} \underline{\phi}^S_{in,\ell} + \underline{\underline{A}}_\ell^{-1} \underline{\underline{T}}_{\ell,V} \underline{S}^V_\ell \tag{2.35}$$

relating the local volumetric flux vector to the global incoming flux and volumetric source vectors.

The response matrices are found by projecting the local volumetric flux vector onto the global mesh. The angular flux was approximated in Eq. (2.25) as

$$\phi(\underline{r},\underline{\Omega}) \simeq \underline{\psi}_{\ell}^{T}\,\underline{\phi}_{\ell}$$

Because the outgoing surface flux, $\phi_{\ell+}(\underline{r},\underline{\Omega})$ is just the angular flux evaluated on Γ_{ℓ}^{+},

$$\phi_{\ell+}(\underline{r},\underline{\Omega}) = \phi(\underline{r},\underline{\Omega}) \qquad (\underline{r},\underline{\Omega}) \in \Gamma_{\ell}^{+} \tag{2.36}$$

its approximation is written:

$$\phi_{\ell+}(\underline{r},\underline{\Omega}) \simeq \underline{\psi}_{\ell}^{T}\underline{\phi}_{\ell} \qquad (\underline{r},\underline{\Omega}) \in \Gamma_{\ell}^{+} \tag{2.37}$$

An alternate approximation is an expansion in the local surface basis function, $\underline{\psi}_{\ell S}$,

$$\phi_{\ell+}(\underline{r},\underline{\Omega}) \simeq \underline{\psi}_{\ell S}^{T}\,\underline{\phi}_{\ell+}^{\ell S} \tag{2.38}$$

where

$$\psi_{\ell Si}(\underline{r},\underline{\Omega}),\ i = 1,\ 2,\ \ldots,\ N_S$$

spans the local surface function space, $S^{h^{\ell S}} \subset H^{\ell S}$, which is defined only on the boundary of ℓ:

$$H^{\ell S} = \{\psi_{\ell S}(\underline{r},\underline{\Omega}) \mid (\underline{r},\underline{\Omega}) \in \Gamma_{\ell},\ \langle\psi_{\ell S},\psi_{\ell S}\rangle_{+\ell} + \langle\psi_{\ell S},\psi_{\ell S}\rangle_{-\ell} < \infty\}$$

These two approximations can be reconciled using the weighted residual technique. The residual, $g(\underline{r},\underline{\Omega})$, is defined as the difference between the two approximations Eqs. (2.37) and (2.38):

$$g(\underline{r},\underline{\Omega}) = \underline{\psi}_{\ell}^{T}\,\underline{\phi}_{\ell} - \underline{\psi}_{\ell S}^{T}\,\underline{\phi}_{\ell+}^{\ell S} \tag{2.39}$$

If $g(\underline{r},\underline{\Omega})$ is forced to be orthogonal to the local surface basis function space, $S^{h\,\ell S}$, a relationship between the two flux vectors, $\underline{\phi}_{\ell+}^{\ell S}$ and $\underline{\phi}_{\ell}$, is found:

$$\begin{aligned} 0 &= \langle \underline{\psi}_{\ell S}, g(\underline{r},\underline{\Omega}) \rangle_{+\ell} \\ &= \langle \underline{\psi}_{\ell S}, \underline{\psi}_{\ell}^{T}\,\underline{\phi}_{\ell} \rangle_{+\ell} - \langle \underline{\psi}_{\ell S}, \underline{\psi}_{\ell S}^{T}\,\underline{\phi}_{\ell+}^{\ell S} \rangle_{+\ell} \end{aligned} \tag{2.40}$$

or

$$\langle \underline{\psi}_{\ell S}, \underline{\psi}_{\ell S}^{T} \rangle_{+\ell}\,\underline{\phi}_{\ell+}^{\ell S} = \langle \underline{\psi}_{\ell S}, \underline{\psi}_{\ell}^{T} \rangle_{+\ell}\,\underline{\phi}_{\ell} \tag{2.41}$$

which can be expressed as

$$\underline{\underline{T}}_{\ell S,\ell S}\,\underline{\phi}_{\ell+}^{\ell S} = \underline{\underline{T}}_{\ell S,\ell}\,\underline{\phi}_{\ell} \tag{2.42}$$

Solving for $\underline{\phi}_{\ell+}^{\ell S}$,

$$\underline{\phi}_{\ell+}^{\ell S} = \underline{\underline{T}}_{\ell S,\ell S}^{-1}\,\underline{\underline{T}}_{\ell S,\ell}\,\underline{\phi}_{\ell} \tag{2.43}$$

We now have an expression for the local outgoing flux in terms of the internal flux. The next step is to express the global outgoing flux in terms of the local internal flux. Recall the expansion of the outgoing flux in the global surface basis functions (Eq. (2.10)):

$$\phi_{\ell+}(\underline{r},\underline{\Omega}) \simeq \underline{\Psi}_S^T \, \underline{\phi}_{\ell+}^S \tag{2.44}$$

The residual

$$g(\underline{r},\underline{\Omega}) = \underline{\Psi}_S^T \, \underline{\phi}_{\ell+}^S - \underline{\psi}_{\ell S}^T \, \underline{\phi}_{\ell+}^{\ell S}$$

is forced to be orthogonal to the space of global surface basis functions:

$$\langle \underline{\Psi}_S, \underline{\Psi}_S^T \rangle_{+\ell} \, \underline{\phi}_{\ell+}^S = \langle \underline{\Psi}_S, \underline{\psi}_{\ell S}^T \rangle_{+\ell} \, \underline{\phi}_{\ell+}^{\ell S} \tag{2.45}$$

$$\underline{\underline{T}}_{SS} \, \underline{\phi}_{\ell+}^S = \underline{\underline{T}}_{S,\ell S} \, \underline{\phi}_{\ell+}^{\ell S} \tag{2.46}$$

$$\underline{\phi}_{\ell+}^S = \underline{\underline{T}}_{SS}^{-1} \, \underline{\underline{T}}_{S,\ell S} \, \underline{\phi}_{\ell+}^{\ell S} \tag{2.47}$$

By combining Eqs. (2.47) and (2.43) the global surface boundary flux can be expressed in terms of the local volume flux,

$$\underline{\phi}_{\ell+}^S = \underline{\underline{T}}_{SS}^{-1} \, \underline{\underline{T}}_{S,\ell S} \, \underline{\underline{T}}_{\ell S,\ell S}^{-1} \, \underline{\underline{T}}_{\ell S,\ell} \, \underline{\phi}_{\ell} \tag{2.48}$$

or, defining $\underline{\underline{R}}_{S\ell}$,

$$\underline{\phi}^{S}_{\ell+} = \underline{\underline{R}}_{S\ell}\ \underline{\phi}_{\ell} \tag{2.49}$$

Combining Eq. (2.49) with Eq. (2.35)

$$\underline{\phi}^{S}_{\ell+} = \underline{\underline{R}}_{S\ell}\ (\underline{\underline{A}}^{-1}_{\ell}\underline{\underline{T}}_{\ell,S}\ \underline{\phi}^{S}_{in,\ell} + \underline{\underline{A}}^{-1}_{\ell}\underline{\underline{T}}_{\ell,V}\ \underline{S}^{V}_{\ell}) \tag{2.51}$$

results in the response matrix equation given previously (Eq. (2.14)) that gives the outgoing flux for region ℓ:

$$\underline{\phi}^{S}_{\ell+} = \underline{\underline{R}}^{\ell}_{S\leftarrow S}\underline{\phi}^{S}_{in,\ell} + \underline{\underline{R}}^{\ell}_{S\leftarrow V}\underline{S}^{V}_{\ell} \tag{2.52}$$

It should be noted that the response matrices implicitly include the effect of local variations within the region that can be resolved by the fine local mesh. This information has been orthogonally projected onto the global mesh.

The response matrix equation that determines the global volumetric flux (Eq. (2.15)) is found by projecting the volumetric flux from the local mesh onto the global mesh. This is accomplished by requiring the residual of two approximations of the volumetric flux, Eq. (2.25) and

$$\phi(\underline{r},\underline{\Omega}) \simeq \underline{\Psi}^{T}\ \underline{\phi}^{V}_{\ell} \tag{2.53}$$

respectively, to be orthogonal to the global basis functions. Here the residual is defined

$$g(\underline{r},\underline{\Omega}) = \underline{\Psi}^T \underline{\phi}_\ell^V - \underline{\psi}_\ell^T \underline{\phi}_\ell \tag{2.54}$$

The requirement of orthogonality implies

$$(\underline{\Psi},\underline{\Psi}^T)_\ell \underline{\phi}_\ell^V = (\underline{\Psi},\underline{\psi}_\ell^T)_\ell \underline{\phi}_\ell \tag{2.55}$$

$$\underline{\underline{T}}_{VV}^{\ell} \underline{\phi}_\ell^V = \underline{\underline{T}}_{V,\ell} \underline{\phi}_\ell \tag{2.56}$$

$$\underline{\phi}_\ell^V = \underline{\underline{T}}_{VV}^{\ell\ -1} \underline{\underline{T}}_{V,\ell} \underline{\phi}_\ell \tag{2.57}$$

$$\underline{\phi}_\ell^V = \underline{\underline{M}}_{V\ell} \underline{\phi}_\ell \tag{2.58}$$

Again, substituting Eq. (2.35) into the above expression

$$\underline{\phi}_\ell^V = \underline{\underline{M}}_{V\ell} (\underline{\underline{A}}_\ell^{-1} \underline{\underline{T}}_{\ell,S} \underline{\phi}_{in,\ell}^S + \underline{\underline{A}}_\ell^{-1} \underline{\underline{T}}_{\ell,V} \underline{S}^V) \tag{2.59}$$

results in the ancillary response matrix equation:

$$\underline{\phi}_\ell^V = \underline{\underline{M}}_{V\leftarrow S}^{\ell} \underline{\phi}_{in,\ell}^S + \underline{\underline{M}}_{V\leftarrow V}^{\ell} \underline{S}_\ell^V \tag{2.60}$$

The response matrix equations derived above (Eqs. (2.52) and (2.60)) provide a means of finding, for a single region ℓ, the outgoing surface flux and the volumet-

ric flux, both described on a coarse global mesh, from the coarse-mesh flux entering the region and the coarse-mesh source within the region. The response matrices, as well as the flux and source vectors, for a particular region have non-zero elements only in those locations corresponding to mesh points contained in the region or on its boundary. By combining the response matrices calculated for the remaining L-1 regions, a global system of response matrix equations can be found. If some regions are not unique, the matrices for these regions need be calculated only once and then used repeatedly for all identical regions. Global flux and source vectors are defined as the sum of all region vectors:

$$\underline{\phi}_{+}^{S} = \sum_{\ell=1}^{L} \underline{\phi}_{\ell+}^{S}$$

$$\underline{\phi}_{in}^{S} = \sum_{\ell=1}^{L} \underline{\phi}_{in,\ell}^{S} \qquad (2.61)$$

$$\underline{S}^{V} = \sum_{\ell=1}^{L} \underline{S}_{\ell}^{V}$$

$$\underline{\phi}^{V} = \sum_{\ell=1}^{L} \underline{\phi}_{\ell}^{V}$$

Global matrices are block diagonal matrices found by summing individual region matrices:

$$\underline{\underline{R}}_{S\leftarrow S} = \sum_{\ell=1}^{L} \underline{\underline{R}}^{\ell}_{S\leftarrow S}$$

$$\underline{\underline{R}}_{S\leftarrow V} = \sum_{\ell=1}^{L} \underline{\underline{R}}^{\ell}_{S\leftarrow V} \qquad (2.62)$$

$$\underline{\underline{M}}_{V\leftarrow S} = \sum_{\ell=1}^{L} \underline{\underline{M}}^{\ell}_{V\leftarrow S}$$

$$\underline{\underline{M}}_{V\leftarrow V} = \sum_{\ell=1}^{L} \underline{\underline{M}}^{\ell}_{V\leftarrow V}$$

The global matrix equations are written

$$\underline{\varphi}^{S}_{+} = \underline{\underline{R}}_{S\leftarrow S}\underline{\varphi}^{S}_{in} + \underline{\underline{R}}_{S\leftarrow V}\underline{S}^{V} \qquad (2.63)$$

$$\underline{\varphi}^{V} = \underline{\underline{M}}_{V\leftarrow S}\underline{\varphi}^{S}_{in} + \underline{\underline{M}}_{V\leftarrow V}\underline{S}^{V} \qquad (2.64)$$

The individual matrices that make up the global matrix $\underline{\underline{R}}_{S\leftarrow S}$ represent the transfer of neutrons from the incoming surface to the outgoing surface of each region. These neutrons may undergo absorption or scattering during the transfer but may not experience a fission event (or a downscatter for multi-group problems). The fission process is treated explicitly, removed from the response matrices, as will be seen below. The response matrices, therefore, are independ-

ent of the multiplication constant--a significant result. The other response matrices, $\underline{\underline{R}}_{S\leftarrow V}$, $\underline{\underline{M}}_{V\leftarrow S}$, and $\underline{\underline{M}}_{V\leftarrow V}$, represent the volume-to-surface, surface-to-volume, and volume-to-volume transfer of neutrons, respectively.

The response matrices would be subject to a different interpretation if, in Eq. (2.20), the inner product containing the scattering operator, K_{scat}, were considered a known quantity, moved to the right side of the equation, and combined with the source term. In that case, the scattering source and fission source would be treated similarly; the response matrices would represent the transfer of **uncollided** neutrons from surface-to-surface, volume-to-surface, etc.

Iterative Solution Scheme

The global response matrix equations can be formulated into an iteration solution scheme by considering the continuity of angular flux across the interfaces separating neighboring regions. A neighbor of region m is a region that shares a boundary or part of a boundary with region m. To be more specific, part of the neighbor's outgoing boundary and part of the incoming boundary of region m must intersect. The set of neighbors of region m is defined

$$\{n\}_m = \{n_i: \quad i=1, 2, \ldots, L \mid n_i \neq m, \quad \Gamma^+_{n_i} \cap \Gamma^-_m \neq \emptyset\}$$

If one defines the following angular fluxes,

$$\phi_{in,m}(\underline{r},\underline{\Omega}) = \phi(\underline{r},\underline{\Omega}) \qquad \text{for } (\underline{r},\underline{\Omega})\epsilon\Gamma_m^-$$

and

$$\phi_{n_i^+}(\underline{r},\underline{\Omega}) = \phi(\underline{r},\underline{\Omega}) \qquad \text{for } (\underline{r},\underline{\Omega})\epsilon\Gamma_{n_i}^+$$

continuity of angular flux requires

$$\phi_{in,m}(\underline{r},\underline{\Omega}) = \phi_{\{n\}_m^+}(\underline{r},\underline{\Omega}) \qquad \text{for } (\underline{r},\underline{\Omega})\epsilon\Gamma_m^-$$

The angular flux can be expanded in terms of the global surface basis function (Eq. (2.44)) to obtain

$$\underline{\Psi}_S^T \underline{\phi}_{in,m}^S = \underline{\Psi}_S^T \underline{\phi}_{\{n\}_m^+}^S \qquad \text{for } (\underline{r},\underline{\Omega})\epsilon\Gamma_m^- \qquad (2.66)$$

A relationship between the incoming and outgoing flux vectors is provided once more by the weighted residual technique. Here, require the residual

$$g(\underline{r},\underline{\Omega}) = \underline{\Psi}_S^T \underline{\phi}_{in,m}^S - \underline{\Psi}_S^T \underline{\phi}_{\{n\}_m^+}^S \qquad (2.67)$$

to be orthogonal to the global basis functions:

$$0 = \langle \underline{\Psi}_S, g(\underline{r},\underline{\Omega}) \rangle_{-m} \qquad (2.68)$$

$$\langle \underline{\Psi}_S, \underline{\Psi}_S^T \rangle_{-m} \, \underline{\phi}^S_{in,m} = \langle \underline{\Psi}_S, \underline{\Psi}_S^T \rangle_{-m} \, \underline{\phi}^S_{\{n\}_{m^+}} \tag{2.69}$$

$$\underline{\underline{T}}_{SS} \, \underline{\phi}^S_{in,m} = \underline{\underline{T}}_{SS} \, \underline{\phi}^S_{\{n\}_{m^+}} \tag{2.70}$$

$$\underline{\phi}^S_{in,m} = \underline{\underline{T}}_{SS}^{-1} \underline{\underline{T}}_{SS} \, \underline{\phi}^S_{\{n\}_{m^+}} \tag{2.71}$$

$$\underline{\phi}^S_{in,m} = \underline{\underline{H}} \, \underline{\phi}^S_{\{n\}_{m^+}} = \underline{\underline{I}} \, \underline{\phi}^S_{\{n\}_{m^+}} \tag{2.72}$$

The coupling matrix is thus the identity matrix because the support points for the incoming flux vector and the neighbor's exiting flux vector are identical. The fact that $\underline{\underline{H}}$ is actually the identity matrix leads one to the erroneous conclusion that the interface continuity condition is an essential, not natural, condition. This is not the case, however, because the weak form of the transport equation was solved with a natural, not essential, boundary condition. The incoming angular flux distribution is, in fact, this boundary condition. Furthermore, the **incoming** flux vector for a particular region has components of value zero at locations corresponding to the **outgoing** boundary support points. In practice, however, in order to avoid storage of meaningless zeros, the incoming flux vector is shortened to just the components representing the incoming boundary support points. The outgoing flux vector is shortened likewise. The coupling matrix, then, is simply a renumber-

ing matrix that assigns the elements of the outgoing flux vector to the proper location in the incoming flux vector:

$$\underline{\underline{H}} = \{H_{ij}\} \quad \left(\frac{M_S}{2} \times \frac{M_S}{2} \text{ matrix}\right)$$

$$H_{ij} = \begin{cases} 1 \text{ if } (\underline{r},\underline{\Omega})_i^{S-} = (\underline{r},\underline{\Omega})_j^{S+} \\ 0 \text{ if } (\underline{r},\underline{\Omega})_i^{S-} \neq (\underline{r},\underline{\Omega})_j^{S+} \end{cases} \tag{2.73}$$

where $(\underline{r},\underline{\Omega})_i^{S-}$ is the mesh point associated with Ψ_{S_i} on the incoming boundary and $(\underline{r},\underline{\Omega})_j^{S+}$ is that on the outgoing boundary. This shortening of surface vectors reduces the storage required for the response matrices $\underline{\underline{R}}_{S\leftarrow S}$, $\underline{\underline{R}}_{S\leftarrow V}$, and $\underline{\underline{M}}_{V\leftarrow S}$, as well.

Consider now the angular flux impinging all L regions:

$$\phi(\underline{r},\underline{\Omega}) \simeq \Psi_S^T \, \underline{\phi}_{in}^S \qquad \text{for } (\underline{r},\underline{\Omega}) \in \bigcup_{\ell=1}^{L} \Gamma_\ell^-$$

A relationship relating all the incoming interface fluxes to all the outgoing interface fluxes is written

$$\underline{\phi}_{in}^S = \underline{\underline{H}} \, \underline{\phi}_+^S \tag{2.74}$$

The $\underline{\underline{H}}$ matrix can also provide for reflecting or periodic boundary conditions. In order to differentiate between the $\underline{\underline{H}}$ matrix described above that accounts only for con-

tinuity across interfaces and one that includes boundary conditions, the former is renamed $\underline{\underline{H}}_{cont}$. The latter, then, is the sum of $\underline{\underline{H}}_{cont}$ and a boundary condition matrix, $\underline{\underline{H}}_{BC}$, described below:

$$\underline{\underline{H}} = \underline{\underline{H}}_{cont} + \underline{\underline{H}}_{BC}$$

The description of $\underline{\underline{H}}_{BC}$ in the event of periodic boundary conditions will be deferred until the discussion of implementation to specific geometries in Chapter III as it is difficult to specify periodicity in a general geometry. At present, consider a reflecting boundary condition,

$$\phi^{\mathcal{R}}_{in}(\underline{r},\underline{\Omega}) = \phi^{\mathcal{R}}_{+}(\underline{r},\underline{\Omega}_{out}) \qquad (\underline{r},\underline{\Omega}) \epsilon \Gamma^{-}$$

and

$$\underline{\underline{H}}_{BC} = \underline{\underline{H}}_{refl}$$

where, recall,

$\mathcal{R}$ = spatial domain of global region

$\partial\mathcal{R}$ = boundary of global region

$\underline{n}$ = unit outward normal to $\partial\mathcal{R}$

Γ = $\partial\mathcal{R} x 4\pi$

Γ^+ = outgoing boundary:
all $(\underline{r},\underline{\Omega}) \in \Gamma$ for $\underline{n}\cdot\underline{\Omega}>0$

Γ^- = incoming boundary:
all $(\underline{r},\underline{\Omega}) \in \Gamma$ for $\underline{n}\cdot\underline{\Omega}<0$

$\underline{\phi}_{in}^{\mathcal{R}}$ = flux entering $\partial\mathcal{R}$

$\underline{\phi}_{+}^{\mathcal{R}}$ = flux exiting $\partial\mathcal{R}$

and $\underline{\Omega}_{out}$ is determined from $\underline{\Omega}$. The angle of incoming neutron travel can be broken into two components

$$\underline{\Omega} = \underline{\Omega}^{n} + \underline{\Omega}^{\bar{n}}$$

where $\underline{\Omega}^{n}$ and $\underline{\Omega}^{\bar{n}}$ are the components parallel and perpendicular to $\underline{n}$, respectively:

$$\underline{\Omega}^{n} = (\underline{n}\cdot\underline{\Omega})\ \underline{n} \tag{85.4}$$

The outgoing angle is simply

$$\underline{\Omega}_{out} = -\underline{\Omega}^{n} + \underline{\Omega}^{\bar{n}} \tag{85.5}$$

The matrix $\underline{\underline{H}}_{refl}$ assigns elements of the outgoing flux vector that correspond to flux leaking from $\partial\mathcal{R}$, i.e., $(\underline{r},\underline{\Omega}) \in \Gamma^+$, to the proper locations in the incoming flux vector corresponding to reflected flux entering $\partial\mathcal{R}$ (Γ^-).

Another boundary condition, that of specified incoming flux, can be accounted for by adding to Eq. (2.74) an interface flux vector, $\underline{\phi}_{\Gamma^-}$,

$$\underline{\phi}^S_{in} = \underline{\underline{H}}\, \underline{\phi}^S_+ + \underline{\phi}_{\Gamma^-} \tag{2.75}$$

that has zero valued elements at all locations corresponding to interior interface fluxes and, at locations corresponding to the incoming boundary, the specified values of the flux. The remaining boundary condition--vacuum--is automatically provided for by Eq. (85), that is $\underline{\phi}_{\Gamma^-}$ identically zero.

As mentioned earlier in this chapter, the source term may be due to either an external source or a fission source--or, if the alternative scattering treatment is used, a scattering source--or any combination. Consider the case for which the source is solely an external source. The iteration scheme depicted in Fig. 2-1 is constructed by combining the response matrix equations, Eqs. (2.63) and (2.64), and the coupling equation, Eq. (2.75). The external source ($\underline{S}_{ex}$), an initial guess for the incoming flux distribution ($\underline{\phi}_{guess}$), and appropriate boundary conditions ($\underline{\underline{H}}_{BC}$ and $\underline{\phi}_{\Gamma^-}$) must be specified. The maximum norm,

$$\|\underline{\phi}\|_\infty = \max_i |\phi_i|$$

is used as the convergence test, with ϵ as the convergence criterion.

If the medium contains multiplying material, the $\underline{S}^V$ term of Eqs. (2.63) and (2.64) must include the fission source necessitating an additional iteration loop because the fission source is dependent on the volumetric flux distribution. Consider the case of no external source; the source is entirely due to fission. Recalling Eq. (2.3):

$$S(\underline{r},\underline{\Omega}) = \frac{1}{k} \frac{\nu\Sigma_f(\underline{r})}{4\pi} \int_{4\pi} d\underline{\Omega}' \phi(\underline{r},\underline{\Omega}')$$

Inverting $\underline{\underline{T}}_{\ell,V}$ in Eq. (2.31) results in a equation defining the global volumetric source:

$$\underline{S}_\ell^V = \underline{\underline{T}}_{\ell,V}^{-1} \underline{S}_\ell \tag{2.76}$$

Substitute the definition for $\underline{S}_\ell^V$ and Eq. (2.3) into (2.76):

$$\begin{aligned} \underline{S}_\ell^V &= \underline{\underline{T}}_{\ell,V}^{-1} (S(\underline{r},\underline{\Omega}),\underline{\psi}_\ell)_\ell \\ &= \underline{\underline{T}}_{\ell,V}^{-1} \left(\frac{1}{k} \frac{\nu\Sigma_f(\underline{r})}{4\pi} \int_{4\pi} d\underline{\Omega}' \phi(\underline{r},\underline{\Omega}'),\underline{\psi}_\ell(\underline{r},\underline{\Omega})\right)_\ell \end{aligned} \tag{2.77}$$

The angular flux has been approximated in Eq. (2.53) as

$$\phi(\underline{r},\underline{\Omega}') = \sum_{m=1}^{M} \Psi_m(\underline{r},\underline{\Omega}') \phi_{\ell m}^V$$

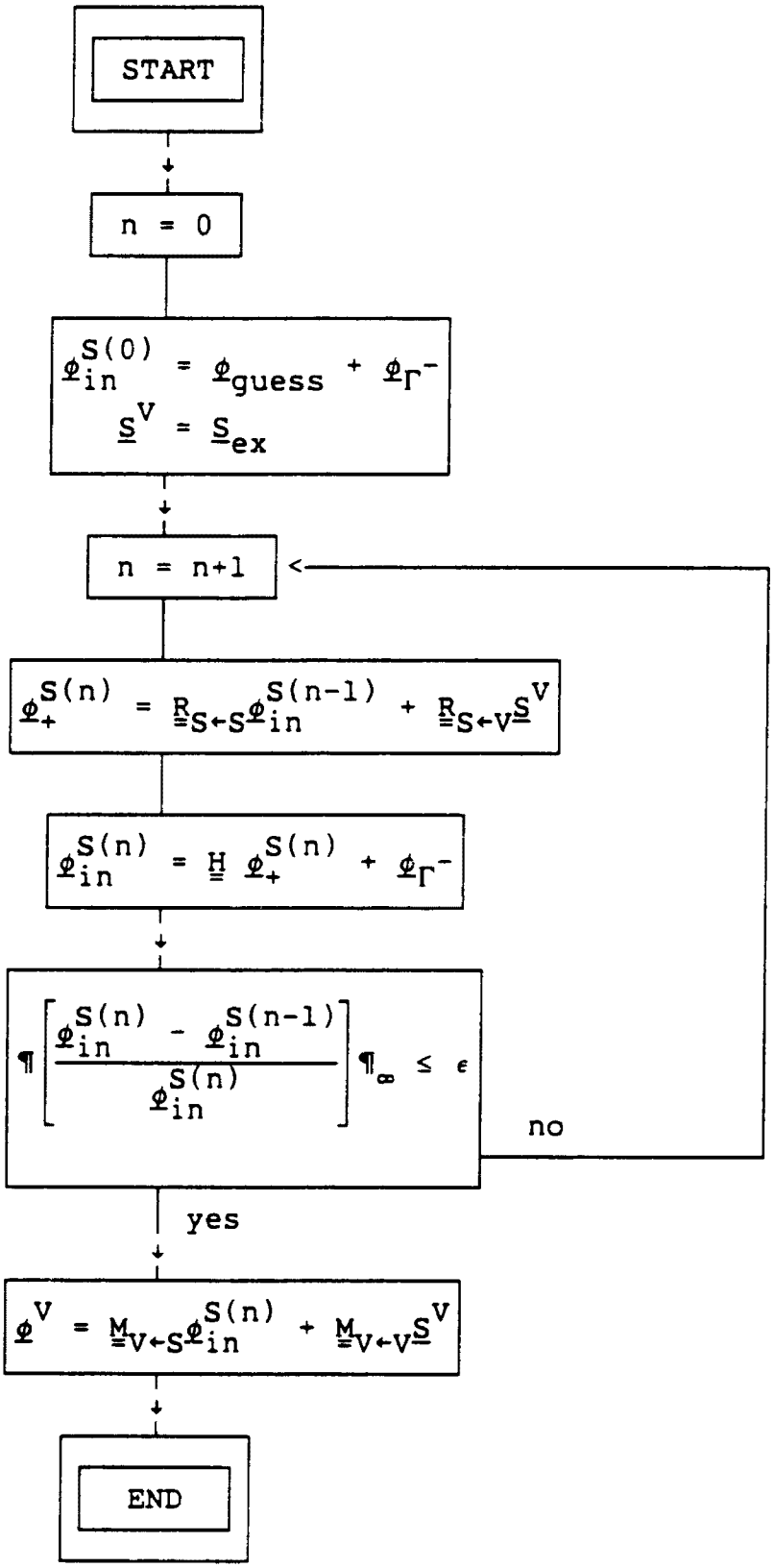


Fig. 2-1. Iterative solution scheme with external source.

Consider the i^{th} component of $\underline{S}_\ell^V$:

$$S_{\ell_i}^V = \frac{1}{k} \sum_{j=1}^{M} (\underline{\underline{T}}_{\ell,V}^{-1})_{ij} \left(\frac{\nu\Sigma_f(\underline{r})}{4\pi} \int_{4\pi} d\underline{\Omega}' \Psi_m(\underline{r},\underline{\Omega}') \sum_{m=1}^{M} \phi_{\ell m}^V, \psi_{\ell j}(\underline{r},\underline{\Omega})\right)_\ell \tag{2.79}$$

Moving the integral over $d\underline{\Omega}'$ within the summation over m and defining

$$\tilde{\Psi}_m(\underline{r}) = \int_{4\pi} d\underline{\Omega}' \Psi_m(\underline{r},\underline{\Omega}') \tag{2.79}$$

and

$$F_{jm}^\ell = \left(\frac{\nu\Sigma_f(\underline{r})}{4\pi} \psi_{\ell j}(\underline{r},\underline{\Omega}), \tilde{\Psi}_m(\underline{r})\right)_\ell \tag{2.80}$$

results in

$$S_{\ell_i}^V = \frac{1}{k} \sum_{j=1}^{M} (\underline{\underline{T}}_{\ell,V}^{-1})_{ij} \sum_{m=1}^{M} F_{jm}^\ell \phi_{\ell m}^V \tag{2.81}$$

or

$$\underline{S}_\ell^V = \frac{1}{k} \underline{\underline{T}}_{\ell,V}^{-1} \underline{\underline{F}}^\ell \underline{\phi}_\ell^V \tag{2.82}$$

or, introducing $\underline{\underline{F}}^\ell$,

$$\underline{S}_\ell^V = \frac{1}{k} \underline{\underline{F}}^\ell \underline{\phi}_\ell^V \tag{2.83}$$

The global fission matrix, like all global matrices, is defined by summing individual region matrices:

$$\underline{F} = \sum_{\ell=1}^{L} \underline{F}^{\ell} \tag{2.84}$$

The incorporation of the additional, outer iteration loop to the iteration scheme of Fig. 2-1 is depicted in Fig. 2-2. The norm ¶$\underline{S}$¶ represents a weighted summation of components of $\underline{S}$, for example, that results in an integration over phase-space of the finite element function approximation. The fission source iteration scheme requires guesses for the multiplication constant (k_{guess}), the incoming interface flux distribution ($\underline{\phi}_{guess}$), and the fission source ($\underline{S}_{guess}$). Convergence criteria for the same three quantities (ϵ_k, ϵ_{in}, and ϵ_{out}, respectively) are used to terminate the iteration loops.

Special Case: Identical Local and Global Mesh

Certain simplifying identifications can be made for many of the intermediate matrices used in the derivation (and, later, calculation) of the response matrices if the local and global mesh are identical. In that case, no distinction between local and global basis functions need be made and the local-global projection *per se* is not performed. By identical, we mean

$$S^{h^V} = \bigcup_{\ell=1}^{L} S^{h^{\ell}}$$

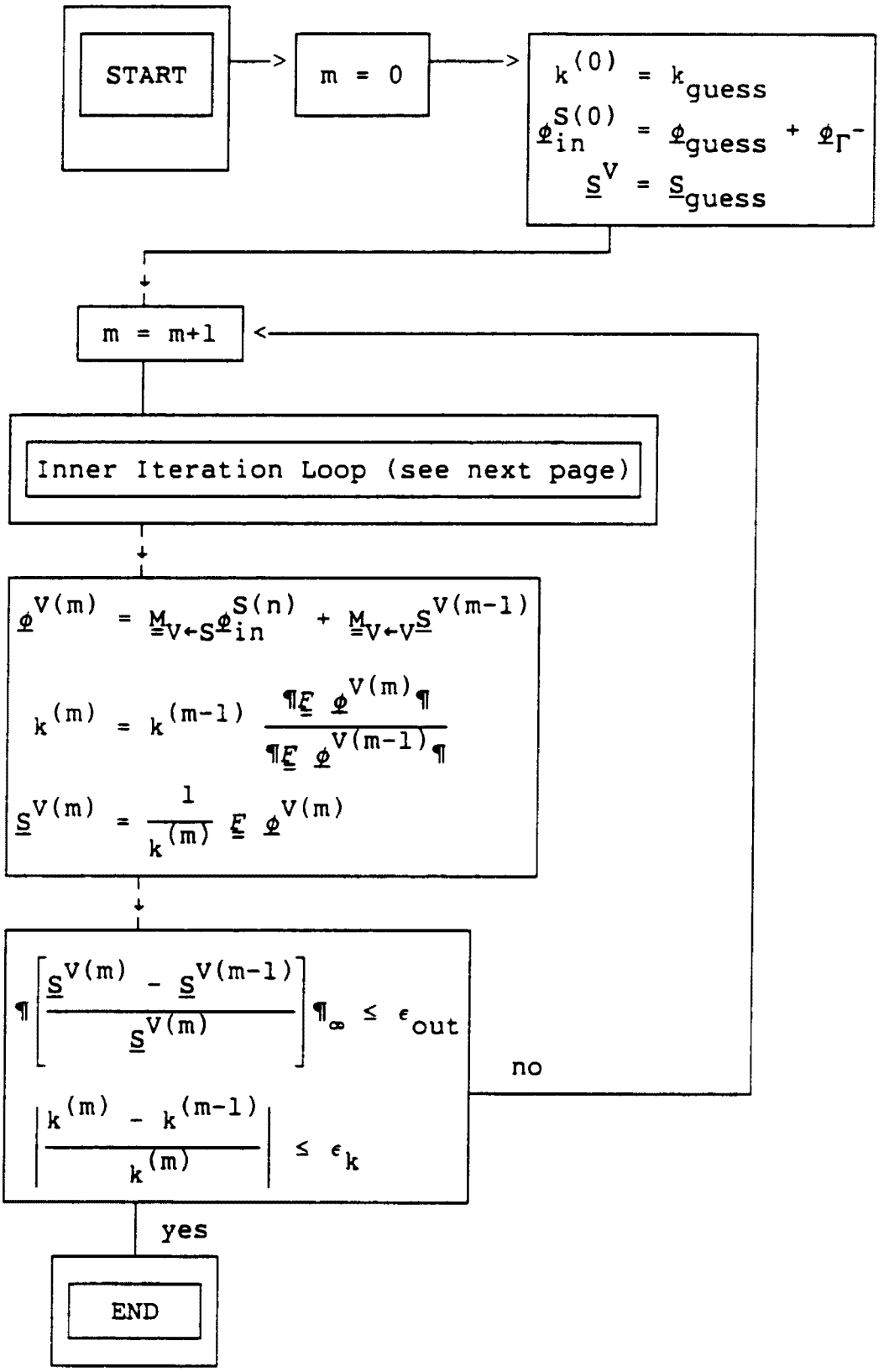


Fig. 2-2. Iterative solution scheme with fission source.

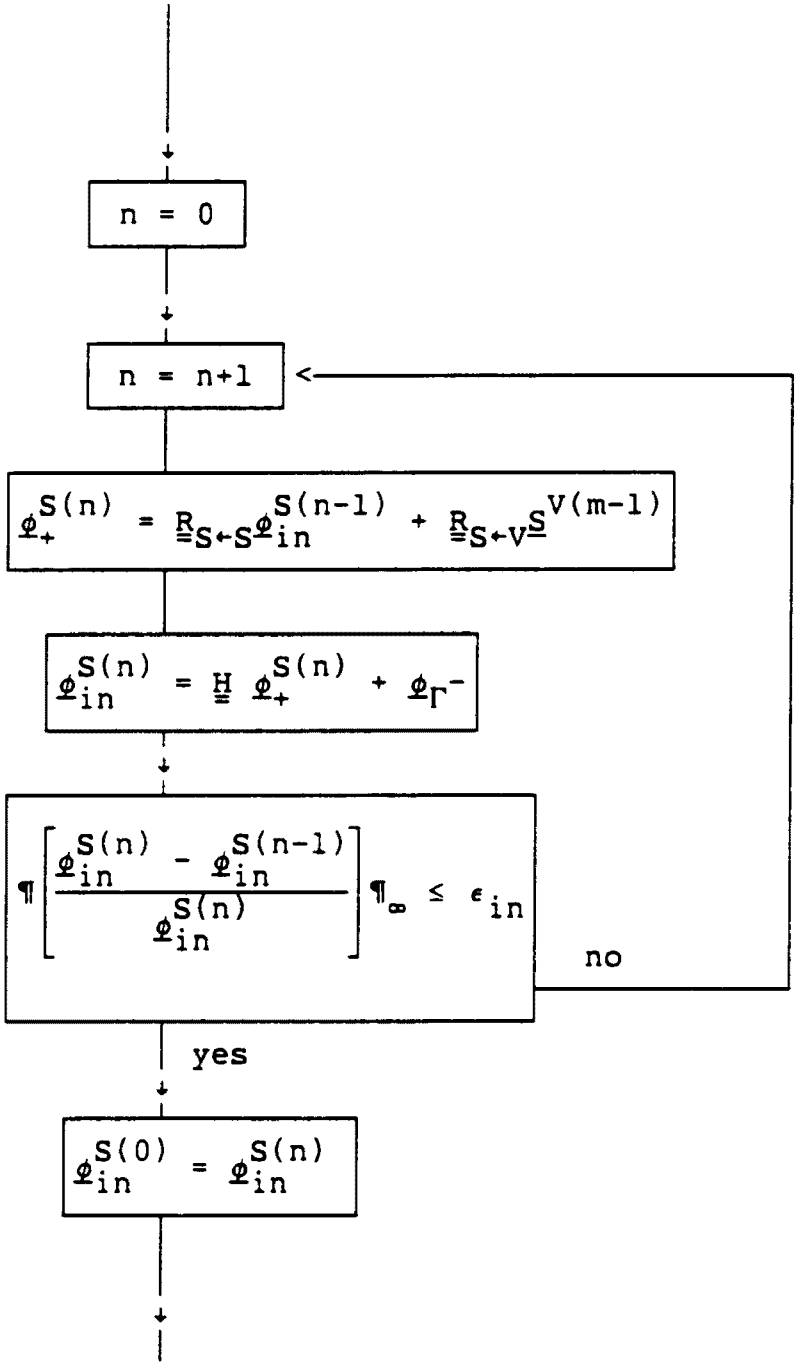


Fig. 2-2.(cont'd) Iterative solution scheme with fission source. (Inner Iteration Loop)

The response matrices of Eq. (2.60) result from the two matrix multiplications in Eq. (2.35) without any further manipulation:

$$\underline{\underline{M}}^{\ell}_{V\leftarrow S} = \underline{\underline{A}}^{-1}_{\ell}\underline{\underline{T}}_{\ell,S} \tag{2.85}$$

$$\underline{\underline{M}}^{\ell}_{V\leftarrow V} = \underline{\underline{A}}^{-1}_{\ell}\underline{\underline{T}}_{\ell,V} \tag{2.86}$$

The response matrices of Eq. (2.52) can be found simply from Eq. (2.35) as well if, in addition to the requirement that the local and global mesh be identical, the global mesh is constructed such that the surface and volumetric mesh are identical on the boundary and the basis functions are Lagrangian polynomials. The outgoing surface and volumetric mesh are said to be identical if

$$\underline{\Psi}_S(\underline{r},\underline{\Omega}) = \underline{\underline{H}}_{S+,V}\,\underline{\Psi}(\underline{r},\underline{\Omega}) \quad \text{for } (\underline{r},\underline{\Omega}) \in \bigcup_{\ell=1}^{L}\Gamma_{\ell}$$

where $\underline{\underline{H}}_{S+,V}$ is a renumbering matrix:

$$\underline{\underline{H}}_{S+,V} = \{H_{ij}\} \quad \left(\frac{M_{S^+}}{2} \text{ x } M \text{ matrix}\right)$$

$$H_{ij} = \begin{cases} 1 \text{ if } (\underline{r},\underline{\Omega})^{V}_{i} = (\underline{r},\underline{\Omega})^{S+}_{j} \\ 0 \text{ if } (\underline{r},\underline{\Omega})^{V}_{i} \neq (\underline{r},\underline{\Omega})^{S+}_{j} \end{cases} \tag{2.87}$$

and $(\underline{r},\underline{\Omega})_j^V$ is the mesh point associated with $\Psi_j(\underline{r},\underline{\Omega})$ and $(\underline{r},\underline{\Omega})_j^{S+}$ is that associated with $\Psi_{S_j}(\underline{r},\underline{\Omega})$ on the outgoing boundary. Defining the outgoing surface flux vector

$$\underline{\phi}_{\ell+}^S = \underline{\underline{H}}_{S+,V}\ \underline{\phi}_\ell \tag{2.88}$$

and the surface-to-surface and volume-to-surface response matrices

$$\underline{\underline{R}}_{S\leftarrow S}^{\ell} = \underline{\underline{H}}_{S+,V}\ \underline{\underline{A}}_\ell^{-1}\ \underline{\underline{T}}_{\ell,S} \tag{2.89}$$

$$\underline{\underline{R}}_{S\leftarrow V}^{\ell} = \underline{\underline{H}}_{S+,V}\ \underline{\underline{A}}_\ell^{-1}\ \underline{\underline{T}}_{\ell,V} \tag{2.90}$$

results in the first response matrix equation (Eq. (2.52)).

Table 2-1 provides a summary of the definitions of all the matrices needed to generate the four final response matrices, the interface coupling matrix, and the fission source matrix. Also presented in the table are comments for each matrix for the special case where the local and global mesh are identical.

Table 2-1. Summary of Response Matrix Definitions

matrix or vector	definition	if local and global are identical
$A_{\ell}{}_{ji}$	$a_{\ell}(\psi_{\ell i}, \psi_{\ell j})$	no effect
$\underline{\Phi}_{in,\ell}$	$\langle \phi_{in,\ell}, \underline{\Psi}_{\ell} \rangle_{-\ell} = \underline{\underline{T}}_{\ell,S} \, \underline{\Phi}^{S}_{in,\ell}$	no effect
$\underline{\underline{T}}_{\ell,S}$	$\langle \underline{\Psi}_{\ell}, \underline{\Psi}_{S}^{T} \rangle_{-\ell}$	no effect
$\underline{S}_{\ell}$	$(S, \underline{\Psi}_{\ell})_{\ell} = \underline{\underline{T}}_{\ell,V} \, \underline{S}^{V}{}_{\ell}$	no effect
$\underline{\underline{T}}_{\ell,V}$	$(\underline{\Psi}_{\ell}, \underline{\Psi}^{T})_{\ell}$	no effect
$\underline{\Phi}^{\ell S}_{\ell +}$	$\underline{\underline{T}}^{-1}_{\ell S,\ell S} \, \underline{\underline{T}}_{\ell S,\ell} \, \underline{\Phi}_{\ell}$	$\underline{\underline{H}}_{S+,V} \, \underline{\Phi}_{\ell}{}^{1}$
$\underline{\underline{T}}_{\ell S,\ell S}$	$\langle \underline{\Psi}_{\ell S}, \underline{\Psi}_{\ell S}^{T} \rangle_{+\ell}$	no effect
$\underline{\underline{T}}_{\ell S,\ell}$	$\langle \underline{\Psi}_{\ell S}, \underline{\Psi}_{\ell}^{T} \rangle_{+\ell}$	no effect
$\underline{\Phi}^{S}_{\ell +}$	$\underline{\underline{R}}_{S\ell} \, \underline{\Phi}_{\ell}$	$\underline{\Phi}^{\ell S}_{\ell +}$
$\underline{\underline{R}}_{S\ell}$	$\underline{\underline{T}}^{-1}_{SS} \, \underline{\underline{T}}_{S,\ell S} \, \underline{\underline{T}}^{-1}_{\ell S,\ell S} \, \underline{\underline{T}}_{\ell S,\ell}$	$\underline{\underline{H}}_{S+,V}{}^{1}$

Table 2-1.(cont'd) Summary of Response Matrix Definitions

matrix or vector	definition	if local and global are identical
$\underline{\underline{T}}_{SS}$	$\langle \underline{\Psi}_S, \underline{\Psi}_S^T \rangle_{+\ell}$	unnecessary
$\underline{\underline{T}}_{S,\ell S}$	$\langle \underline{\Psi}_S, \underline{\psi}_{\ell S}^T \rangle_{+\ell}$	unnecessary
$\underline{\underline{R}}^{\ell}_{S\leftarrow S}$	$\underline{\underline{R}}_{S\ell}\ \underline{\underline{A}}_{\ell}^{-1}\underline{\underline{T}}_{\ell,S}$	$\underline{\underline{H}}_{S+,V}\ \underline{\underline{A}}_{\ell}^{-1}\ \underline{\underline{T}}_{\ell,S}$
$\underline{\underline{R}}^{\ell}_{S\leftarrow V}$	$\underline{\underline{R}}_{S\ell}\ \underline{\underline{A}}_{\ell}^{-1}\underline{\underline{T}}_{\ell,V}$	$\underline{\underline{H}}_{S+,V}\ \underline{\underline{A}}_{\ell}^{-1}\ \underline{\underline{T}}_{\ell,V}$
$\underline{\underline{M}}_{V\ell}$	$\underline{\underline{T}}_{VV}^{-1}\ \underline{\underline{T}}_{V,\ell}$	unnecessary
$\underline{\underline{T}}^{\ell}_{VV}$	$(\underline{\Psi}, \underline{\Psi}^T)_{\ell}$	unnecessary
$\underline{\underline{T}}_{V,\ell}$	$(\underline{\Psi}, \underline{\psi}_{\ell}^T)_{\ell}$	unnecessary
$\underline{\underline{M}}^{\ell}_{V\leftarrow S}$	$\underline{\underline{M}}_{V\ell}\ \underline{\underline{A}}_{\ell}^{-1}\underline{\underline{T}}_{\ell,S}$	$\underline{\underline{A}}_{\ell}^{-1}\underline{\underline{T}}_{\ell,S}$
$\underline{\underline{M}}^{\ell}_{V\leftarrow V}$	$\underline{\underline{M}}_{V\ell}\ \underline{\underline{A}}_{\ell}^{-1}\underline{\underline{T}}_{\ell,V}$	$\underline{\underline{A}}_{\ell}^{-1}\underline{\underline{T}}_{\ell,V}$
$\underline{\underline{S}}^{V_2}_{\ell}$	$\frac{1}{k}\ \underline{\underline{F}}^{\ell}\ \underline{\phi}_{\ell}^{V}$	$\underline{\underline{A}}_{\ell}^{-1}\underline{\underline{T}}_{\ell,V}$
$\underline{\underline{F}}^{\ell}$	$\underline{\underline{T}}_{\ell,V}^{-1}\ \underline{\underline{F}}^{\ell}$	$\underline{\underline{A}}_{\ell}^{-1}\underline{\underline{T}}_{\ell,V}$

Table 2-1.(cont'd) Summary of Response Matrix Definitions

matrix or vector	definition	if local and global are identical
$\underline{\underline{F}}^{\ell}$	$(\frac{\nu\Sigma_f(\underline{r})}{4\pi}\,\underline{\psi}_{\ell},\tilde{\underline{\Psi}}(\underline{r}))_{\ell}$	$\underline{\underline{A}}_{\ell}^{-1}\underline{\underline{T}}_{\ell,V}$
$\tilde{\underline{\Psi}}(\underline{r})$	$\int_{4\pi} d\underline{\Omega}'\,\underline{\Psi}(\underline{r},\underline{\Omega}')$	$\underline{\underline{A}}_{\ell}^{-1}\underline{\underline{T}}_{\ell,V}$

notes:

[1] $\underline{\underline{H}}$ matrices are simple renumbering matrices

[2] fission source

CHAPTER III

APPLICATION TO SPECIFIC GEOMETRIES

In this chapter the details of the application of the method to one- and two-dimensional geometries are discussed. Specific topics covered include the form of the transport equation, the configuration of the multi-regional spatial domain, the specification of the angular domain, and the definition of terms of the matrix equations. First, the one-dimensional application is presented, then the two-dimensional case.

Application of the Method in One Dimension

The one-dimensional slab geometry, to which the method is applied in this section, is constructed so that the spatial variation of all physical quantities is specified in terms of one variable, x. The physical space extends from $-\infty$ to $+\infty$ in the other two dimensions, y and z. Because there is no variation in these directions, only a single angle is needed to specify the direction of neutron travel. This angle, θ, is defined as the angle of neutron travel measured from the x-axis, as shown in Fig. 3-1.

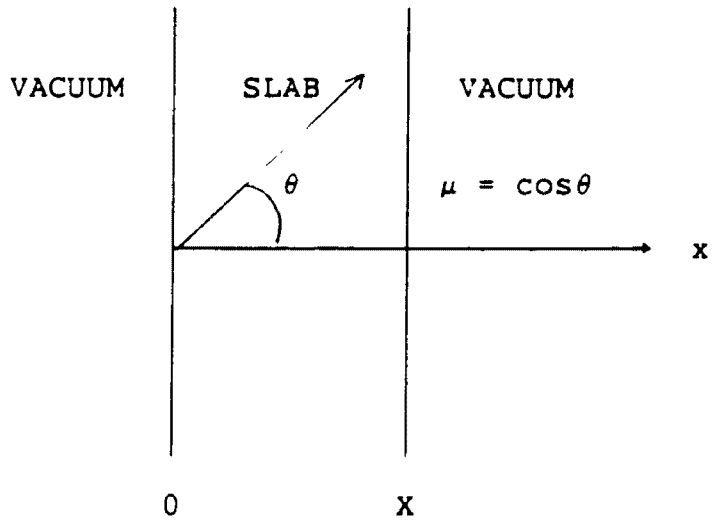


Fig. 3-1. Physical domain of one-dimensional slab geometry.

The one-dimensional, first-order neutron transport equation is written

$$\mu\frac{\partial\phi}{\partial x} + \Sigma_t(x)\phi(x,\mu) = \int_{-1}^{1} d\mu\Sigma_s(x,|\mu'-\mu|)\phi(x,\mu') + S(x,\mu) \tag{3.1}$$

where $\mu = \cos\theta$. The two phase-space dimensions necessary to specify the angular flux distribution in one dimension are x and μ.

The spatial domain, $\mathcal{R}$, which extends from x=0 to x=X is divided into L distinct, contiguous regions,

$$\mathcal{R}_\ell, \ \ell = 1, 2, \ldots, L$$

such that x is in $\mathcal{R}_\ell$ if

$$x_{\ell-} \leq x \leq x_{\ell+}$$

The interval Δx_ℓ is defined

$$\Delta x_\ell = x_{\ell+} - x_{\ell-} \tag{3.2}$$

Furthermore, the regions are numbered from left to right, as shown in Fig. 3-2, such that

$$
\begin{aligned}
x_{1-} &= 0 \\
x_{2-} &= x_{1+} = x_{1-} + \Delta x_1 \\
x_{3-} &= x_{2+} = x_{2-} + \Delta x_2 \\
&\vdots \\
x_{L-} &= x_{(L-1)+} = x_{(L-1)-} + \Delta x_{L-1} \\
x_{L+} &= X = x_{L-} + \Delta x_L
\end{aligned}
\tag{3.3}
$$

Here, we will consider isotropic scattering,

$$\Sigma_s(x,|\mu' \to \mu|) = \frac{\Sigma_s(x)}{2}$$

but the extension to general anisotropic scattering is straight-forward as demonstrated by Martin [Mar77]. The transport equation for region ℓ

$$\mu \frac{\partial \phi}{\partial x} + \Sigma_t(x)\phi(x,\mu) = \frac{1}{2}\int_{-1}^{1} d\mu' \Sigma_s(x)\phi(x,\mu') + S(x,\mu) \tag{3.4}$$

subject to a specified incoming boundary condition

$$\phi(x,\mu) = \phi_{in,\ell}(x,\mu) \quad \begin{cases} x = x_{\ell-}, & \mu>0, \\ x = x_{\ell+}, & \mu<0 \end{cases} \tag{3.5}$$

serves as the starting point for the response matrix development. The boundary condition applies to the analytical domain for region ℓ shown in Fig. 3-3. As before, the

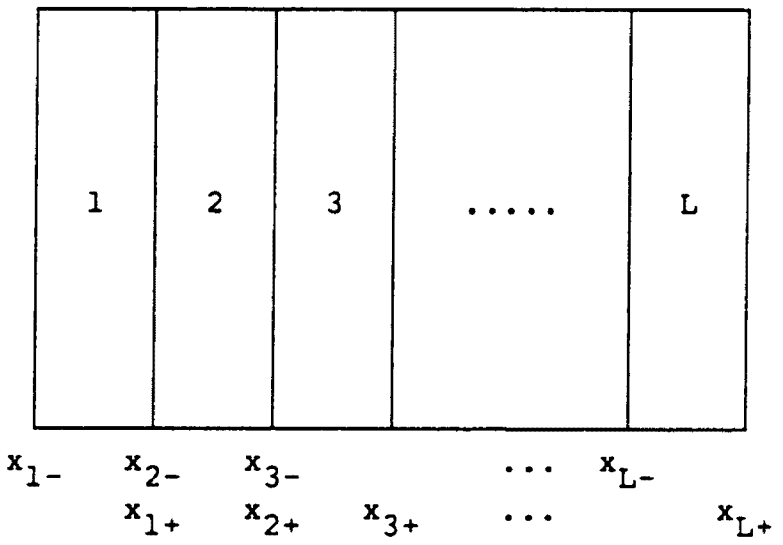


Fig. 3-2. Division of one-dimensional spatial domain.

source, $S(x,\mu)$, may represent any combination of external or fission source. The latter, in one dimension, is written

$$S(x,\mu) = \frac{1}{k} \frac{\nu\Sigma_f(x)}{2} \int_{-1}^{1} d\mu' \phi(x,\mu') \tag{3.6}$$

The derivation of the finite element matrix representation of the transport equation proceeds analogously to the general derivation in the Chapter II. The weak form is written

$$\begin{aligned} -(\phi, \mu\frac{\partial\psi_\ell}{\partial x})_\ell + \langle\phi,\psi_\ell\rangle_{+\ell} \\ - (\frac{\Sigma_s(x)}{2} \int_{-1}^{1} d\mu' \phi(x,\mu'), \psi_\ell(x,\mu))_\ell \\ + (\Sigma_t\phi,\psi_\ell)_\ell = \langle\phi_{in,\ell},\psi_\ell\rangle_{-\ell} + (S,\psi_\ell)_\ell \end{aligned} \tag{3.7}$$

where the local volume and surface inner products are defined

$$(\phi,\psi)_\ell = \int_{\Delta x_\ell} dx \int_{-1}^{1} d\mu \phi(x,\mu)\psi(x,\mu)$$

$$\langle\phi,\psi\rangle_{+\ell} = \int_{0}^{1} d\mu\mu\phi(x_{\ell+},\mu)\psi(x_{\ell+},\mu) - \int_{-1}^{0} d\mu\mu\phi(x_{\ell-},\mu)\psi(x_{\ell-},\mu)$$

$$\langle\phi,\psi\rangle_{-\ell} = \int_{0}^{1} d\mu\mu\phi(x_{\ell-},\mu)\psi(x_{\ell-},\mu) - \int_{-1}^{0} d\mu\mu\phi(x_{\ell+},\mu)\psi(x_{\ell+},\mu)$$

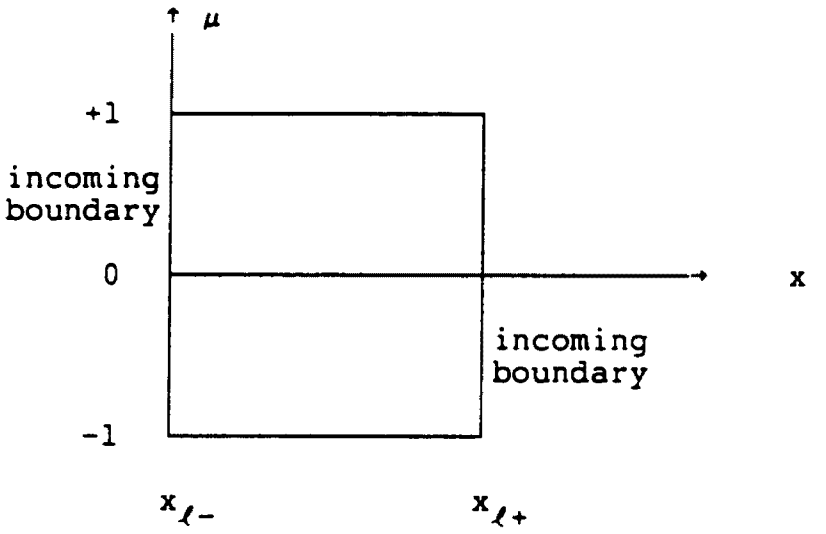


Fig. 3-3. Analytical domain for one-dimensional region ℓ.

Approximating the angular flux by an N-term expansion

$$\phi(x,\mu) \simeq \sum_{i=1}^{N} \psi_{\ell i}(x,\mu)\phi_{\ell i} = \underline{\psi}_{\ell}^{T}\underline{\phi}_{\ell} \tag{3.8}$$

where N is the dimension of the basis function space $S^{h^{\ell}}$ leads to the matrix equation,

$$\underline{\underline{A}}_{\ell}\underline{\phi}_{\ell} = \underline{\phi}_{in,\ell} + \underline{S}_{\ell} \tag{3.9}$$

which is made up of the terms defined in Eq. (2.26) and Eqs. (2.27) and repeated below with some minor modification.

$$A_{\ell_{ji}} = a_{\ell}(\psi_{\ell i},\psi_{\ell j})$$

$$= -(\psi_{\ell i},\mu\frac{\partial\psi_{\ell j}}{\partial x})_{\ell} + \langle\psi_{\ell i},\psi_{\ell j}\rangle_{+\ell}$$

$$- (K_{scat}\psi_{\ell i},\psi_{\ell j})_{\ell} + (\Sigma_{t}\psi_{\ell i},\psi_{\ell j})_{\ell}$$

$$\underline{\underline{A}}_{\ell} = \{A_{\ell_{ji}}\} \quad (N \times N \text{ matrix})$$

$$\phi_{in,\ell_{j}} = \langle\phi_{in,\ell},\psi_{\ell j}\rangle_{-\ell}$$

$$\underline{\phi}_{in,\ell} = \text{col}(\phi_{in,\ell_1}, \phi_{in,\ell_2}, \ldots, \phi_{in,\ell_N})$$

$$S_{\ell_j} = (S, \psi_{\ell j})_\ell$$

$$\underline{S}_\ell = \text{col}(S_{\ell_1}, S_{\ell_2}, \ldots, S_{\ell_N})$$

where the scattering operator, K_{scat} is defined

$$K_{scat}\phi(x,\mu) = \frac{1}{2}\int_{-1}^{1} d\mu' \Sigma_s(x)\phi(x,\mu') \qquad (3.10)$$

The response matrices are generated using the definitions of Table 2-1 with the one-dimensional interpretation of surface and volume inner products and making the proper substitutions for the $\underline{\Omega}\cdot\underline{\nabla}$ dot product $(\mu\frac{\partial}{\partial x})$, the position vector $\underline{r}$ (x), and the direction vector $\underline{\Omega}$ (μ).

Application of the Method in Two Dimensions

The application to a two-dimensional Cartesian geometry is significantly more complicated than the application in one dimension. In one dimension, two phase-space dimensions are considered: configuration space, x, and angle, μ. In two dimensions, four phase-space dimensions must be accounted for: two in configuration space, x and y, and two in the angular domain, μ and Φ. This complexity is reflected in the two-dimensional neutron transport equation with isotropic scattering:

$$\mu\frac{\partial\phi}{\partial x} + \sqrt{1-\mu^2}\cos\Phi\frac{\partial\phi}{\partial y} + \Sigma_t(x,y)\phi(x,y;\mu,\Phi) = \frac{\Sigma_s(x,y)}{4\pi}\int_0^{2\pi}d\Phi'\int_{-1}^{1}d\mu'\phi(x,y;\mu',\Phi') + S(x,y;\mu,\Phi) \tag{3.11}$$

where

θ = polar angle of neutron travel with respect to x-axis

Φ = azimuthal angle of neutron travel with respect to y-axis

$\mu = \cos\theta$

Central to the concept of a two-dimensional geometry is the invariance in any physical parameter in the third dimension, in this case the z-direction. Because a neutron cannot distinguish between up and down (+z and -z), there is symmetry in Φ; only half the Φ-domain, i.e., 0 to π, need be considered.

The spatial domain, $\mathcal{R}$, is a rectangular region (Fig. 3-4)

$$\mathcal{R} = \{x,y \mid 0 \le x \le X,\ 0 \le y \le Y\}$$

divided into L sub-regions, as shown in Fig. 3-5,

$$\mathcal{R}_\ell,\ \ell = 1, 2, \ldots, L$$

with L_x sub-regions in the x-direction and L_y in the y-direction so that each region $\mathcal{R}_\ell$ can be uniquely specified by the pair pq:

$$\mathcal{R}_\ell = \mathcal{R}_{pq} = \{x,y \mid x_{p-} \le x \le x_{p+},\ y_{q-} \le y \le y_{q+}\};$$

$$p = 1, 2, \ldots, L_x;$$

$$q = 1, 2, \ldots, L_y$$

In two dimensions, the angular domain, 4π, is defined

$$4\pi = \{\mu,\Phi \mid -1 \le \mu \le +1,\ 0 \le \Phi \le \pi\}$$

The orientation of μ and Φ is shown in Fig. 3-6.

The specification of the outgoing and incoming boundary domains requires some care. For convenience, the convention of numbering the sides of the rectangular region shown in Fig. 3-7 will be used throughout this work. The angular domains distinguishing incoming neutrons from outgoing neutrons are summarized in Table 3-1 for each of the four sides together with the spatial specifications of all sides. The arrangement depicted in Fig. 3-8 provides a graphical illustration of the incoming angular domains.

Formally, we can write the boundary of region ℓ as the union of all four sides,

$$\partial\mathcal{R}_\ell = \partial\mathcal{R}_\ell^1 \cup \partial\mathcal{R}_\ell^2 \cup \partial\mathcal{R}_\ell^3 \cup \partial\mathcal{R}_\ell^4$$

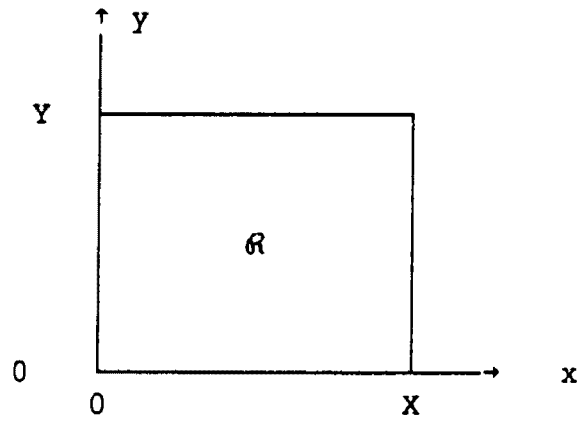


Fig. 3-4. Two-dimensional spatial domain.

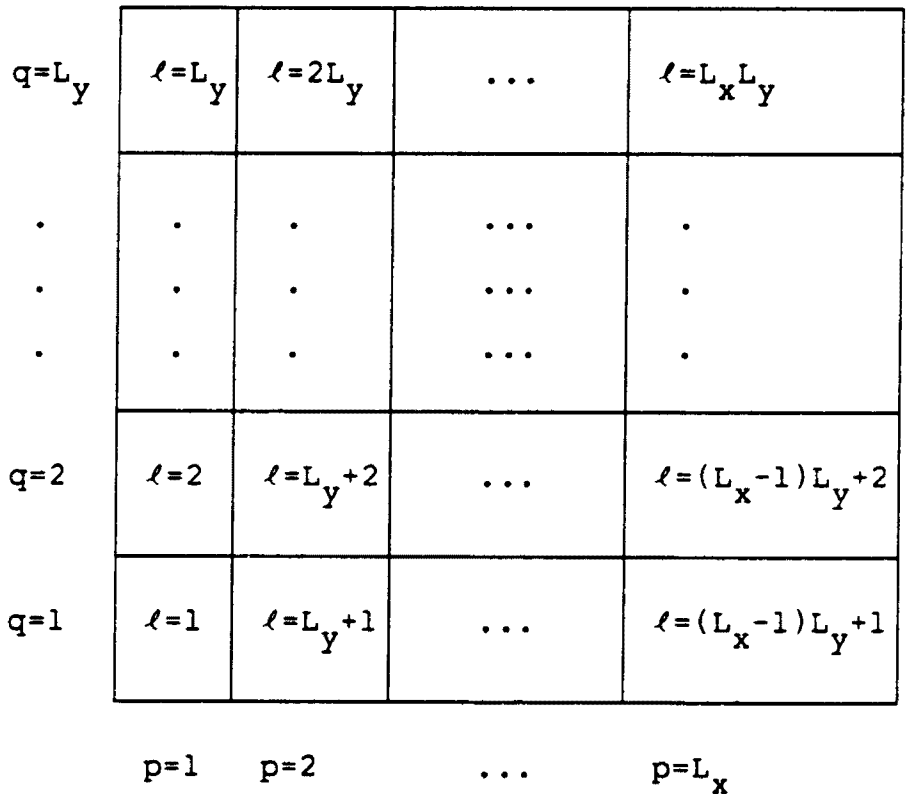


Fig. 3-5. Division of two-dimensional spatial domain.

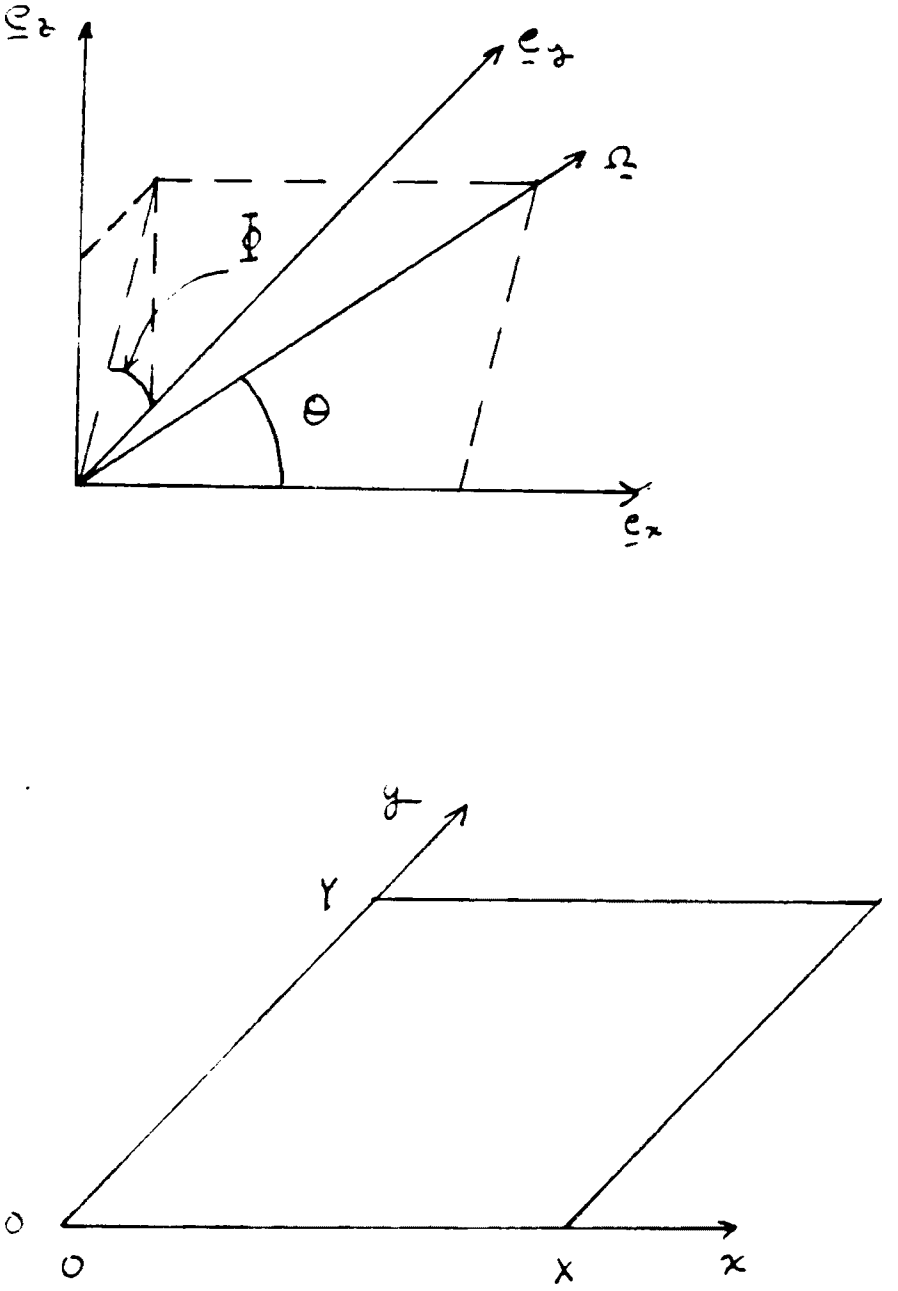


Fig. 3-6. Two-dimensional angular coordinate system.

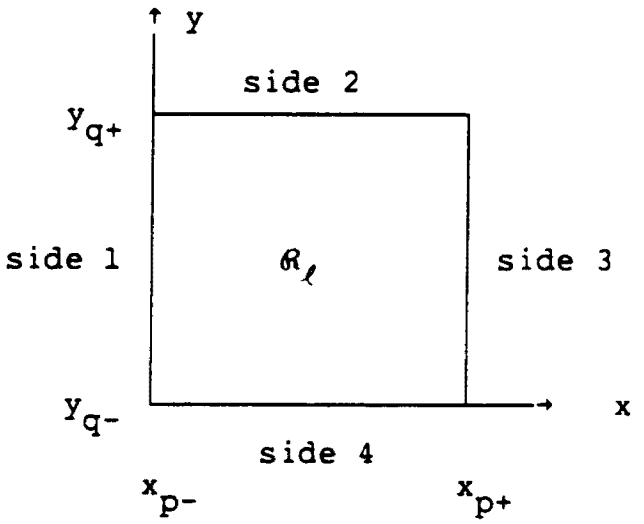


Fig. 3-7. Side numbering convention in two dimensions.

Table 3-1. Boundary Domains in Two Dimensions

side (m)	angular domain		spatial domain ($\mathcal{R}_\ell^m$)	
	incoming (Θ^{m-})	outgoing (Θ^{m+})	x	y
1	$0 < \mu \leq +1$ $0 \leq \Phi \leq \pi$	$-1 \leq \mu < 0$ $0 \leq \Phi \leq \pi$	x_{p-}	y_{q-}, y_{q+}
2	$-1 \leq \mu \leq +1$ $\pi/2 < \Phi \leq \pi$	$-1 \leq \mu \leq +1$ $0 \leq \Phi < \pi/2$	x_{p-}, x_{p+}	y_{q+}
3	$-1 \leq \mu < 0$ $0 \leq \Phi \leq \pi$	$0 < \mu \leq +1$ $0 \leq \Phi \leq \pi$	x_{p+}	y_{q-}, y_{q+}
4	$-1 \leq \mu \leq +1$ $0 \leq \Phi < \pi/2$	$-1 \leq \mu \leq +1$ $\pi/2 < \Phi \leq \pi$	x_{p-}, x_{p+}	y_{q-}

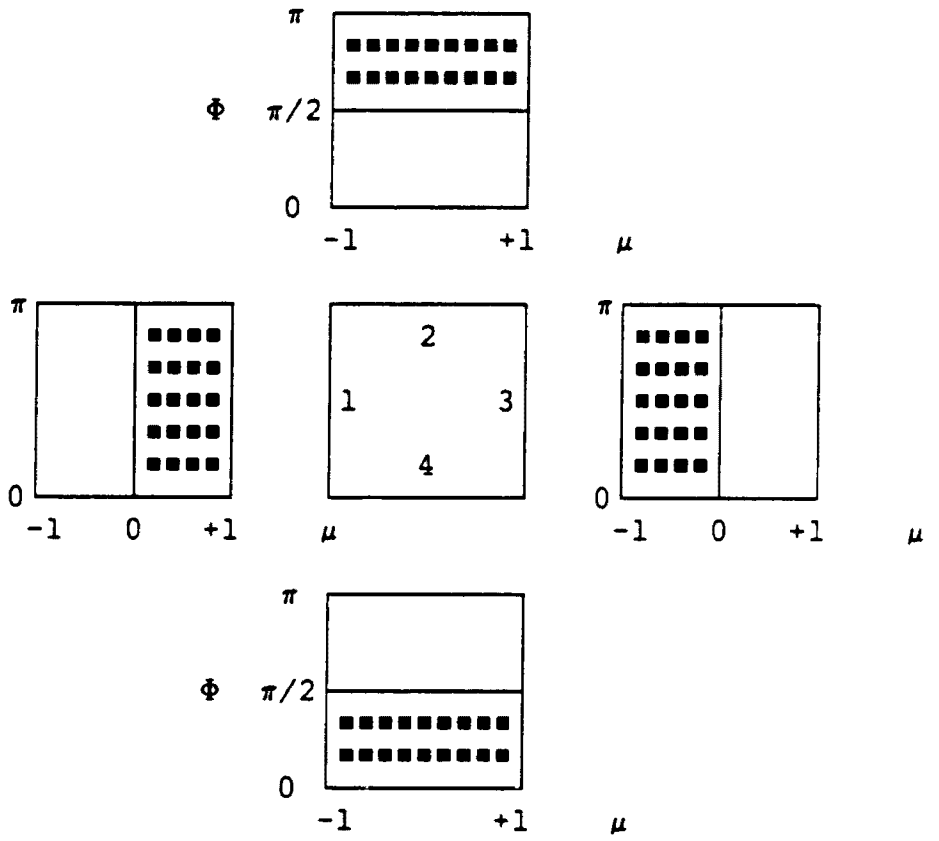


Fig. 3-8. Incoming boundary angular and spatial two-dimensional domain.

where ∂R_ℓ^1, ∂R_ℓ^2, ∂R_ℓ^3, and ∂R_ℓ^4 are defined in Table 3-1. The phase space boundary, Γ_ℓ, is defined as the tensor product of the whole angular domain and the physical boundary:

$$\Gamma_\ell = \partial R_\ell \times 4\pi$$

The outgoing/incoming boundaries are defined as the union of the respective boundaries of the four sides

$$\Gamma_\ell^{\pm} = \Gamma_\ell^{1\pm} \cup \Gamma_\ell^{2\pm} \cup \Gamma_\ell^{3\pm} \cup \Gamma_\ell^{4\pm}$$

that are defined as the tensor product of the spatial and angular components:

$$\Gamma_\ell^{m\pm} = \partial R_\ell^m \Theta^{m\pm}$$

The two-dimensional response matrices are found by first applying the finite element method to the neutron transport equation,

$$\mu\frac{\partial\phi}{\partial x} + \eta\frac{\partial\phi}{\partial y} + \Sigma_t(x,y)\phi(x,y;\mu,\Phi) = \frac{\Sigma_s(x,y)}{4\pi} 2\int_0^{\pi} d\Phi' \int_{-1}^{1} d\mu' \phi(x,y;\mu',\Phi') + S(x,y;\mu,\Phi) \tag{3.12}$$

where

$$\eta = \sqrt{1-\mu^2}\cos\Phi$$

subject to the specified boundary conditions on the incoming flux:

$$\phi(x,y;\mu,\Phi) = \phi_{in,\ell}(x,y;\mu,\Phi) \quad \text{on } \Gamma_\ell^- \tag{3.13}$$

If the source is solely due to fission, it is written

$$S(x,y;\mu,\Phi) = \frac{1}{k}\frac{\nu\Sigma_f(x,y)}{4\pi} 2\int_0^\pi d\Phi' \int_{-1}^{1} d\mu' \phi(x,y;\mu',\Phi') \tag{3.14}$$

The weak form is

$$\begin{aligned} &-(\phi,\mu\frac{\partial\psi_\ell}{\partial x})_\ell - (\phi,\eta\frac{\partial\psi_\ell}{\partial y})_\ell + \langle\phi,\psi_\ell\rangle_{+\ell} \\ &- (\frac{\Sigma_s(x,y)}{4\pi} 2\int_0^\pi d\Phi' \int_{-1}^{1} d\mu' \phi(x,y;\mu',\Phi'),\psi_\ell(x,y;\mu,\Phi))_\ell \\ &\qquad + (\Sigma_t\phi,\psi_\ell)_\ell = \langle\phi_{in,\ell},\psi_\ell\rangle_{-\ell} + (S,\psi_\ell)_\ell \end{aligned} \tag{3.15}$$

where the inner products are defined

$$(\phi,\psi)_\ell = \int_{\Delta x_p} dx \int_{\Delta y_q} dy \; 2\int_0^\pi d\Phi \int_{-1}^{1} d\mu \phi(x,y;\mu,\Phi)\psi(x,y;\mu,\Phi)$$

$$\langle \phi, \psi \rangle_{+\ell} =$$

$$\int_{\Delta y_q} dy \; 2 \int_0^{\pi} d\Phi \int_0^1 d\mu \mu \phi(x=x_{p+}, y; \mu, \Phi) \psi(x=x_{p+}, y; \mu, \Phi)$$

$$- \int_{\Delta y_q} dy \; 2 \int_0^{\pi} d\Phi \int_{-1}^0 d\mu \mu \phi(x=x_{p-}, y; \mu, \Phi) \psi(x=x_{p-}, y; \mu, \Phi)$$

$$+ \int_{\Delta x_p} dx \int_{-1}^1 d\mu \; 2 \int_0^{\pi/2} d\Phi \eta \phi(x, y=y_{q+}; \mu, \Phi) \psi(x, y=y_{q+}; \mu, \Phi)$$

$$- \int_{\Delta x_p} dx \int_{-1}^1 d\mu \; 2 \int_{\pi/2}^{\pi} d\Phi \eta \phi(x, y=y_{q-}; \mu, \Phi) \psi(x, y=y_{q-}; \mu, \Phi)$$

$$\langle \phi, \psi \rangle_{-\ell} =$$

$$- \int_{\Delta y_q} dy \; 2 \int_0^{\pi} d\Phi \int_{-1}^0 d\mu \mu \phi(x=x_{p+}, y; \mu, \Phi) \psi(x=x_{p+}, y; \mu, \Phi)$$

$$+ \int_{\Delta y_q} dy \; 2 \int_0^{\pi} d\Phi \int_0^1 d\mu \mu \phi(x=x_{p-}, y; \mu, \Phi) \psi(x=x_{p-}, y; \mu, \Phi)$$

$$- \int_{\Delta x_p} dx \int_{-1}^1 d\mu \; 2 \int_{\pi/2}^{\pi} d\Phi \eta \phi(x, y=y_{q+}; \mu, \Phi) \psi(x, y=y_{q+}; \mu, \Phi)$$

$$+ \int_{\Delta x_p} dx \int_{-1}^1 d\mu \; 2 \int_0^{\pi/2} d\Phi \eta \phi(x, y=y_{q-}; \mu, \Phi) \psi(x, y=y_{q-}; \mu, \Phi)$$

The angular flux is approximated by an expansion in terms of the basis functions of the N-dimensional function space S^{h^ℓ}

$$\phi(x,y;\mu,\Phi) \simeq \sum_{i=1}^{N} \psi_{\ell i}(x,y;\mu,\Phi)\phi_{\ell i} = \underline{\psi}_\ell^T \underline{\phi}_\ell \qquad (3.16)$$

Substituting this expression into the weak form, Eq. (3.15), results in the finite element matrix equation,

$$\underline{\underline{A}}_\ell \underline{\phi}_\ell = \underline{\phi}_{in,\ell} + \underline{S}_\ell \qquad (3.17)$$

where $\underline{\underline{A}}_\ell$ is made of elements $A_{\ell_{ji}}$ defined

$$A_{\ell_{ji}} = a_\ell(\psi_{\ell i}, \psi_{\ell j})$$

$$= -(\psi_{\ell i}, \mu\frac{\partial\psi_{\ell j}}{\partial x})_\ell - (\psi_{\ell i}, \eta\frac{\partial\psi_{\ell j}}{\partial y})_\ell + \langle\psi_{\ell i}, \psi_{\ell j}\rangle_{+\ell} \qquad (3.18)$$

$$- (K_{scat}\psi_{\ell i}, \psi_{\ell j})_\ell + (\Sigma_t\psi_{\ell i}, \psi_{\ell j})_\ell$$

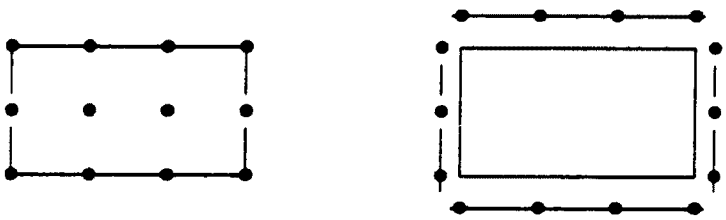
where the scattering operator in two dimensions is written

$$K_{scat}\phi(x,y;\mu,\Phi) = \frac{\Sigma_s(x,y)}{4\pi} \int_0^{2\pi} d\Phi' \int_{-1}^{1} d\mu' \phi(x,y;\mu',\Phi') \qquad (3.19)$$

Response matrices for each rectangular region are calculated using the prescriptions given in Table 2-1. Again, substitutions must be made for the $\underline{\Omega}\cdot\underline{\nabla}$ $(\mu\frac{\partial}{\partial x} + \Phi\frac{\partial}{\partial y})$, $\underline{r}$ (x,y) and $\underline{\Omega}$ (μ, Φ). Special attention must be paid the surface basis functions. Consider the volume and surface mesh depicted in in Fig. 3-9 where each '•' represents the spatial location of a support point for volume or surface basis functions. The outgoing surface basis functions, for example, are defined on the outgoing boundary, Γ_ℓ^+. Recall:

$$\Gamma_\ell^+ = \text{all } (\underline{r},\underline{\Omega}) \in \Gamma_\ell \quad \text{for } \underline{n}_\ell\cdot\underline{\Omega}>0$$

$\underline{n}_\ell$ = unit outward normal to ∂R_ℓ



(a) volume (b) surface

Fig. 3-9. Volume and surface support points in two dimensions.

The difficulty arises at the corners of the regions where the meaning of $\underline{n}_\ell$ is ambiguous. The surface basis functions, therefore, are defined at the corners spatial support points as the limit as the corner is approached along the side in question.

CHAPTER IV

COMPUTER IMPLEMENTATION

The general features of the method as applied to a general multidimensional geometry as well as to specific one- and two-dimensional geometries were discussed in the previous two chapters. In this chapter, some specifics necessary to implement the method on a computer are addressed, such as the specification of the finite element basis functions, how the integrals of the finite element matrix are calculated, generation of the four response matrices, and various types of iterative solution methods. This information is presented first as applied to one dimension, then in two. In Chapter V, the effectiveness of the method and the associated computer codes will be discussed.

Computer Implementation in One Dimension

Finite Element Basis Function Construction

As mentioned earlier, the basis functions used in this work are Lagrangian polynomials. Multi-dimensional polynomials are constructed by a simple tensor product of basis functions of lower dimension. Consider, for example, the one-dimensional basis function, $\hat{\psi}_j(z)$, with associated sup-

port point z_j. Because $\hat{\psi}_j$ is a Lagrangian polynomial it has value 1 at z_j and 0 at all other support points, or

$$\hat{\psi}_j(z_i) = \delta_{ij} \tag{4.1}$$

Linear basis functions vary to the first order with z and are written

$$\hat{\psi}_j(z) = \begin{cases} \psi_j^-(z), & z_{j-1} \le z \le z_j, \\ \psi_j^+(z), & z_j \le z \le z_{j+1}, \\ 0, & z < z_{j-1},\ z_{j+1} < z \end{cases} \tag{4.2}$$

where

$$\psi_j^-(z) = \frac{z - z_{j-1}}{z_j - z_{j-1}} \tag{4.3}$$

and

$$\psi_j^+(z) = \frac{z_{j+1} - z}{z_{j+1} - z_j} \tag{4.4}$$

Substitution of z_i into Eq. (4.2) verifies Eq. (4.1). A linear basis function is presented in Fig. 4-1.

Quadratic Lagrangian polynomials vary quadratically with the determining variable, z. They are defined

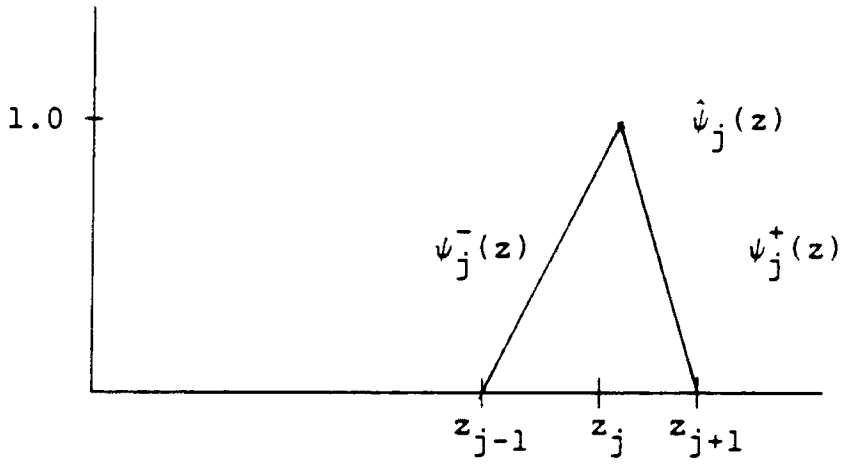


Fig. 4-1. One-dimensional linear basis function.

$$\hat{\psi}_j(z) = \begin{cases} \psi_j^-(z), & z_{j-2} \le z \le z_j, \\ \psi_j^+(z), & z_j \le z \le z_{j+2}, \\ 0, & z < z_{j-2},\ z_{j+2} < z \end{cases} \tag{4.5}$$

for odd j's, and

$$\hat{\psi}_j(z) = \begin{cases} \psi_j^0(z), & z_{j-1} \le z \le z_{j+1}, \\ 0, & z < z_{j-1},\ z_{j+1} < z \end{cases} \tag{4.6}$$

for even j's, where

$$\begin{aligned} \psi_j^-(z) &= \frac{z - z_{j-2}}{z_j - z_{j-2}} \frac{z - z_{j-1}}{z_j - z_{j-1}} \\ \psi_j^+(z) &= \frac{z_{j+2} - z}{z_{j+2} - z_j} \frac{z_{j+1} - z}{z_{j+1} - z_j} \\ \psi_j^0(z) &= \frac{z_{j+1} - z}{z_{j+1} - z_j} \frac{z - z_{j-1}}{z_j - z_{j-1}} \end{aligned} \tag{4.7}$$

and the support points are numbered such that the edges of the z-domain coincide with odd numbered support points. For convenience, the even numbered support points are known as principal support points; odd numbered are interior points; and interior support points are usually placed at the mid-point between adjoining principal support points. Examples of quadratic basis functions are shown in Fig. 4-2.

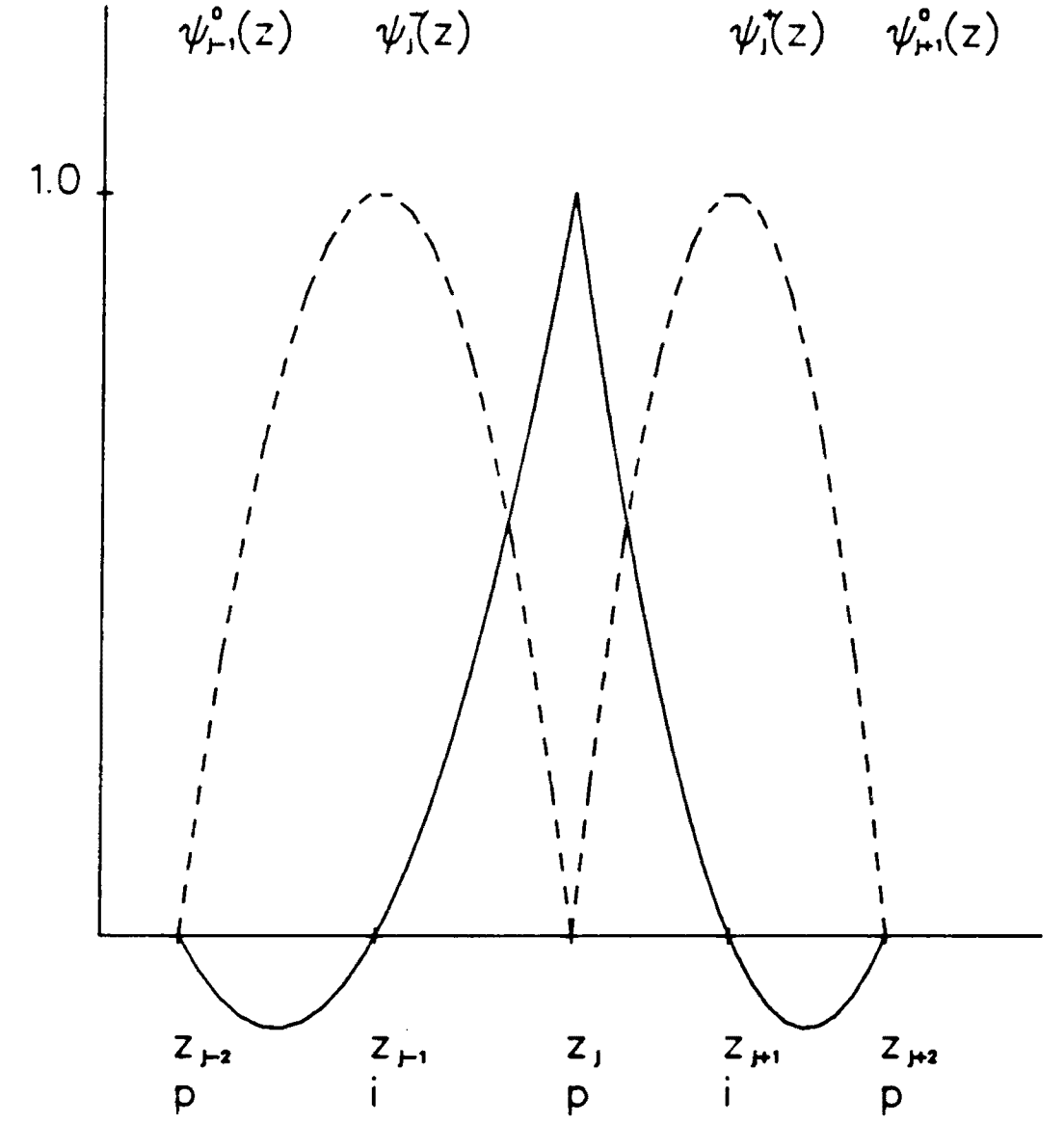


Fig. 4-2. One-dimensional quadratic basis functions.

The function f(z) can be approximated by an expansion, $f_{exp}(z)$, in Lagrangian polynomials,

$$f_{exp}(z) \simeq \sum_{j=1}^{N} f_j \hat{\psi}_j(z)$$

where a particular expansion coefficient is simply the value of the function at that support point

$$f_j = f(z_j)$$

For linear polynomials, the resulting expansion approximation will be piecewise continuous, with the derivative undefined at the support points. For the quadratic case, the approximation will be piecewise quadratic, with derivatives undefined only at the principal support points.

In the one-dimensional implementation of the method, basis functions must be functions of two variables, x and μ. A support point location in the x,μ analytical domain can be uniquely identified in two ways: as a single number, m, or a pair, ij:

$$(x,\mu)_m = (x_i,\mu_j)$$

The basis function for the support point $(x,\mu)_m$ is the product of the one-dimensional basis function of x_i and that of μ_j:

$$\psi_m(x,\mu) = \hat{\psi}_i(x)\hat{\psi}_j(\mu)$$

For linear basis functions, for example,

$$\psi_m(x,\mu) = \begin{cases} \psi_i^-(x)\psi_j^-(\mu), & x_{i-1} \le x \le x_i, \\ & \mu_{j-1} \le \mu \le \mu_j, \\ \psi_i^+(x)\psi_j^-(\mu), & x_i \le x \le x_{i+1}, \\ & \mu_{j-1} \le \mu \le \mu_j, \\ \psi_i^+(x)\psi_j^+(\mu), & x_i \le x \le x_{i+1}, \\ & \mu_j \le \mu \le \mu_{j+1}, \\ \psi_i^-(x)\psi_j^+(\mu), & x_{i-1} \le x \le x_i, \\ & \mu_j \le \mu \le \mu_{j+1}, \\ 0, & x < x_{i-1},\ x_{i+1} < x, \\ & \mu < \mu_{j-1},\ \mu_{j+1} < \mu \end{cases} \tag{4.8}$$

An illustration of this basis function is presented in Fig. 4-3. Two-dimensional quadratic basis functions are shown in Fig. 4-4.

To complete the description of the basis functions a grid of support points in x and μ must be specified. A set of intervals in each direction suffices. In principle, any arrangement of support points in the μ-direction is permitted. In practice, however, at least one support point coincides with μ=0, as shown in Fig. 4-6. Moreover, because in a non-scattering medium there is no coupling between neutrons with μ>0 and those with μ<0, superior results have been observed if a discontinuity in the expansion approximation is allowed at μ=0. This is accomplished by placing two support points at μ=0: one extends toward μ=-1, the other toward μ=+1. Fig. 4-5 shows typical support point arrange-

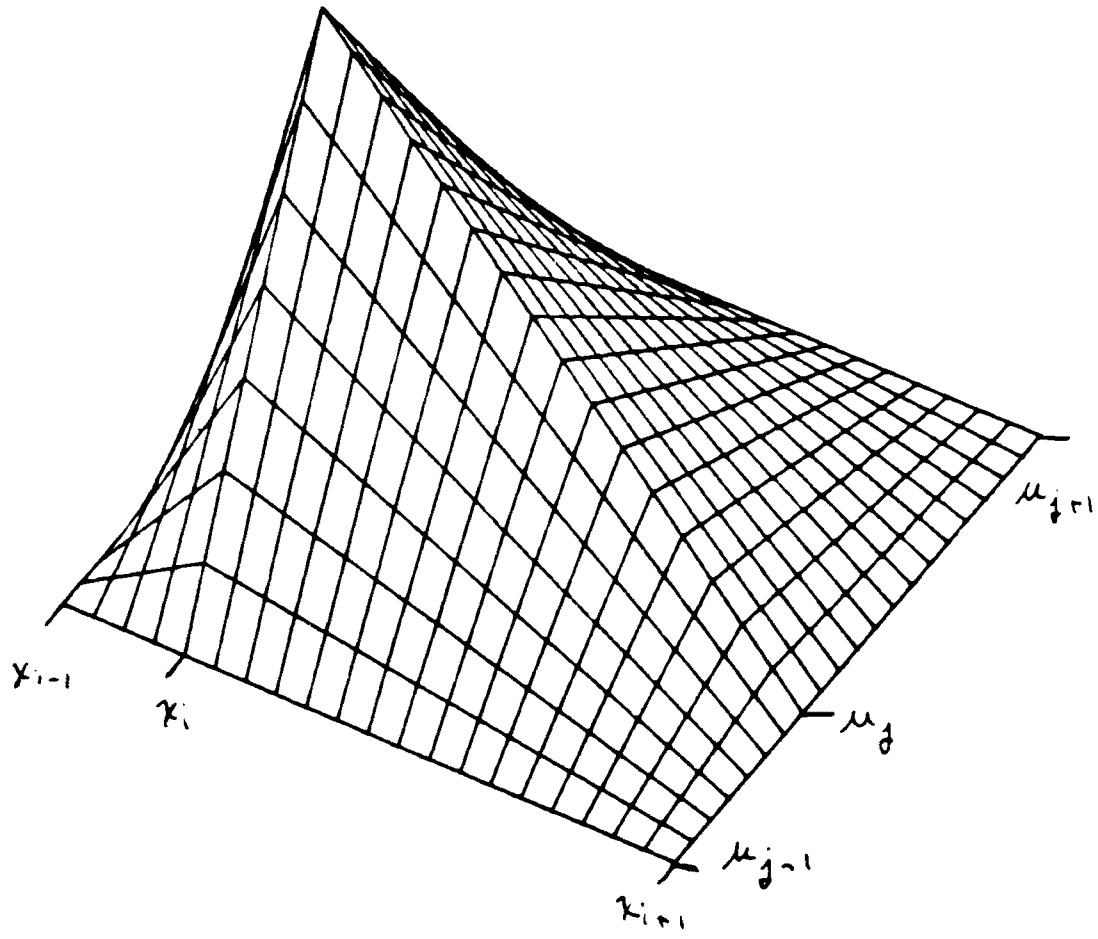


Fig. 4-3. Two-dimensional linear basis function.

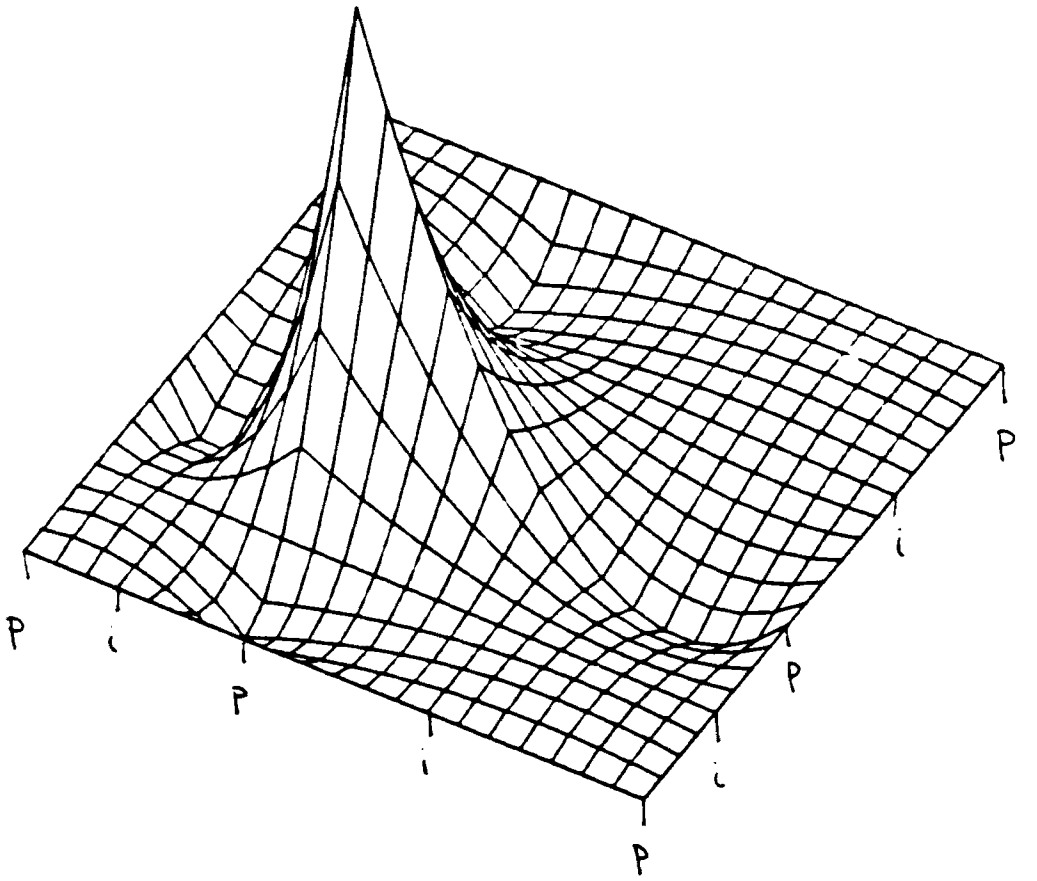


Fig. 4-4. Two-dimensional quadratic basis functions.

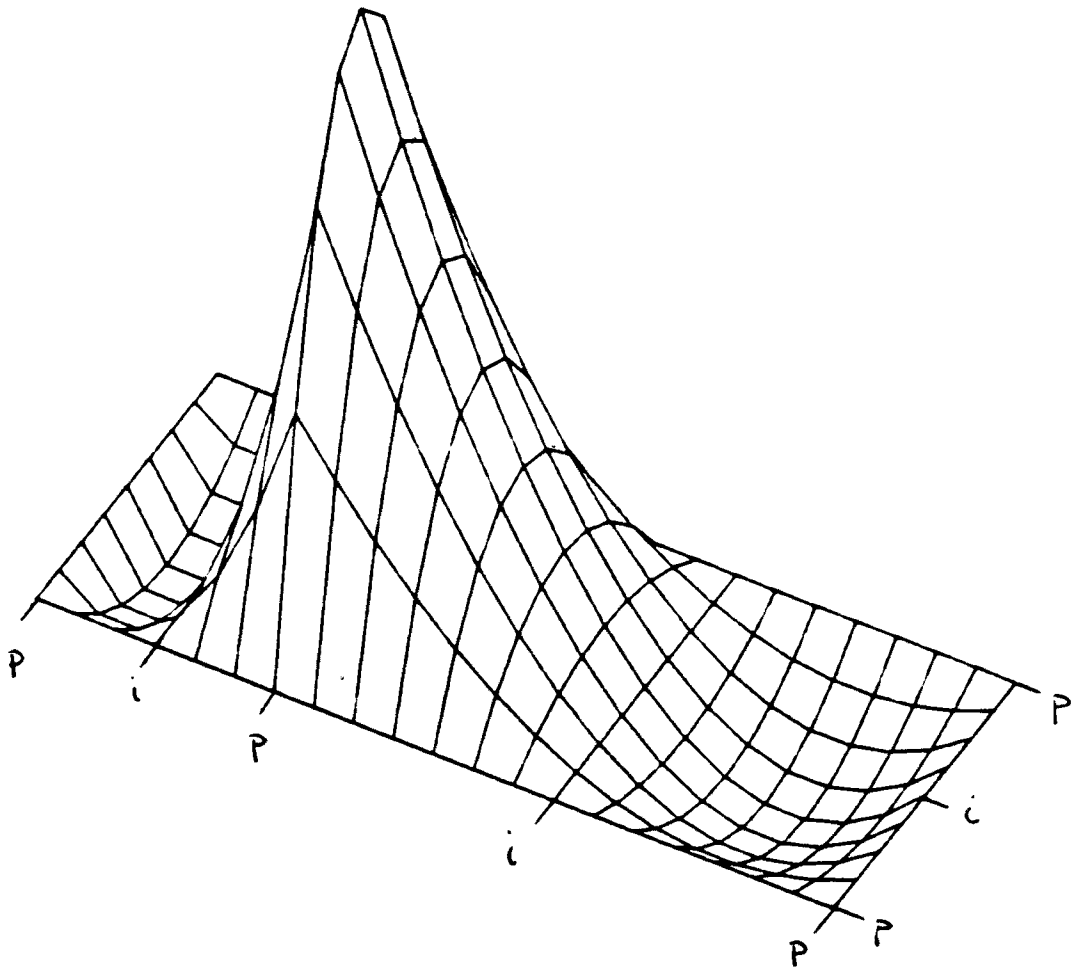


Fig. 4-4.(cont'd.) Two-dimensional quadratic basis functions.

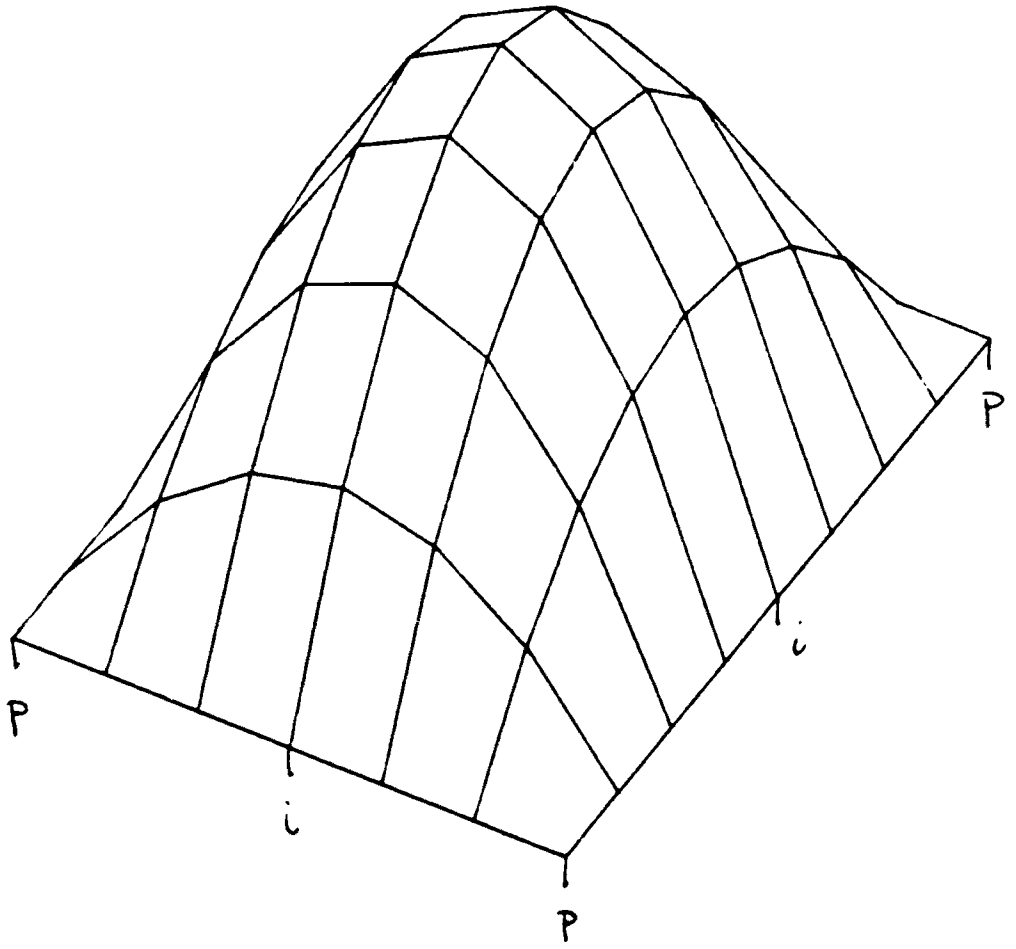


Fig. 4-4.(cont'd.) Two-dimensional quadratic basis functions.

ments of basis functions both with and without a discontinuity at μ=0; a two-dimensional grid is shown in Fig. 4-6.

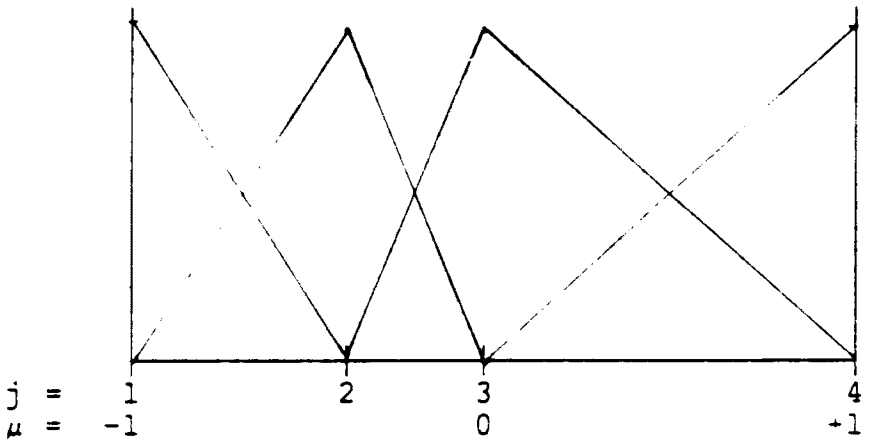
Finite Element Matrix Calculation

Because the two-dimensional basis function $\psi_m(x,\mu)$ is constructed from two one-dimensional parts, $\hat{\psi}_i(x)$ and $\hat{\psi}_j(\mu)$, two-dimensional integrals containing one or more basis functions can be split into two one-dimensional integrals. Consider, for example, the local volume inner product:

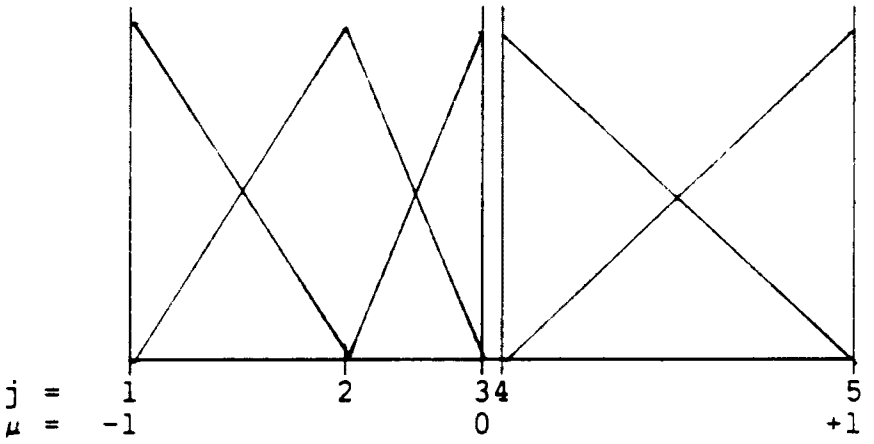
$$
\begin{aligned}
(\psi_{m_1},\psi_{m_2})_\ell &= \int_{\Delta x_\ell} dx \int_{-1}^{1} d\mu \psi_{m_1}(x,\mu)\psi_{m_2}(x,\mu) \\
&= \int_{\Delta x_\ell} dx \hat{\psi}_{i_1}(x)\hat{\psi}_{i_2}(x) \int_{-1}^{1} d\mu \hat{\psi}_{j_1}(\mu)\hat{\psi}_{j_2}(\mu) \qquad (4.9) \\
&= (\hat{\psi}_{i_1},\hat{\psi}_{i_2})_{\Delta x_\ell} (\hat{\psi}_{j_1},\hat{\psi}_{j_2})_\mu
\end{aligned}
$$

The two-dimensional volume inner product is seen to be the tensor product of two one-dimensional inner products.

The individual integrals need not be calculated for each pair of one-dimensional basis functions. Instead, because each basis function is non-zero over only a finite interval, only a few pairs of functions will result in non-zero integrals. In the case of linear basis functions, $(\hat{\psi}_i,\hat{\psi}_j)$ will be non-zero only if i=j or |i-j|=1; only neighboring functions interact. For quadratic basis functions, the one-dimensional inner product will be non-zero in

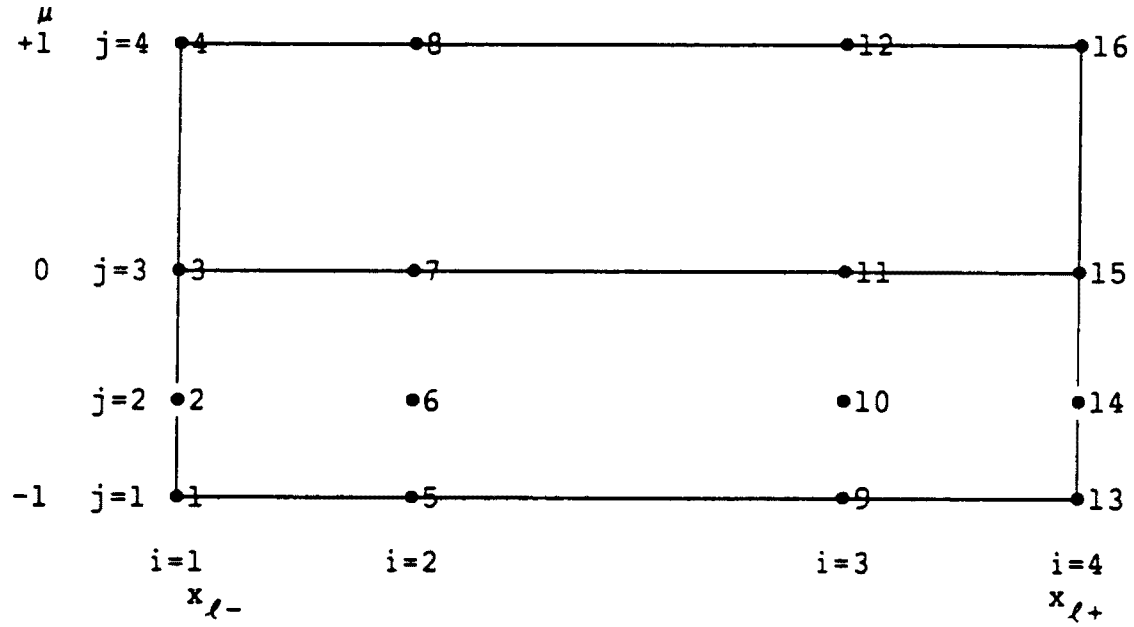


(a) without discontinuity

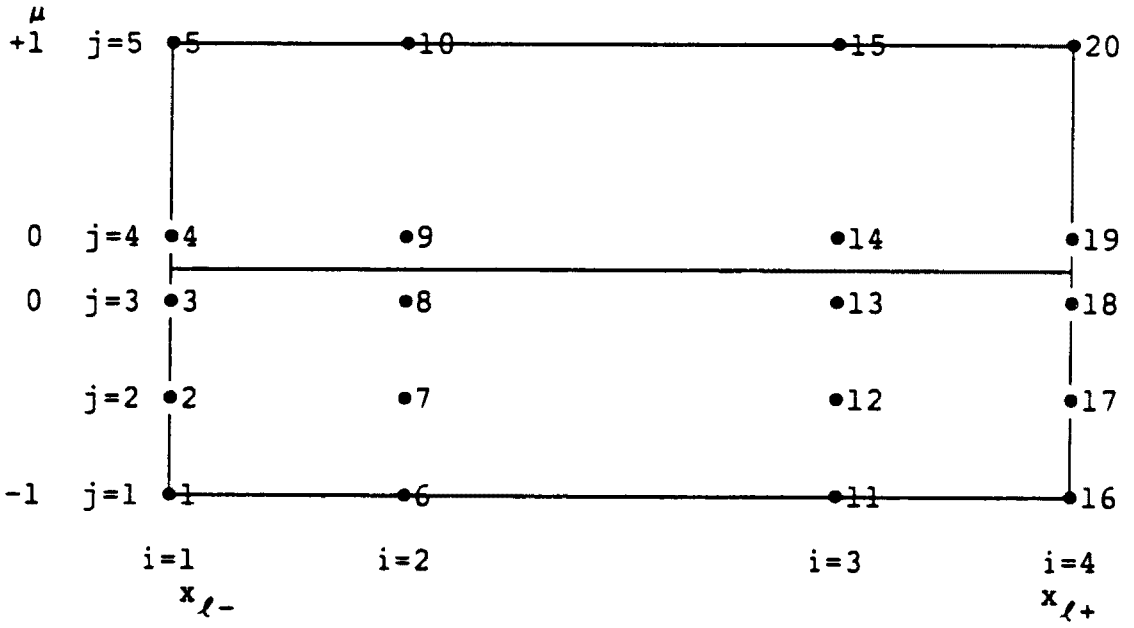


(b) with discontinuity

Fig. 4-5. Arrangement of one-dimensional linear basis functions in angle.



(a) continuous support at μ=0



(b) discontinuous support at μ=0

Fig. 4-6. Volume one-dimensional phase-space support points.

two cases: (1) $|i-j| \leq 2$ and z_i and z_j are both principal support points and (2) $|i-j| \leq 1$ and either z_i or z_j or both are interior support points. That is, support point interaction does not extend past adjacent principal support points. Furthermore, only a few unique integrals need be calculated on a standard interval--then transformed to the specific interval in x or μ--because all the basis functions in a particular direction are of the same order. For example, to calculate the array of integrals $(\hat{\psi}_i, \hat{\psi}_j)_{\Delta x_\ell}$ for linear basis functions, only two fundamental integrals must be calculated:

$$I_{++} = \int_{-1}^{1} d\xi \psi^+(\xi)\psi^+(\xi)$$

and

$$I_{+-} = \int_{-1}^{1} d\xi \psi^+(\xi)\psi^-(\xi)$$

where

$$\psi^+(\xi) = \psi_1^+(\xi)$$

and

$$\psi^-(\xi) = \psi_2^-(\xi)$$

as defined in Eqs. (4.3) and (4.4) where $\xi_1=-1$ and $\xi_2=+1$ as seen in Fig. 4-7. The integrals I_{++} and I_{+-} are calculated using Gauss's formula [Abr70]. The transformation to the inner product on x is

$$(\hat{\psi}_i,\hat{\psi}_j) = \begin{cases} \dfrac{|x_i - x_j|}{2} I_{+-}, & |i-j|=1 \\ \dfrac{x_i - x_{i-1}}{2} I_{++} + \dfrac{x_{i+1} - x_i}{2} I_{++}, & i=j \\ 0, & |i-j|>1 \end{cases} \tag{4.10}$$

The calculation of the four components of each element of the matrix $\underline{\underline{A}}_\ell$ proceeds as described above. For all but one of the components, non-zero integrals will result for all but a few pairs of support points. The exception is the scattering term which, in effect, couples all angular support points. This is a consequence of the physical nature of the scattering process which redistributes neutrons to all angles--with equal probability in the case of isotropic scattering. Recall the scattering term:

$$\begin{aligned} &(K_{scat}\psi_{m_1},\psi_{m_2})_\ell \\ &= \int_{\Delta x_\ell} dx \int_{-1}^{1} d\mu \frac{1}{2} \int_{-1}^{1} d\mu' \Sigma_s(x)\psi_{m_1}(x,\mu')\psi_{m_2}(x,\mu) \qquad (4.11) \\ &= \frac{1}{2}\int_{\Delta x_\ell} dx \Sigma_s(x)\hat{\psi}_{i_1}(x)\hat{\psi}_{i_2}(x) \int_{-1}^{1} d\mu' \hat{\psi}_{j_1}(\mu') \int_{-1}^{1} d\mu \hat{\psi}_{j_2}(\mu) \end{aligned}$$

The angular coupling is a manifestation of the presence of two angular integrals each containing one basis function

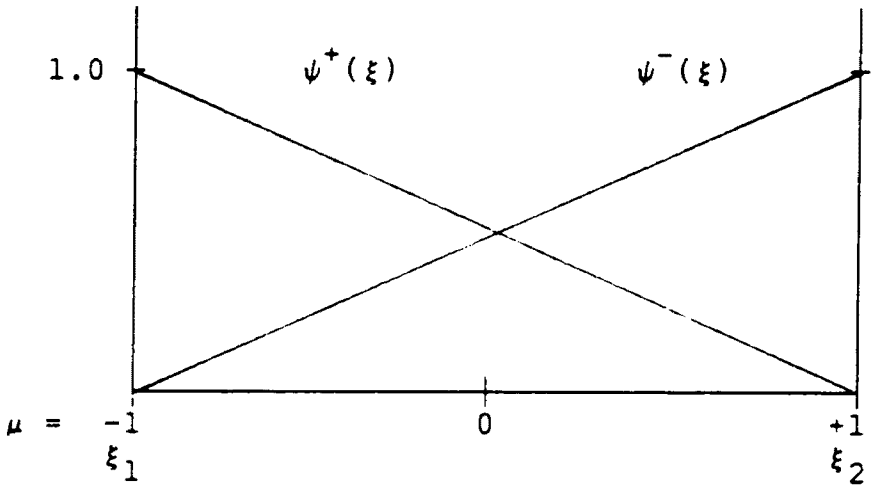


Fig. 4-7. Linear basis functions on the standard interval.

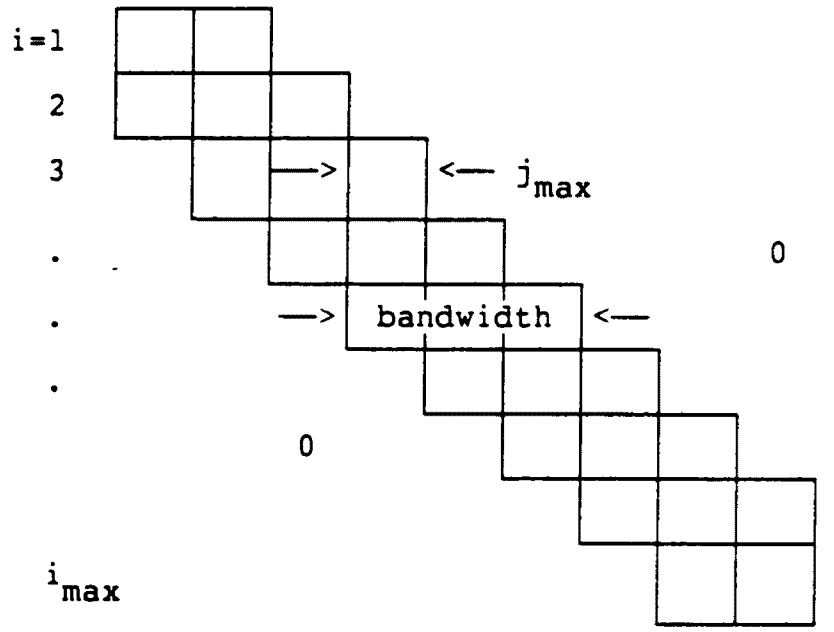
rather than a single integral of a pair of basis functions. Note the inclusion of $\Sigma_s(x)$ in the spatial integration. Other terms in $\underline{\underline{A}}_\ell$ include physical parameters that may vary in space. Although, theoretically, most parameters may take any shape, for the sake of computational simplicity, mesh point positions are chosen so that spatially varying physical parameters are constant between principal mesh points. Hence, discontinuities in the cross section, for instance, may exist at mesh points.

Following the support point numbering scheme of Fig. 4-6 results in a band structure for $\underline{\underline{A}}_\ell$ that depends on the order of basis functions and the number of support points in the μ-direction. Within this band structure is imbedded another if $\Sigma_s=0$. The bandwidth of $\underline{\underline{A}}_\ell$, as defined in Fig. 4-8, is $3j_{max}$ for linear basis functions in x and $5j_{max}$ for quadratic, where j_{max} is the total number of support points in the μ-direction.

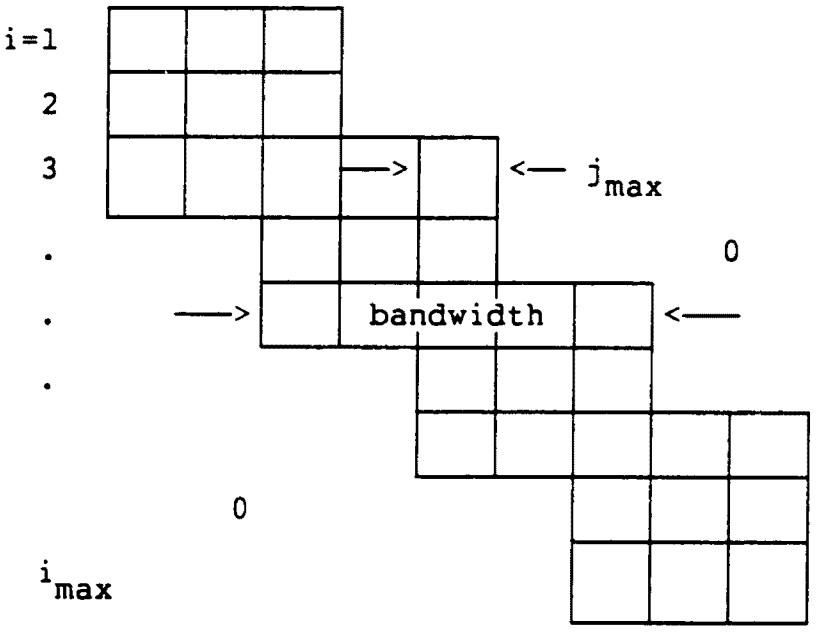
The matrix $\underline{\underline{A}}_\ell$ is inverted by means of LU-decomposition [Dah74]. First $\underline{\underline{A}}_\ell$ is decomposed using Gauss elimination into upper and lower triangular matrices

$$\underline{\underline{A}}_\ell = \underline{\underline{L}}\,\underline{\underline{U}}$$

during which the band structure of $\underline{\underline{A}}_\ell$ reduces the computational effort required and is retained in $\underline{\underline{L}}$ and $\underline{\underline{U}}$. Then, the inverses of $\underline{\underline{L}}$ and $\underline{\underline{U}}$ are found by means of repeated



(a) linear basis functions in x



(b) quadratic basis functions in x

Fig. 4-8. Block structure of $\underline{\underline{A}}_\ell$ in one dimension.

forward substitution and back elimination, respectively. These inverses are multiplied to find $\underline{\underline{A}}_{\ell}^{-1}$:

$$\underline{\underline{A}}_{\ell}^{-1} = \underline{\underline{U}}^{-1}\underline{\underline{L}}^{-1} \tag{4.12}$$

The band structure of $\underline{\underline{A}}_{\ell}$, $\underline{\underline{U}}$, and $\underline{\underline{L}}$ is not, of course, preserved in $\underline{\underline{A}}_{\ell}^{-1}$.

Response Matrix Generation

Before the response matrices themselves are calculated, support points for basis functions other than local volume basis functions, as stated in Chapter II, must be specified. Examples are given in Fig. 4-9 where the following notation is used:

- N - dimension of local volume function space
- i_{max} - number of x-support points in local volume functi-on space
- j_{max} - number of μ-support points in local volume function space
- N_S - dimension of local surface function space
- j_+ - number of local surface support points ($\mu>0$)
- j_- - number of local surface support points ($\mu<0$)

M - dimension of global volume function space

M_ℓ - number of global volume support points in region ℓ

I^ℓ_{max} - number of global volume support points in x-direction in region ℓ

J^ℓ_{max} - number of global volume support points in μ-direction in region ℓ

M_S - dimension of global surface function space

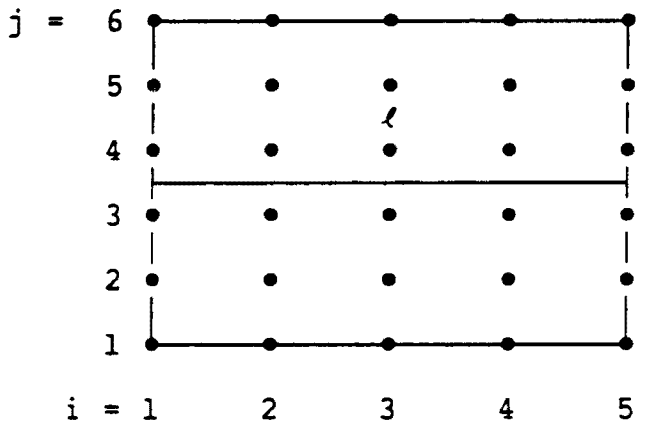
J_+ - number of global surface support points ($\mu>0$) in a single region

J_- - number of global surface support points ($\mu<0$) in a single region

Surface basis functions are defined only at region boundaries and are thus one-dimensional basis functions in μ. In this work, surface basis function support points always coincide with those volume basis function support points that lie on the surface, although, theoretically, any arrangement is permitted.

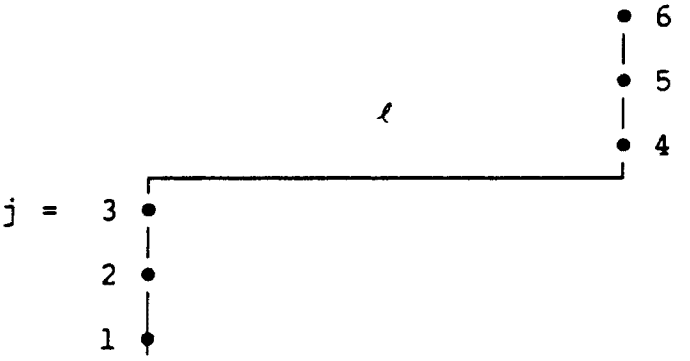
Response matrices are found using the definitions of Table T1. First, the $\underline{\underline{T}}$ matrices are calculated as described below. Then, after multiplying the various matrices in the many combinations described in the table, the response matrices result. Throughout this manipulation the band structure of the matrices, which will also be discussed below, is utilized to reduce computational requirements.

The $\underline{\underline{T}}$ matrices are calculated much in the same manner as were the components of $\underline{\underline{A}}$: the multidimensional inner



$$N = i_{max}\, j_{max} = 30$$

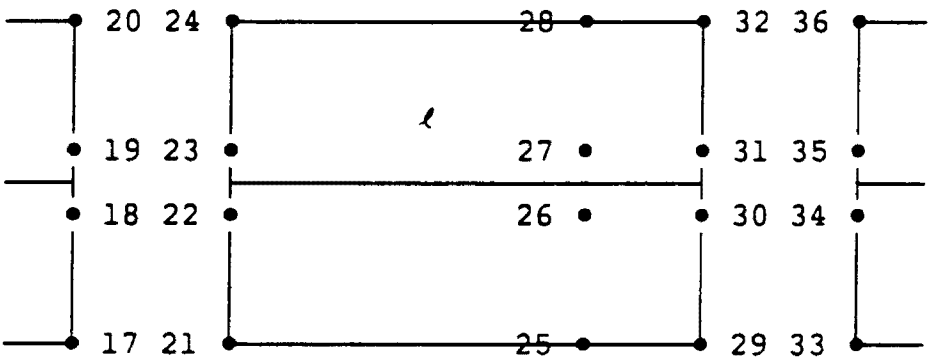
(a) local volume



$$\frac{N_S}{2} = j_+ + j_- = 6$$

(b) local outgoing surface

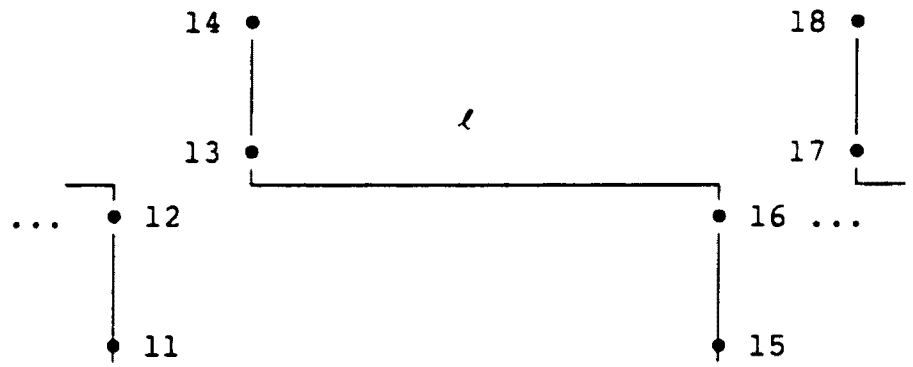
Fig. 4-9. Volume and surface one-dimensional phase-space support points.



$$M = \sum_{m=1}^{L} M_m, \quad M_\ell = I_{max}^{\ell} \; J_{max}^{\ell} = 12$$

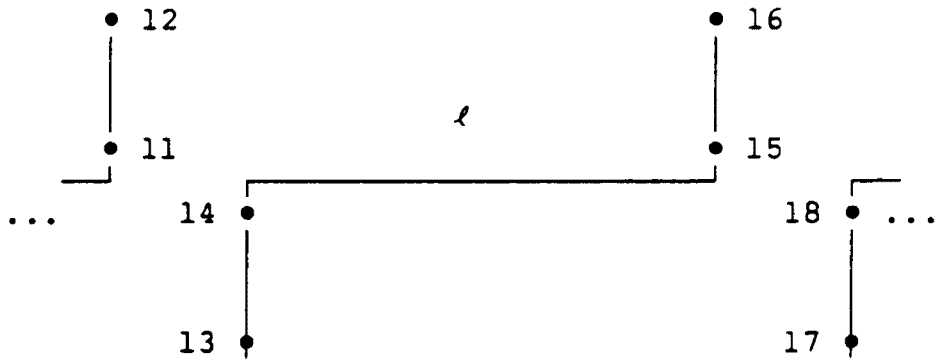
(c) global volume

Fig. 4-9.(cont'd) Volume and surface phase-space support points.



$$\frac{M_S}{2} = L(J_+ + J_-) = 4L$$

(d) global incoming surface



$$\frac{M_S}{2} = L(J_- + J_+) = 4L$$

(e) local outgoing surface

Fig. 4-9.(cont'd) Volume and surface phase-space support points.

products are tensor products of one-dimensional inner products. For the purpose of illustration, consider $\underline{\underline{T}}_{V,\ell}$. Recall

$$\underline{\underline{T}}_{V,\ell} = (\underline{\Psi},\underline{\psi}_{\ell}^{T})_{\ell} \tag{4.13}$$

Hence, the element of $\underline{\underline{T}}_{V,\ell}$ corresponding to support points at $(x,\mu)_{m_1}$ and $(x,\mu)_{m_2}$ is defined

$$\begin{aligned}(\underline{\underline{T}}_{V,\ell})_{m_1 m_2} &= (\Psi_{m_1},\psi_{\ell m_2})_{\ell} \\ &= (\hat{\Psi}_{i_1},\hat{\psi}_{\ell i_2})_{\Delta x_{\ell}} \; (\hat{\Psi}_{j_1},\hat{\psi}_{\ell j_2})_{\mu}\end{aligned} \tag{4.14}$$

Fig. 4-10 is an example of local and global basis functions in x. The one-dimensional integrals are, once again, found using Gauss's formula. Furthermore, when an inverse of a $\underline{\underline{T}}$ matrix must be found, the entire matrix need not be inverted. Instead, the individual, one-dimensional matrices are inverted and then used to create the inverted multidimensional matrix by tensor multiplication. An explanation follows.

Consider the meaning of the tensor multiplication of two matrices

$$(\underline{\underline{T}}_{V,\ell})_{m_1 m_2} = (\hat{\Psi}_{i_1},\hat{\psi}_{\ell i_2})_{\Delta x_{\ell}} \; (\hat{\Psi}_{j_1},\hat{\psi}_{\ell j_2})_{\mu}$$

$$= (\underline{\underline{T}}^{x}_{V,\ell} \bullet \underline{\underline{T}}^{\mu}_{V,\ell})_{m_1 m_2}$$

where '•' indicates tensor product. A tensor product, or direct product, is a term by term multiplication of corresponding matrix elements. The matrix $\underline{\underline{T}}_{V,\ell}$ can also be considered the **matrix** product of two matrices

$$(\underline{\underline{T}}_{V,\ell})_{m_1 m_2} = \sum_{m_3} (\underline{\underline{T}}_x)_{m_1 m_3} (\underline{\underline{T}}_\mu)_{m_3 m_2}$$

The matrix $\underline{\underline{T}}_x$ is made up of sub-matrices defined

$$\underline{\underline{T}}_x^{sub}{}_{AB} = (\underline{\underline{T}}_{V,\ell}^x)_{AB} \underline{\underline{I}}$$

where $\underline{\underline{T}}_x^{sub}{}_{AB}$ is the sub-matrix at position AB and $\underline{\underline{T}}_\mu$ is a block diagonal matrix where each block is $\underline{\underline{T}}_{V,\ell}^\mu$. Thus,

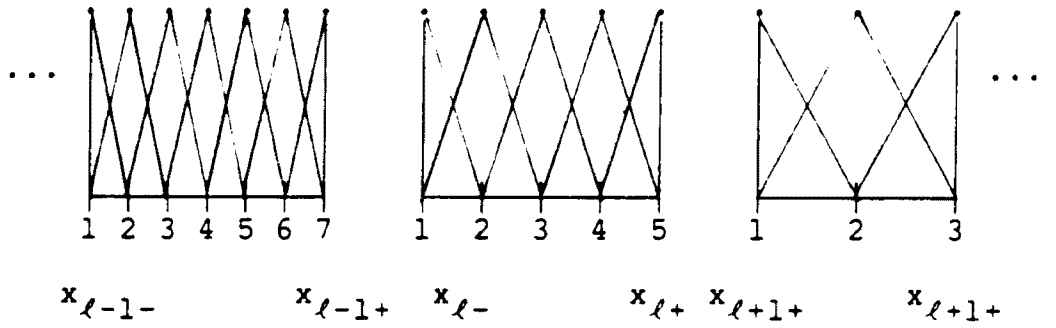
$$\underline{\underline{T}}_{V,\ell}^{-1} = \underline{\underline{T}}_\mu^{-1} \; \underline{\underline{T}}_x^{-1}$$

The inverse of $\underline{\underline{T}}_\mu$ is a block diagonal matrix where each block is $\underline{\underline{T}}_{V,\ell}^{\mu\ -1}$. Moreover, $\underline{\underline{T}}_x^{-1}$ has the same structure as $\underline{\underline{T}}_x$ but the sub-matrices of $\underline{\underline{T}}_x^{-1}$ are defined

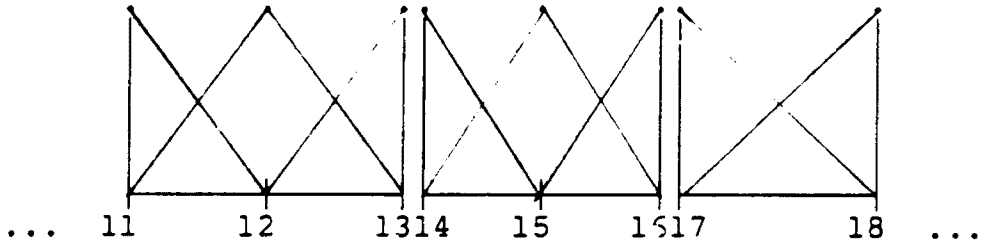
$$\underline{\underline{T}}_x^{-1sub}{}_{AB} = (\underline{\underline{T}}_{V,\ell}^{x\ -1})_{AB} \underline{\underline{I}}$$

Then

$$(\underline{\underline{T}}_{V,\ell}^{-1})_{n_1 n_2} = \sum_{n_3} (\underline{\underline{T}}_\mu^{-1})_{n_1 n_3} (\underline{\underline{T}}_x^{-1})_{m_3 m_2}$$



(a) local



(b) global

Fig. 4-10. Local and global one-dimensional spatial basis functions.

which also results in a tensor product

$$(\underline{\underline{T}}^{-1}_{V,\ell})_{n_1 n_2} = (\underline{\underline{T}}^{\mu}_{V,\ell}{}^{-1} \bullet \underline{\underline{T}}^{x}_{V,\ell}{}^{-1})_{n_1 n_2}$$

For a particular region, many of the one-dimensional inner products are used more than once. Table 4-1 provides a list of the inner products that make up the $\underline{\underline{T}}$ matrices where the following definitions for μ-weighted one-dimensional inner products are used:

$$(\pm\mu\hat{\psi}_i, \hat{\psi}_j)_{\mu\pm} = \int_0^1 d\mu\, \mu \hat{\psi}_i(\mu)\hat{\psi}_j(\mu) - \int_{-1}^0 d\mu\, \mu \hat{\psi}_i(\mu)\hat{\psi}_j(\mu)$$

$$(\mp\mu\hat{\psi}_i, \hat{\psi}_j)_{\mu\mp} = -\int_{-1}^0 d\mu\, \mu \hat{\psi}_i(\mu)\hat{\psi}_j(\mu) + \int_0^1 d\mu\, \mu \hat{\psi}_i(\mu)\hat{\psi}_j(\mu)$$

From Table 4-1, the following unique inner products are identified:

1) $(\mp\mu\hat{\psi}_\ell, \hat{\Psi})_{\mu\mp}$

2) $(\hat{\psi}_\ell, \hat{\Psi})_{\Delta x_\ell}$

3) $(\hat{\psi}_\ell, \hat{\Psi})_{\mu}$

4) $(\pm\mu\hat{\psi}_\ell, \hat{\psi}_\ell)_{\mu\pm}$

Table 4-1. One-Dimensional Projection Matrices and their Inner Products

matrix	definition	inner products
$\underline{\underline{T}}_{\ell,S}$	$\langle \underline{\Psi}_\ell, \underline{\Psi}_S^T \rangle_{-\ell}$	$(\mp\mu\hat{\underline{\psi}}_\ell, \hat{\Psi})_{\mu\mp}$
$\underline{\underline{T}}_{\ell,V}$	$(\underline{\Psi}_\ell, \underline{\Psi}^T)_\ell$	$(\hat{\underline{\psi}}_\ell, \hat{\Psi})_{\Delta x_\ell} (\hat{\underline{\psi}}_\ell, \hat{\Psi})_\mu$
$\underline{\underline{T}}_{\ell S,\ell S}$	$\langle \underline{\Psi}_{\ell S}, \underline{\Psi}_{\ell S}^T \rangle_{+\ell}$	$(\pm\mu\hat{\underline{\psi}}_\ell, \hat{\underline{\psi}}_\ell)_{\mu\pm}$
$\underline{\underline{T}}_{\ell S,\ell}$	$\langle \underline{\Psi}_{\ell S}, \underline{\Psi}_\ell^T \rangle_{+\ell}$	$(\pm\mu\hat{\underline{\psi}}_\ell, \hat{\underline{\psi}}_\ell)_{\mu\pm}$
$\underline{\underline{T}}_{SS}$	$\langle \underline{\Psi}_S, \underline{\Psi}_S^T \rangle_{+\ell}$	$(\pm\mu\hat{\Psi}, \hat{\Psi})_{\mu\pm}$
$\underline{\underline{T}}_{S,\ell S}$	$\langle \underline{\Psi}_S, \underline{\Psi}_{\ell S}^T \rangle_{+\ell}$	$(\pm\mu\hat{\Psi}, \hat{\underline{\psi}}_\ell)_{\mu\pm}$
$\underline{\underline{T}}_{VV}$	$(\underline{\Psi}, \underline{\Psi}^T)_\ell$	$(\hat{\Psi}, \hat{\Psi})_{\Delta x_\ell} (\hat{\Psi}, \hat{\Psi})_\mu$
$\underline{\underline{T}}_{V,\ell}$	$[\underline{\underline{T}}_{\ell,V}]^T$	$(\hat{\underline{\psi}}_\ell, \hat{\Psi})_{\Delta x_\ell} (\hat{\underline{\psi}}_\ell, \hat{\Psi})_\mu$

5) $(\pm\mu\hat{\Psi},\hat{\Psi})_{\mu\pm}$

6) $(\hat{\Psi},\hat{\Psi})_{\Delta x_\ell}$

7) $(\hat{\Psi},\hat{\Psi})_{\mu}$

Because the surface and volume basis functions reside on the same support points at the surface, the only difference between matrices such as $\underline{\underline{T}}_{\ell S,\ell S}$ and $\underline{\underline{T}}_{\ell S,\ell}$ is the **location** of matrix elements, not the values. For this reason, the product $\underline{\underline{T}}_{\ell S,\ell S}^{-1}\ \underline{\underline{T}}_{\ell S,\ell}$ contains only zeros and ones and acts as a renumbering matrix.

The band structure of the one-dimensional $\underline{\underline{T}}$ matrices for individual regions is determined by the order of basis functions and the number of local and global support points. They all have structure similar to $\underline{\underline{A}}_\ell$ where each of the blocks of Fig. 4-8 contains a single element; the matrices, however, are not necessarily square.

One of the advantages of a response matrix method, as mentioned earlier, is that identical regions share response matrices resulting in a reduction in the number of matrices that must be calculated in order to solve a global problem. Response matrices are thus calculated separately; the only information that must be shared by all regions during calculation of matrices is the global specification of the angular mesh, and, in the case of two spatial dimensions, the global specification of the spatial mesh.

The response matrix $\underline{\underline{R}}_{S\leftarrow S}$ has the following block diagonal structure:

$$\underline{\underline{R}}_{S\leftarrow S} = \begin{bmatrix} \underline{\underline{R}}^{1}_{S\leftarrow S} & 0 & \cdot & \cdot & \cdot \\ 0 & \underline{\underline{R}}^{2}_{S\leftarrow S} & \cdot & \cdot & \cdot \\ \cdot & \cdot & \cdot & \cdot & \cdot \\ \cdot & \cdot & \cdot & \cdot & \underline{\underline{R}}^{L}_{S\leftarrow S} \end{bmatrix} \tag{4.15}$$

where the response matrix for region ℓ is partitioned into four parts:

$$\underline{\underline{R}}^{\ell}_{S\leftarrow S} = \begin{bmatrix} \underline{\underline{r}}^{\ell}_{--+} & \underline{\underline{t}}^{\ell}_{---} \\ \underline{\underline{t}}^{\ell}_{++} & \underline{\underline{r}}^{\ell}_{+-} \end{bmatrix}$$

The diagonal submatrices, $\underline{\underline{r}}^{\ell}_{--+}$ and $\underline{\underline{r}}^{\ell}_{+-}$, represent the reflection of neutrons striking region ℓ. The off-diagonal submatrices, $\underline{\underline{t}}^{\ell}_{---}$ and $\underline{\underline{t}}^{\ell}_{++}$, give the transmission of neutrons through the region.

Iterative Solution Method

The coupling and boundary condition matrix, $\underline{\underline{H}}$, that is used in the iterative solution procedure is a block matrix that has a modified block-tridiagonal structure:

$$\underline{\underline{H}} = \begin{bmatrix} \underline{\underline{H}}^{L}_{refl} & \underline{\underline{H}}_{-} & 0 & . & . & . & . & \underline{\underline{H}}^{+}_{per} \\ \underline{\underline{H}}_{+} & 0 & \underline{\underline{H}}_{-} & . & . & & & . \\ 0 & \underline{\underline{H}}_{+} & 0 & . & . & & & . \\ . & . & . & . & . & . & & . \\ \underline{\underline{H}}^{-}_{per} & . & . & . & . & . & . & \underline{\underline{H}}^{R}_{refl} \end{bmatrix} \qquad (4.16)$$

All the sub-matrices are of size $(J_{+}+J_{-})x(J_{-}+J_{+})$. The sub-matrices $\underline{\underline{H}}_{-}$ and $\underline{\underline{H}}_{+}$ represent the coupling of adjoining regions,

$$\underline{\underline{H}}_{-} = \begin{bmatrix} 0 & 0 \\ \underline{\underline{I}}_{-} & 0 \end{bmatrix}$$

and

$$\underline{\underline{H}}_{+} = \begin{bmatrix} 0 & \underline{\underline{I}}_{+} \\ 0 & 0 \end{bmatrix}$$

where $\underline{\underline{I}}_{-}$ and $\underline{\underline{I}}_{+}$ are identity matrices with dimensions J_{-} and J_{+}, respectively. All elements of the left and right reflection matrices, $\underline{\underline{H}}^{L}_{refl}$ and $\underline{\underline{H}}^{R}_{refl}$, are zero unless a reflecting boundary condition is specified. In that case, $J_{-} = J_{+} = J_{\pm}$; if the left side is reflecting

$$\underline{\underline{H}}^{L}_{refl} = \begin{bmatrix} \underline{\underline{P}} & 0 \\ 0 & 0 \end{bmatrix}$$

if the right side is reflecting

$$\underline{\underline{H}}^{R}_{refl} = \begin{bmatrix} 0 & 0 \\ 0 & \underline{\underline{P}} \end{bmatrix}$$

where

$$\underline{\underline{P}} = \begin{bmatrix} 0 & 0 & . & . & . & 0 & 1 \\ 0 & 0 & . & . & . & 1 & 0 \\ . & . & & & & & . \\ 0 & 1 & & & & & . \\ 1 & 0 & . & . & . & . & 0 \end{bmatrix}$$

and has dimension $J_{\pm}$.

The periodic boundary condition is a means of simulating a repeating lattice. In the case of one dimension, the flux exiting the right edge is taken to be the incoming flux at the left edge and vice versa. If such a boundary condition is specified, $\underline{\underline{H}}^{+}_{per}$ and $\underline{\underline{H}}^{-}_{per}$ will take the form

$$\underline{\underline{H}}^{+}_{per} = \begin{bmatrix} 0 & \underline{\underline{I}}_{+} \\ 0 & 0 \end{bmatrix}$$

and

$$\underline{\underline{H}}^{-}_{per} = \begin{bmatrix} 0 & 0 \\ \underline{\underline{I}}_{-} & 0 \end{bmatrix}$$

Otherwise, all elements in $\underline{\underline{H}}^{+}_{per}$ and $\underline{\underline{H}}^{-}_{per}$ will have value zero.

The remaining boundary conditions--specified incoming flux and zero incoming flux--are accounted for by $\underline{\phi}_{\Gamma^-}$, where

$$\underline{\phi}_{\Gamma^-} = \text{col}(\underline{\phi}^{L}_{-}, 0, \ldots, 0, \underline{\phi}^{R}_{-}) \tag{4.17}$$

and $\underline{\phi}^{L}_{-}$ and $\underline{\phi}^{R}_{-}$ are vectors specifying the incoming flux at the left and right and are of length J_{+} and J_{-}, respectively.

In practice, the coupling-boundary condition matrix is never calculated nor the multiplication performed. Instead, since multiplication by $\underline{\underline{H}}$ simply renumbers values of the interface flux, it is, in fact, this reassignment that is performed. The multiplication is, however, a convenient means of representing this reassignment and shall be used as such in the remainder of this work.

In Chapter II, the iteration procedure used to find the interface flux distribution was written

$$\underline{\phi}_{+}^{S(n)} = \underline{\underline{R}}_{S\leftarrow S}\underline{\phi}_{in}^{S(n-1)} + \underline{\underline{R}}_{S\leftarrow V}\underline{S}^{V}$$

$$\underline{\phi}_{in}^{S(n)} = \underline{\underline{H}}\,\underline{\phi}_{+}^{S(n)} + \underline{\phi}_{\Gamma^-}$$

By combining these two equations,

$$\underline{\phi}_{in}^{S(n)} = \underline{\underline{H}}\underline{\underline{R}}_{S\leftarrow S}\underline{\phi}_{in}^{S(n-1)} + \underline{\underline{H}}\underline{\underline{R}}_{S\leftarrow V}\underline{S}^{V} + \underline{\phi}_{\Gamma^-} \qquad (4.18)$$

and defining

$$\underline{\underline{B}} = \underline{\underline{H}}\underline{\underline{R}}_{S\leftarrow S}$$

and

$$\underline{\phi}_{SV} = \underline{\underline{H}}\underline{\underline{R}}_{S\leftarrow V}\underline{S}^{V} + \underline{\phi}_{\Gamma^-} \qquad (4.19)$$

the familiar form of Jacobi's method [Dah74] emerges:

$$\underline{\phi}_{in}^{S(n)} = \underline{\underline{B}}\underline{\phi}_{in}^{S(n-1)} + \underline{\phi}_{SV} \qquad (4.21)$$

The iteration matrix is a block-triangular matrix with zero diagonal elements,

$$\underline{\underline{HR}}_{S\leftarrow S} = \begin{bmatrix} 0 & \underline{\underline{b}}_{-}^{2} & 0 & . & . & . & . \\ \underline{\underline{b}}_{+}^{1} & 0 & \underline{\underline{b}}_{-}^{3} & 0 & . & . & . \\ 0 & \underline{\underline{b}}_{+}^{2} & 0 & \underline{\underline{b}}_{-}^{4} & . & . & . \\ . & 0 & \underline{\underline{b}}_{+}^{3} & 0 & \underline{\underline{b}}_{-}^{5} & . & . \\ . & . & . & . & . & . & . \end{bmatrix} \tag{4.22}$$

where

$$\underline{\underline{b}}_{+}^{\ell} = \begin{bmatrix} \underline{\underline{t}}_{++}^{\ell} & \underline{\underline{r}}_{+-}^{\ell} \\ 0 & 0 \end{bmatrix}$$

and

$$\underline{\underline{b}}_{-}^{\ell} = \begin{bmatrix} 0 & 0 \\ \underline{\underline{r}}_{-+}^{\ell} & \underline{\underline{t}}_{--}^{\ell} \end{bmatrix}$$

It can thus be considered the sum of a lower triangle matrix and an upper triangle matrix

$$\underline{\underline{HR}}_{S\leftarrow S} = \underline{\underline{L}}_{HR} + \underline{\underline{U}}_{HR} \tag{4.23}$$

which leads conveniently to a Gauss-Seidel method. If $\underline{\underline{L}}_{HR}$ operates on the updated flux, the Gauss-Seidel formulation,

$$\underline{\phi}_{in}^{S(n)} = \underline{\underline{L}}_{HR}\underline{\phi}_{in}^{S(n)} + \underline{\underline{U}}_{HR}\underline{\phi}_{in}^{S(n-1)} + \underline{\phi}_{SV} \qquad (4.24)$$

represents a left-to-right sweep. A right-to-left sweep results with the interchange of $\underline{\underline{L}}_{HR}$ and $\underline{\underline{U}}_{HR}$:

$$\underline{\phi}_{in}^{S(n)} = \underline{\underline{U}}_{HR}\underline{\phi}_{in}^{S(n)} + \underline{\underline{L}}_{HR}\underline{\phi}_{in}^{S(n-1)} + \underline{\phi}_{SV} \qquad (4.25)$$

Note that if $\Sigma_s=0$, the reflection matrices, $\underline{\underline{r}}_{-+}^{\ell}$ and $\underline{\underline{r}}_{+-}^{\ell}$, also become zero and a converged interface flux distribution can be found after at most a single iteration in each direction.

The logical extension of the Gauss-Seidel method is, of course, the successive overrelaxation (SOR) method which results from the simple inclusion of the relaxation parameter, ω. The left-to-right SOR iteration is written

$$\underline{\phi}_{in}^{S(n)} = \omega\underline{\underline{L}}_{HR}\underline{\phi}_{in}^{S(n)} + \omega\underline{\underline{U}}_{HR}\underline{\phi}_{in}^{S(n-1)} + (1-\omega)\underline{\phi}_{in}^{S(n-1)} + \omega\underline{\phi}_{SV}$$

As before, a right-to-left scheme can be written by interchanging $\underline{\underline{L}}_{HR}$ and $\underline{\underline{U}}_{HR}$.

Computer Implementation in Two Dimensions

The implementation of the method to two-dimensional geometries is similar to that in one dimension with the added complexity of four phase-space dimensions rather than two.

Finite Element Basis Function Construction

As before, four-dimensional finite element polynomials are formed by a tensor product of one-dimensional basis functions. A support point in the $x,y;\mu,\Phi$ phase-space is labeled in one of two ways, with a single index, m, or a group, *ijkl*:

$$(x,y;\mu,\Phi)_m = (x_i,y_j;\mu_k,\Phi_l)$$

The four-dimensional basis function is written

$$\psi_m(x,y;\mu,\Phi) = \hat{\psi}_i(x)\hat{\psi}_j(y)\hat{\psi}_k(\mu)\hat{\psi}_l(\Phi)$$

For linear basis functions this multidimensional "tent" function, although difficult to visualize, much less draw, has a unit value at $(x,y;\mu,\Phi)_m$ and value zero outside the range

$$\{x,y,;\mu,\Phi \mid x_{i-1} \le x \le x_{i+1},$$

$$y_{j-1} \le y \le y_{j+1},$$

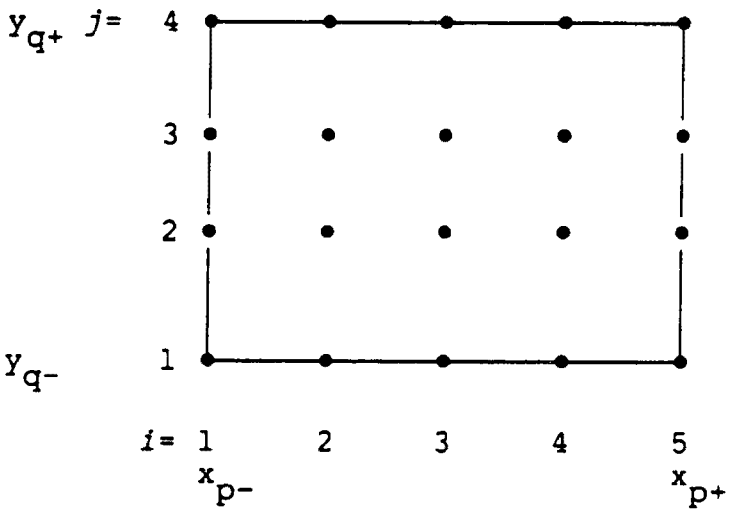
$$\mu_{k-1} \le \mu \le \mu_{k+1},$$

$$\Phi_{l-1} \le \Phi \le \Phi_{l+1}\}$$

A grid of basis function support points is established by specifying a set of intervals in each of the four directions. As was the case in one dimension, superior results are obtained when a discontinuity in angular flux is allowed at the angles distinguishing outgoing neutrons from incoming neutrons. For the rectangular regions considered in this work, these angles are μ=0 and $\Phi=\pi/2$. The two sample angular grids shown in Fig. 4-11 illustrate cases both with and without angular discontinuities. Also shown in Fig. 4-11 is a sample spatial mesh arrangement. Because the angular mesh is replicated at each spatial support point, the index of a particular mesh point is found from the following formula,

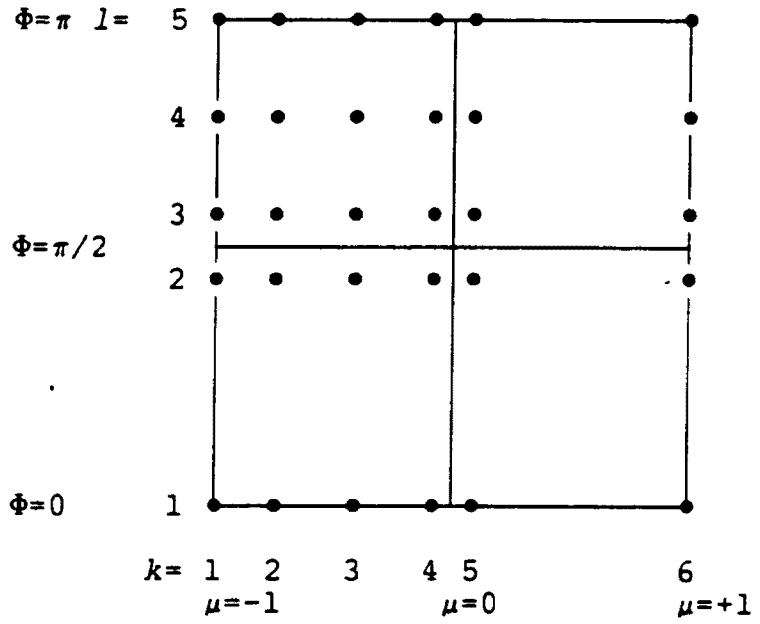
$$m = (((i-1)j_{max} + j-1)k_{max} + k-1)l_{max} + l \quad (4.27)$$

where the subscript 'max' indicates the maximum value of the one-dimensional index.

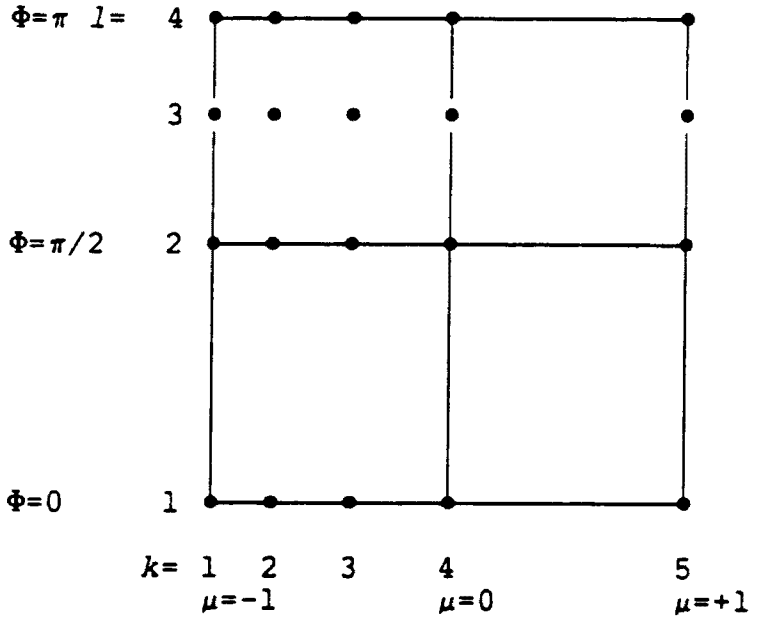


(a) spatial support points

Fig. 4-11. Volume two-dimensional phase-space support points.



(b) angular support points
(discontinuous support at $\mu=0$, $\Phi=\pi/2$)



(c) angular support points
(continuous support at $\mu=0$, $\Phi=\pi/2$)

Fig. 4-11.(cont'd) Volume two-dimensional phase-space support points.

Finite Element Matrix Calculation

The volume inner product, which has been defined in Chapter III,

$$(\phi_{m_1},\psi_{m_2})_\ell = \int_{\Delta x_p} dx \int_{\Delta y_q} dy \; 2\int_0^\pi d\Phi \int_{-1}^{1} d\mu \phi_{m_1}(x,y;\mu,\Phi)\psi_{m_2}(x,y;\mu,\Phi)$$

is the product of four separate one-dimensional inner products:

$$(\phi_{m_1},\phi_{m_2})_\ell = \int_{\Delta x_p} dx \hat{\psi}_{\ell i_1}(x)\hat{\psi}_{\ell i_2}(x) \int_{\Delta y_q} dy \hat{\psi}_{\ell j_1}(y)\hat{\psi}_{\ell j_2}(y)$$
$$\int_{-1}^{1} d\mu \hat{\psi}_{\ell k_1}(\mu)\hat{\psi}_{\ell k_2}(\mu) \; 2\int_0^\pi d\Phi \hat{\psi}_{\ell l_1}(\Phi)\hat{\psi}_{\ell l_2}(\Phi)$$
$$= (\hat{\psi}_{\ell i_1},\hat{\psi}_{\ell i_2})_{\Delta x_p} (\hat{\psi}_{\ell j_1},\hat{\psi}_{\ell j_2})_{\Delta y_q}$$
$$(\hat{\psi}_{\ell k_1},\hat{\psi}_{\ell k_2})_\mu \; (2\hat{\psi}_{\ell l_1},\hat{\psi}_{\ell l_2})_\Phi$$

The surface inner products, too, can be separated into one-dimensional components:

$$<\psi_{m_1},\psi_{m_2}>_{+\ell} =$$

$$\int_{\Delta y_q} dy \; 2\int_0^{\pi} d\Phi \int_0^{1} d\mu\mu\psi_{m_1}(x=x_{p+},y;\mu,\Phi)\psi_{m_2}(x=x_{p+},y;\mu,\Phi)$$

$$- \int_{\Delta y_q} dy \; 2\int_0^{\pi} d\Phi \int_{-1}^{0} d\mu\mu\psi_{m_1}(x=x_{p-},y;\mu,\Phi)\psi_{m_2}(x=x_{p-},y;\mu,\Phi)$$

$$+ \int_{\Delta x_p} dx \int_{-1}^{1} d\mu \; 2\int_0^{\pi/2} d\Phi\eta\psi_{m_1}(x,y=y_{q+};\mu,\Phi)\psi_{m_2}(x,y=y_{q+};\mu,\Phi)$$

$$- \int_{\Delta x_p} dx \int_{-1}^{1} d\mu \; 2\int_{\pi/2}^{\pi} d\Phi\eta\psi_{m_1}(x,y=y_{q-};\mu,\Phi)\psi_{m_2}(x,y=y_{q-};\mu,\Phi)$$

$$<\psi_{m_1},\psi_{m_2}>_{+\ell} =$$

$$\int_{\Delta y_q} dy\hat{\psi}_{\ell j_1}(y)\hat{\psi}_{\ell j_2}(y) \; 2\int_0^{\pi} d\Phi\hat{\psi}_{\ell l_1}(\Phi)\hat{\psi}_{\ell l_2}(\Phi)$$

$$[\hat{\psi}_{\ell i_1}(x_{p+})\hat{\psi}_{\ell i_2}(x_{p+}) \int_0^{1} d\mu\hat{\psi}_{\ell k_1}(\mu)\hat{\psi}_{\ell k_2}(\mu)$$

$$- \hat{\psi}_{\ell i_1}(x_{p-})\hat{\psi}_{\ell i_2}(x_{p-}) \int_{-1}^{0} d\mu\hat{\psi}_{\ell k_1}(\mu)\hat{\psi}_{\ell k_2}(\mu)]$$

$$+ \int_{\Delta x_p} dx\hat{\psi}_{\ell i_1}(x)\hat{\psi}_{\ell i_2}(x) \int_{-1}^{1} d\mu\sqrt{1-\mu^2}\hat{\psi}_{\ell k_1}(\mu)\hat{\psi}_{\ell k_2}(\mu)$$

$$[\hat{\psi}_{\ell j_1}(y_{q+})\hat{\psi}_{\ell j_2}(y_{q+}) \; 2\int_0^{\pi/2} d\Phi\cos\Phi\hat{\psi}_{\ell l_1}(\Phi)\hat{\psi}_{\ell l_2}(\Phi)$$

$$- \hat{\psi}_{\ell j_1}(y_{q-})\hat{\psi}_{\ell j_2}(y_{q-}) \; 2\int_{\pi/2}^{\pi} d\Phi\cos\Phi\hat{\psi}_{\ell l_1}(\Phi)\hat{\psi}_{\ell l_2}(\Phi)]$$

$$= (\hat{\psi}_{\ell j_1},\hat{\psi}_{\ell j_2})_{\Delta y_q} \; (2\hat{\psi}_{\ell l_1},\hat{\psi}_{\ell l_2})_{\Phi} \; (\pm\mu\hat{\psi}_{\ell k_1},\hat{\psi}_{\ell k_2})^{i_1,i_2}_{\pm\mu}$$

$$+ (\hat{\psi}_{\ell i_1},\hat{\psi}_{\ell i_2})_{\Delta x_p} \; (\sqrt{1-\mu^2}\hat{\psi}_{\ell k_1},\hat{\psi}_{\ell k_2})_{\mu}$$

$$(\pm 2\cos\Phi\hat{\psi}_{\ell k_1},\hat{\psi}_{\ell k_2})^{j_1,j_2}_{\pm\Phi}$$

$$\langle \psi_{m_1}, \psi_{m_2} \rangle_{-\ell} =$$

$$(\hat{\psi}_{\ell j_1}, \hat{\psi}_{\ell j_2})_{\Delta y_q} \; (2\hat{\psi}_{\ell l_1}, \hat{\psi}_{\ell l_2})_{\Phi} \; (\mp\mu\hat{\psi}_{\ell k_1}, \hat{\psi}_{\ell k_2})^{i_1, i_2}_{\mp\mu}$$

$$+ \; (\hat{\psi}_{\ell i_1}, \hat{\psi}_{\ell i_2})_{\Delta x_p} \; (\sqrt{1-\mu^2}\hat{\psi}_{\ell k_1}, \hat{\psi}_{\ell k_2})_{\mu}$$

$$(\mp 2\cos\Phi\hat{\psi}_{\ell k_1}, \hat{\psi}_{\ell k_2})^{j_1, j_2}_{\mp\Phi}$$

where

$$(\mp\mu\hat{\psi}_{\ell k_1}, \hat{\psi}_{\ell k_2})^{i_1, i_2}_{\mp\mu} =$$

$$- \hat{\psi}_{\ell i_1}(x_{p+})\hat{\psi}_{\ell i_2}(x_{p+}) \int_{-1}^{0} d\mu \hat{\psi}_{\ell k_1}(\mu)\hat{\psi}_{\ell k_2}(\mu)$$

$$+ \hat{\psi}_{\ell i_1}(x_{p-})\hat{\psi}_{\ell i_2}(x_{p-}) \int_{0}^{1} d\mu \hat{\psi}_{\ell k_1}(\mu)\hat{\psi}_{\ell k_2}(\mu)$$

and

$$(\mp 2\cos\Phi\hat{\psi}_{\ell k_1}, \hat{\psi}_{\ell k_2})^{j_1, j_2}_{\mp\Phi} =$$

$$- \hat{\psi}_{\ell j_1}(y_{q+})\hat{\psi}_{\ell j_2}(y_{q+}) \; 2\int_{\pi/2}^{\pi} d\Phi \cos\Phi \hat{\psi}_{\ell l_1}(\Phi)\hat{\psi}_{\ell l_2}(\Phi)$$

$$+ \hat{\psi}_{\ell j_1}(y_{q-})\hat{\psi}_{\ell j_2}(y_{q-}) \; 2\int_{0}^{\pi/2} d\Phi \cos\Phi \hat{\psi}_{\ell l_1}(\Phi)\hat{\psi}_{\ell l_2}(\Phi)$$

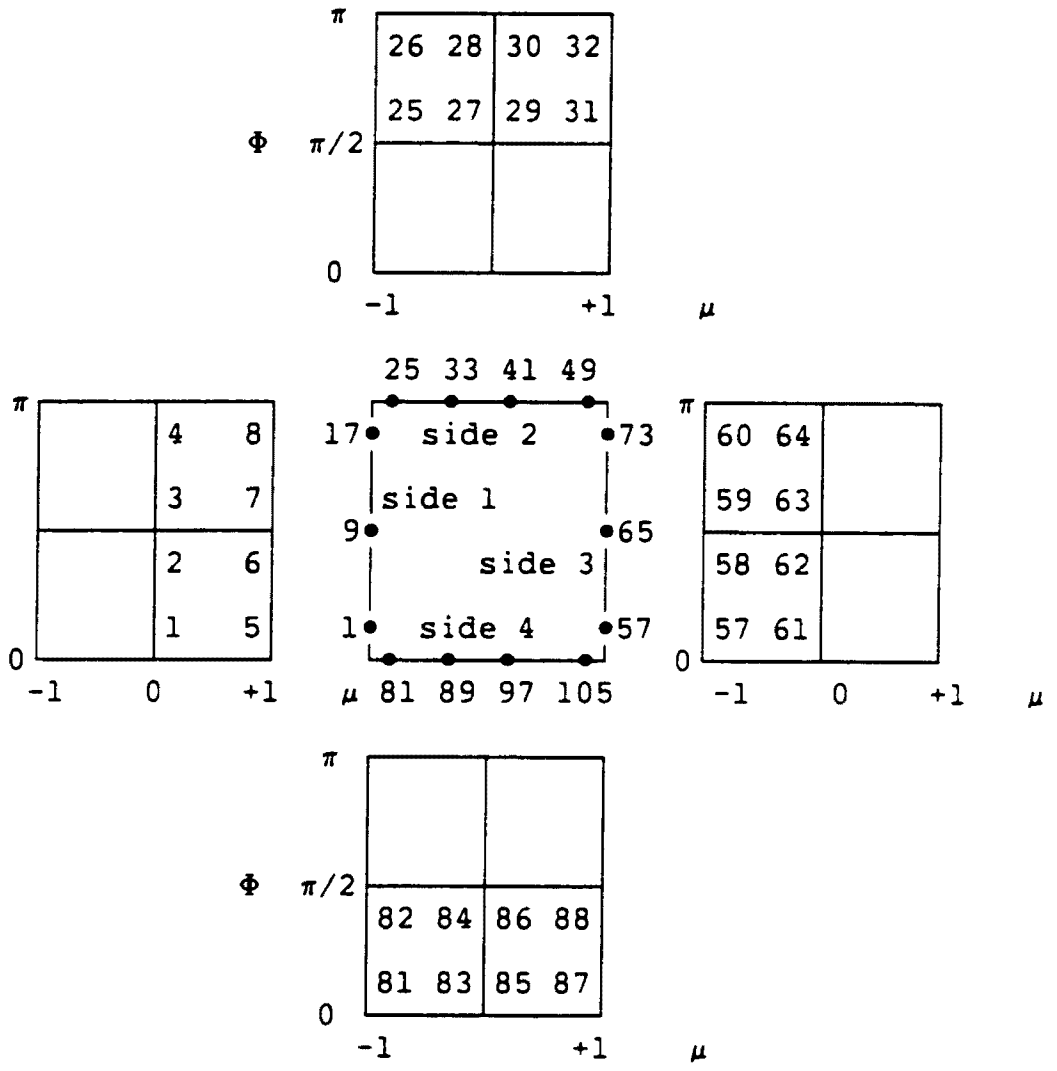
The band structure of $\underline{\underline{A}}_{\ell}$ is like that of the one-dimensional $\underline{A}_{\ell}$ presented in Fig. 4-8 with block size $j_{max}k_{max}l_{max}$. Moreover, within each block is another band structure of the same type, dependent on the order of the basis function in y, with blocks of size $k_{max}l_{max}$.

Response Matrix Generation

In order to generate response matrices that simulate the transfer of neutrons to or from surfaces, a surface mesh must be specified in addition to the volume mesh already described. Fig. 4-12 illustrates example incoming and outgoing surface grids. Because a mesh which occupies one-half of the angular domain is repeated at every point on the surface, the index written at each surface support point represents the starting index for the angular grid at that point. In this example, the outgoing mesh is of the same dimension as the incoming mesh, although this is not necessarily always the case. However, the mesh structure must be consistent in a particular direction of neutron travel.

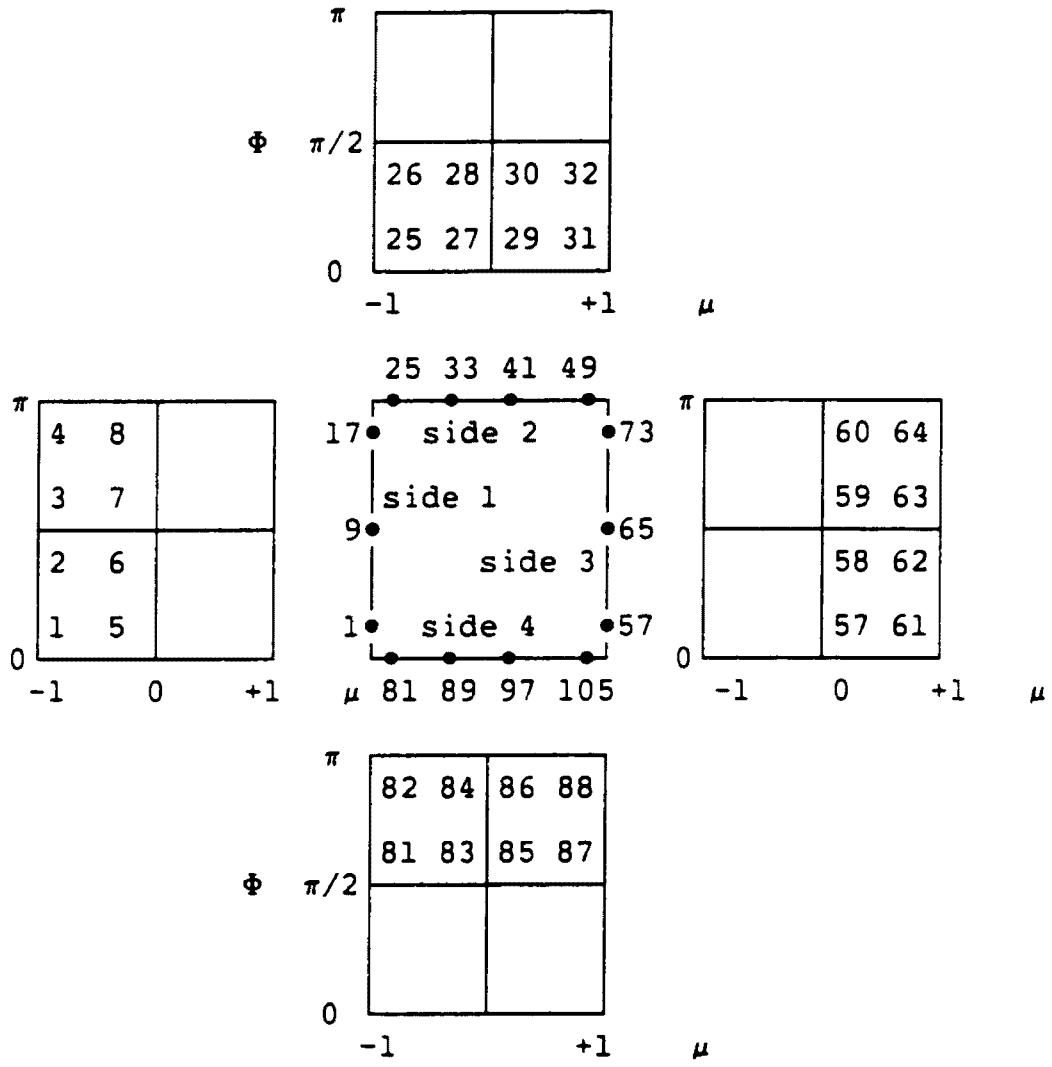
The global mesh structure is specified over the entire problem domain. Fig. 4-13 is an example of spatial volume support points; Fig. 4-14 shows a spatial surface support point grid. Again, at each spatial support point an angular grid exists: over the full angular domain in the case of volume basis functions but over only half of the angular domain for surface basis functions.

The $\underline{\underline{T}}$ matrices are calculated by combining a series of one-dimensional local/global inner products by taking tensor products. Table 4-2 provides definitions of the various matrices that are used according to the prescriptions of Table T1 to generate two-dimensional response matrices. Some of the previously defined notation must be updated to



(a) incoming surface

Fig. 4-12. Two-dimensional surface support points.



(b) outgoing surface

Fig. 4-12.(cont'd.) Two-dimensional surface support points.

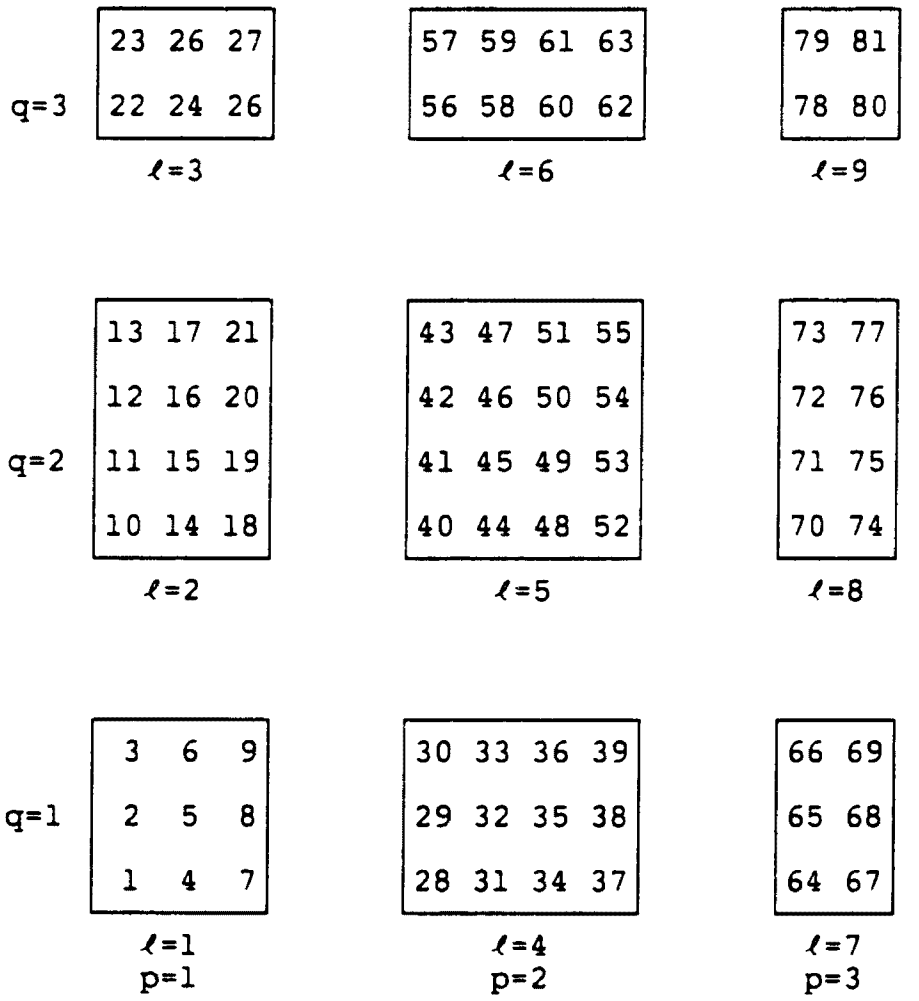


Fig. 4-13. Two-dimensional spatial volume support point numbering system.

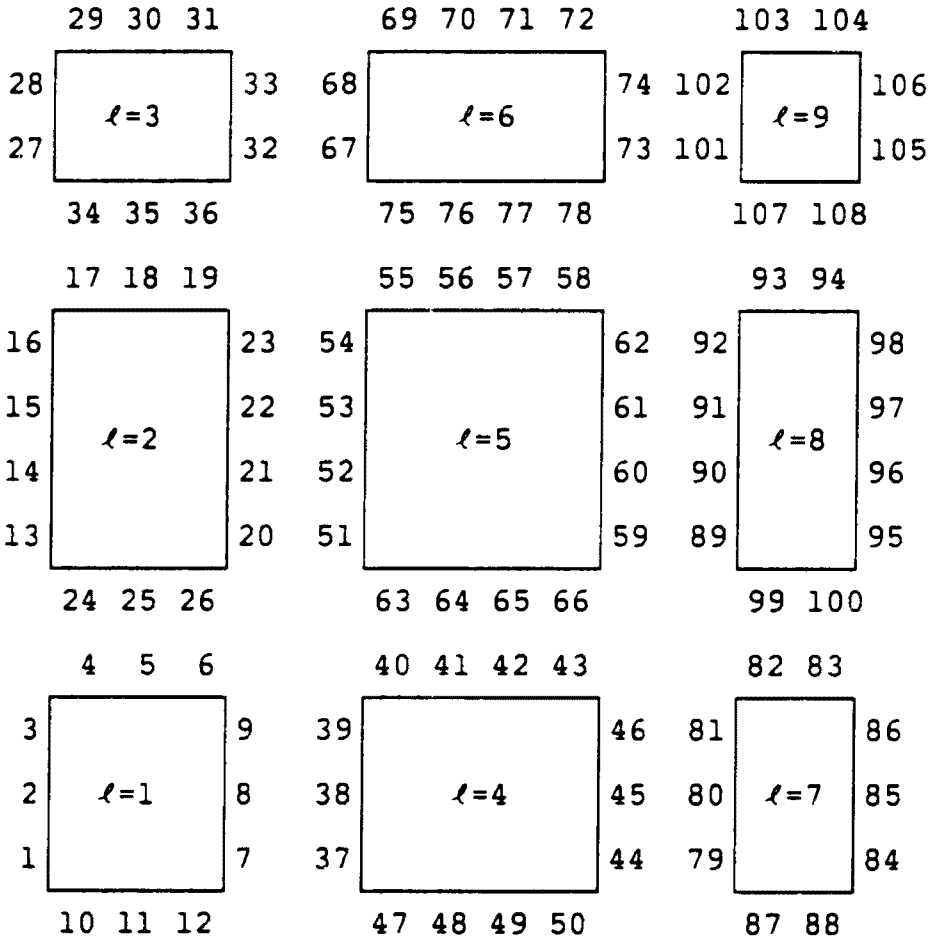


Fig. 4-14. Two-dimensional spatial surface support point numbering system.

account for surface basis functions that are defined only at region interfaces. A surface support point, m, can be represented by a group of four indices: either $s^x jkl$ or $is^y kl$ where s^x refers to side 1 or 3 and s^y is 2 or 4. Then the weighted angular inner products are redefined,

$$(\pm\mu\hat{\psi}_{\ell k_1}, \hat{\psi}_{\ell k_2})^{i_1, i_2}_{\pm\mu} =$$
$$\xi^+_{i_1}\xi^+_{i_2}\int_0^1 d\mu\hat{\psi}_{\ell k_1}(\mu)\hat{\psi}_{\ell k_2}(\mu)$$
$$- \xi^-_{i_1}\xi^-_{i_2}\int_{-1}^0 d\mu\hat{\psi}_{\ell k_1}(\mu)\hat{\psi}_{\ell k_2}(\mu)$$

$$(\mp\mu\hat{\psi}_{\ell k_1}, \hat{\psi}_{\ell k_2})^{i_1, i_2}_{\mp\mu} =$$
$$- \xi^+_{i_1}\xi^+_{i_2}\int_{-1}^0 d\mu\hat{\psi}_{\ell k_1}(\mu)\hat{\psi}_{\ell k_2}(\mu)$$
$$+ \xi^-_{i_1}\xi^-_{i_2}\int_0^1 d\mu\hat{\psi}_{\ell k_1}(\mu)\hat{\psi}_{\ell k_2}(\mu)$$

$$(\pm 2\cos\Phi\hat{\psi}_{\ell k_1}, \hat{\psi}_{\ell k_2})^{j_1, j_2}_{\pm\Phi} =$$
$$\xi^+_{j_1}\xi^+_{j_2}\, 2\int_0^{\pi/2} d\Phi\cos\Phi\hat{\psi}_{\ell l_1}(\Phi)\hat{\psi}_{\ell l_2}(\Phi)$$
$$- \xi^-_{j_1}\xi^-_{j_2}\, 2\int_{\pi/2}^{\pi} d\Phi\cos\Phi\hat{\psi}_{\ell l_1}(\Phi)\hat{\psi}_{\ell l_2}(\Phi)$$

and

$$(\mp 2\cos\Phi\hat{\psi}_{\ell k_1}, \hat{\psi}_{\ell k_2})^{j_1, j_2}_{\mp\Phi} =$$

$$- \xi^{+}_{j_1}\xi^{+}_{j_2}\, 2\int_{\pi/2}^{\pi} d\Phi\cos\Phi\hat{\psi}_{\ell l_1}(\Phi)\hat{\psi}_{\ell l_2}(\Phi)$$

$$+ \xi^{-}_{j_1}\xi^{-}_{j_2}\, 2\int_{0}^{\pi/2} d\Phi\cos\Phi\hat{\psi}_{\ell l_1}(\Phi)\hat{\psi}_{\ell l_2}(\Phi)$$

where

$$\xi^{+}_{m_n} = \begin{cases} \hat{\psi}_{\ell i_n}(x_{p+}) & \text{if } m_n = i_n \\ \hat{\psi}_{\ell j_n}(y_{q+}) & \text{if } m_n = i_n \\ \delta_{KR}(s^x_n - 3) & \text{if } m_n = s^x_n \\ \delta_{KR}(s^y_n - 2) & \text{if } m_n = s^y_n \end{cases}$$

$$\xi^{-}_{m_n} = \begin{cases} \hat{\psi}_{\ell i_n}(x_{p-}) & \text{if } m_n = i_n \\ \hat{\psi}_{\ell j_n}(y_{q-}) & \text{if } m_n = i_n \\ \delta_{KR}(s^x_n - 1) & \text{if } m_n = s^x_n \\ \delta_{KR}(s^y_n - 4) & \text{if } m_n = s^y_n \end{cases}$$

The response matrix $\underline{\underline{R}}_{S\leftarrow S}$ has the same block diagonal structure (Eq. J29.1) in both one and two dimensions. The composition of the individual blocks, however, is different. In two dimensions, side-transmission (denoted below by the matrix $\underline{\underline{s}}^{\ell}$) must be considered in addition to reflection ($\underline{\underline{r}}^{\ell}$) and through-transmission ($\underline{\underline{t}}^{\ell}$):

Table 4-2. Two-Dimensional Projection Matrices and their Inner Products

matrix	definition	inner products
$\underline{\underline{T}}_{\ell,S}$	$\langle \underline{\Psi}_\ell, \underline{\Psi}_S^T \rangle_{-\ell}$	$(\vartheta_\ell,\Psi)_{\delta y_q}(2\vartheta_\ell,\Psi)_\Phi(\mp\mu\vartheta_\ell,\Psi)_{\mp\mu}^{i,s^x}$ + $(\vartheta_\ell,\Psi)_{\delta x_p}(\sqrt{1-\mu^2}\vartheta_\ell,\Psi)_\mu(\mp 2\cos\Phi\vartheta_\ell,\Psi)_{\mp\Phi}^{j,s^y}$
$\underline{\underline{T}}_{\ell,V}$	$(\underline{\Psi}_\ell, \underline{\Psi}^T)_\ell$	$(\vartheta_\ell,\Psi)_{\Delta x_p}(\vartheta_\ell,\Psi)_{\Delta y_q}(\vartheta_\ell,\Psi)_\mu(2\vartheta_\ell,\Psi)_\Phi$
$\underline{\underline{T}}_{\ell S,\ell S}$	$\langle \underline{\Psi}_{\ell S}, \underline{\Psi}_{\ell S}^T \rangle_{+\ell}$	$(\vartheta_\ell,\vartheta_\ell)_{\delta y_q}(2\vartheta_\ell,\vartheta_\ell)_\Phi(\pm\mu\vartheta_\ell,\vartheta_\ell)_{\pm\mu}^{s^x,s^x}$ + $(\vartheta_\ell,\vartheta_\ell)_{\delta x_p}(\sqrt{1-\mu^2}\vartheta_\ell,\vartheta_\ell)_\mu(\pm 2\cos\Phi\vartheta_\ell,\vartheta_\ell)_{\pm\Phi}^{s^y,s^y}$
$\underline{\underline{T}}_{\ell S,\ell}$	$\langle \underline{\Psi}_{\ell S}, \underline{\Psi}_\ell^T \rangle_{+\ell}$	$(\vartheta_\ell,\vartheta_\ell)_{\delta y_q}(2\vartheta_\ell,\vartheta_\ell)_\Phi(\pm\mu\vartheta_\ell,\vartheta_\ell)_{\pm\mu}^{s^x,i}$ + $(\vartheta_\ell,\vartheta_\ell)_{\Delta x_p}(\sqrt{1-\mu^2}\vartheta_\ell,\vartheta_\ell)_\mu(\pm 2\cos\Phi\vartheta_\ell,\vartheta_\ell)_{\pm\Phi}^{s^y,j}$

Table 4-2.(cont'd.) Two-Dimensional Projection Matrices and their Inner Products

matrix	definition	inner products
$\underline{\underline{T}}_{SS}$	$\langle \underline{\Psi}_S, \underline{\Psi}_S^T \rangle_{+\ell}$	$(\Psi,\Psi)_{\Delta y_q} (2\Psi,\Psi)_{\Phi} (\pm\mu\Psi,\hat{\psi}_\ell)^{s^x, s^x}_{\pm\mu}$ $+ (\Psi,\Psi)_{\Delta x_p} (\sqrt{1-\mu^2}\Psi,\Psi)_{\mu} (\pm 2\cos\Phi\Psi,\Psi)^{s^y, s^y}_{\pm\Phi}$
$\underline{\underline{T}}_{S,\ell S}$	$\langle \underline{\Psi}_S, \underline{\Psi}_{\ell S}^T \rangle_{+\ell}$	$(\Psi,\hat{\psi}_\ell)_{\Delta y_q} (2\Psi,\hat{\psi}_\ell)_{\Phi} (\pm\mu\Psi,\hat{\psi}_\ell)^{s^x, s^x}_{\pm\mu}$ $+ (\Psi,\hat{\psi}_\ell)_{\Delta x_p} (\sqrt{1-\mu^2}\Psi,\hat{\psi}_\ell)_{\mu} (\pm 2\cos\Phi\Psi,\hat{\psi}_\ell)^{s^y, s^y}_{\pm\Phi}$
$\underline{\underline{T}}_{VV}$	$(\underline{\Psi}, \underline{\Psi}^T)_\ell$	$(\Psi,\Psi)_{\Delta x_p} (\Psi,\Psi)_{\Delta y_q} (\Psi,\Psi)_{\mu} (2\Psi,\Psi)_{\Phi}$
$\underline{\underline{T}}_{V,\ell}$	$[\underline{\underline{T}}_{\ell,V}]^T$	$(\hat{\psi}_\ell,\Psi)_{\Delta x_p} (\hat{\psi}_\ell,\Psi)_{\Delta y_q} (\hat{\psi}_\ell,\Psi)_{\mu} (2\hat{\psi}_\ell,\Psi)_{\Phi}$

$$\underline{\underline{R}}_{S\leftarrow S} = \begin{bmatrix} \underline{\underline{r}}_1^{\ell} & \underline{\underline{s}}_{12}^{\ell} & \underline{\underline{t}}_{13}^{\ell} & \underline{\underline{s}}_{14}^{\ell} \\ \underline{\underline{s}}_{21}^{\ell} & \underline{\underline{r}}_2^{\ell} & \underline{\underline{s}}_{23}^{\ell} & \underline{\underline{t}}_{24}^{\ell} \\ \underline{\underline{t}}_{31}^{\ell} & \underline{\underline{s}}_{22}^{\ell} & \underline{\underline{r}}_3^{\ell} & \underline{\underline{s}}_{34}^{\ell} \\ \underline{\underline{s}}_{41}^{\ell} & \underline{\underline{t}}_{42}^{\ell} & \underline{\underline{s}}_{43}^{\ell} & \underline{\underline{r}}_4^{\ell} \end{bmatrix} \tag{4.28}$$

The subscript '12', for example, indicates neutrons exiting side 1 that originally entered side 2.

Iterative Solution Method

Recall that the $\underline{\underline{H}}$ matrix is of the form,

$$\underline{\underline{H}} = \underline{\underline{H}}_{cont} + \underline{\underline{H}}_{BC}$$

where the continuity matrix is block tridiagonal

$$\underline{\underline{H}}_{cont} = \begin{bmatrix} \underline{\underline{H}}_D & \underline{\underline{H}}_U & 0 & \cdot & \cdot & \cdot & \cdot \\ \underline{\underline{H}}_L & \underline{\underline{H}}_D & \underline{\underline{H}}_U & 0 & \cdot & \cdot & \cdot \\ 0 & \underline{\underline{H}}_L & \underline{\underline{H}}_D & \underline{\underline{H}}_U & \cdot & \cdot & \cdot \\ \cdot & \cdot & \cdot & \cdot & \cdot & \cdot & \cdot \end{bmatrix} \tag{4.29}$$

The block components are defined

$$\underline{\underline{H}}_D = \begin{bmatrix} 0 & \underline{\underline{P}}_{24} & 0 & . & . & . & . \\ \underline{\underline{P}}_{42} & 0 & \underline{\underline{P}}_{24} & 0 & . & . & . \\ 0 & \underline{\underline{P}}_{42} & 0 & \underline{\underline{P}}_{24} & . & . & . \\ . & . & . & . & . & . & . \end{bmatrix}$$

$$\underline{\underline{H}}_U = \begin{bmatrix} \underline{\underline{P}}_{31} & 0 & . & . & . \\ 0 & \underline{\underline{P}}_{31} & 0 & . & . \\ . & 0 & \underline{\underline{P}}_{31} & . & . \\ . & . & . & . & . \end{bmatrix}$$

and

$$\underline{\underline{H}}_L = \begin{bmatrix} \underline{\underline{P}}_{13} & 0 & . & . & . \\ 0 & \underline{\underline{P}}_{13} & 0 & . & . \\ . & 0 & \underline{\underline{P}}_{13} & . & . \\ . & . & . & . & . \end{bmatrix}$$

where the permutation matrices contain the identity matrix at unique locations:

$$\underline{\underline{P}}_{13} = \begin{bmatrix} 0 & 0 & \underline{\underline{I}} & 0 \\ 0 & 0 & 0 & 0 \\ 0 & 0 & 0 & 0 \\ 0 & 0 & 0 & 0 \end{bmatrix}$$

$$\underline{\underline{P}}_{24} = \begin{bmatrix} 0 & 0 & 0 & 0 \\ 0 & 0 & 0 & \underline{\underline{I}} \\ 0 & 0 & 0 & 0 \\ 0 & 0 & 0 & 0 \end{bmatrix}$$

$$\underline{\underline{P}}_{31} = \begin{bmatrix} 0 & 0 & 0 & 0 \\ 0 & 0 & 0 & 0 \\ \underline{\underline{I}} & 0 & 0 & 0 \\ 0 & 0 & 0 & 0 \end{bmatrix}$$

$$\underline{\underline{P}}_{42} = \begin{bmatrix} 0 & 0 & 0 & 0 \\ 0 & 0 & 0 & 0 \\ 0 & 0 & 0 & 0 \\ 0 & \underline{\underline{I}} & 0 & 0 \end{bmatrix}$$

The boundary condition matrix the sum of two parts,

$$\underline{\underline{H}}_{BC} = \underline{\underline{H}}_{refl} + \underline{\underline{H}}_{per}$$

that account for reflection and periodicity, respectively. The reflection matrix is the sum of four matrices, one for

each side for which a reflecting boundary condition is specified,

$$\underline{\underline{H}}_{refl} = \underline{\underline{H}}^{1}_{refl} + \underline{\underline{H}}^{2}_{refl} + \underline{\underline{H}}^{3}_{refl} + \underline{\underline{H}}^{4}_{refl} \tag{4.30}$$

where

$$\underline{\underline{H}}^{1}_{refl} = \begin{bmatrix} \underline{\underline{H}}^{1} & 0 & . & . \\ 0 & 0 & . & . \\ . & . & . & . \\ . & . & . & . \end{bmatrix} \tag{4.31}$$

$$\underline{\underline{H}}^{1} = \begin{bmatrix} \underline{\underline{H}}^{1'} & 0 & . & . \\ 0 & \underline{\underline{H}}^{1'} & 0 & . \\ . & . & . & . \\ . & . & . & . \end{bmatrix}$$

$$\underline{\underline{H}}^{1'} = \begin{bmatrix} \underline{\underline{H}}^{1''} & 0 & 0 & 0 \\ 0 & 0 & 0 & 0 \\ 0 & 0 & 0 & 0 \\ 0 & 0 & 0 & 0 \end{bmatrix}$$

$$\underline{\underline{H}}^{2'} = \begin{bmatrix} 0 & 0 & 0 & 0 \\ 0 & \underline{\underline{H}}^{2''} & 0 & 0 \\ 0 & 0 & 0 & 0 \\ 0 & 0 & 0 & 0 \end{bmatrix}$$

$$\underline{\underline{H}}^{1''} = \begin{bmatrix} 0 & 0 & . & . & . & 0 & \underline{\underline{I}} \\ 0 & 0 & . & . & . & \underline{\underline{I}} & 0 \\ . & . & & & & & . \\ 0 & \underline{\underline{I}} & & & & & . \\ \underline{\underline{I}} & 0 & . & . & . & . & 0 \end{bmatrix}$$

For side 2

$$\underline{\underline{H}}^{2}_{refl} = \begin{bmatrix} \underline{\underline{H}}^{2} & 0 & . & . \\ 0 & \underline{\underline{H}}^{2} & 0 & . \\ . & . & . & . \\ . & . & . & . \end{bmatrix} \qquad (4.32)$$

$$\underline{\underline{H}}^{2} = \begin{bmatrix} 0 & . & . & . & . \\ . & . & . & . & . \\ . & . & . & 0 & 0 \\ . & . & . & 0 & \underline{\underline{H}}^{2'} \end{bmatrix}$$

$$\underline{\underline{H}}^{2''} = \begin{bmatrix} \underline{\underline{P}} & 0 & . & . \\ 0 & \underline{\underline{P}} & 0 & . \\ . & . & . & . \\ . & . & . & . \end{bmatrix}$$

where $\underline{\underline{P}}$ was defined earlier. The reflection matrices for sides 3 and 4 are

$$\underline{\underline{H}}^{3}_{refl} = \begin{bmatrix} 0 & . & . & . & . \\ . & . & . & . & . \\ . & . & . & 0 & 0 \\ . & . & . & 0 & \underline{\underline{H}}^{3} \end{bmatrix} \tag{4.33}$$

$$\underline{\underline{H}}^{3} = \begin{bmatrix} \underline{\underline{H}}^{3'} & 0 & . & . \\ 0 & \underline{\underline{H}}^{3'} & 0 & . \\ . & . & . & . \\ . & . & . & . \end{bmatrix}$$

$$\underline{\underline{H}}^{3'} = \begin{bmatrix} 0 & 0 & 0 & 0 \\ 0 & 0 & 0 & 0 \\ 0 & 0 & \underline{\underline{H}}^{1''} & 0 \\ 0 & 0 & 0 & 0 \end{bmatrix}$$

and

$$\underline{\underline{H}}^{4}_{refl} = \begin{bmatrix} \underline{\underline{H}}^{4} & 0 & . & . \\ 0 & \underline{\underline{H}}^{4} & 0 & . \\ . & . & . & . \\ . & . & . & . \end{bmatrix} \tag{4.34}$$

$$\underline{\underline{H}}^{4} = \begin{bmatrix} \underline{\underline{H}}^{4'} & 0 & . & . \\ 0 & 0 & . & . \\ . & . & . & . \\ . & . & . & . \end{bmatrix}$$

$$\underline{\underline{H}}^{4'} = \begin{bmatrix} 0 & 0 & 0 & 0 \\ 0 & 0 & 0 & 0 \\ 0 & 0 & 0 & 0 \\ 0 & 0 & 0 & \underline{\underline{H}}^{2''} \end{bmatrix}$$

The periodic boundary condition matrix is the sum of two matrices if periodicity is desired in both x- and y-directions,

$$\underline{\underline{H}}_{per} = \underline{\underline{H}}^{x}_{per} + \underline{\underline{H}}^{y}_{per} \tag{4.35}$$

where

$$\underline{\underline{H}}^{x}_{per} = \begin{bmatrix} 0 & . & . & . & \underline{\underline{H}}^{13}_{per} \\ . & . & . & . & . \\ . & . & . & . & . \\ \underline{\underline{H}}^{31}_{per} & . & . & . & 0 \end{bmatrix} \tag{4.36}$$

$$\underline{\underline{H}}^{31}_{per} = \begin{bmatrix} \underline{\underline{P}}_{31} & 0 & . & . & . \\ 0 & \underline{\underline{P}}_{31} & 0 & . & . \\ . & 0 & \underline{\underline{P}}_{31} & . & . \\ . & . & . & . & . \end{bmatrix}$$

$$\underline{\underline{H}}^{13}_{per} = \begin{bmatrix} \underline{\underline{P}}_{13} & 0 & . & . & . \\ 0 & \underline{\underline{P}}_{13} & 0 & . & . \\ . & 0 & \underline{\underline{P}}_{13} & . & . \\ . & . & . & . & . \end{bmatrix}$$

and

$$\underline{\underline{H}}^{Y}_{per} = \begin{bmatrix} \underline{\underline{H}}^{Y} & 0 & . & . & . \\ 0 & \underline{\underline{H}}^{Y} & 0 & . & . \\ . & 0 & \underline{\underline{H}}^{Y} & . & . \\ . & . & . & . & . \end{bmatrix} \qquad (4.37)$$

$$\underline{\underline{H}}^{Y} = \begin{bmatrix} 0 & . & . & . & \underline{\underline{P}}^{42} \\ . & . & . & . & . \\ . & . & . & . & . \\ \underline{\underline{P}}^{24} & . & . & . & 0 \end{bmatrix}$$

The product $\underline{\underline{HR}}_{S\leftarrow S}$, from which various iteration schemes can be formulated, has a block tridiagonal structure (if $\underline{\underline{H}}_{BC}=0$):

$$\underline{\underline{HR}}_{S\leftarrow S} = \begin{bmatrix} \underline{\underline{B}}_D^1 & \underline{\underline{B}}_U^2 & 0 & . & . & . & . & . \\ \underline{\underline{B}}_L^1 & \underline{\underline{B}}_D^2 & \underline{\underline{B}}_U^3 & 0 & . & . & . & . \\ 0 & \underline{\underline{B}}_L^2 & \underline{\underline{B}}_D^3 & \underline{\underline{B}}_U^4 & . & . & . & . \\ . & . & . & . & . & . & . & . \\ . & . & . & . & . & . & \underline{\underline{B}}_L^{p_{max-1}} & \underline{\underline{B}}_D^{p_{max}} \end{bmatrix} \qquad (4.38)$$

with

$$\underline{\underline{B}}_D^p = \begin{bmatrix} 0 & \underline{b}_4^{p2} & 0 & . & . & . & . & . \\ \underline{b}_2^{p1} & 0 & \underline{b}_4^{p3} & 0 & . & . & . & . \\ 0 & \underline{b}_2^{p2} & 0 & \underline{b}_4^{p4} & . & . & . & . \\ . & 0 & \underline{b}_2^{p3} & 0 & \underline{b}_4^{p5} & . & . & . \\ . & . & . & . & . & . & . & . \\ . & . & . & . & . & . & \underline{b}_2^{pq_{max}} & 0 \end{bmatrix}$$

$$\underline{\underline{B}}_U^p = \begin{bmatrix} \underline{\underline{b}}_1^{p1} & 0 & . & . & . & . \\ 0 & \underline{\underline{b}}_1^{p2} & 0 & . & . & . \\ . & . & . & . & . & . \\ . & . & . & . & 0 & \underline{\underline{b}}_1^{pq_{max}} \end{bmatrix}$$

$$\underline{\underline{B}}_L^p = \begin{bmatrix} \underline{\underline{b}}_3^{p1} & 0 & . & . & . & . \\ 0 & \underline{\underline{b}}_3^{p2} & 0 & . & . & . \\ . & . & . & . & . & . \\ . & . & . & . & 0 & \underline{\underline{b}}_3^{pq_{max}} \end{bmatrix}$$

where

$$\underline{\underline{b}}_1^{pq} = \underline{\underline{b}}_1^{\ell} = \begin{bmatrix} 0 & 0 & 0 & 0 \\ 0 & 0 & 0 & 0 \\ \underline{\underline{r}}_1^{\ell} & \underline{\underline{s}}_{12}^{\ell} & \underline{\underline{t}}_{13}^{\ell} & \underline{\underline{s}}_{14}^{\ell} \\ 0 & 0 & 0 & 0 \end{bmatrix}$$

$$\underline{\underline{b}}_2^{pq} = \underline{\underline{b}}_2^{\ell} = \begin{bmatrix} 0 & 0 & 0 & 0 \\ 0 & 0 & 0 & 0 \\ 0 & 0 & 0 & 0 \\ \underline{\underline{s}}_{21}^{\ell} & \underline{\underline{r}}_2^{\ell} & \underline{\underline{s}}_{23}^{\ell} & \underline{\underline{t}}_{24}^{\ell} \end{bmatrix}$$

$$\underline{\underline{b}}_3^{pq} = \underline{\underline{b}}_3^{\ell} = \begin{bmatrix} \underline{\underline{t}}_{31}^{\ell} & \underline{\underline{s}}_{32}^{\ell} & \underline{\underline{r}}_3^{\ell} & \underline{\underline{s}}_{34}^{\ell} \\ 0 & 0 & 0 & 0 \\ 0 & 0 & 0 & 0 \\ 0 & 0 & 0 & 0 \end{bmatrix}$$

$$\underline{\underline{b}}_4^{pq} = \underline{\underline{b}}_4^{\ell} = \begin{bmatrix} 0 & 0 & 0 & 0 \\ \underline{\underline{s}}_{41}^{\ell} & \underline{\underline{t}}_{42}^{\ell} & \underline{\underline{s}}_{43}^{\ell} & \underline{\underline{r}}_4^{\ell} \\ 0 & 0 & 0 & 0 \\ 0 & 0 & 0 & 0 \end{bmatrix}$$

Thus

$$\underline{\underline{HR}}_{S\leftarrow S} = \underline{\underline{L}}_{HR} + \underline{\underline{U}}_{HR}$$

The resulting Gauss-Seidel method

$$\underline{\phi}_{in}^{S(n)} = \underline{\underline{L}}_{HR}\underline{\phi}_{in}^{S(n)} + \underline{\underline{U}}_{HR}\underline{\phi}_{in}^{S(n-1)} + \underline{\phi}_{SV} \qquad (4.39)$$

results in a sweep through the regions as pictured in Fig. 4-15(a), i.e. sweeping each column bottom to top starting with the left-most column. By interchanging $\underline{\underline{L}}_{HR}$ and $\underline{\underline{U}}_{HR}$ so that $\underline{\underline{U}}_{HR}$ multiplies the updated interface flux vector,

$$\underline{\phi}_{in}^{S(n)} = \underline{\underline{U}}_{HR}\underline{\phi}_{in}^{S(n)} + \underline{\underline{L}}_{HR}\underline{\phi}_{in}^{S(n-1)} + \underline{\phi}_{SV} \qquad (4.40)$$

the sweep scheme labeled 'b' results. Sweeps 'a' and 'd' result if the regions are numbered from top to bottom rather than bottom to top before assembling $\underline{\underline{H}}$ and $\underline{\underline{R}}_{S\leftarrow S}$. By imposing other numbering conventions, the other sweeps can be obtained. But for the purposes of this work there is no difference between schemes 'a' and 'c', 'b' and 'f', 'c' and 'g', 'd' and 'h'. That is, whether the rows are first swept

or the columns is of no consequence to the numerical results.

The procedure chosen here is to use schemes 'a', 'b', 'c', and 'd' in a cyclical fashion. If a problem consists of purely absorbing material ($\Sigma_s=0$), a converged solution can be found with at most one iteration in each of the four directions because, as was the case in one dimension, the reflecting sub-matrices, $\underline{\underline{r}}^{\ell}$, vanish.

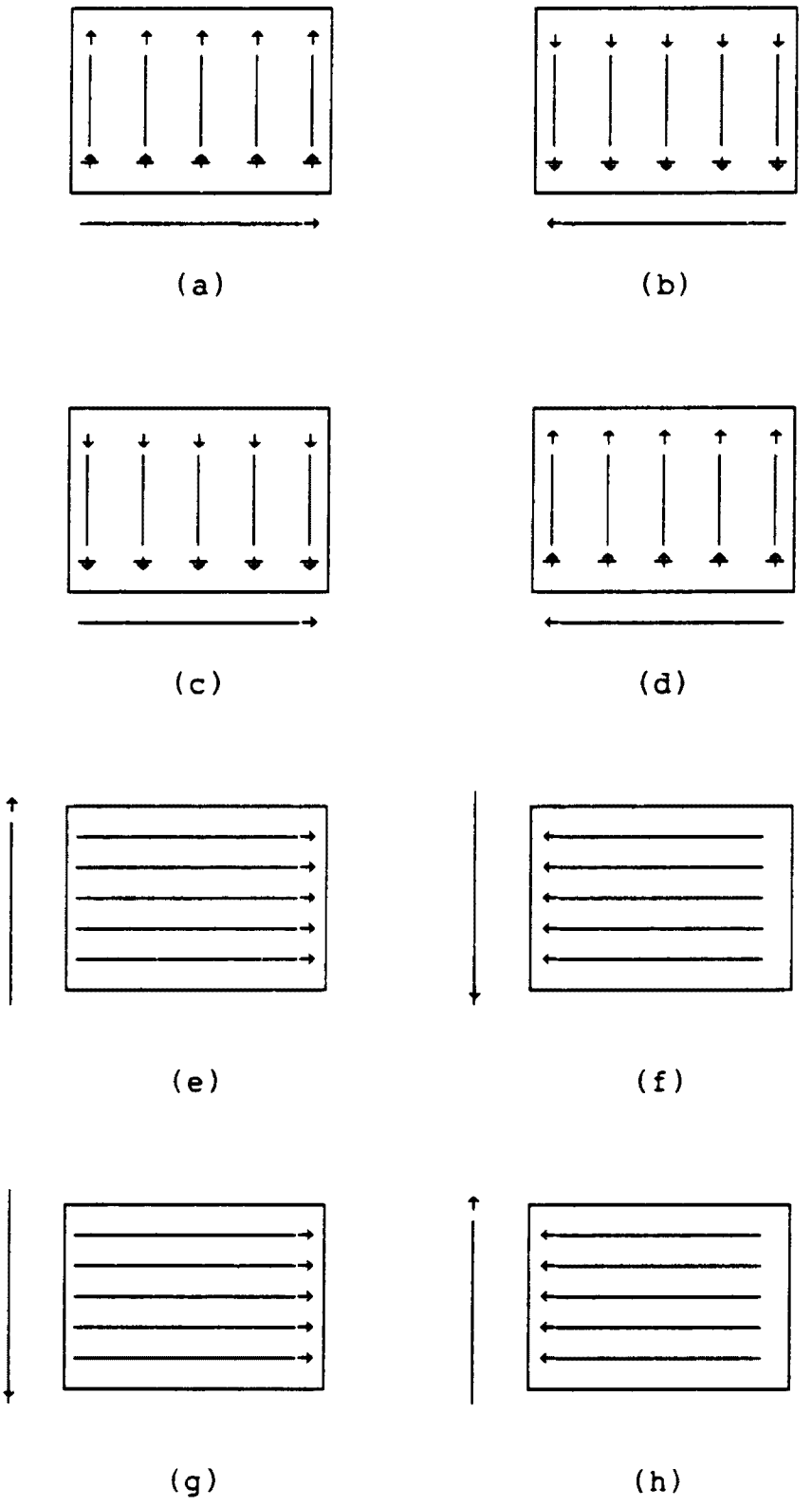


Fig. 4-15. Two-dimensional sweep schemes.

CHAPTER V

COMPUTATIONAL TESTING

The specific means of implementing the method, as discussed in Chapter IV, have been incorporated in two series of computer codes--one for the analysis of one-dimensional problems and the other for two-dimensional problems. The one-dimensional method served primarily as a testing ground of fundamental concepts for the potentially more rewarding two-dimensional method. In this chapter, the organization of these codes will be discussed. In addition, a collection of test problems, in both one and two dimensions will be described together with the results of the analysis of these problems by the response matrix method. The test problems enable verification of the coding and demonstration of the capability of the method. They provide a means to study the effects of parameters such as response matrix region size and the size of the local and global meshes in space and angle on solution accuracy. Other issues addressed are the computational efficiency of the method and the relative merits of the iteration schemes discussed in previous chapters.

Following this chapter is the final chapter presenting a summary of conclusions drawn from the current chapter and recommendations for future study.

Computer Code Organization

Two series of computer codes have been programmed in FORTRAN66 and are operational on the AMDAHL 5860 of the Michigan Terminal System (MTS), the operating system of The University of Michigan. The purpose of the two series are identical: generate response matrices and then find the global neutron distribution of a physical configuration. One handles one-dimensional problems, the other two-dimensional problems. Each series consists of four programs. Three programs are used to generate the response matrices; the fourth accepts response matrices as input and finds the global solution by the iteration technique described in Chapter II.

The interaction of the three codes which generate response matrices is depicted in Fig. 5-1. Using a common input file as their data base, the codes

1) generate the finite element matrix $\underline{\underline{A}}$ on the local mesh,

2) invert $\underline{\underline{A}}$, and

3) find the four global response matrices by projecting $\underline{\underline{A}}^{-1}$ from the local mesh to the global mesh.

Data flows from one code to another via standardized binary files.

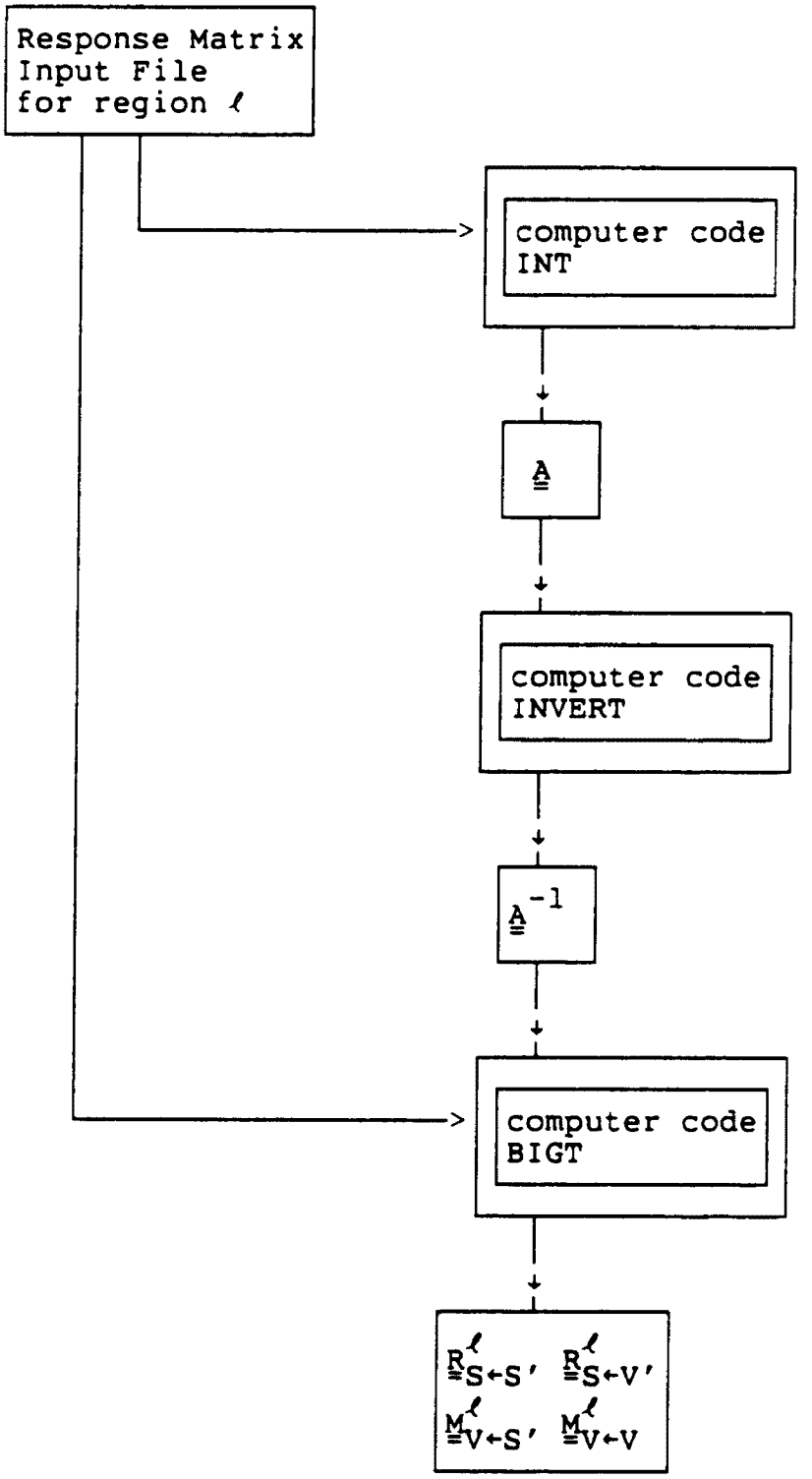


Fig. 5-1. Computer codes used to generate response matrices for region ℓ.

The global solution is found by specifying the problem configuration (iteration input file), reading in the response matrices, and iterating until a converged solution is obtained. Fig. 5-2 depicts this procedure.

One-Dimensional Numerical Experimentation

Four different one-dimensional test problems are analyzed here: two are problems with strong heterogeneities, another is a repeating lattice, and the fourth is a series of homogeneous eigenvalue problems

Reed's Problem

Reed's problem [Ree71], as depicted in Fig. 5-3, was originally devised to test differencing schemes of discrete ordinates codes. It is a problem of four different material regions with a non-uniform, isotropic source distribution, a reflecting boundary condition on the left, and a vacuum on the right.

Fig. 5-4 is a plot of the scalar flux distribution in Reed's problem obtained with the Monte Carlo code TART [Ple76]. The solution was provided by the authors of TART. This solution shall be considered a benchmark. The obvious features of this profile includes a peak at the source zone of the scattering material, a plateau in the void due to neutrons traveling from the scatterer on the right to the gray and black regions on the left, a depression to nearly zero in the sourceless gray region as the left-ward travel-

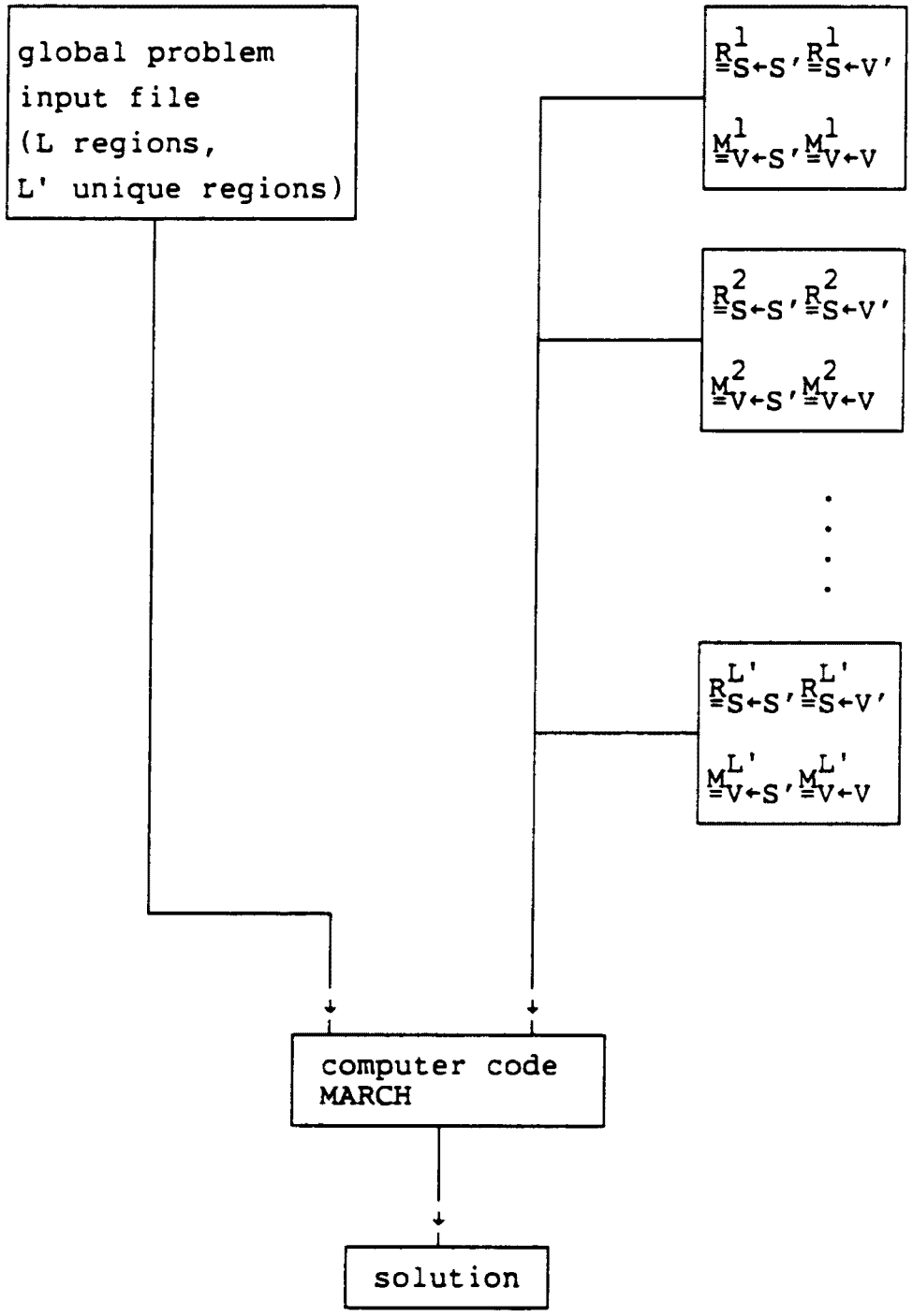
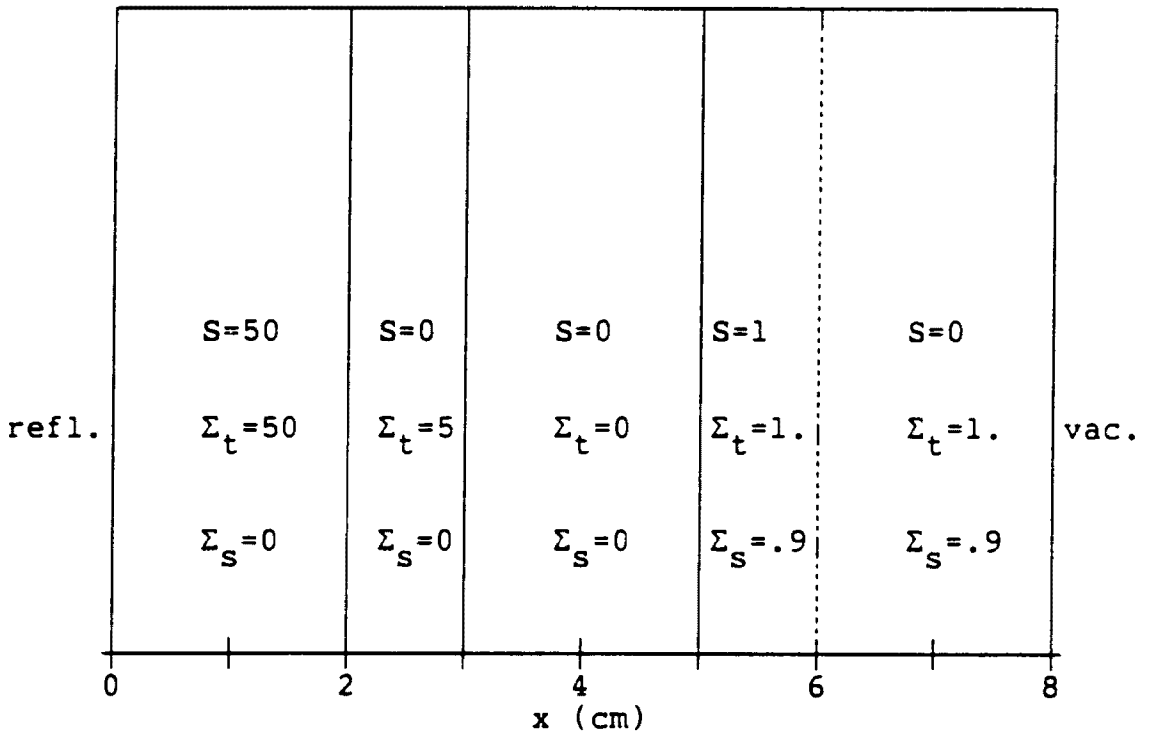


Fig. 5-2. Use of global solution computer codes.



(units: Σ_t, Σ_s, S [cm^{-1}])

Fig. 5-3. Reed's Problem.

ing neutrons are absorbed, and another plateau of value 1.0 in the intensely absorbing region with the large source. Examination of the angular flux profiles indicates that neutrons born in the region on the left are also absorbed there. For this reason, the flux distribution in both the void and gray region is due to neutrons from the scattering source. The flux, therefore, is extremely anisotropic throughout the problem, except in the scattering region and in the black absorbing region where the source itself forces isotropy.

Reed's problem has been analyzed using FTRAN [Mar77], the conventional one-dimensional finite element code, and using the response matrix method with two different approaches: (1) scattering included in the $\underline{\underline{A}}$ matrix and hence the response matrices, and (2) $\underline{\underline{A}}$ including only absorption with the scattering source found in the outer iteration from the volumetric flux distribution. In case (1) the scattering operator is retained on the left side of the transport equation; in case (2) the operator is moved to the right. The local and global mesh structures are identical for both cases, with a spacing of 0.25 cm. The scalar flux profile (Fig. 5-5) and Table 5-1, which lists the errors of the finite element results with respect to the TART calculation, indicate that the three cases are nearly identical. Furthermore, they reproduce the benchmark results very well. The errors listed in Table 5-1 and succeeding tables of this type are defined

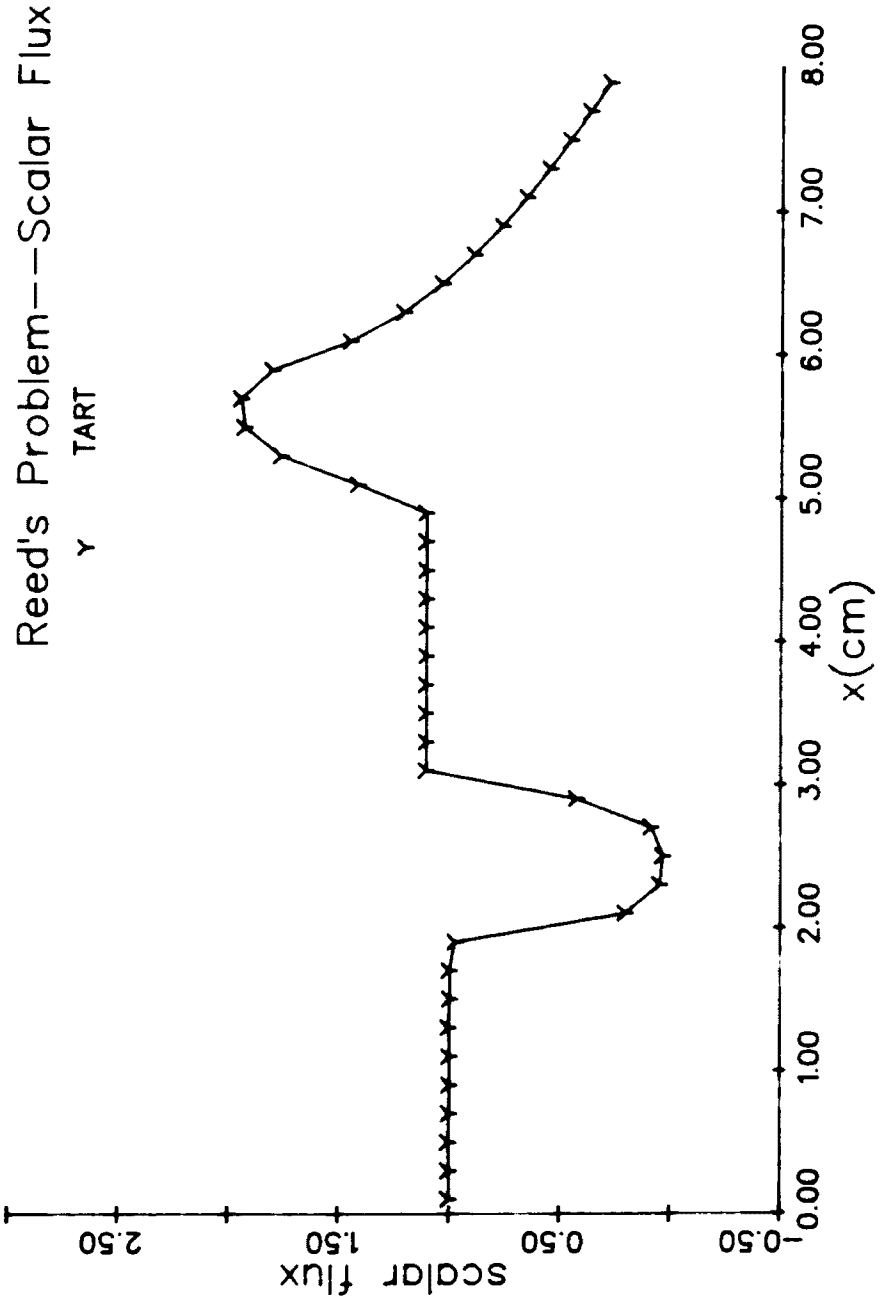


Fig. 5-4. Reed's Problem: Monte Carlo benchmark.

$$\text{relative error} = \frac{\int_{x_a}^{x_b} [\phi_{ref}(x) - \phi(x)]dx}{\int_{x_a}^{x_b} \phi_{ref}(x)dx}$$

and

$$\text{RMS error} = \frac{\left[\int_{x_a}^{x_b} [\phi_{ref}(x) - \phi(x)]^2 dx\right]^{1/2}}{\left[\int_{x_a}^{x_b} [\phi_{ref}(x)]^2 dx\right]^{1/2}}$$

where $\phi_{ref}(x)$ is the reference scalar flux (TART), $\phi(x)$ is the scalar flux in question, and x_a and x_b are determined by the region definitions. The flux found is assumed to vary linearly between the points plotted in Fig. 5-4. The regions of Table 5-1 are the material regions as depicted in Fig. 5-3 numbered from left to right, with the scattering region divided into source and sourceless regions. For all of the response matrix cases listed in Table 5-1, a set of response matrices were generated for each region 1 cm wide. Five such sets were necessary for Reed's problem.

Also shown in Table 5-1 are the errors for two cases in which the global mesh is 0.5 cm (cases 5/3 and 3/3). The local mesh size, however, is 0.25 cm for 5/3 and 0.5 for 3/3, i.e. for case 5/3 a fine mesh local solution is projected onto a coarser global mesh. The RMS errors demonstrate that although both the coarse mesh solutions provide less agree-

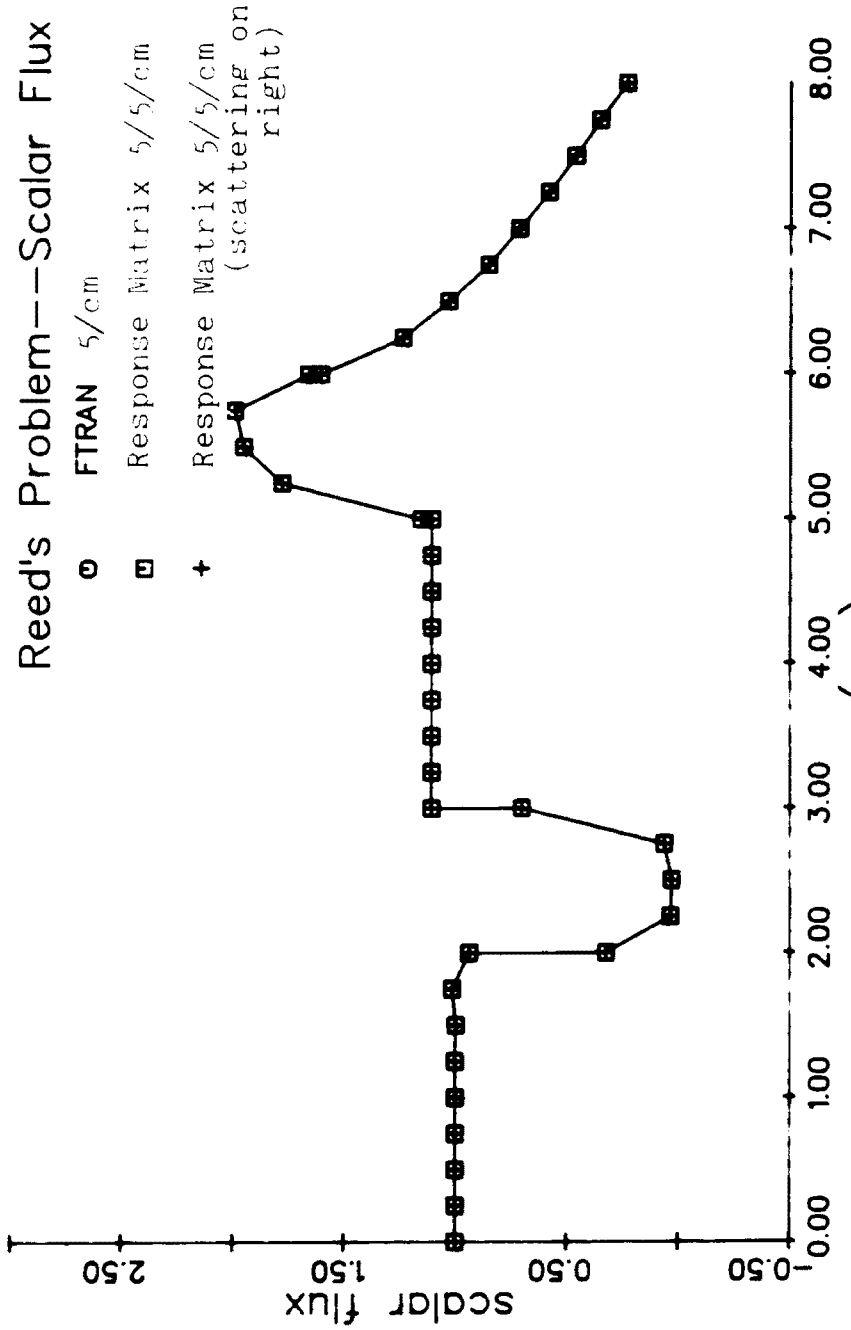


Fig. 5-5. Reed's Problem: FTRAN and response matrix (mesh size = 0.25cm)

Table 5-1. Errors in Scalar Flux for Reed's Problem

(Errors with respect to Monte Carlo benchmark;
angular support points: 6;
Response Matrix convergence criteria: 10^{-5})

case	error					
	total	region				
		1	2	3	4	5
			relative error			
FTRAN[1]	0.069%	-0.002%	-3.312%	0.039%	0.722%	-0.216%
5/5[2]	0.069%	-0.002%	-3.311%	0.039%	0.723%	-0.216%
5/5[3]	0.067%	-0.022%	-3.313%	0.036%	0.720%	-0.220%
5/3	0.055%	-0.024%	-6.142%	0.038%	0.953%	-0.294%
3/3	0.274%	-0.025%	-5.524%	0.621%	1.061%	-0.243%
			RMS error			
FTRAN	1.169%	0.434%	8.522%	0.039%	1.556%	0.789%
5/5	1.169%	0.434%	8.522%	0.035%	1.556%	0.788%
5/5[3]	1.168%	0.434%	8.521%	0.036%	1.555%	0.780%
5/3	2.860%	0.483%	29.17 %	0.038%	3.128%	1.424%
3/3	3.317%	0.468%	26.21 %	0.621%	4.414%	1.672%

[1]FTRAN mesh structure: 5 support points/cm
[2]5/3 indicates Response Matrix mesh structure of 5 local support points/cm and 3 global support points/cm
[3]scattering source is calculated in outer, not inner, loop

ment with the benchmark than the fine mesh solution (especially in the gray region, 2, although the per cent errors here are misleading because the flux itself is nearly zero), the 5/3 solution is in better agreement than the 3/3 solution in the void and region 4, the source-scattering region. Projecting the solution from a fine mesh, therefore, improves the results of a coarse mesh calculation. Fig. 5-6 is a plot of these results.

To further demonstrate the local/global projection method, a series of coarse mesh calculations with a spacing of 1.0 cm were performed, as listed in Table 5-2. In all of the response matrix calculations, a global mesh of 2 support points per cm is used with each response matrix region spanning 1 cm. The local mesh, however, varies from a fine mesh of 5/cm to coarser meshes of 3/cm and 2/cm. The case in which the local and global mesh are identical (2/2) gives nearly identical results as the FTRAN calculation performed with the same 1 cm mesh spacing. With decreased local mesh size, however, better agreement is seen with the benchmark, even though the same coarse global mesh is used throughout. The overall improvement is not dramatic but in several regions--the void, in particular, and region 4--it is significant. Differences between the cases are apparent in the scalar flux profiles of Fig. 5-7.

The results obtained by the response matrix method appear to be independent of the response matrix region size if the mesh spacing is held constant. The errors listed in

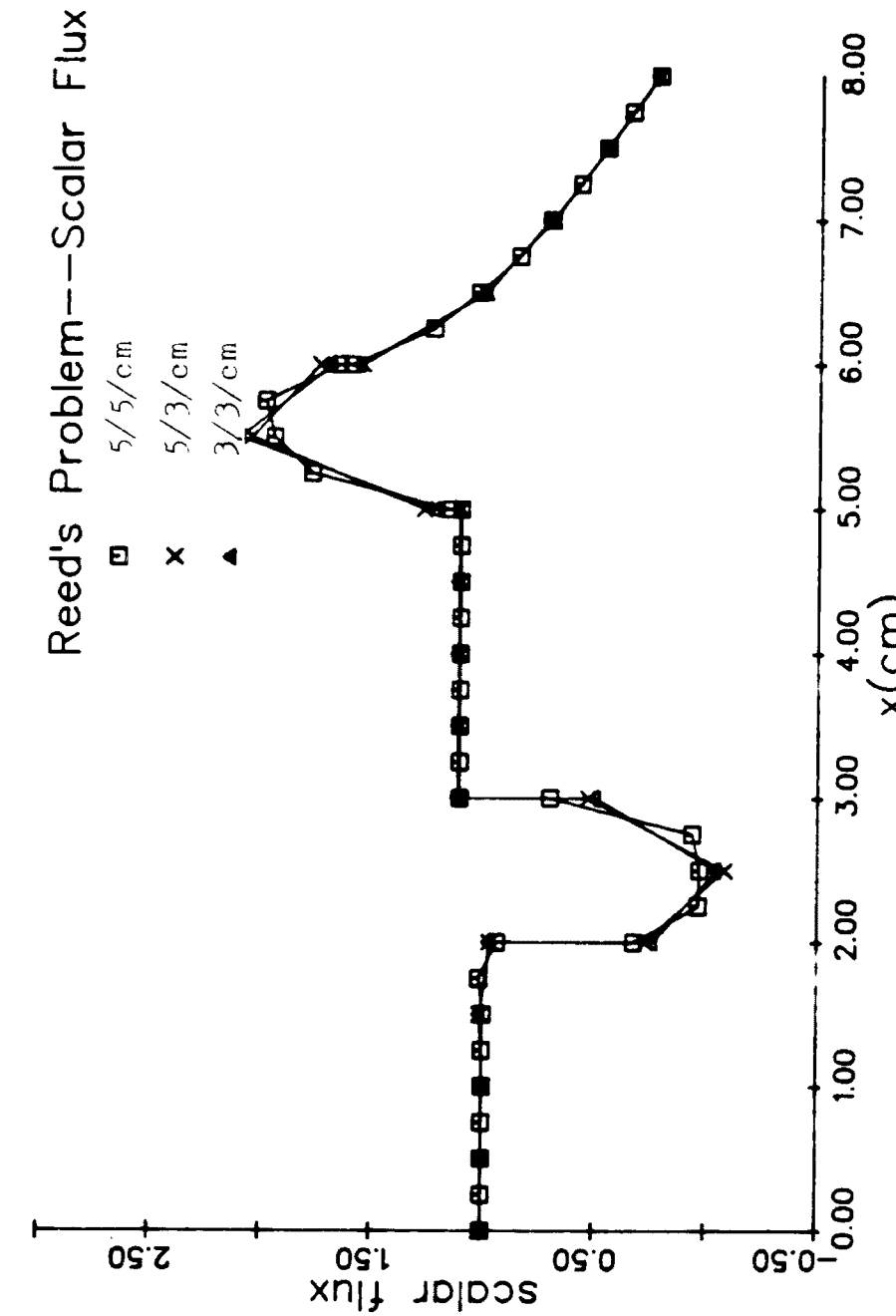


Fig. 5-6. Reed's Problem: response matrix (mesh size = 0.5 and 0.25 cm)

Table 5-2. Errors in Scalar Flux for Coarse Mesh Reed's Problem: Constant Global Mesh

(Errors with respect to Monte Carlo benchmark; angular support points: 6; Response Matrix convergence criteria: 10^{-5})

case	error					
	total	region				
		1	2	3	4	5
relative error						
FTRAN[1]	-2.190%	-0.046%	8.132%	-2.104%	-5.918%	-1.700%
2/2[2]	-2.104%	-0.055%	8.133%	-2.126%	-5.958%	-1.176%
3/2	0.252%	-0.004%	-0.249%	-0.621%	0.334%	-0.011%
5/2	0.071%	-0.004%	-0.064%	-0.038%	0.342%	-0.101%
RMS error						
FTRAN	7.392%	0.604%	60.39 %	2.104%	9.579%	3.783%
2/2	7.349%	0.569%	60.39 %	2.126%	9.603%	3.030%
3/2	6.322%	0.557%	60.04 %	0.621%	7.565%	2.685%
5/2	6.313%	0.556%	60.03 %	0.038%	7.565%	2.691%

[1] FTRAN mesh structure: 2 support points/cm
[2] 3/2 indicates Response Matrix mesh structure of 3 local support points/cm and 2 global support points/cm

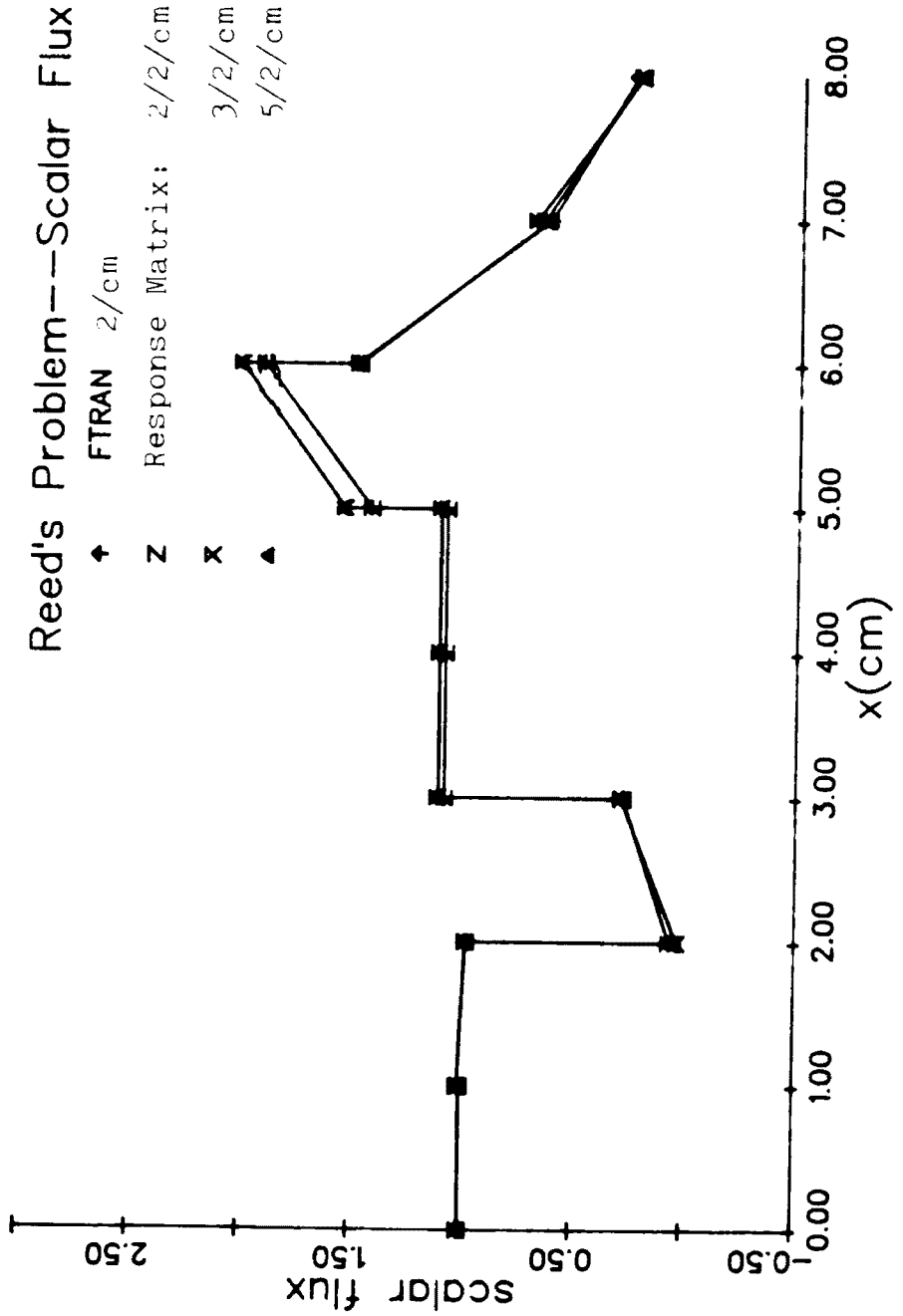


Fig. 5-7. Reed's Problem: coarse mesh (1.0 cm).

Table 5-3 and the flux profiles of Fig. 5-8 indicate that nearly identical results are obtained with response matrix regions varying from as large as 2 cm to as small as 0.25 cm. In all cases the local and global mesh are identical with 0.25 cm between support points.

In all the calculations described above, linear basis functions were used in space and angle. The cases presented in Table 5-4 provide a comparison between linear and quadratic basis functions. For the cases marked "quad.", quadratic basis functions are used in both phase-space dimensions. Linear basis functions are used similarly. The cases plotted in Fig. 5-9 use identical local and global mesh spacing. Fig. 5-10 shows the flux profiles obtained with response matrices with which a local-to-global projection has been performed. In both situations the quadratic results are slightly superior to the linear results.

Table 5-3. Errors in Scalar Flux for Fine Mesh Reed's Problem

(Errors with respect to Monte Carlo benchmark;
angular support points: 6;
spatial support points: 5/cm;
convergence criteria: 10^{-5})

case	error					
	total	region				
		1	2	3	4	5
relative error						
9:9,5:5[1]	0.069%	-0.002%	-3.312%	0.038%	0.722%	-0.213%
5:5	0.069%	-0.002%	-3.311%	0.039%	0.723%	-0.216%
2:2	0.072%	-0.053%	-2.975%	0.078%	0.720%	-0.226%
RMS error						
9:9,5:5	1.169%	0.434%	8.522%	0.038%	1.555%	0.789%
5:5	1.169%	0.434%	8.522%	0.035%	1.556%	0.788%
2:2	1.064%	0.249%	7.724%	0.078%	1.422%	0.781%

[1]5:3 indicates Response Matrix mesh structure of 5 local support points/region and 3 global support points/region

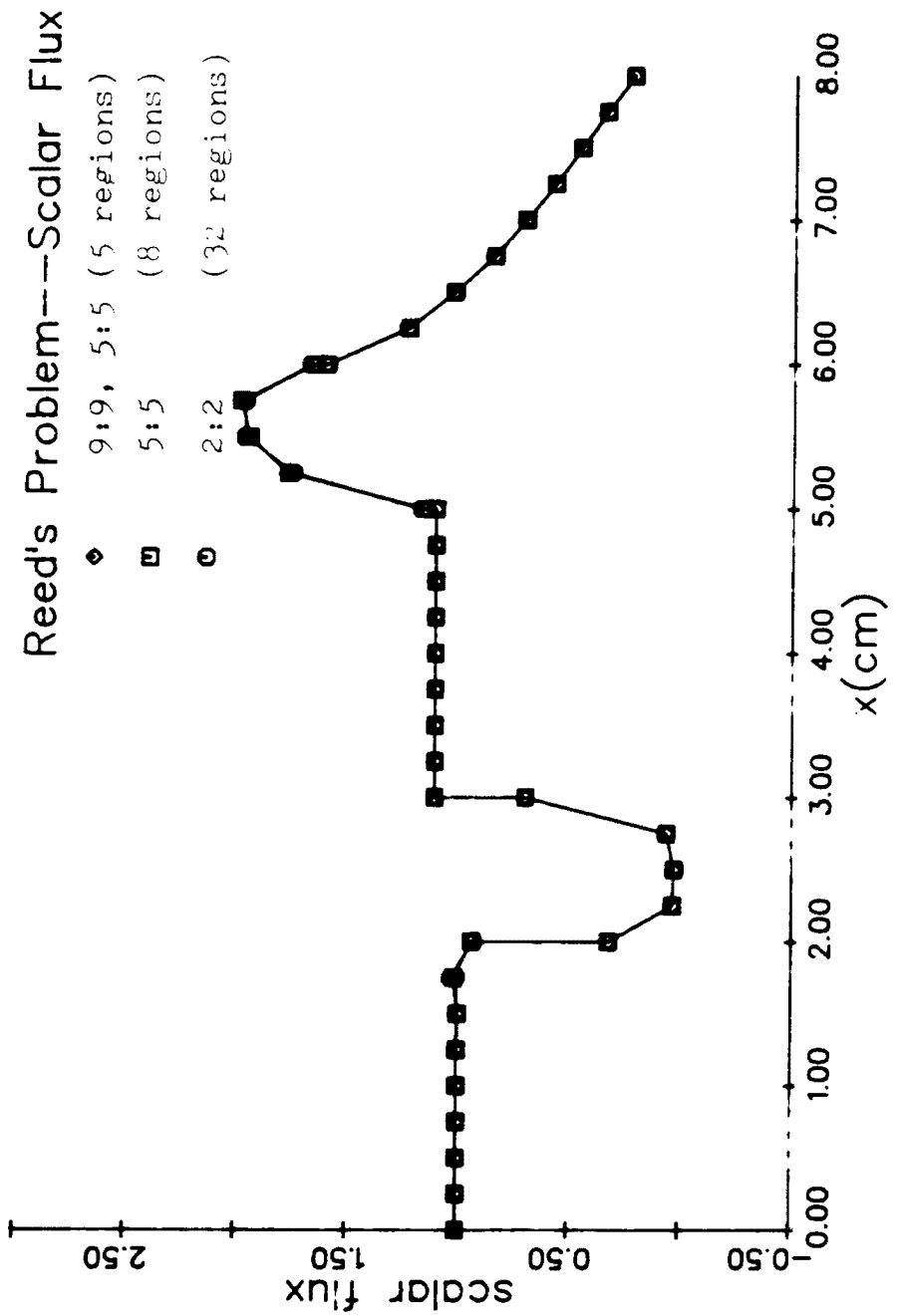


Fig. 5-8. Reed's Problem: fine mesh (0.25 cm).

Table 5-4. Errors in Scalar Flux for Reed's Problem: Quadratic vs. Linear Basis Functions

(Errors with respect to Monte Carlo benchmark; convergence criteria: 10^{-5})

case	order basis func.	no. principal angular support points	mesh spacing (cm)	error					
				total	region				
					1	2	3	4	5
relative error									
5:5,3:3[1]	quad.	4	0.25/0.25[2]	0.097%	-0.017%	-2.642%	0.091%	0.682%	-0.152%
9:9,5:5	linear	6	0.25/0.25	0.069%	-0.002%	-3.312%	0.038%	0.722%	-0.213%
5:2,3:2	quad.	4	0.25/1.0,0.5	0.052%	0.024%	-4.495%	0.092%	0.734%	-0.302%
9:3,5:3	linear	6	0.25/1.0,0.5	0.075%	0.003%	-6.142%	0.038%	0.953%	-0.164%
RMS error									
5:5,3:3	quad.	4	0.25/0.25	0.940%	0.538%	9.072%	0.091%	0.972%	0.645%
9:9,5:5	linear	6	0.25/0.25	1.169%	0.434%	8.522%	0.038%	1.555%	0.789%
5:2,3:2	quad.	4	0.25/1.0,0.5	1.487%	0.537%	13.93 %	0.092%	1.057%	2.189%
9:3,5:3	linear	6	0.25/1.0,0.5	3.052%	0.595%	29.17 %	0.038%	3.128%	3.005%

[1] 5:3 indicates Response Matrix mesh structure of 5 local principal support points/region and 3 global principal support points/region

[2] 0.25/1.0 indicates a local mesh spacing of 0.25 and a global mesh spacing of 1.0

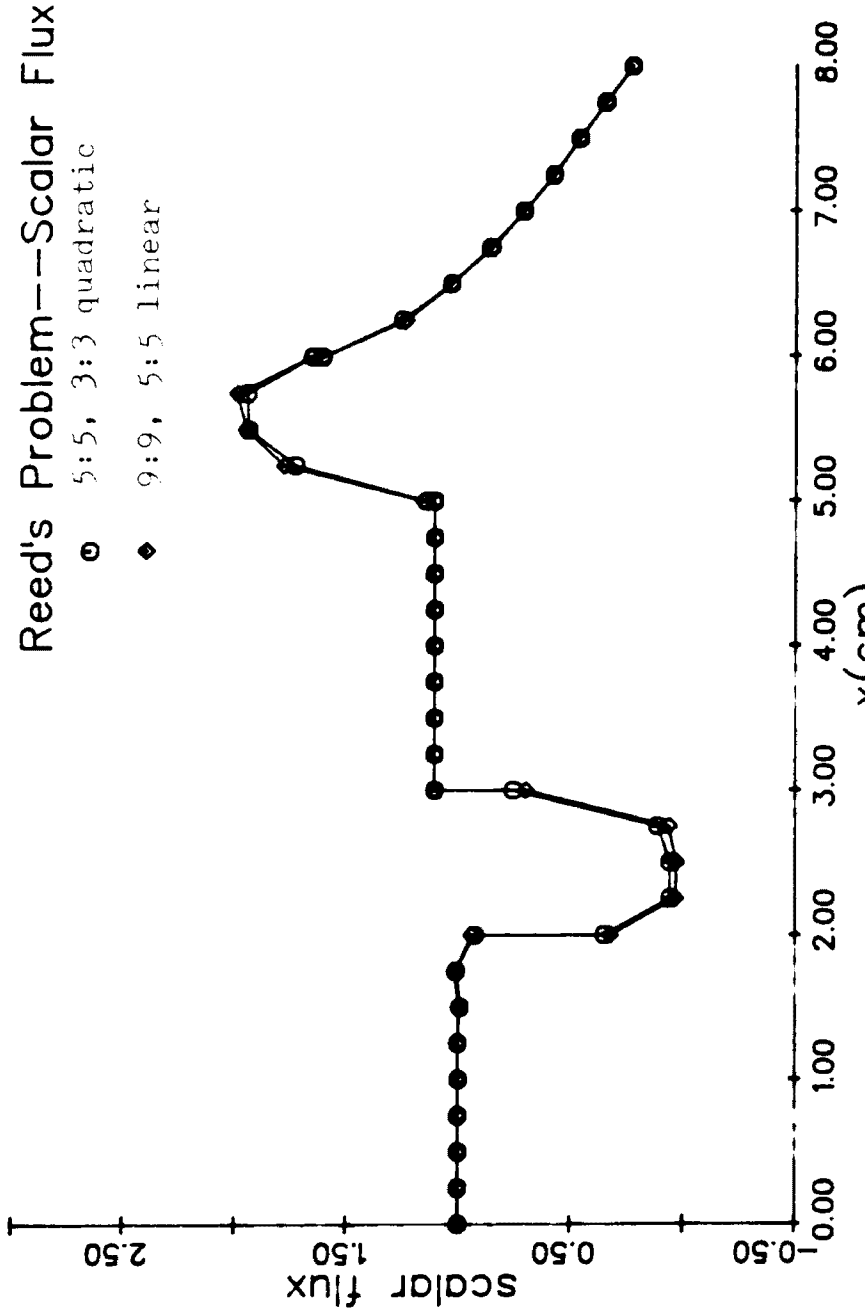


Fig. 5-9. Reed's Problem: quadratic vs. linear (no projection)

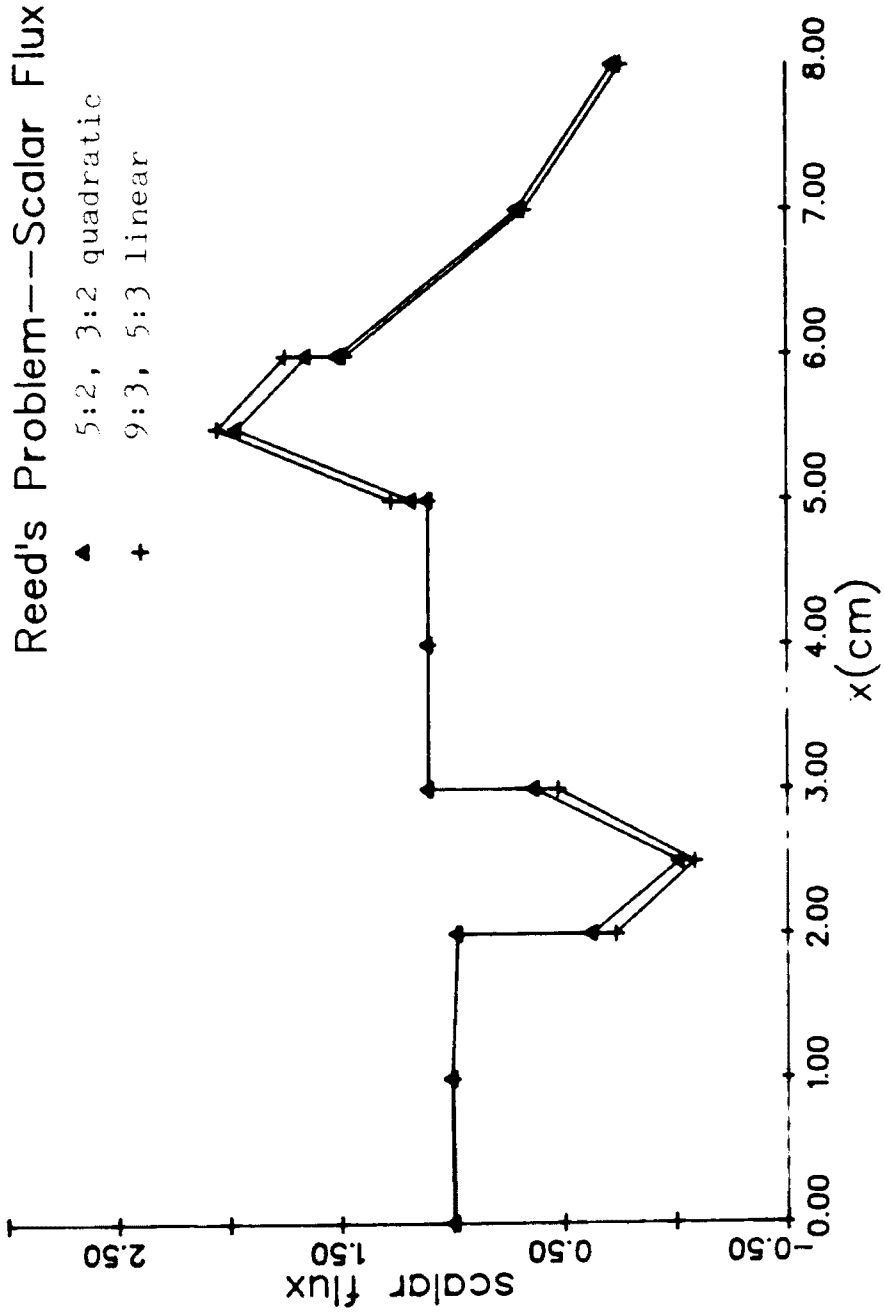
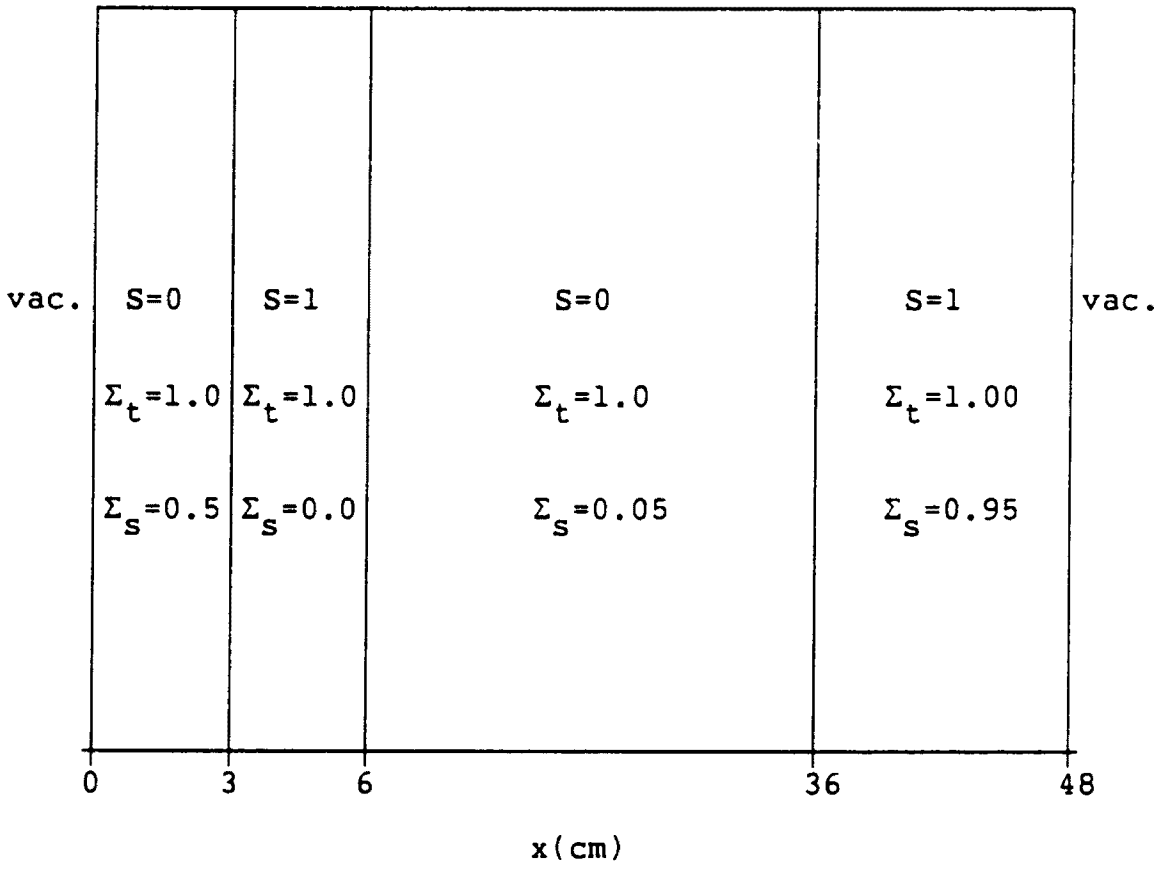


Fig. 5-10. Reed's Problem: quadratic vs. linear (with local/global projection)

NSE 71 Problem

A second test problem, the NSE 71 problem [Alc79] (for lack of a better name), provides a vivid demonstration of the effectiveness of the response matrix method in solving coarse mesh problems. This problem, shown in Fig. 5-11, has been analyzed by three different local/global configurations: 5:5, 5:2, and 2:2, where 5:2 indicates 5 local support points/region and 2 global support points/region. In all cases, regions are 3 cm wide and an angular mesh with 6 support points is used. Fig. 5-12 shows the dramatic disagreement of 2:2 with 5:5 and 5:2 in the region with the source and strongly scattering material. The latter two cases are drawn again in Fig. 5-13. Here, the agreement over the entire problem is obvious. Once again, the coarse mesh calculation using response matrices that have a fine local mesh produces superior solutions.



(not to scale; units: Σ_t, Σ_s, S [cm^{-1}])

Fig. 5-11. NSE 71 Problem.

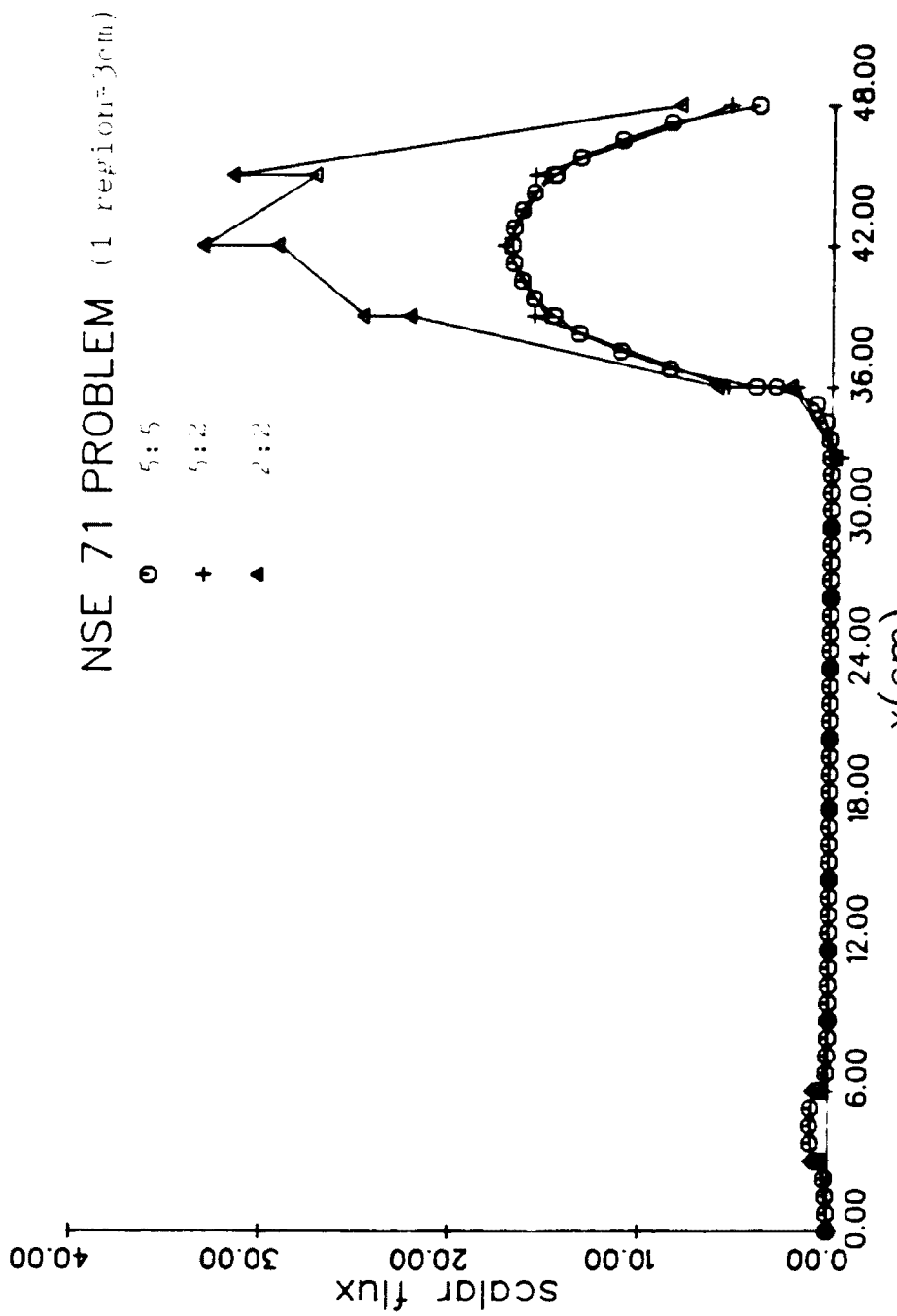


Fig. 5-12. NSE 71 Problem: scalar flux.

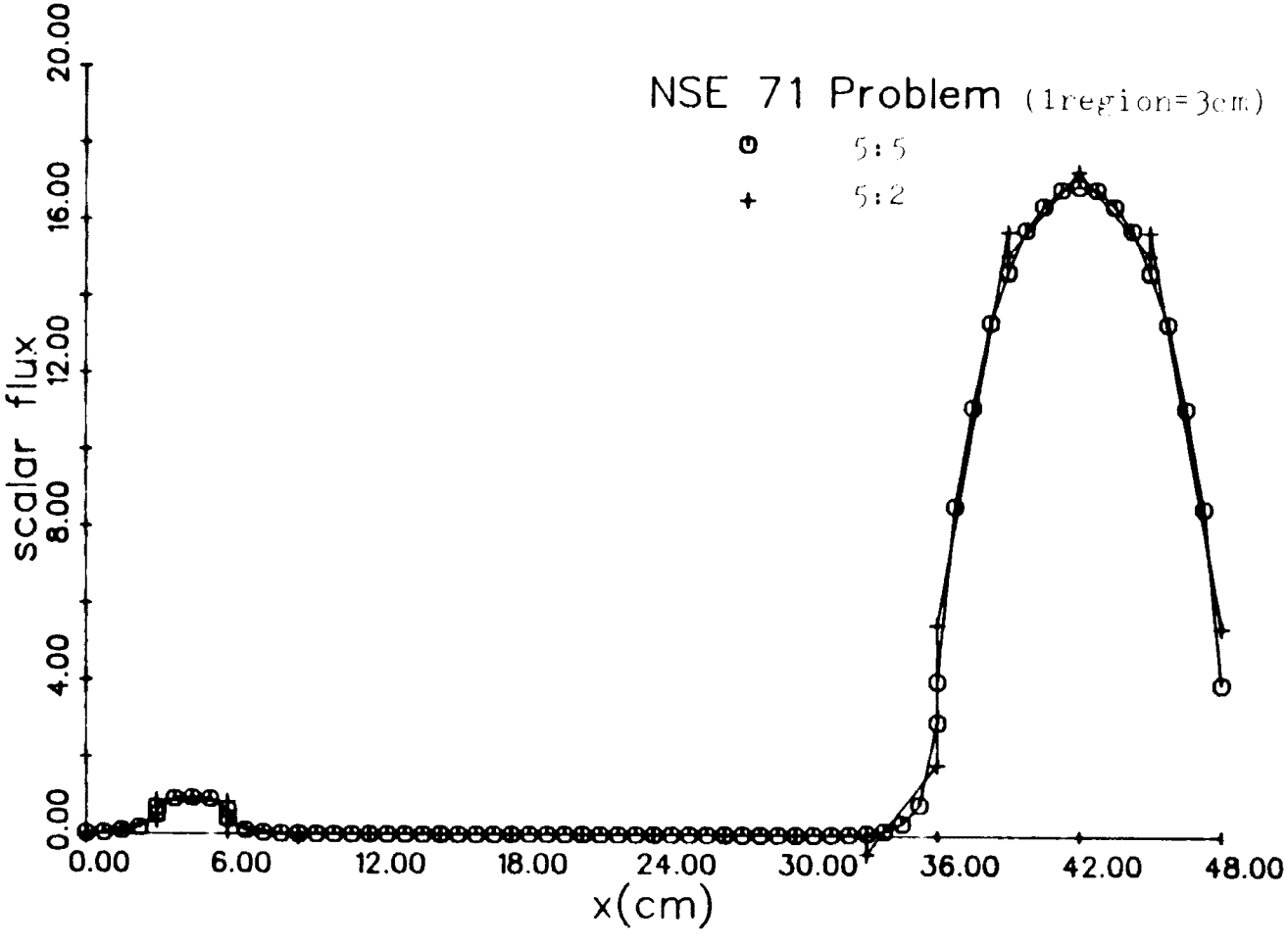
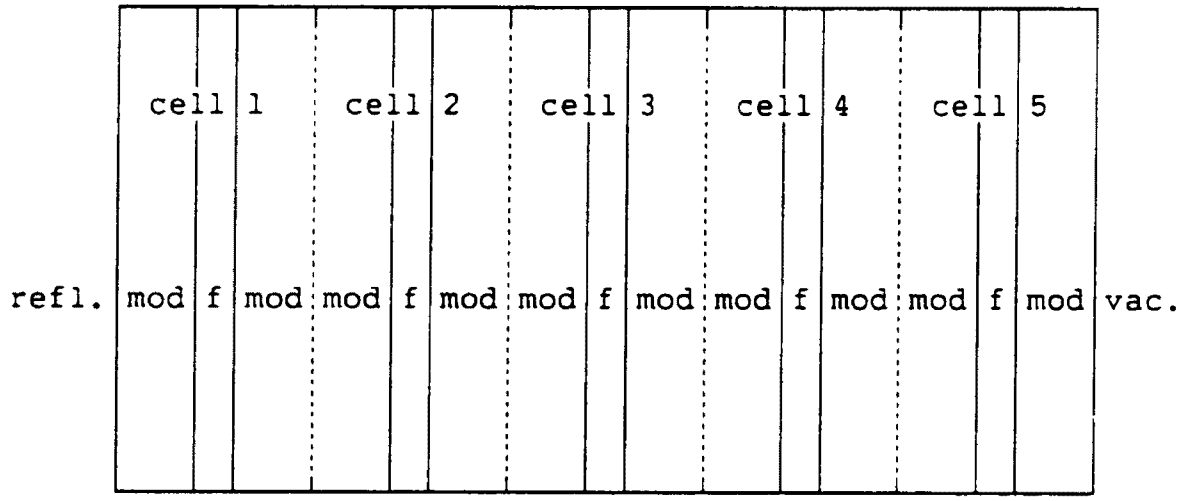


Fig. 5-13. NSE 71 Problem: scalar flux (scale reduced).

Lattice Problem

The repeating lattice problem [Bri77] depicted in Fig. 5-14 provides a demonstration of the heterogeneous capability of the method. Plotted in Fig. 5-15 are two response matrix calculations, both with a local angular mesh of 10 support points but with different global angular mesh. Linear basis functions are used in all cases. One case uses a global angular mesh of 10 support points, the other one with 4 support points. Any differences between the two are indiscernible. Separate response matrix regions are used for the moderator and fuel regions with four spatial support points in each. This is the homogeneous region problem. Excellent agreement is seen between the region averaged flux of the 10/10 problem and the reference S_8 calculation.

Results of a heterogeneous response matrix region problem are plotted in Fig. 5-16. A single set of response matrices is generated for a heterogeneous region consisting of two half-width moderator slabs and a fuel slab. Of the 10 spatial support points, points 4 and 7 fall at the fuel-moderator interface and nodes 1 and 10 are located at the region edge, the moderator midpoint. Region averaged scalar fluxes for the heterogeneous case are also listed in Table 5-5. The disagreement between the homogeneous and heterogeneous cases is due to the inability of the present implementation of the response matrix method to allow an internal discontinuity in the source distribution. Such a feature is



mat'l	abbre-viation	1/2 width (cm)	Σ_t (cm^{-1})	Σ_s (cm^{-1})
fuel	f	0.4	0.717	0.397
moderator	mod	1.4	2.35	2.33

(source of value 1.0 cm^{-1} in moderator)

Fig. 5-14. Lattice Problem.

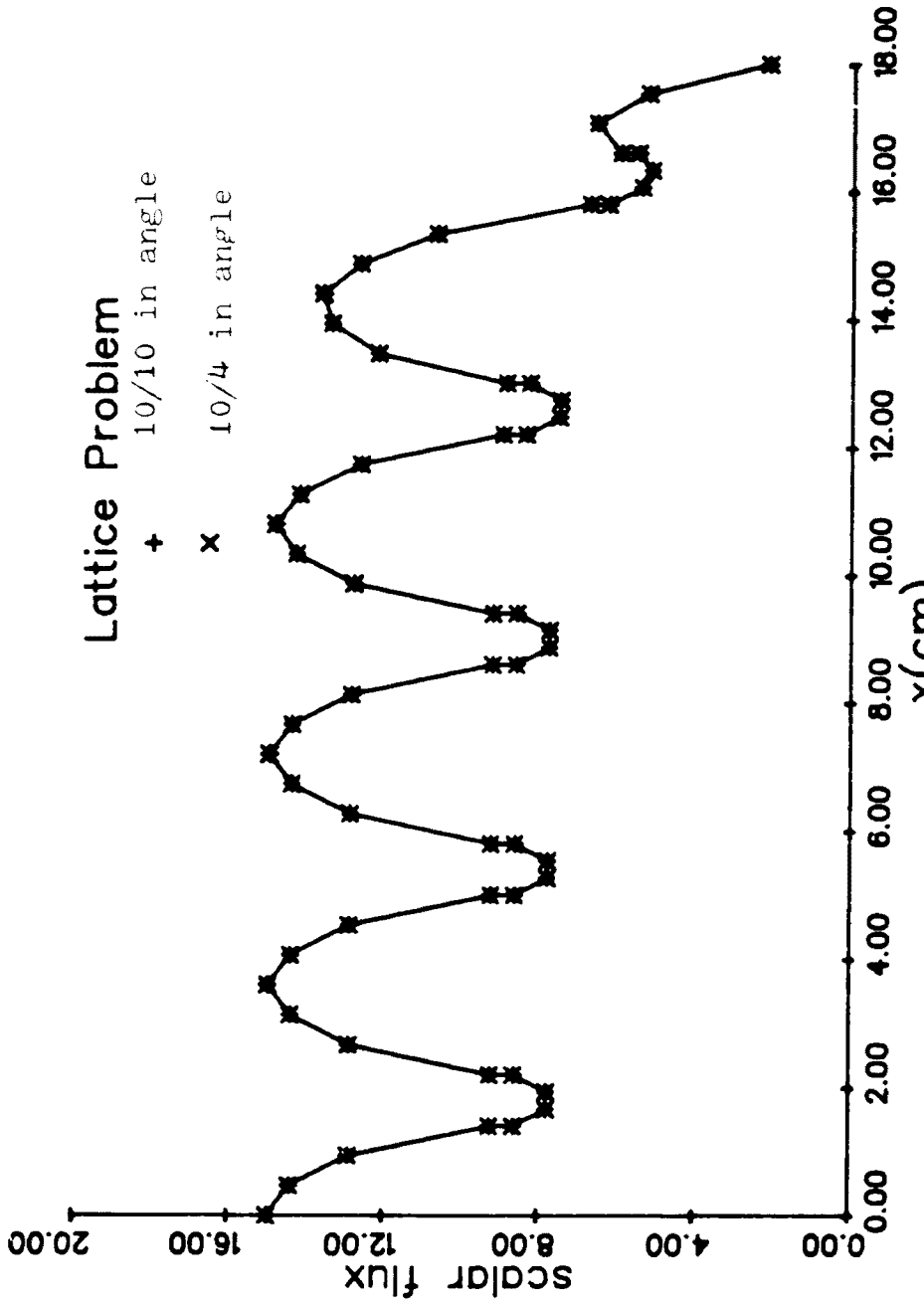


Fig. 5-15. Lattice Problem: homogeneous regions.

Table 5-5. Lattice Problem Scalar Fluxes

cell	fuel			moderator		
	S_8[1] ref. [Bri77]	response matrix method[2]		S_8[1] ref. [Bri77]	response matrix method[2]	
		homog.	hetero.		homog.	hetero.
1	8.062	8.062	8.949	13.133	13.133	13.841
2	8.059	8.059	8.946	13.126	13.127	13.836
3	8.033	8.032	8.919	13.077	13.077	13.784
4	7.788	7.785	8.660	12.612	12.607	13.298
5	5.515	5.501	6.263	8.259	8.362	8.753

[1]normalized so S_8 fluxes equal homogeneous fluxes at cell 1

[2]10/10 in angle

necessary in order to truly simulate the source distribution of this problem.

One-Dimensional Eigenvalue Problem

The results of analysis of a series of homogeneous eigenvalue problems are presented in Table 5-6. For all cases the local and global mesh structures are identical and cross sections of Σ_t=1.0 cm^{-1}, Σ_s=0.5 cm^{-1}, and $\nu\Sigma_f$=0.5 cm^{-1} were used. Thus, one mean free path (mfp) is equivalent to 1 cm. Scattering is included in the response matrices. Eigenvalues are presented in two forms: the conventional multiplication constant, k, and the number of secondary neutrons required to obtain criticality, c. The response matrix method calculates k directly, as described earlier, from the ratio of the integrated fission source of consecutive outer iterations. The value c can be calculated from k by

$$c = \frac{1}{\Sigma_t}\left[\Sigma_s + \frac{\nu\Sigma_f}{k}\right]$$

and is presented for comparative purposes.

It is apparent that the response matrix method calculates k quite well. For the smallest problem (1/2 width=0.5mfp) poor results are obtained because the angular resolution is not fine enough. Note that the FTRAN case with 8 angular support points agrees well with the

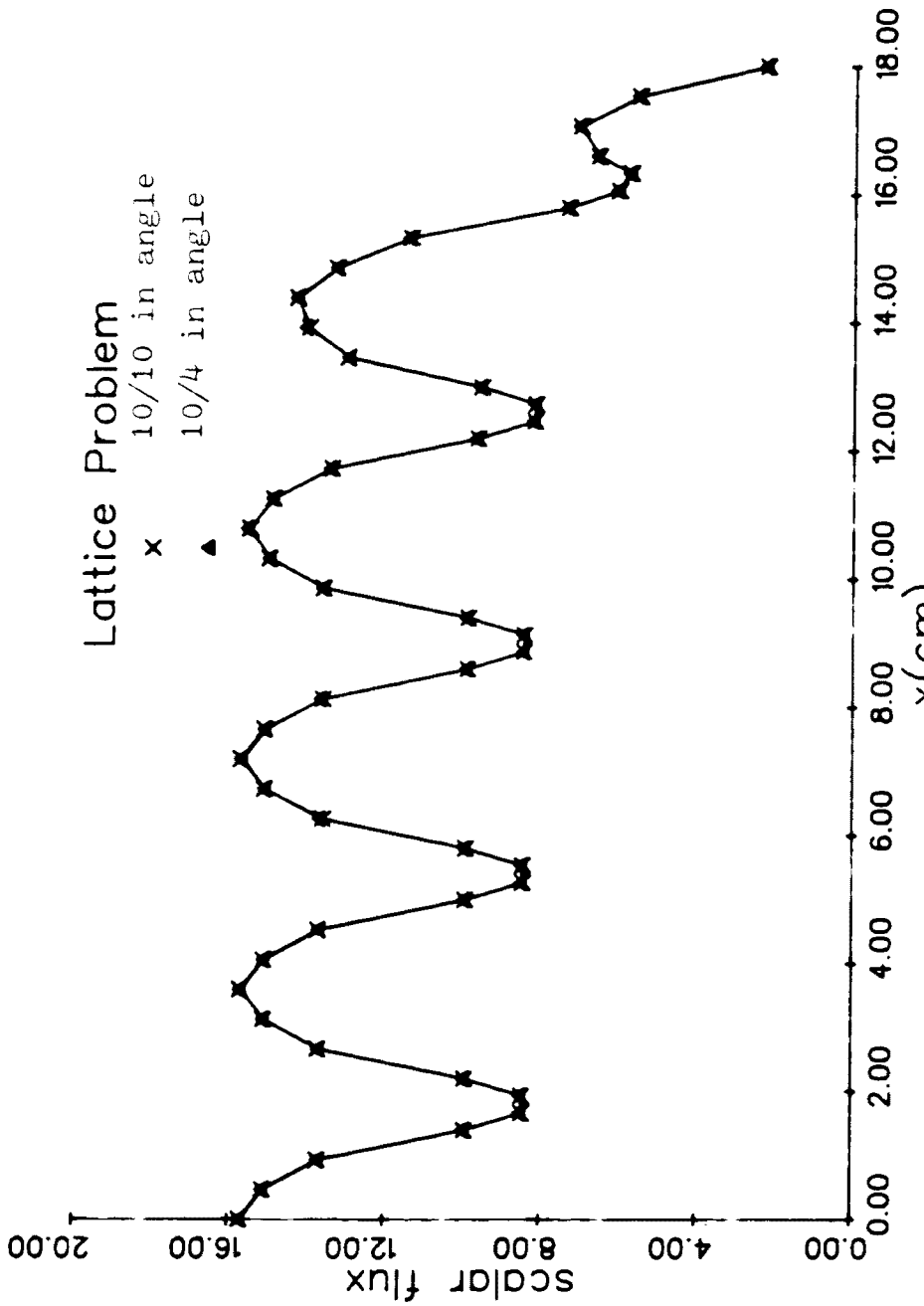


Fig. 5-16. Lattice Problem: heterogeneous regions.

Table 5-6. One-Dimensional Eigenvalues

1/2 width (mfp)	Response Matrix Method (convergence criteria: inner, outer, $k--10^{-6}$; angular support points: 4)								FTRAN ref. [Mar77] convergence criteria: flux--10^{-5}, $k--10^{-6}$				Benchmark[1] ref [Kap74]
	mesh spacing (mfp)	Iteration: no. regions	Iteration: no. outers	Iteration: total no. inners	Iteration: CPU time[2] (sec)	total CPU time[2] (sec)	Eigenvalue: k	Eigenvalue: c	mesh spacing (mfp)	no. angular support pts.	CPU time[2] (sec)	Eigenvalue c	Eigenvalue c
0.5	0.25	2	10	39	0.005	0.030	0.453229	1.60320	0.25	4	. . .	1.60319	1.615379
0.5	0.0625	2	10	42	0.009	0.069	0.453048	1.60364	0.125	6	. . .	1.61140	. . .
0.5	0.025	20	9	243	0.157	0.182	0.453041	1.60365	0.0833	8	. .	1.61462	. . .
1.0	0.25	2	13	73	0.011	0.036	0.647382	1.27234	0.25	4	0.016	1.27233	1.277102
1.0	0.25	4	14	70	0.013	0.038	0.647383	1.27234	0.50	4	0.009	1.27193	. . .
1.0									0.50	4	0.015[3]	1.27193[3]	. . .
1.0									0.25	6	0.033	1.27676	. . .
1.0									0.1667	8	0.055	1.27705	. . .
5.0	2.5	2	44	184	0.023	0.048	0.952779	1.02478	2.5	4	. . .	1.02479	1.024879
5.0	0.25	10	44	696	0.247	0.272	0.952599	1.02488	1.25	6	. . .	1.02488	. . .
5.0									0.833	8	. . .	1.02493	. . .
10.0	2.5	2	112	461	0.059	0.084	0.985827	1.00714	2.5	4	0.128	1.00714	1.007135
10.0	0.25	20	88	501	0.364	0.389	0.985911[4]	1.00715[4]	0.25	4	0.845	1.00714	. . .
10.0									5.0	4	0.077	1.00712	. . .
10.0									2.5	6	0.224	1.00714	. . .
10.0									1.667	8	0.516	1.00714	. . .

[1] rounded to seven significant figures
[2] AMDAHL 5860
[3] convergence criteria: flux, $k--10^{-6}$
[4] convergence criteria: inner, outer, $k--10^{-5}$

benchmark. For the largest problems, however, the small angular mesh is not as critical. Comparable, if not better, values are found using the response matrix method, particularly when a finer mesh is used. Such a fine mesh is feasible because many identical regions can be used in the global solution procedure but only one set of response matrices must be calculated.

The effect of problem size on iteration count and computational costs will be discussed in the following section.

Computational Considerations

The computational cost associated with finding a global neutron flux distribution by the response matrix method can be divided into two components: the cost of generating one or more response matrix sets and the cost of the iteration solution procedure itself.

The response matrix generation cost is dependent on the local and global mesh size desired and if the two mesh structures are identical. Table 5-7 provides a break-down of these costs for various combinations of space and angle support point arrangements. The costs, of course, increase with the number of support points. If, however, the global mesh is identical to the local mesh, the costs are somewhat reduced because some calculations may be bypassed, as explained in Chapter II.

The costs of finding the global solution is dependent on a number of factors, including the number of iterations

Table 5-7. One-Dimensional Response Matrix Generation Costs (AMDAHL 5860)

mesh structure				CPU time (sec)			
space		angle		finite element matrix generation	finite element matrix inversion	response matrix generation	total
local	global	local	global				
3	3	4	4	0.002	0.001	0.018	0.021
9	9	4	4	0.002	0.020	0.034	0.056
2	2	6	6	0.002	0.002	0.023	0.027
3	2	6	6	0.002	0.004	0.026	0.032
3	3	6	6	0.002	0.005	0.025	0.032
5	2	6	6	0.002	0.015	0.038	0.055
5	5	6	6	0.002	0.015	0.032	0.049
9	3	6	6	0.003	0.060	0.059	0.122
9	9	6	6	0.003	0.059	0.053	0.115

required to reach convergence and the cost per iteration. The iteration count depends on the number of regions in the problem, the physical characteristics of the problem, and the iteration scheme chosen.

Fig. 5-17 is a plot of the number of inner iterations required to solve Reed's problem (case 5/5/cm) as a function of the relaxation parameter (ω) used by the successive over-relaxation method. At the optimal ω of 1.2 a minimum of 13 iterations is required. For a Jacobi iteration procedure, 23 iterations are used. If the scattering is removed from the response matrices, a converged interface flux distribution is found in just 3 iterations given a source distribution, as promised in Chapter IV. To find a converged scattering source distribution, however, many outer iterations, together with the associated inner iterations, must be performed.

For most of the Reed's problem solutions, the iteration costs are much less than the cost of generating response matrices, as seen from Table 5-8. The only exception is the 32 region problem. For that case the response matrix generation costs are less because the regions contain few support points. The iteration costs are high because the many regions cause an increase in both the cost per iteration and the iteration count.

The iteration cost required with scattering calculated in the outer iteration is, of course, much greater than the alternative treatment. The cost of generating the response

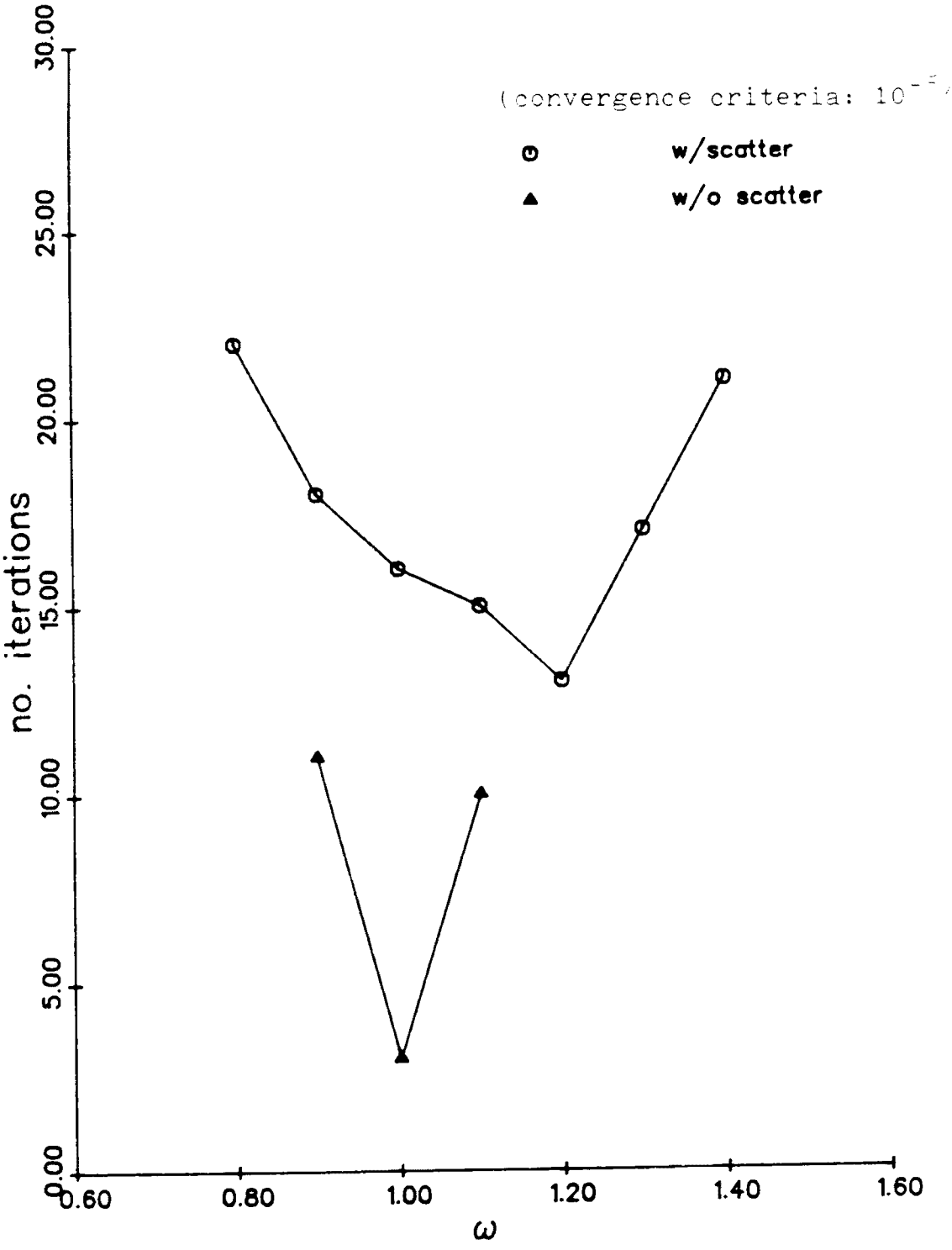


Fig. 5-17. Number of iterations vs. relaxation parameter (Reed's Problem--5/5/cm)

matrices is greater, too, because a scattering operator must be found. No advantage is seen for adopting this approach. Note, however, that the number of inner iterations per outer averages 3.

The FTRAN times quoted in Table 5-8 indicate that the response matrix method is not competitive with FTRAN for this type of problem. This is a consequence of the explicit inversion necessary to generate response matrices. FTRAN solves the finite element matrix directly (but does not invert it) while taking advantage of its band structure which results in a linear dependence of costs to the number of spatial mesh points. In two dimensions, as will be seen later, the response matrix method is more efficient than FTRAN2 (the two-dimensional version of the standard finite element code).

The iteration counts and CPU times quoted in Table 5-6 were found using an optimal relaxation parameter of 1.0, i.e. no relaxation at all. Once again, the inner iteration count increases with the number of regions. As the half-width increases approaching a critical configuration, more outer iterations are required. For the eigenvalue problems, iteration is required to find the solution with both FTRAN and the response matrix method. In FTRAN the finite element matrix equation must be solved at each iteration, although only backsubstitutions are required for each iteration because the $\underline{\underline{A}}$ matrix is LU-decomposed in advance. The response matrix iteration consists of simple multiplication

Table 5-8. Computational Costs to Solve Reed's Problem (AMDAHL 5860)

mesh structure		no. regions	total response matrix generation time (sec)	iteration			total CPU time (sec)
local	global			no. outers	total no. inners	CPU time (sec)	
...	33	..	.....	...	...	.....	0.065[1]
5	5	8	0.196	1	13	0.016	0.212
5	5	8	0.223	44[2]	132	0.088[2]	0.311
5	3	8	0.220	1	13	0.011	0.231
3	3	8	0.128	1	13	0.012	0.140
9,5	9,5	5	0.443	1	14	0.019	0.462
2	2	32	0.108	1	59	0.115	0.223
...	9	..	.....	...	...	.....	0.017[1]
2	2	8	0.108	1	13	0.009	0.117
3	2	8	0.128	1	13	0.012	0.140
5	2	8	0.200	1	13	0.011	0.211

[1] FTRAN

[2] scattering source is calculated in outer, not inner, loop

of flux vectors by matrices. The cost of response matrix generation overhead is overcome by the cheaper iteration procedure which enables the response matrix method to be competitive with FTRAN.

Summary

The one-dimensional implementation of the response matrix method provides a solution identical to the conventional finite element method regardless of the response matrix region size or the scattering treatment. The alternate method of finding the scattering source from the interior flux is less efficient than including scattering in the response matrices. Improved coarse mesh solutions can be obtained using response matrices found by projecting from a fine local mesh. The most obvious improvement is in regions of scattering material containing a source. Quadratic basis functions yield slightly better solutions than linear basis functions. Only in some cases is the response matrix method computationally competitive with the conventional method, and then only marginally. This is expected on the basis of calculation of operation counts.

Two-Dimensional Numerical Experimentation

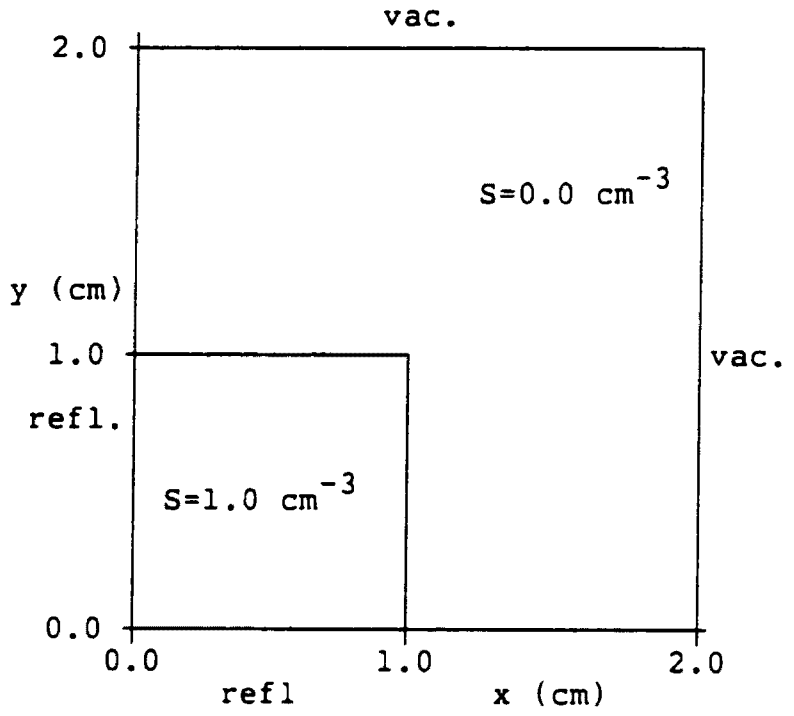
Due to the increased computational expense of the two-dimensional method over that of one dimension, numerical testing was limited to one test problem--the ray effect problem [Bri75]--under a variety of conditions.

Ray Effect Problem

The two-dimensional configuration depicted in Fig. 5-18 was devised to test the ability of neutron transport codes to eliminate the ray effect--a phenomenon characterized by incorrectly calculated distortions of the scalar flux due to the presence of localized sources. Because scattering tends to redistribute the neutron density toward isotropy, the effect is more pronounced in strong absorbers. The majority of the cases presented here are of the ray effect problem with c=1/3, a reasonably small scattering fraction.

To analyze this problem by the response matrix method, the spatial domain must be divided into a set of rectangular regions. If all of the regions are of the same geometry, only one set of response matrices must be calculated because the material properties of the problem are homogeneous. In order to maintain uniform geometry and allow a discontinuity in the source distribution at the source-sourceless region interface, the largest region possible is 1.0 cm square, resulting in a 2x2 array of regions.

The ray effect problem is used as originally intended--to test the response matrix method's susceptibility to the ray effect--as well as a general two-dimensional test problem. First, a series of calculations are presented that used a variety of response matrix region sizes, in order to test the basic premise of the method, i.e., the spatial domain can be subdivided with no adverse consequences. Second, the effect of increasing the angular mesh and



(uniform material: Σ_t=0.75 cm^{-1}, c=Σ_s/Σ_t)

Fig. 5-18. Ray Effect Problem.

projecting from a fine local angular mesh to a coarser global angular mesh is studied. Here, ray effect mitigation is important. Lastly, the projection in space is examined.

A convention has been established to identify the discretization used in a particular calculation. The arrangement of response matrix regions in a rectangular array is referred to as the problem's region configuration. A 2x6 configuration indicates an array of 2 regions in the x-direction and 6 in the y-direction. The arrangement of support points in the four phase-space dimensions is described by a sequence of four digits indicating the number of support points in the x-, y-, μ- and Φ-directions, respectively. In all cases, constant intervals are used and discontinuities in angular flux are allowed at $\mu=0$ and $\Phi=\pi/2$. In the event of projection with non-identical local and global mesh, two sequences of digits are presented separated by a slash. The first describes the local mesh; the second describes the global mesh.

The Effect of Region Size

The intent of this section is to demonstrate the ability of the method to analyze two-dimensional systems by subdividing the spatial domain into many small regions. No projection is performed; identical local and global meshes are used. The results of a series of calculations using square regions with angular mesh structures of 4x4 are presented in Table 5-9 and Figs. 5-19 through 5-23. The

plots show the scalar flux at the edge of the problem along side 2 (the top edge). The dip in the scalar flux followed by a peak around x=1.0 cm is characteristic of the ray effect. The errors in Table 5-9 (and in all the error tables that follow) are calculated using the formulas presented earlier in this chapter along the top edge of the problem. Errors are calculated relative to the results of a fine mesh calculation (8x8-3344). Although the per cent errors are written out to two significant figures, these errors should be viewed carefully because the point-wise angular flux convergence criteria itself is only 1%.

The plots and errors indicate that for a given mesh size, results are consistent regardless of the size of the response matrix region and the number of support points in the region (Figs. 5-19 and 5-21). Solutions with mesh intervals larger than 0.1667 cm (Figs. 5-22 and 5-23) appear to differ greatly from the solutions with mesh intervals of 0.1667 cm and 0.125 cm (Fig. 5-20).

Fig. 5-24 presents FTRAN2 [Yeh78] and response matrix results for the ray effect problem (c=1/3) analyzed with a mesh size of 0.25 cm and an angular mesh of 4x4. The two cases cannot be compared directly because the response matrix method, unlike FTRAN2, allows a discontinuity in the flux at x=1.0 cm. From the discontinuity to the vacuum boundary, the two results agree. From x=0.0 cm to x=1.0 cm, there is greater disagreement. The FTRAN2 results, however, must be viewed with skepticism because, as illustrated in

Table 5-9. Errors in Scalar Flux of Ray Effect Problem (c=1/3): Local=Global

(side 2 traverse; errors relative to 8x8-3366-Δx,Δy=0.125; convergence criteria = 1%)

config-uration	mesh structure				mesh spacing		error	RMS error
	i	*j*	*k*	*l*	Δx (cm)	Δy (cm)		
4x4	5	5	4	4	0.125	0.125	-0.18%	0.65%
6x6	3	3	4	4	0.1667	0.1667	0.02%	1.23%
4x4	4	4	4	4	0.1667	0.1667	-0.14%	1.11%
4x4	3	3	4	4	0.25	0.25	0.23%	2.28%
2x2	3	3	4	4	0.5	0.5	0.15%	4.57%

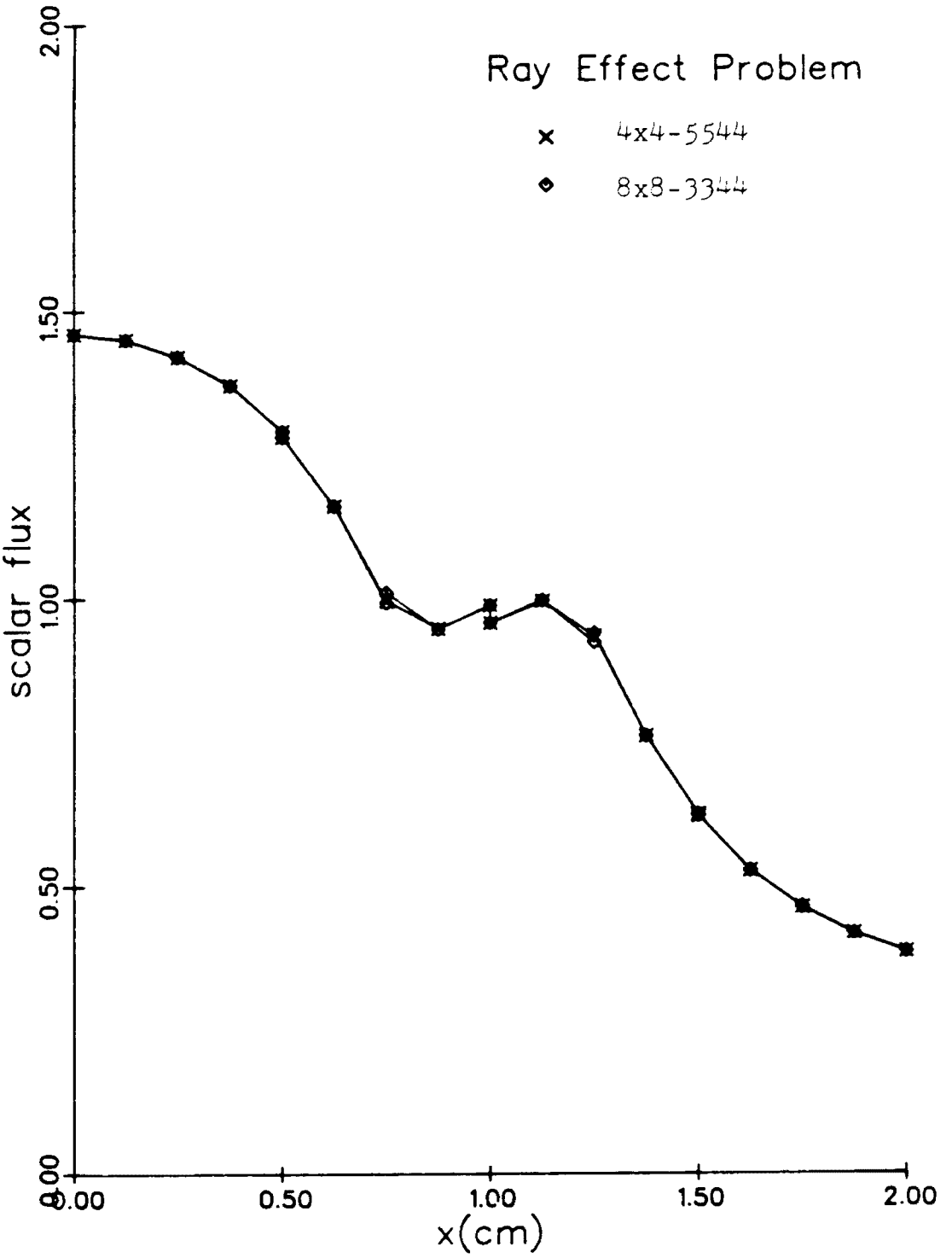


Fig. 5-19. Ray Effect Problem (c=1/3)--scalar flux along side 2: 8x8-3344 vs. 4x4-5544 (local=global).

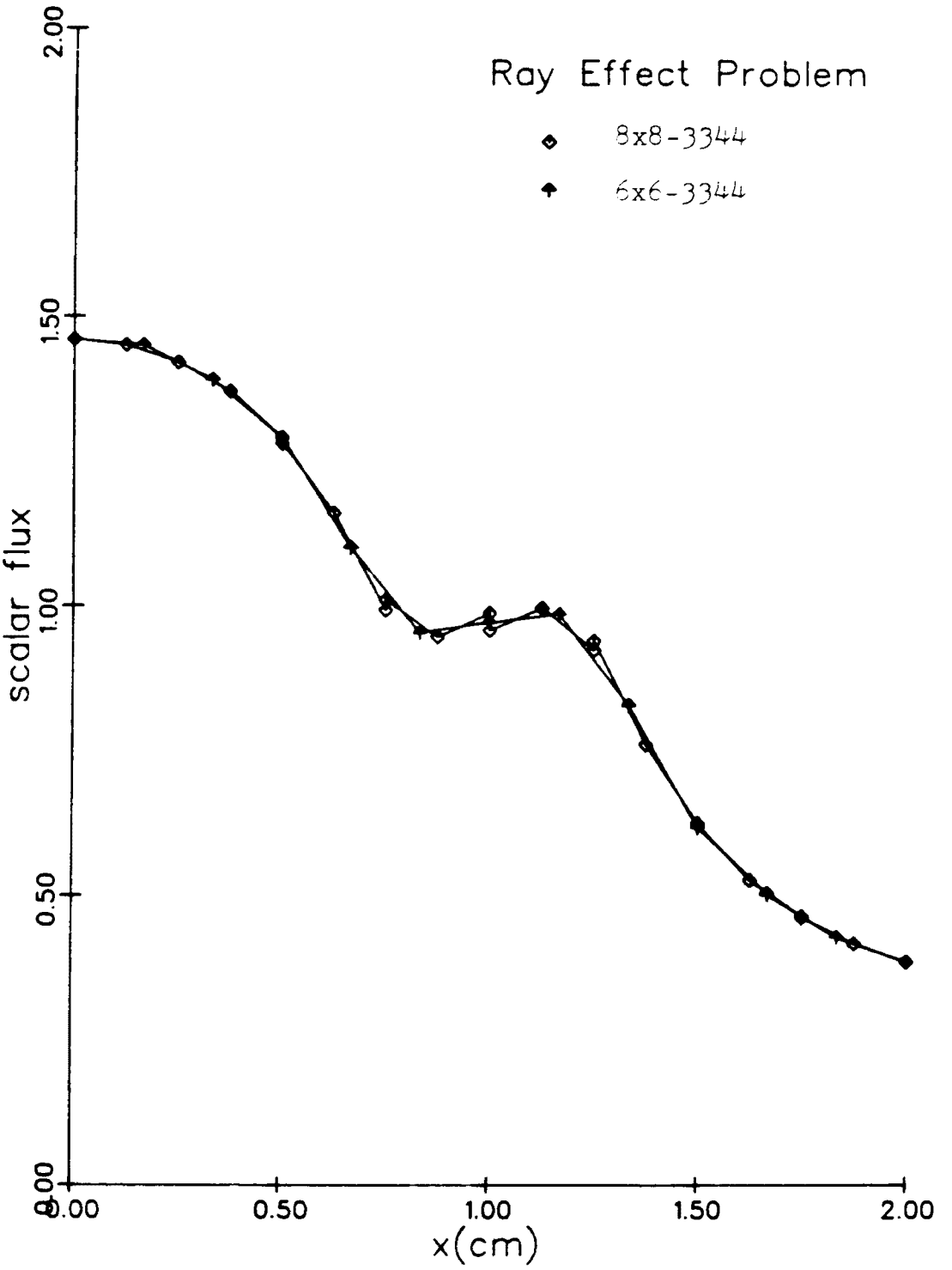


Fig. 5-20. Ray Effect Problem (c=1/3)--scalar flux along side 2: 8x8-3344 vs. 6x6-3344 (local=global).

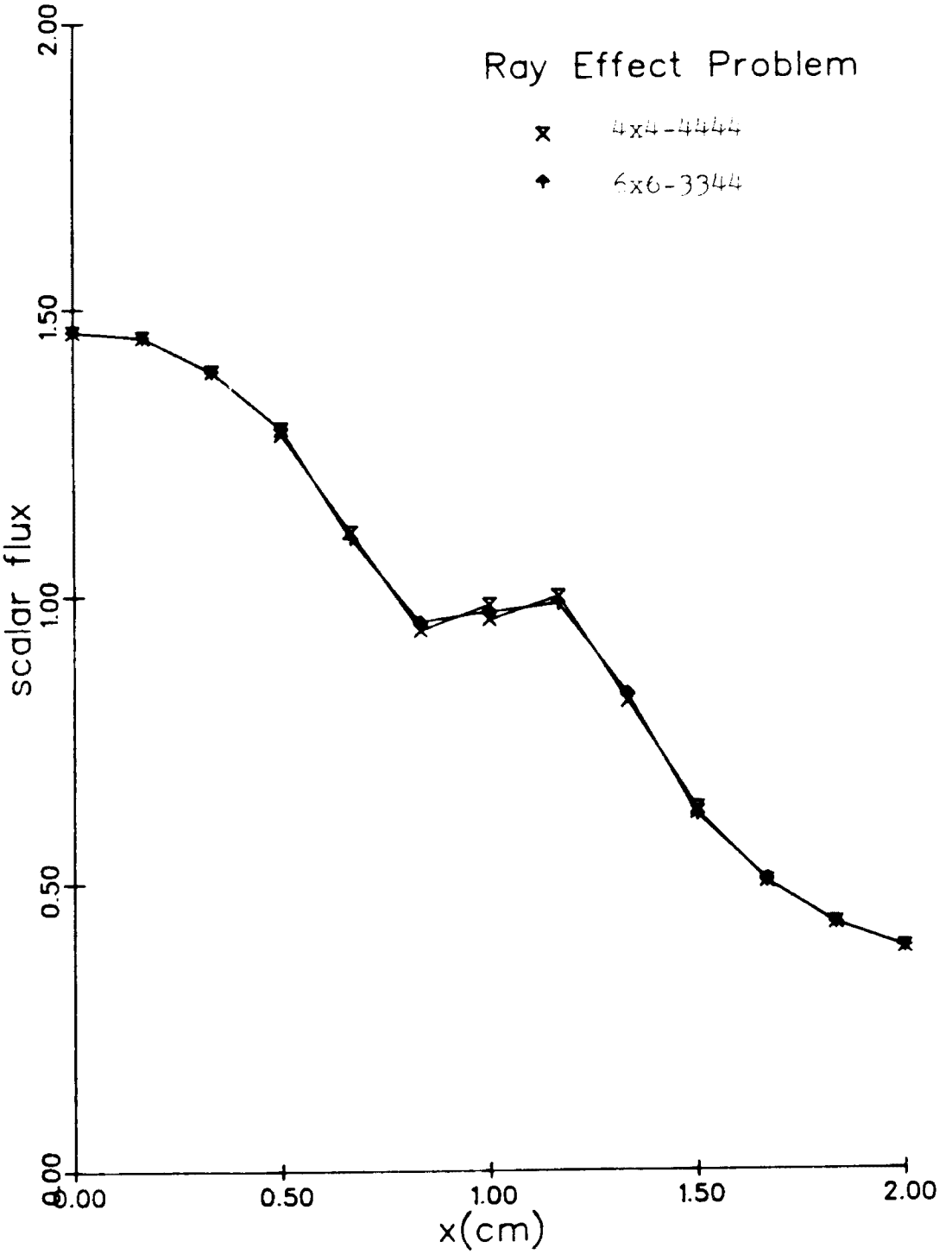


Fig. 5-21. Ray Effect Problem (c=1/3)--scalar flux along side 2: 4x4-4444 vs. 6x6-3344 (local=global).

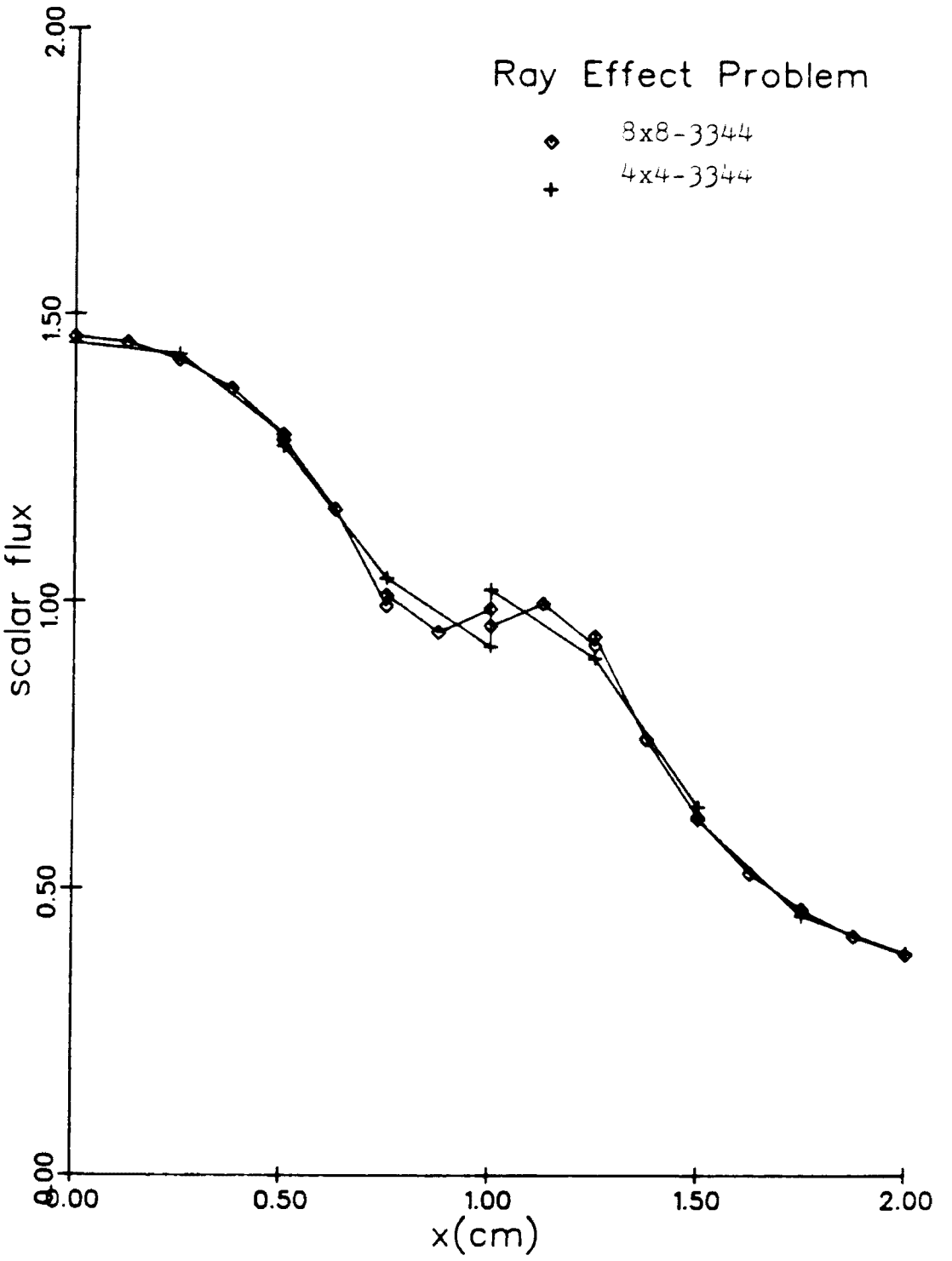


Fig. 5-22. Ray Effect Problem (c=1/3)--scalar flux along side 2: 8x8-3344 vs. 4x4-3344 (local=global).

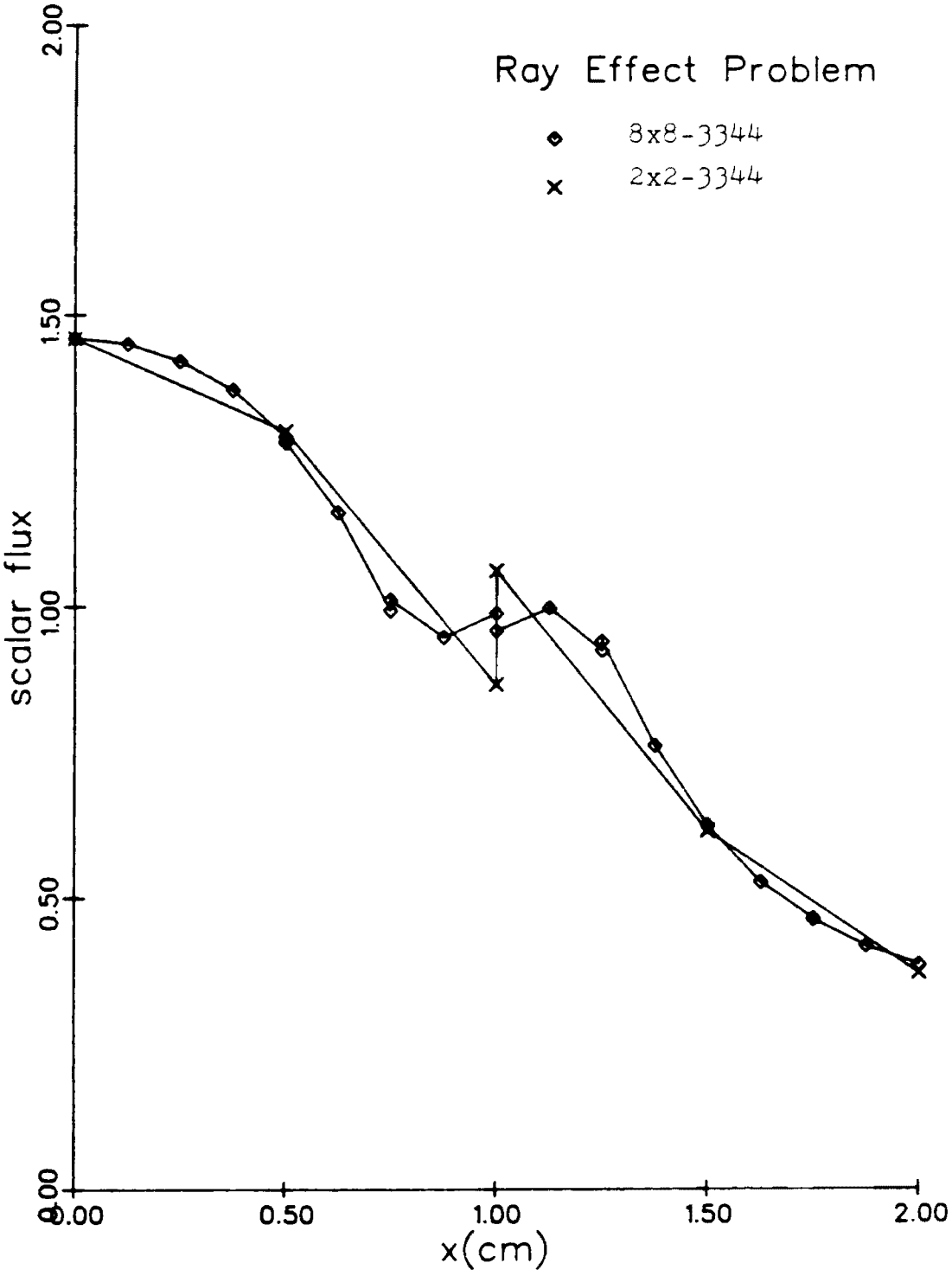


Fig. 5-23. Ray Effect Problem (c=1/3)--scalar flux along side 2: 8x8-3344 vs. 2x2-3344 (local=global).

Fig. 5-25, the scalar flux profiles along y=2.0 cm are extremely sensitive to the choice of spatial support point spacing.

The consistency of results regardless of the response matrix region size indicates that good solutions are possible using the response matrix method if suitable mesh spacing is selected.

Ray Effect Mitigation: Local-Global Projection in Angle

The ray effect can be reduced by increasing the number of angular support points from 4x4 to 6x6 (see Fig. 5-26). Fig. 5-27 is a plot of the scalar fluxes found using a 6x6 angular mesh with 6x6 and 4x4 response matrix region configurations. Note the severe discontinuity at x=1.0 cm, the flat from 0.0 to 0.5 cm, and the lack of the S-shaped dip and peak seen in the previous curves. The FTRAN2 results with the same angular mesh are also included in Fig. 5-27. Again a direct comparison cannot be made because of the discontinuity and because the scalar fluxes found by the response matrix method are along the line y=2.0 cm while the FTRAN2 plot is along y=1.875 cm.

Fig. 5-28 is a plot of three flux profiles found using the 6x6 response matrix region configuration. Two of the profiles have been presented in the preceeding figure (6x6-3344 and 6x6-3366). The third is the result of a projection from the fine 6x6 angular mesh to the coarser 4x4 global angular mesh. The fine-coarse mesh result appears to com-

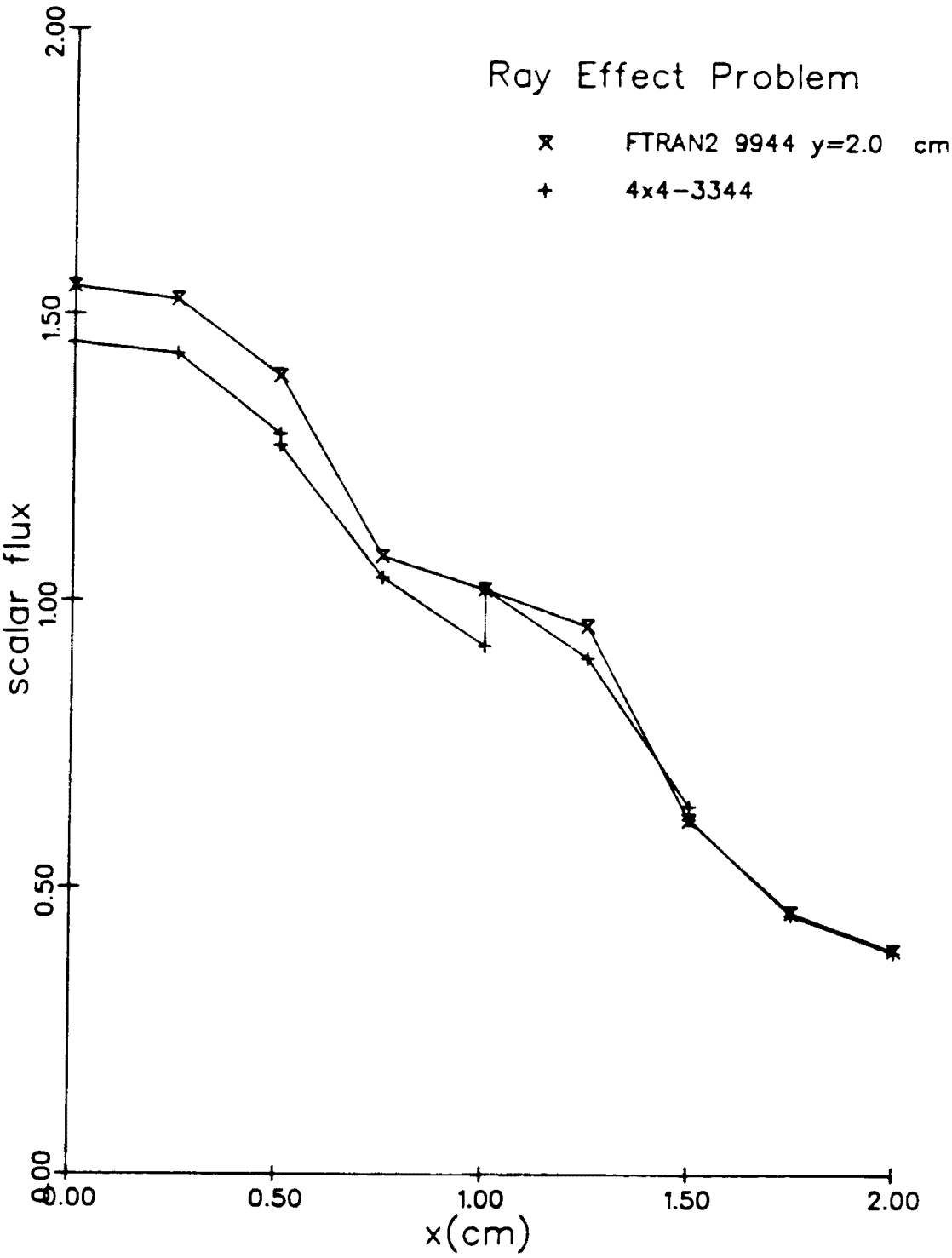


Fig. 5-24. Ray Effect Problem (c=1/3)--scalar flux along side 2: FTRAN2-9944 vs. 4x4-3344.

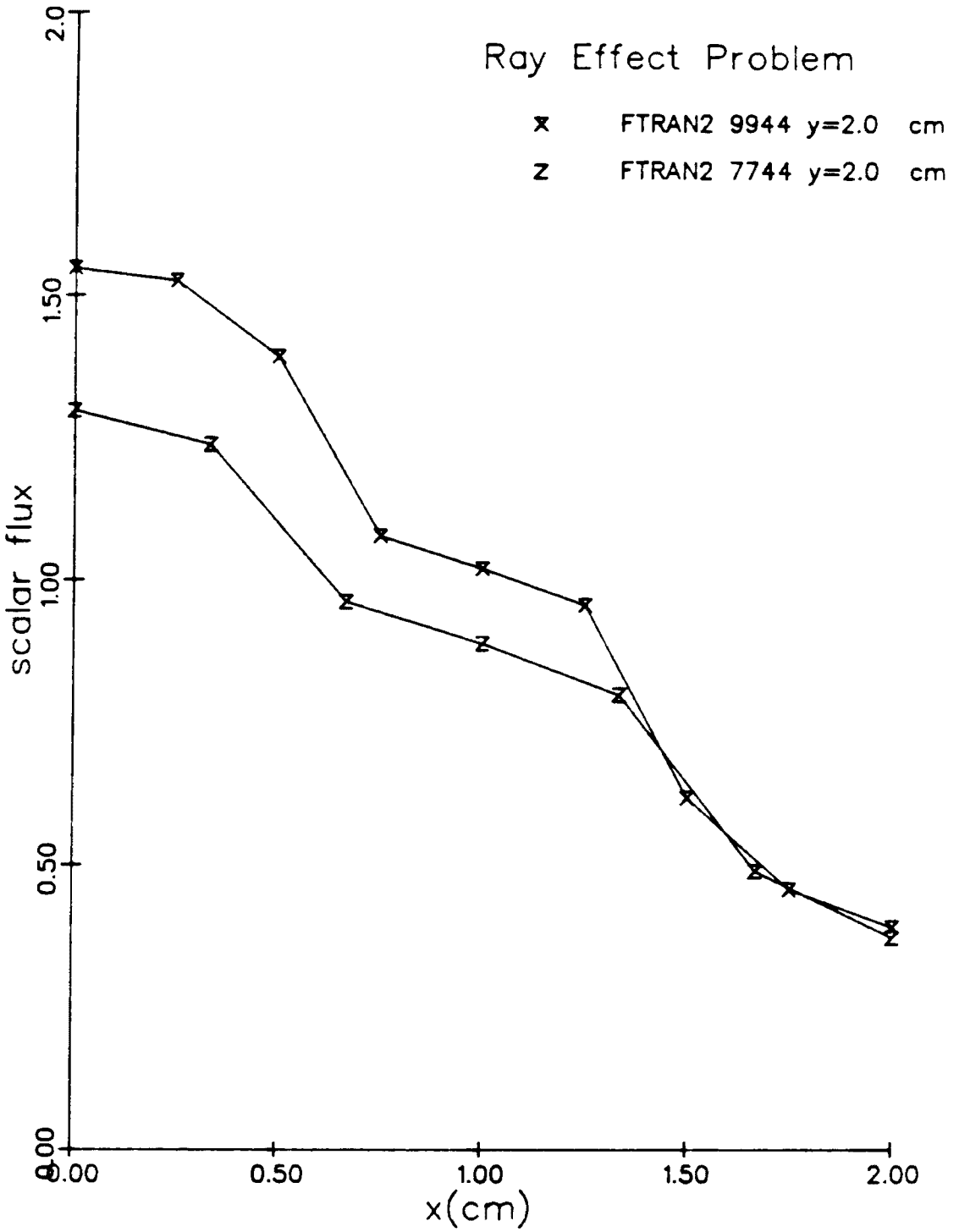
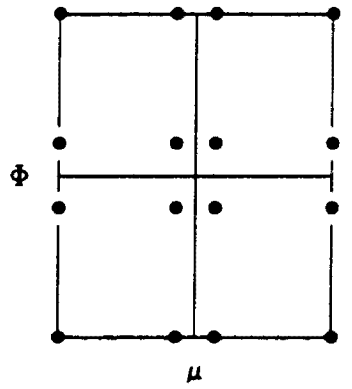
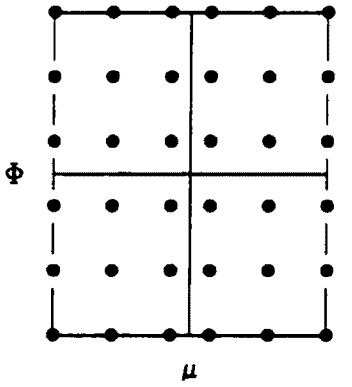


Fig. 5-25. Ray Effect Problem (c=1/3)--scalar flux along side 2: FTRAN2-9944 vs. FTRAN2-7744.



(a) 4x4



(b) 6x6

Fig. 5-26. Two-dimensional angular mesh.

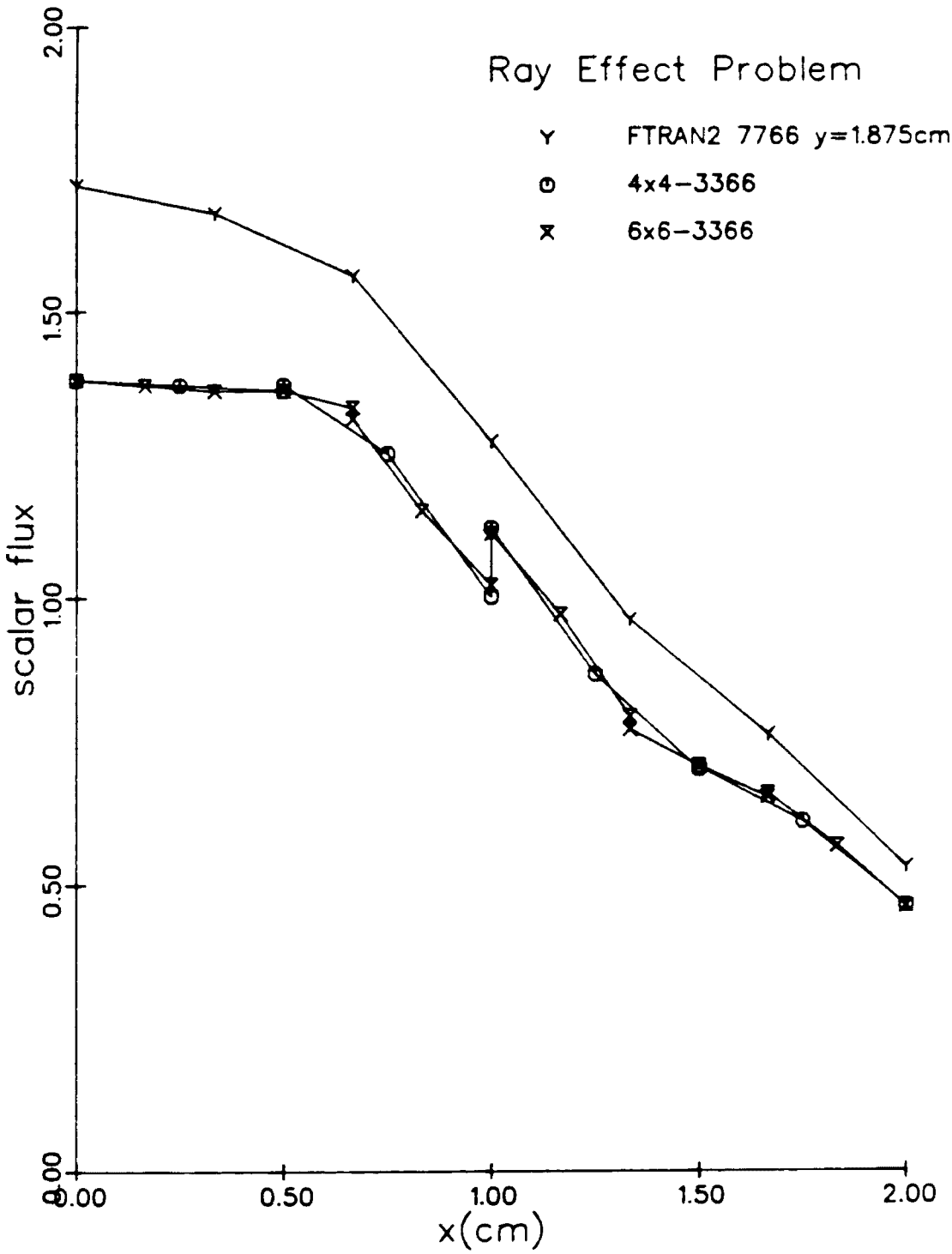


Fig. 5-27. Ray Effect Problem (c=1/3)--scalar flux along side 2, 6x6 angular mesh: FTRAN2 vs. response matrix method.

bine the features of the fine mesh and the coarse mesh. Like the coarse mesh, the profile is high and curved at x=0.0 cm, but further along the traverse it falls between the coarse and fine mesh profiles. The S-shaped dip and peak is less pronounced. From the plot, the effectiveness of the projection procedure in angle is not apparent. The errors in Table 5-10 also indicate that the fine-coarse mesh results agree more closely with the fine mesh results than do the coarse mesh, although not dramatically. Similar observations can be made for the 4x4 configuration plotted in Fig. 5-29.

The selection of the angular mesh is seen to have a large effect on the results obtained by the response matrix method. Fig. 5-30 shows a similar behavior in the standard finite element method.

The ray effect is reduced by decreasing the angular mesh size; a result seen both in the conventional finite element method and the response matrix method. Some of the improvement due to the fine angular mesh is also seen in the coarse angular results obtained using response matrices generated by the fine mesh-coarse mesh projection technique.

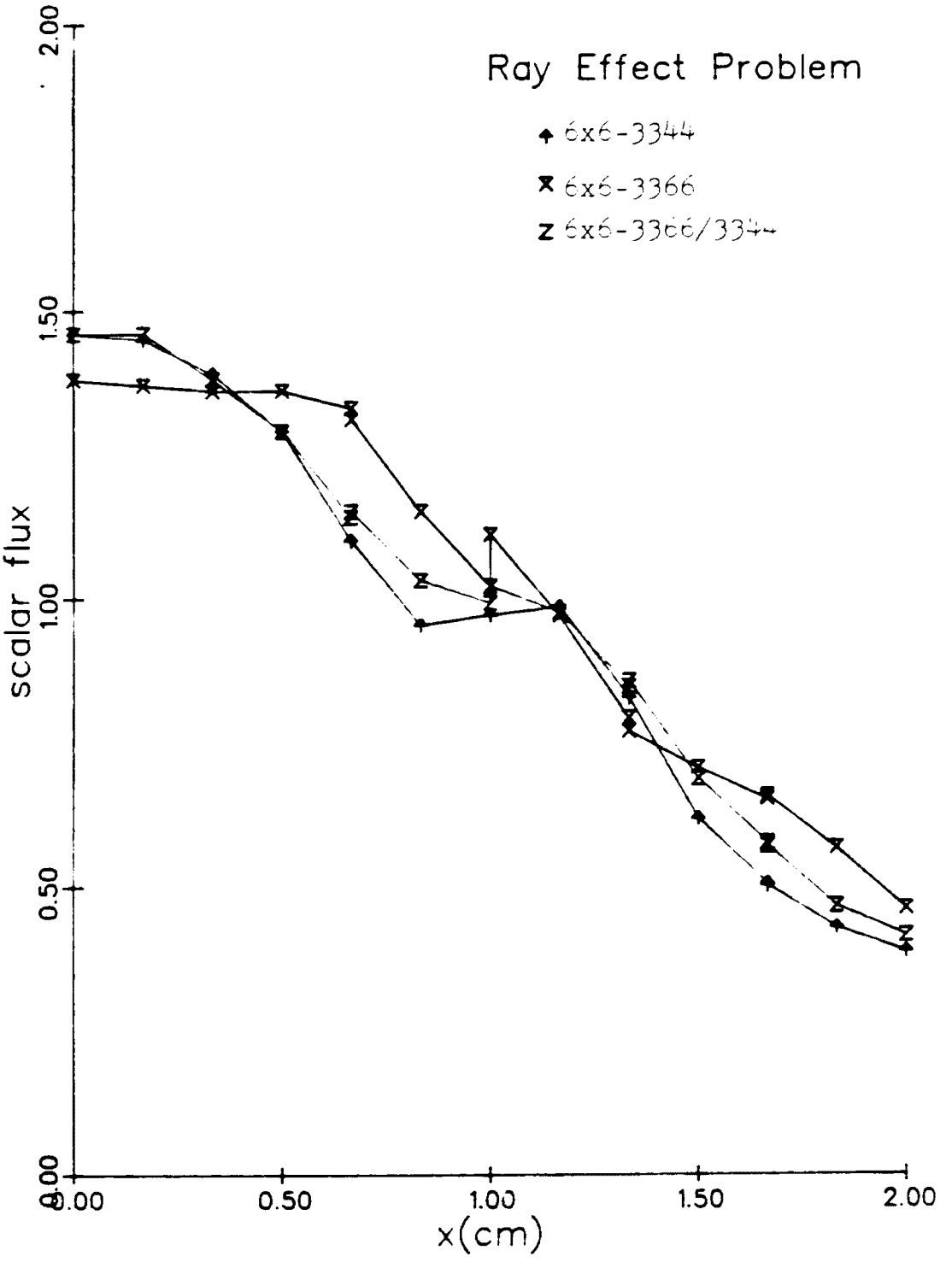


Fig. 5-28. Ray Effect Problem (c=1/3)--scalar flux along side 2: local-global projection in angle (configuration = 6x6).

Table 5-10. Errors in Scalar Flux of Ray Effect Problem (c=1/3): Effect of Fine Angular Mesh

(side 2 traverse; errors relative to 6x6-3366-Δx,Δy=0.1667-local=global; convergence criteria = 1%)

configuration	mesh structure								mesh spacing		error	RMS error
	local				global				Δx (cm)	Δy (cm)		
	i	*j*	*k*	*l*	*i*	*j*	*k*	*l*				
6x6	3	3	6	6	3	3	4	4	0.1667	0.1667	-3.28%	8.08%
6x6	3	3	4	4	3	3	4	4	0.1667	0.1667	-6.42%	11.15%
4x4	3	3	6	6	3	3	6	6	0.25	0.25	0.43%	2.44%
4x4	3	3	6	6	3	3	4	4	0.25	0.25	-1.63%	6.63%
4x4	3	3	4	4	3	3	4	4	0.25	0.25	-6.20%	9.94%

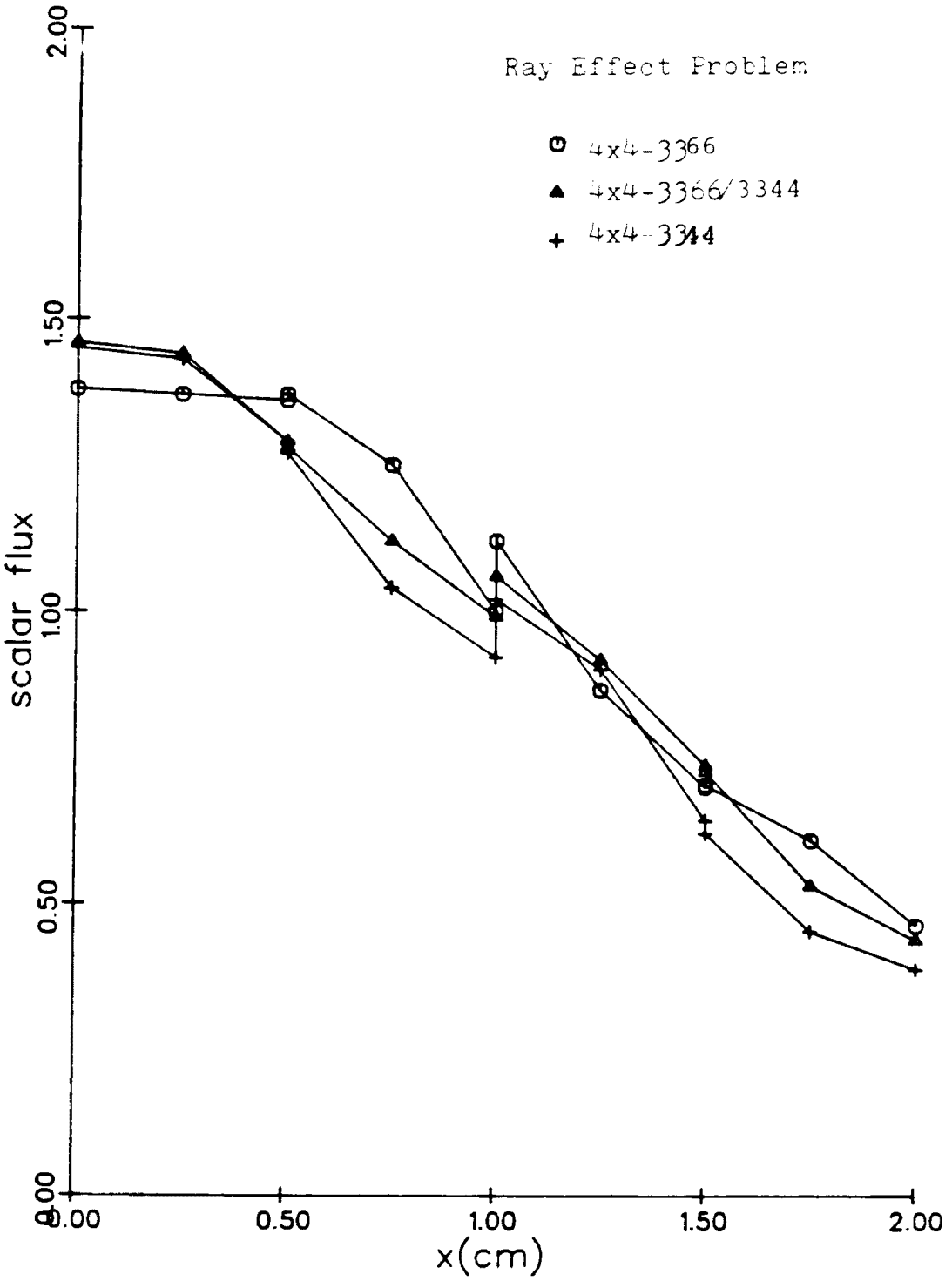


Fig. 5-29. Ray Effect Problem (c=1/3)--scalar flux along side 2: local-global projection in angle (configuration = 4x4).

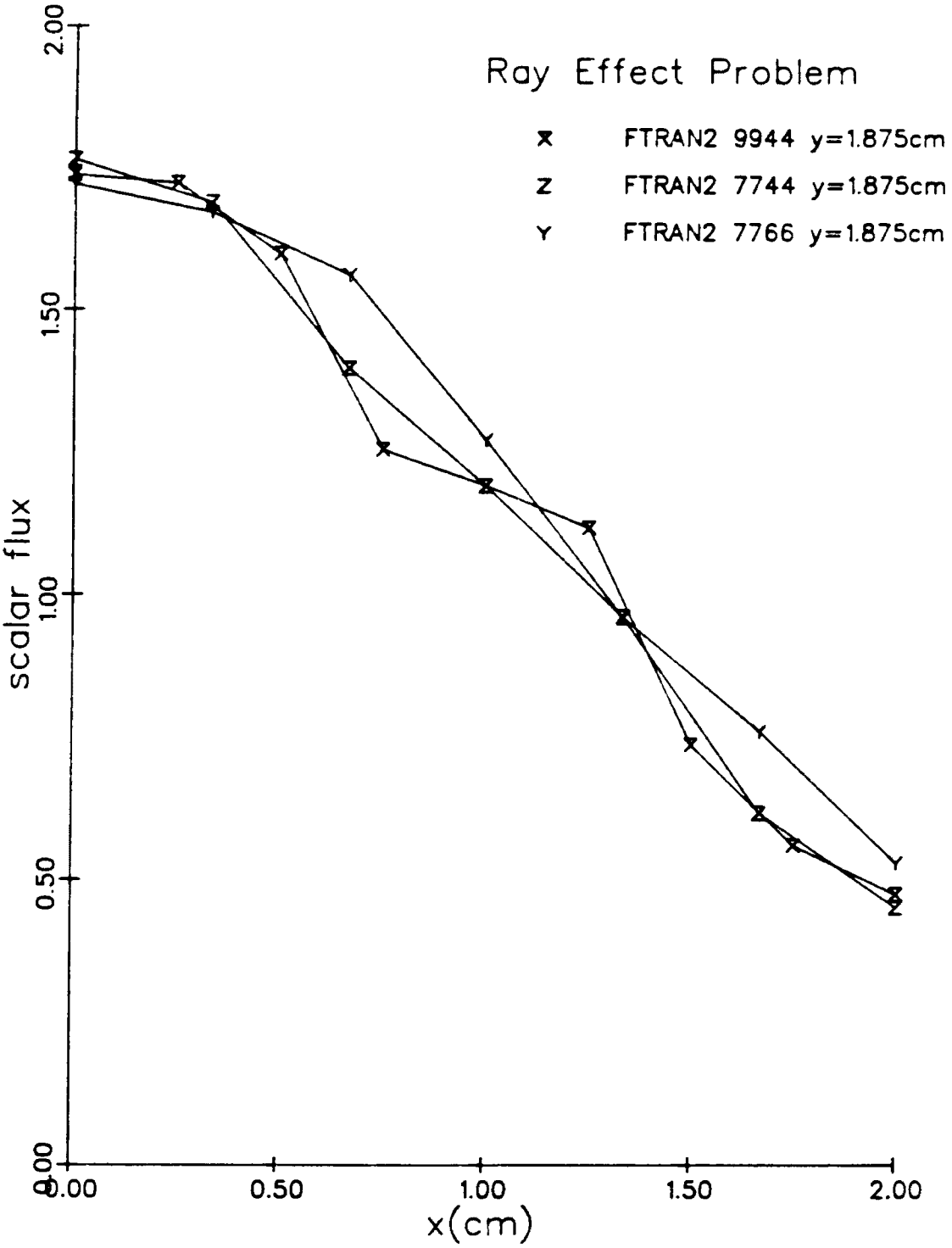


Fig. 5-30. Ray Effect Problem (c=1/3)--scalar flux along side 2: FTRAN2 results.

The Effect of Spatial Projection

Figs. 5-31 and 5-32 indicate the effect of local to global projection in the spatial dimensions. The coarse mesh calculation with response matrices generated using a local mesh spacing of 0.125 cm and a global spacing of 0.25 cm (4x4-5544/3344) agrees more closely with the fine mesh calculation (4x4-5544) than does the coarse mesh calculation (0.25 cm) where local and global mesh are identical (4x4-3344). Table 5-11 verifies this observation. In this case, the projection from a fine mesh improves the coarse mesh calculation.

To further test the spatial projection procedure, a series of calculations using oblong response matrix regions was performed. In all of the following cases, the length of a 1.0x0.3333 cm (or 0.3333x1.0 cm) rectangle is divided into a fine local mesh with 7 support points. Along the width, the local and global mesh spacing is kept constant at 0.1667 cm. During the generation of response matrices the 7 point fine mesh is either retained in the global mesh or projected onto a coarser 4 or 3 point global mesh.

The oblong rectangles and the spatial projection along one side only are necessary because the computational requirements of a 7744 response matrix exceeds the 1 Megabyte single matrix limit of MTS and the AMDAHL 5860.

Once again, the solution is not dependent on the size (or shape) of the response matrices if a constant mesh size is used (see Fig. 5-33). The effect of projection from the

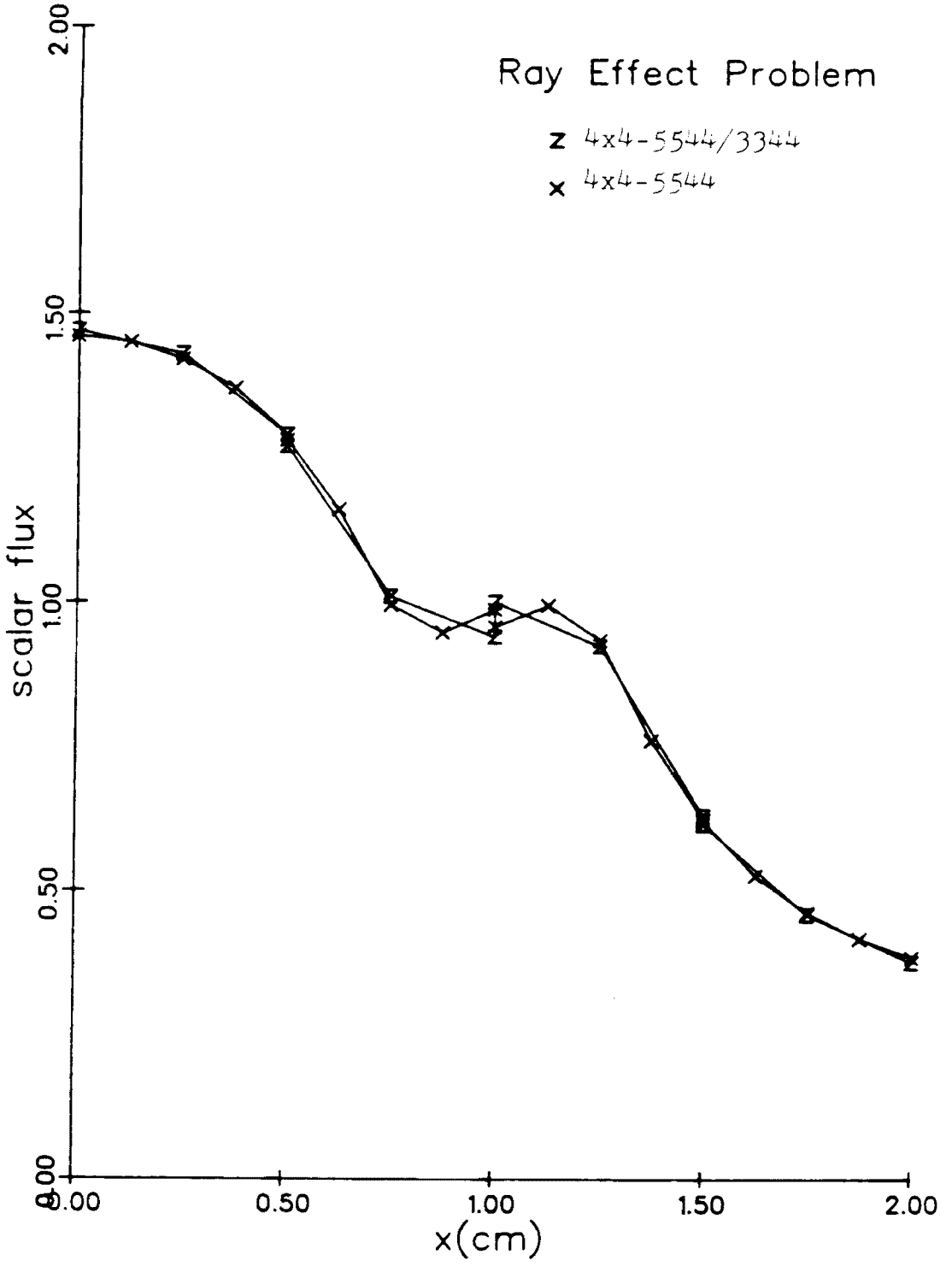


Fig. 5-31. Ray Effect Problem (c=1/3)--scalar flux along side 2: local-global projection in space.

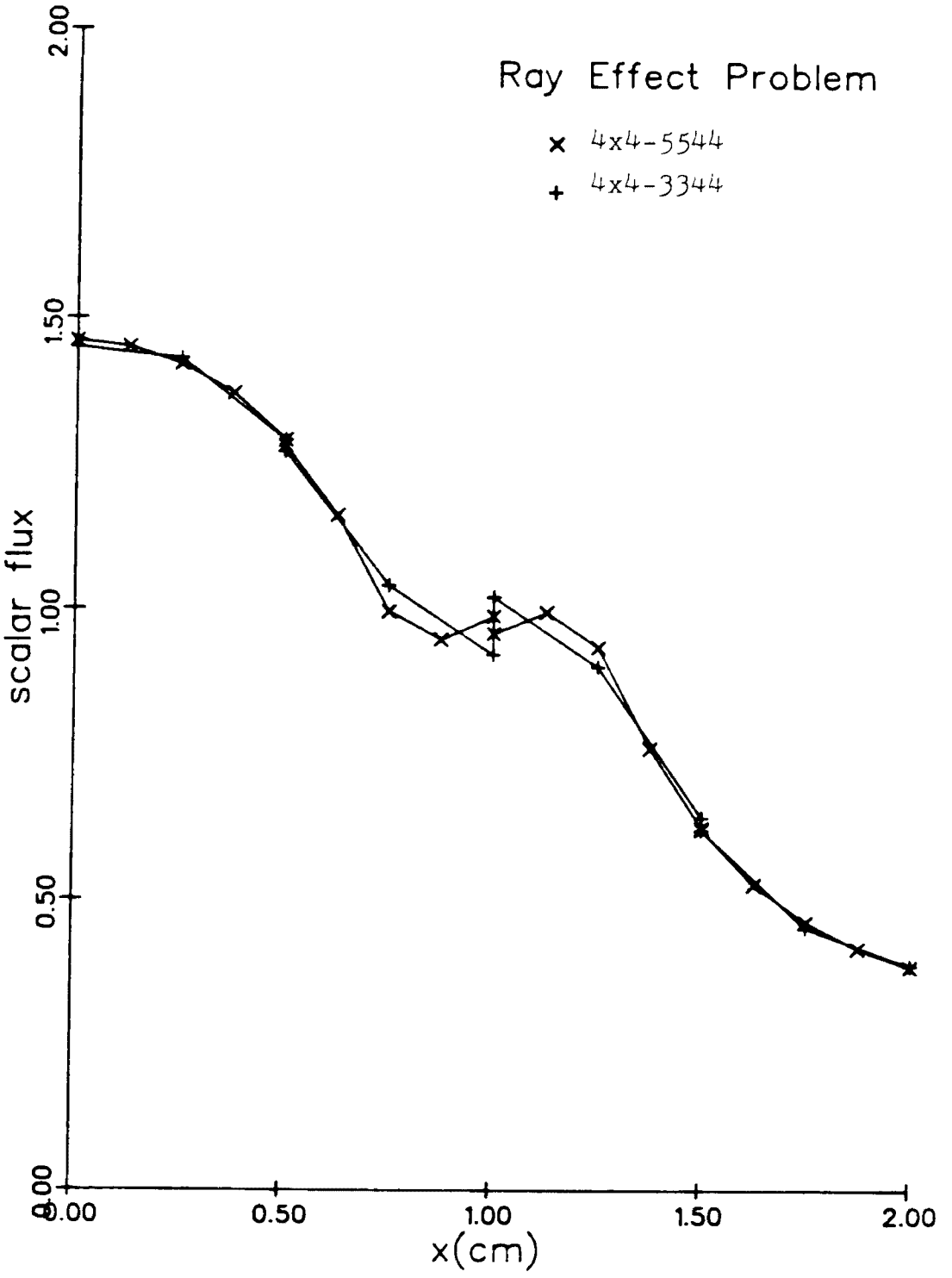


Fig. 5-32. Ray Effect Problem (c=1/3)--scalar flux along side 2: 4x4-5544 vs. 4x4-3344.

Table 5-11. Errors in Scalar Flux of Ray Effect Problem (c=1/3): Effect of Spatial Projection

(side 2 traverse; errors relative to 8x8-3344-Δx,Δy=0.125-local=global; convergence criteria = 1%)

configuration	mesh structure								mesh spacing				error	RMS error
	local				global				local		global			
	i	*j*	*k*	*l*	*i*	*j*	*k*	*l*	Δx (cm)	Δy (cm)	Δx (cm)	Δy (cm)		
4x4	5	5	4	4	5	5	4	4	0.125	0.125	0.125	0.125	-0.18%	0.65%
4x4	5	5	4	4	3	3	4	4	0.125	0.125	0.25	0.25	0.05%	1.69%
4x4	3	3	4	4	3	3	4	4	0.25	0.25	0.25	0.25	0.23%	2.28%
2x6	7	3	4	4	7	3	4	4	0.1667	0.1667	0.1667	0.1667	-0.08%	1.12%
2x6	7	3	4	4	4	3	4	4	0.1667	0.1667	0.3333	0.1667	0.58%	3.31%
2x6	7	3	4	4	3	3	4	4	0.1667	0.1667	0.5	0.1667	0.78%	4.35%
2x2	3	3	4	4	3	3	4	4	0.5	0.5	0.5	0.5	0.15%	4.57%
6x2	3	7	4	4	3	7	4	4	0.1667	0.1667	0.1667	0.1667	-0.02%	1.16%
6x2	3	7	4	4	3	4	4	4	0.1667	0.1667	0.1667	0.3333	-0.04%	1.47%
6x2	3	7	4	4	3	3	4	4	0.1667	0.1667	0.1667	0.5	-0.64%	2.25%

7 support point fine mesh is seen in Fig. 5-34. The coarse mesh solution follows the fine mesh solution reasonably well, but comparing the coarse mesh calculation seen in Fig. 5-35 and examining the errors in Table 5-11 indicate the improvement of a fine-coarse mesh calculation over a simple coarse mesh calculation is insignificant.

The fine mesh 7344 and 3744 calculations are seen to be nearly identical in Fig. 5-36, as expected. The effect of increasing the mesh size from that of the 7 point mesh is less significant because the plots in Fig. 5-37 are along the x-direction, not the y-direction where the coarse mesh resides. Changes in the y-direction mesh spacing affects the x-direction errors nonetheless, as seen in Table 5-11. For these 7 point problems the local-global projection has little benefit.

The projection from a fine local spatial mesh to a coarse global spatial mesh is beneficial in one case presented but not in others. The 5544/3344 calculation provides a result superior to the 3344 calculation. But the projection from the 7 point fine mesh has little advantage over the coarse mesh calculation with no projection.

Three different calculations of the ray effect problem with the scattering fraction increased to 2/3 are presented in Figs. 5-38 and 5-39. In both figures, the S-curve has diminished due to increased scattering which reduces the ray effect.

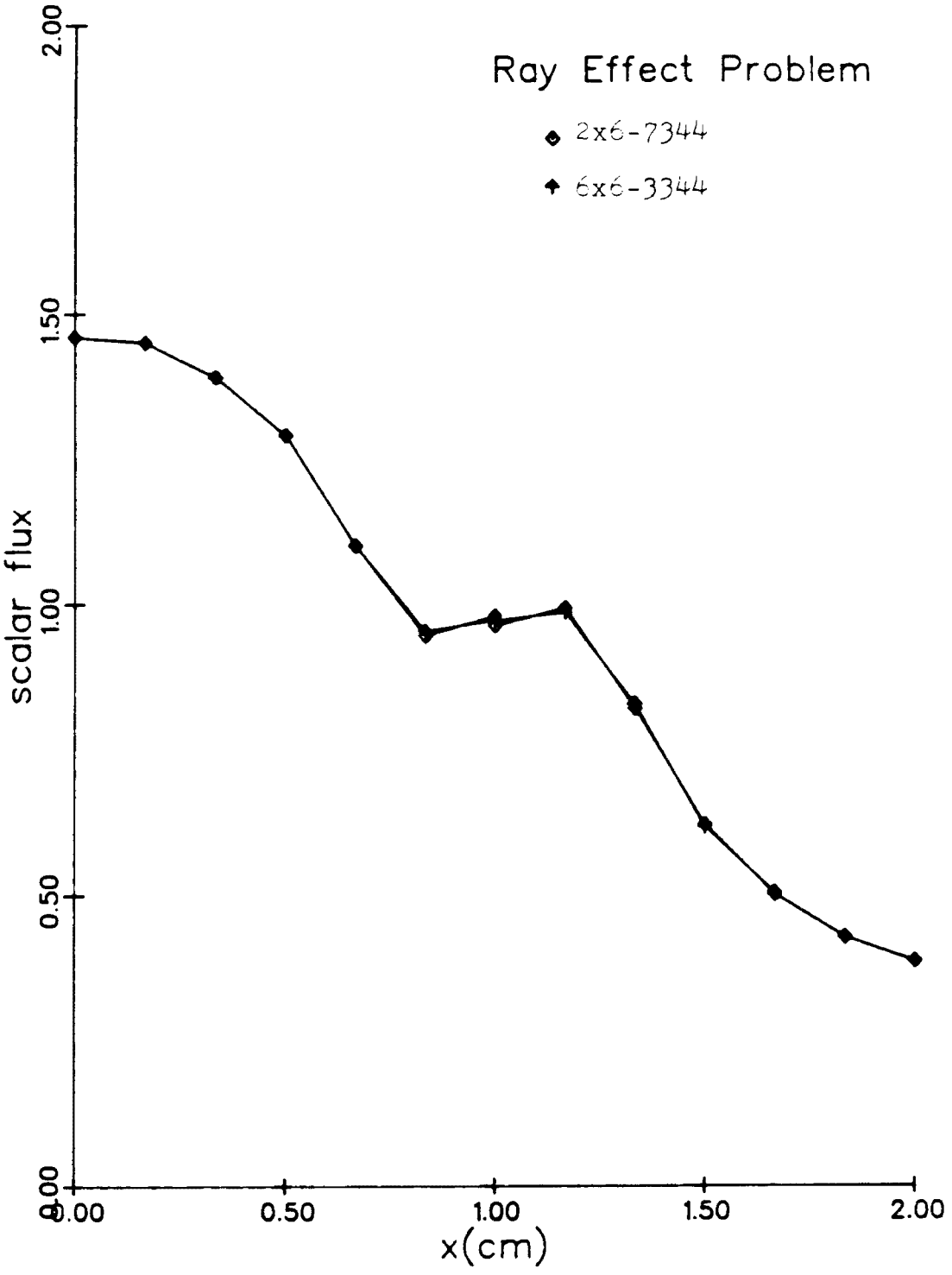


Fig. 5-33. Ray Effect Problem (c=1/3)--scalar flux along side 2: 2x6-7344 vs. 6x6-3344.

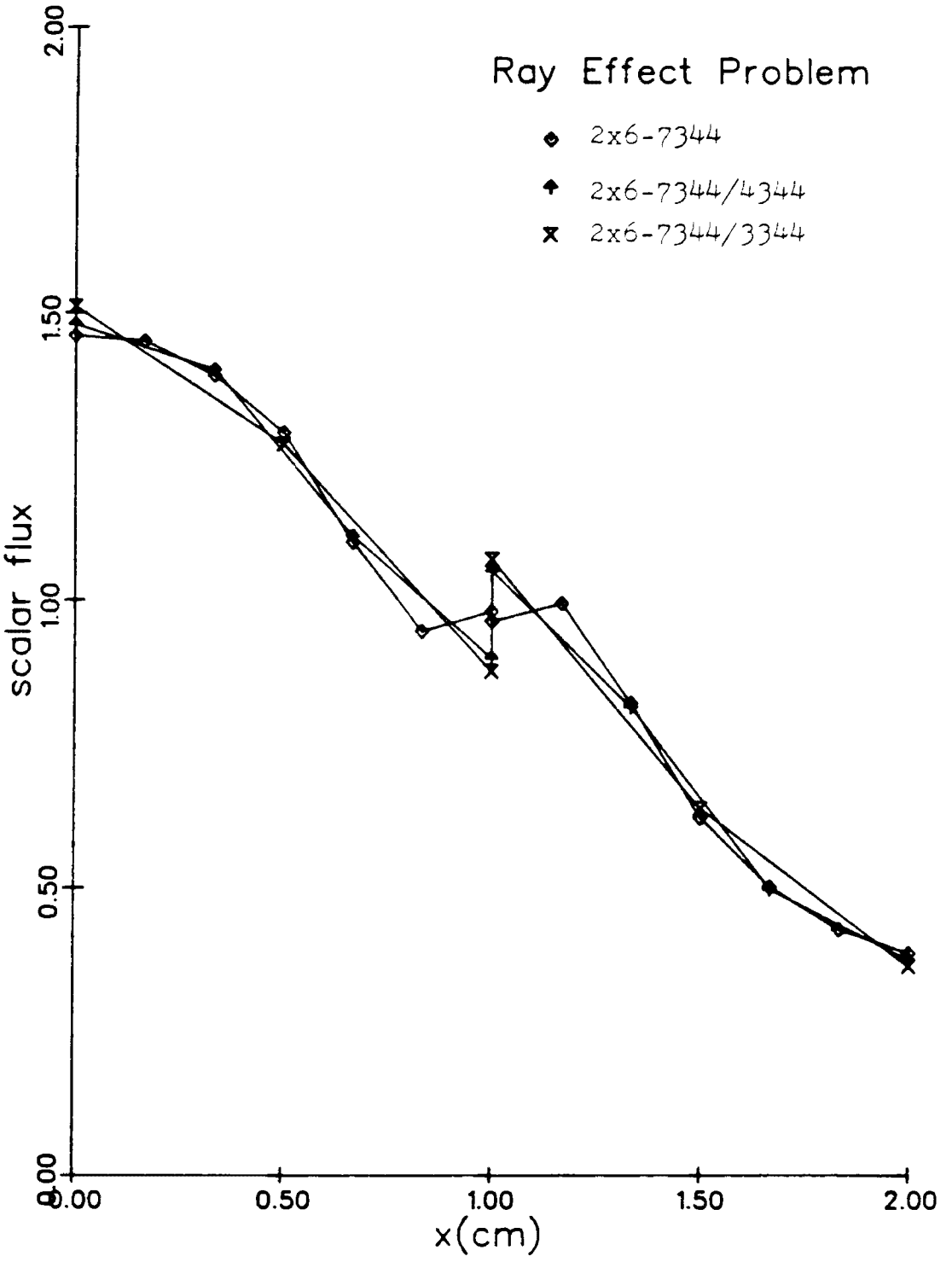


Fig. 5-34. Ray Effect Problem (c=1/3)--scalar flux along side 2: projection in space from 7 point fine mesh (x-direction).

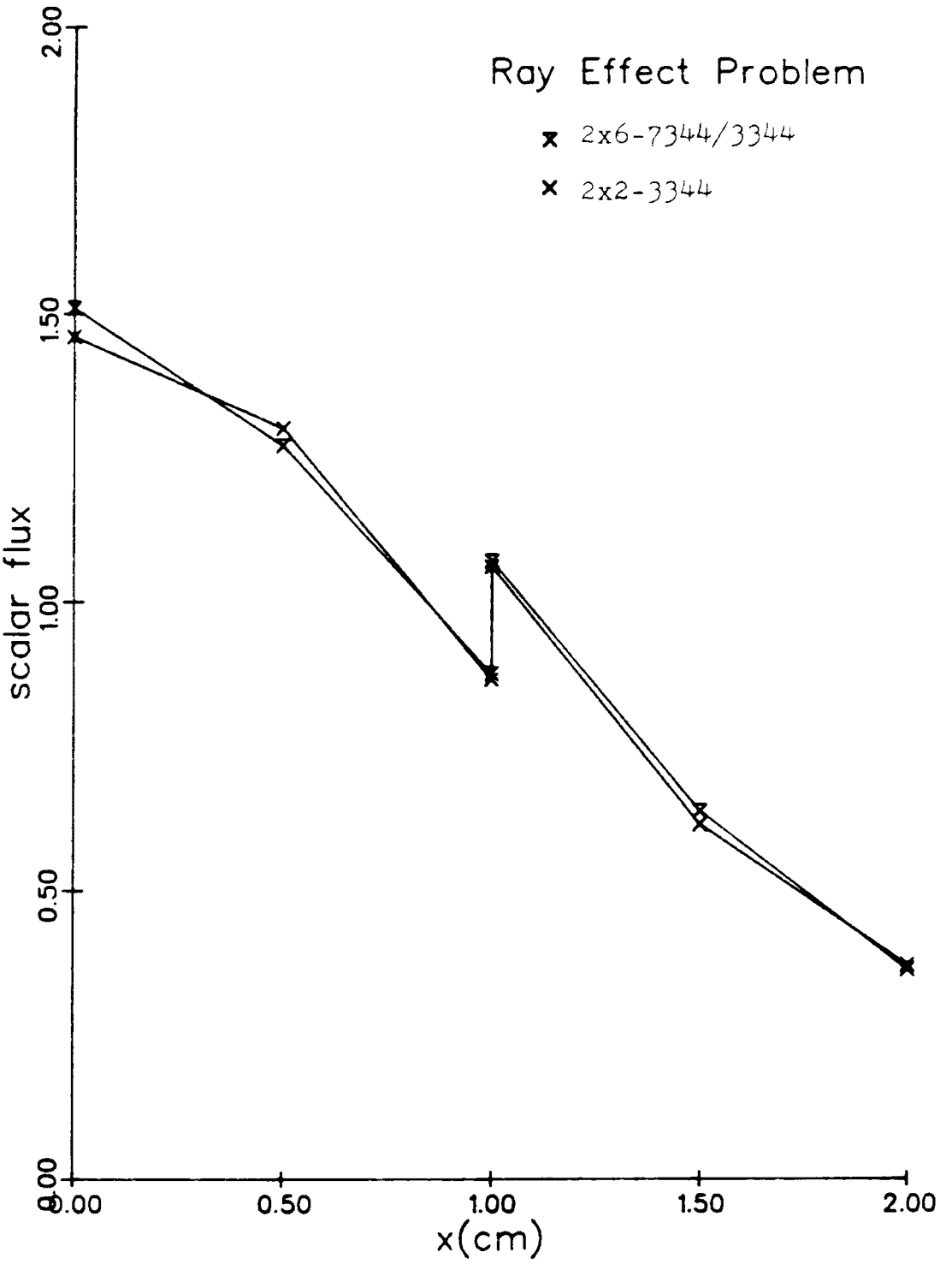


Fig. 5-35. Ray Effect Problem (c=1/3)--scalar flux along side 2: 2x6-7344/3344 vs. 2x2-3344.

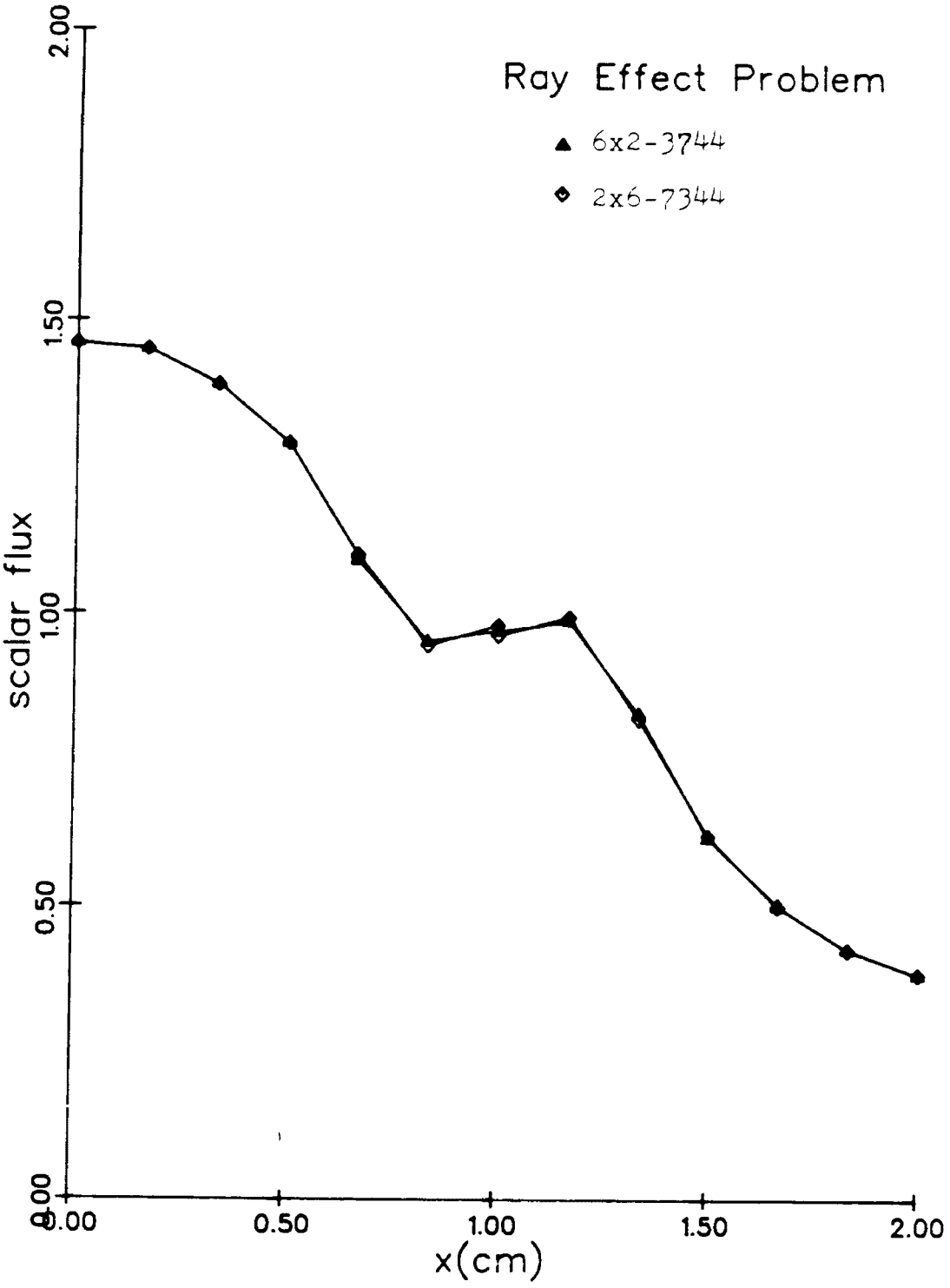


Fig. 5-36. Ray Effect Problem (c=1/3)--scalar flux along side 2: 6x2-3744 vs. 2x6-7344.

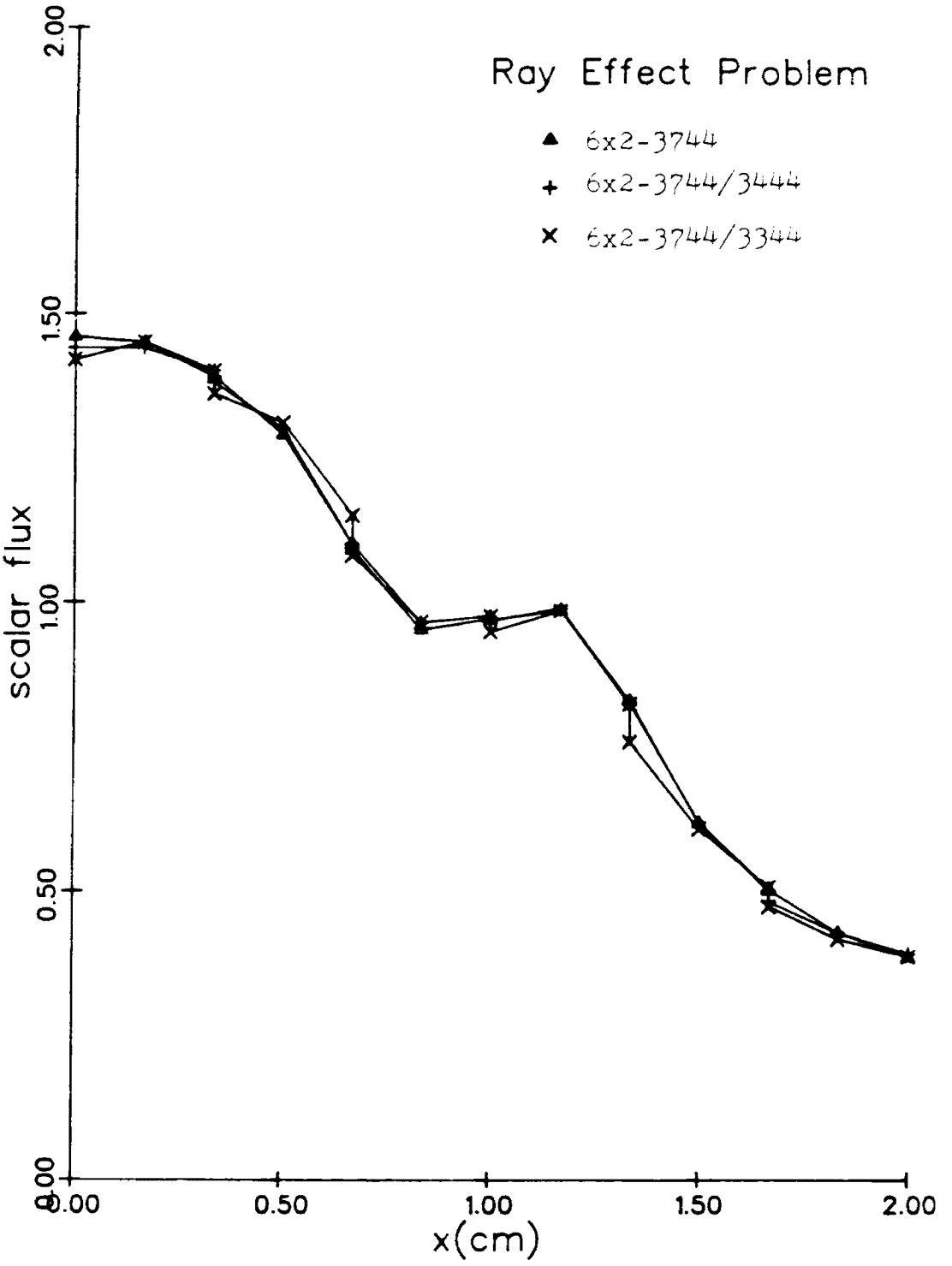


Fig. 5-37. Ray Effect Problem (c=1/3)--scalar flux along side 2: projection in space from 7 point fine mesh (y-direction).

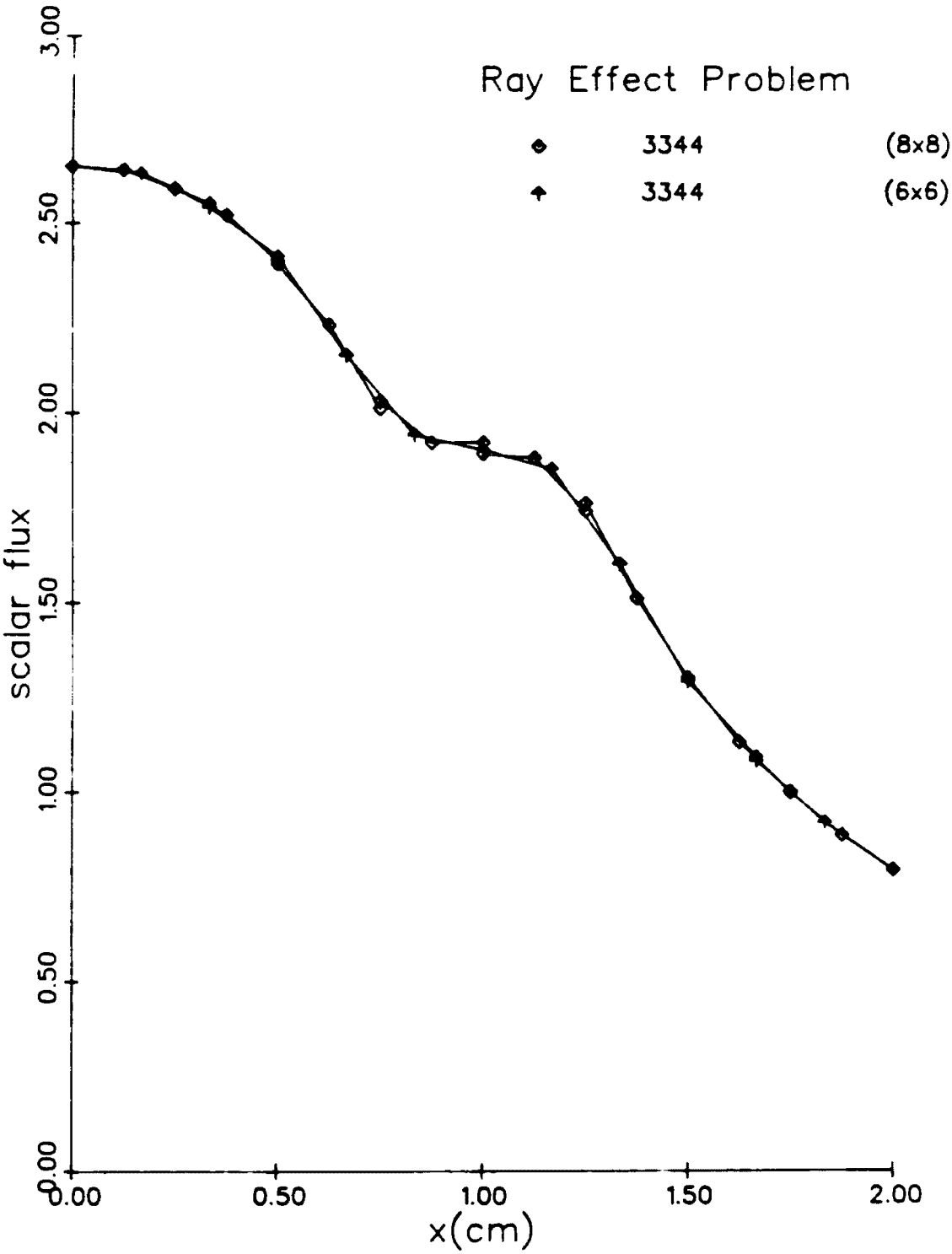


Fig. 5-38. Ray Effect Problem (c=2/3)--scalar flux along side 2: 8x8-3344 vs. 6x6-3344.

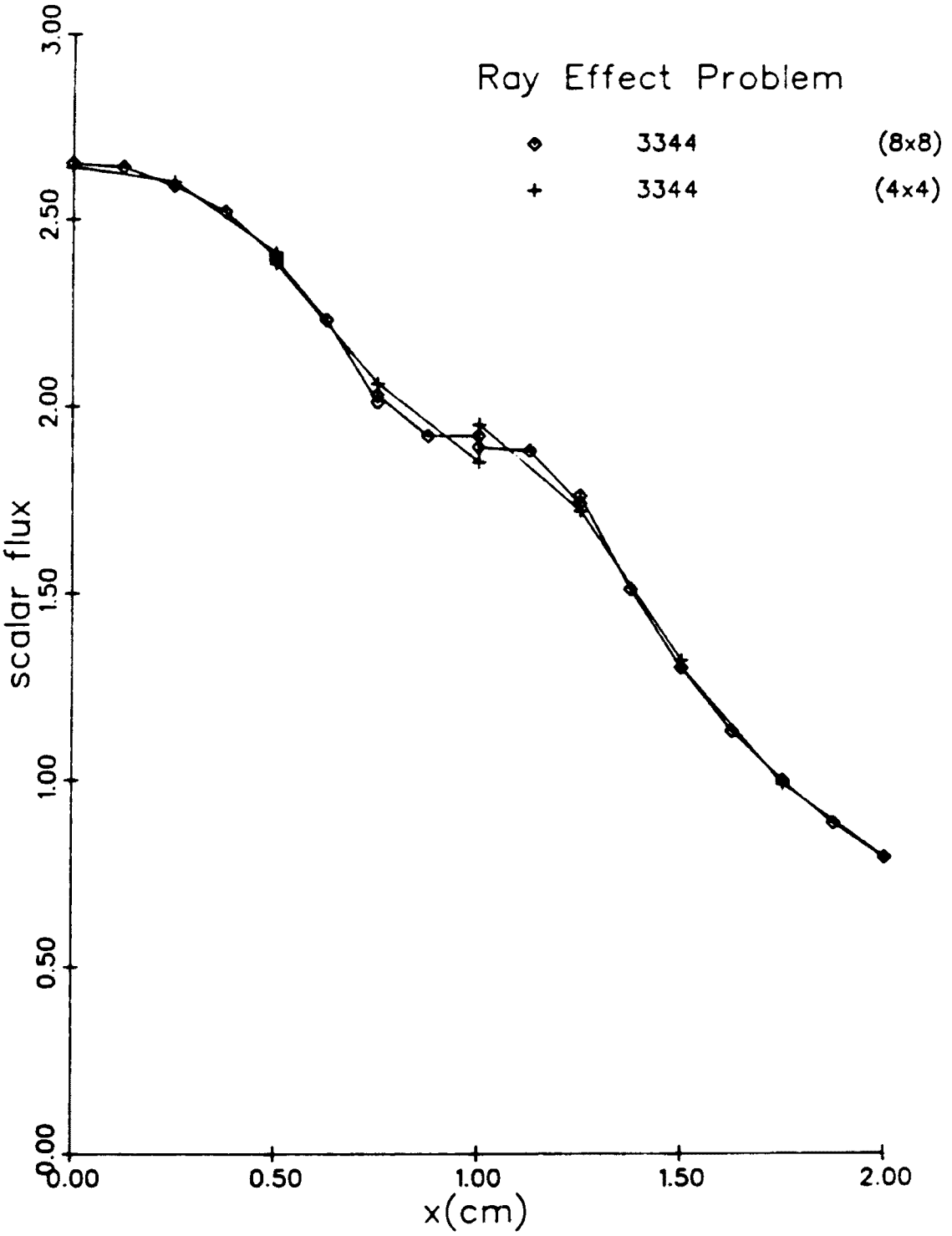


Fig. 5-39. Ray Effect Problem (c=2/3)--scalar flux along side 2: 8x8-3344 vs. 4x4-3344.

Computational Considerations

The computational requirements of the two-dimensional response matrix method are much more demanding than the one-dimensional method both in terms of CPU time and storage. Full fine mesh matrices must be stored during response matrix generation for two reasons: the scattering operator couples all angular support points at common spatial locations, and explicit inversion tends to fill all matrix elements. Table 5-12 lists some storage requirements of square matrices. On the AMDAHL, a single precision word requires 4 bytes.

Some response matrix generation times are presented in Table 5-13. The lion's share of costs belong to the matrix inversion. As was the case for the one-dimensional method, costs are greater if local/global projection is performed. The effect of the exploitation of matrix band structure is seen in the times of the non-symmetric response matrices. The time required to invert a 7344 matrix is less than for a 3744 matrix because for the latter matrix the y-direction block structure is imbedded in the x-direction blocks.

The analysis of the ray effect problem benefits from the use of a relaxation parameter different than 1.0, as was also true for Reed's problem. Fig. 5-40 and 5-41 shows the effect of varying the relaxation parameter for c=1/3 and c=2/3, respectively. If the problem contained no scattering, the optimal relaxation factor would be 1.0. For this reason, the weaker the scattering, the close to 1.0 the

Table 5-12. Two-Dimensional Storage Requirements

local mesh structure				matrix	
i	*j*	*k*	*l*	words	storage (KBytes)
3	3	4	4	20,736	83.
4	4	4	4	65,536	262.
5	5	4	4	160,000	640.
7	7	4	4	614,656	2,459.
3	3	6	6	104,976	420.
4	4	6	6	331,776	1,327.
4	3	4	4	36,864	147.
7	3	4	4	112,896	452.
4	3	6	6	186,624	746.
7	3	6	6	571,536	2,286.

Table 5-13. Two-Dimensional Response Matrix Generation Costs (AMDAHL 5860)

mesh structure								CPU time (sec)			
local				global				finite element matrix generation	finite element matrix inversion	response matrix generation	total
i	*j*	*k*	*l*	*i*	*j*	*k*	*l*				
3	3	6	6	3	3	6	6	0.433	17.553	4.361	22.345
3	3	6	6	3	3	4	4	0.433	17.553	5.706	23.690
3	3	4	4	3	3	4	4	0.117	1.504	0.667	2.288
4	3	4	4	4	3	4	4	0.392	3.302	1.213	4.907
4	4	4	4	4	4	4	4	0.226	11.997	2.254	14.477
5	5	4	4	5	5	4	4	0.377	25.102	5.382	30.821
5	5	4	4	3	3	4	4	0.377	25.102	6.687	32.166
3	7	4	4	3	7	4	4	0.274	19.366	3.733	25.696
3	7	4	4	3	4	4	4	0.274	19.366	8.083	27.736
3	7	4	4	3	3	4	4	0.274	19.366	5.292	24.932
7	3	4	4	7	3	4	4	0.314	12.501	3.696	16.511
7	3	4	4	4	3	4	4	0.314	12.501	8.174	20.989
7	3	4	4	3	3	4	4	0.314	12.501	5.307	18.122

optimal relaxation parameter. For c=1/2, ω_{opt}=1.1; for c=2/3, ω_{opt}=1.2. Note, however, that as the response matrix regions decrease in size, the optimal relaxation parameter tends toward 1.0 because the effect of scattering diminishes for thin regions.

Table 5-14 is a compilation of the total CPU time required to solve the ray effect problem using various combinations of local-global spatial and angular mesh and response matrix sizes. With many small regions, the iteration costs dominate; with few large regions, the response matrix generation costs dominate. An increase in the number of angular support points increases the computational costs greatly. The trade-off between iteration costs and response matrix generation costs favor many small regions as expected. The basic premise of the response matrix philosophy is to analyze a small region in detail and make use of the information in the solution of a large system. The expense associated with the explicit inversion of the fine mesh finite element matrices compared to the relatively inexpensive iteration costs reinforce this philosophy.

Table 5-15 presents a listing of computational costs of equivalent calculations using FTRAN2 and the response matrix method. The times clearly indicate that the response matrix method is vastly more efficient, by as much as 6 times for the 9944 case. Lorence's explicitly interfaced finite element method [Lor84] is nearly 3 times faster than the standard FTRAN2 for the 7766 case.

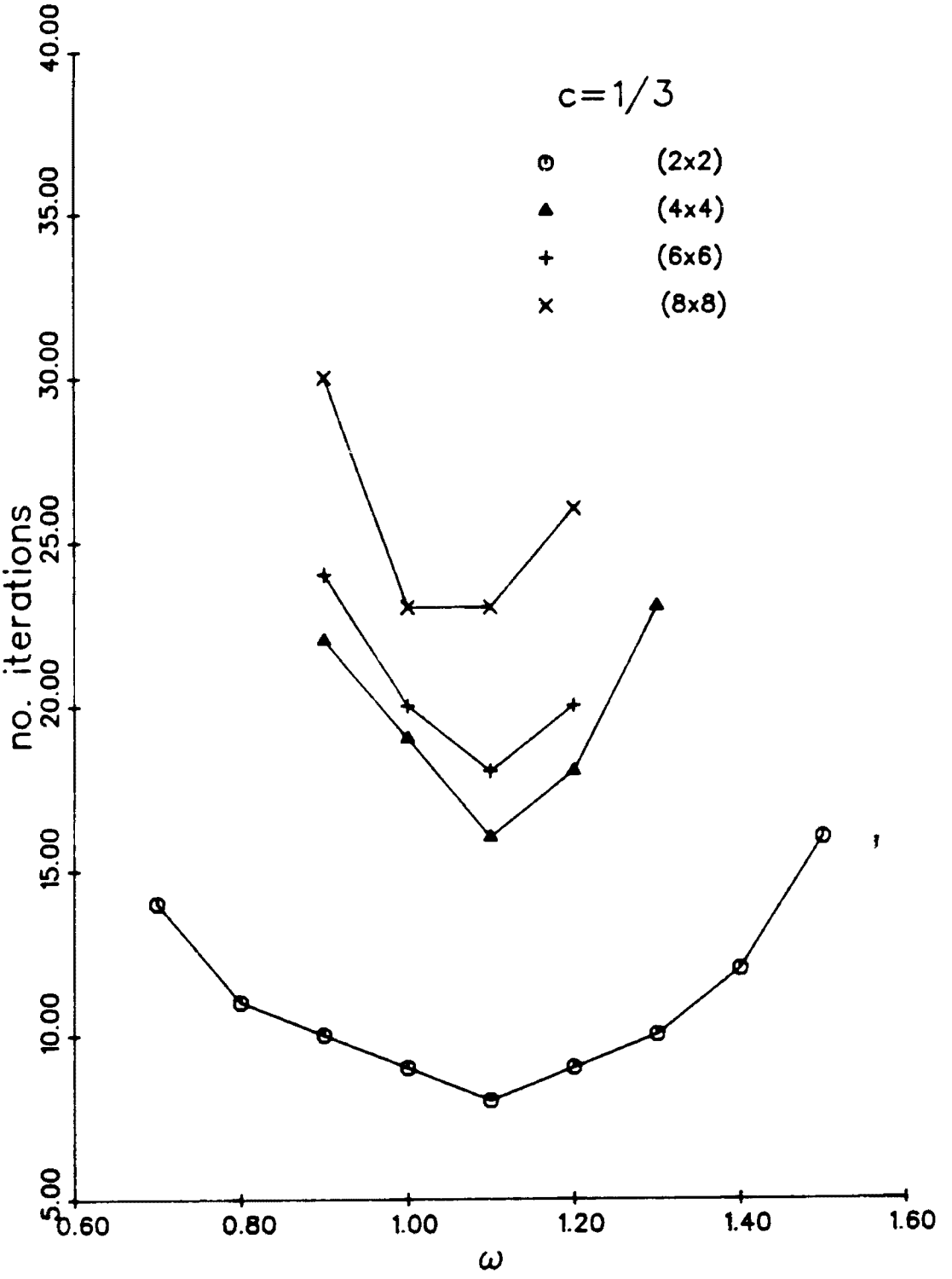


Fig. 5-40. Number of iterations vs. relaxation parameter (Ray Effect Problem, c=1/3).

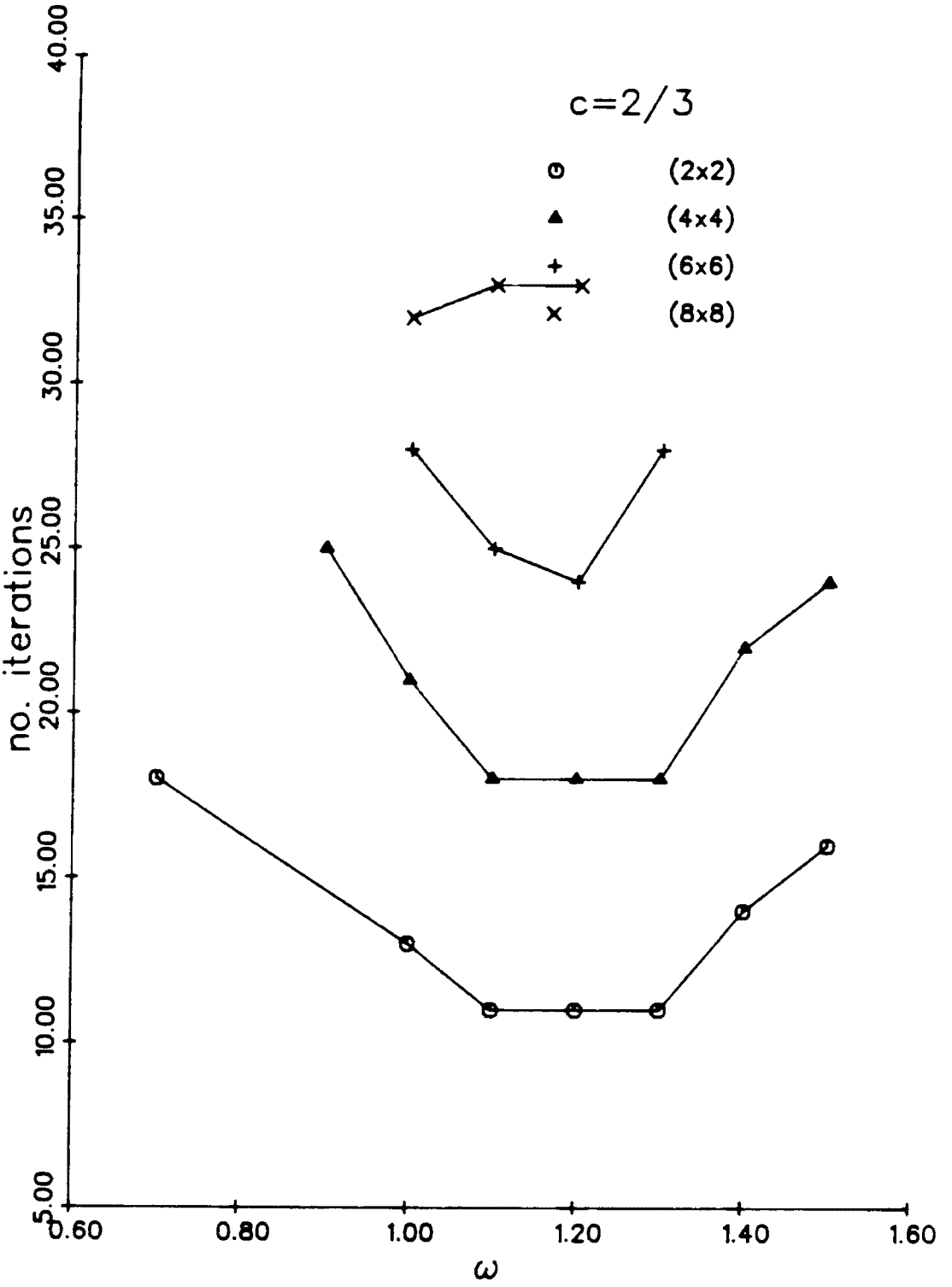


Fig. 5-41. Number of iterations vs. relaxation parameter (Ray Effect Problem, c=2/3).

Table 5-14. Computational Costs to Solve Ray Effect Problem (c=1/3)

(AMDAHL 5860; convergence criteria = 1%)

configuration	mesh structure: local				mesh structure: global				total response matrix generation time (sec)	iteration			total CPU time (sec)
	i	*j*	*k*	*l*	*i*	*j*	*k*	*l*		ω	total no. inners	CPU time (sec)	
8x8	3	3	4	4	3	3	4	4	2.288	1.0	24	17.068	19.356
6x6	3	3	4	4	3	3	4	4	2.288	1.0	21	8.337	10.625
6x6	3	3	6	6	3	3	6	6	22.345	1.1	21	42.116	64.401
6x6	3	3	6	6	3	3	4	4	23.690	1.1	16	6.463	30.153
4x4	3	3	4	4	3	3	4	4	2.288	1.0	20	3.406	5.694
4x4	3	3	6	6	3	3	6	6	22.345	1.0	18	15.668	38.013
4x4	3	3	6	6	3	3	4	4	23.690	1.0	15	2.652	26.342
4x4	4	4	4	4	4	4	4	4	14.477	1.1	16	6.425	20.902
4x4	5	5	4	4	5	5	4	4	30.821	1.1	17	9.030	39.851
4x4	5	5	4	4	3	3	4	4	32.166	1.1	15	2.646	34.812
2x2	3	3	4	4	3	3	4	4	2.288	1.0	10	0.412	2.700
4x6	4	3	4	4	4	3	4	4	4.907	1.1	19	6.880	11.787
6x2	3	7	4	4	3	7	4	4	25.696	1.1	16	8.453	34.149
6x2	3	7	4	4	3	4	4	4	27.723	1.1	14	3.420	41.549
6x2	3	7	4	4	3	3	4	4	24.932	1.1	14	2.275	34.822
2x6	7	3	4	4	7	3	4	4	16.511	1.1	15	8.065	24.576
2x6	7	3	4	4	4	3	4	4	20.989	1.1	14	3.418	24.407
2x6	7	3	4	4	3	3	4	4	18.122	1.1	14	2.274	20.396

Table 5-15. Comparison of Computational Cost: FTRAN2 vs. Response Matrix Method

Δx, Δy	FTRAN2[1] ref. [Yeh78]			Response Matrix Method			
	mesh structure	AMDAHL V/6 CPU time (sec)	AMDAHL 5860 CPU time (sec)	config-uration	mesh structure	AMDAHL 5860 CPU time (sec)	CPU time ratio
0.3333	7744	80	12	2x2	4444	14.9[2]	0.8
0.25	9944	219	34	4x4	3344	5.695	6.0
0.3333	7766	878	132[3]	...	....	.....	....
0.25	9966	2400[2]	360[2,3]	4x4	3366	38.013	9.5[2]

[1]time spent in matrix solving subroutine

[2]estimated

[3]conversion factor of 6.7 used

Summary

Solutions of the ray effect problem can be found efficiently using the response matrix method. The accuracy of these solutions is dependent only on the spatial and angular discretization chosen, not on the size or shape of the response matrix regions. The ray effect is reduced by the use of a fine support grid in angle. Some reduction, although slight, results in the coarse angular grid solution if response matrices are used that have been found by projecting the solution from the fine grid to the coarse grid. For some cases, spatial local-global projection is effective; for others it, is not. In two dimensions, the advantage of the response matrix method appears not to lie in its ability as a coarse mesh method but in the dramatic improvement in computational efficiency over the conventional two-dimensional finite element method.

CHAPTER VI

SUMMARY

In this work, a finite element response matrix method for the solution of the transport equation has been developed. It has been implemented and coded for use on a computer in the analysis of one- and two-dimensional geometries. The finite element method is used to solve the transport equation as a function of an arbitrary volumetric source distribution and an arbitrary incoming angular flux boundary condition on small regions of the spatial domain. The solution is described on a fine local mesh. By projecting this solution onto coarser meshes--one defined only on the region surface, the other defined on the entire volume--a system of response matrices result that is incorporated into an iterative solution scheme. This scheme is used to find a global distribution of particles in space and angle. Because the scheme is iterative, efficiency is increased with coarser global mesh.

If the effect of scattering is considered during the generation of the response matrices (i.e., the scattering operator is retained on the left side of the transport equation), the solution of a fixed source problem can be found with only one outer iteration and as many inner iterations

as are necessary to meet the specified convergence criterion on the interface fluxes. In contrast, if the scattering source is determined explicitly from the volumetric flux distribution, many outer iterations are required to find the converged source distribution. The number of inner iterations in each outer iteration, however, is reduced to a fixed number, 2, independent of the interface flux convergence criterion, because the absence of scattering in the response matrices eliminates reflection by the response matrix regions. If the problem contains a multiplying material, the fission source is found from the volumetric flux distribution in the same manner. A multiplication constant, or eigenvalue, is calculated from the ratio of the fission source distribution found in successive outer iterations.

The method uses multidimensional Lagrange polynomials as the basis functions not only for the determination of the finite element matrix but also as the basis functions for the global surface and volume series expansions. Because the multidimensional polynomials are found by taking the tensor product of one-dimensional polynomials, the intermediate matrices and their inverses needed in the response matrix calculation can be assembled via tensor products of one-dimensional matrices and their inverses.

Computational testing of the method indicates that accurate solutions to the transport equation can be found by this method. If a consistent mesh is used, identical solu-

tions can be found using response matrix regions of different sizes. In one dimension, the method works very well. The projection from a fine mesh solution onto a coarse mesh provides an effective coarse mesh transport method. Response matrices have been calculated and tested for regions with internal heterogeneities although the current implementation of the method must be improved in order to allow discontinuous source distributions on the interior of response matrix regions. With this present limitation taken into account, equally satisfactory results are obtained with both heterogeneous and homogeneous response matrix regions.

For most one-dimensional problems analyzed, the response matrix method proved to be less computationally efficient than the conventional finite element method. The lone exception is problems that require iteration solutions by both methods--specifically, eigenvalue or criticality problems. For all problems analyzed, the effort required to generate response matrices far exceeds that required to find the iterative global solution. By decreasing the number of spatial support points in each response matrix region a large savings is realized. This is a consequence of the direct inversion involved in this part of the calculation. In order to maintain a constant support point spacing, the number of response matrix regions must be increased accordingly resulting in an increase in iteration costs, both in the number of iterations needed and in the cost per iteration. The trade-off, however, favors response matrix

regions with as few spatial support points as possible. The iteration costs can be reduced, however, by using a coarse global mesh.

The computational costs in two dimensions, in terms of both CPU time and memory requirements, are much greater than in one dimension, as one would expect. Due to storage and memory constraints, the local-global projection technique could not be tested to the extent it was examined in the one-dimensional implementation. For some cases the projection in the spatial dimension worked quite well. When projection was performed in only one spatial variable, poorer results were observed perhaps because the effect of the projection was overwhelmed by the absence of projection in the perpendicular direction.

Projection to a coarse mesh in angle was less satisfactory. Again due to practical constraints, only 66 to 44 angular mesh projection calculations were performed. A plausible reason for the disappointing results is that the 66 angular mesh is already too coarse to provide an adequate solution. Projection to a still coarser mesh would, in that case, give poor results.

The two-dimensional response matrix method was found to give good solutions. Moreover, the increase in computational efficiency over the standard two-dimensional finite element method is dramatic: for some cases, from 6 to 10 times more efficient. In two dimensions, the advantage of response matrix regions with as few spatial

support points as possible is all the more apparent. In fact, with 3344 response matrices, the iteration costs for the ray effect problem exceed the matrix generation costs. By just increasing the spatial mesh to 4444, this situation is reversed and the total costs increase.

Any further work with the response matrix method should be directed toward the two-dimensional implementation because there the greatest rewards might be gained. Beyond the needed additional verification of the method with a reliable two-dimensional benchmark solution, improvements could be made in the memory requirements, CPU requirements, and some theoretical aspects.

In all the cases examined in this investigation, symmetric response matrices were found. Although this is generally true for only single energy group formulations, this characteristic can be easily exploited to reduce the storage requirements of the matrices themselves. It is not obvious how one can utilize this feature to reduce the calculational requirements, however.

The effect of scattering can be handled in two ways, as mentioned above. It was found that it is less expensive to include scattering in the response matrices than to calculate the scattering source in the outer iteration from the volumetric flux distribution. No acceleration is included, however, in the outer iteration loop. With a simple acceleration scheme such as the asymptotic source extrapolation method or the Chebyshev polynomial method, convergence

could be reached more quickly with little or no additional work per iteration. Modern source iteration techniques such as synthetic diffusion would dramatically reduce the number of outer iteration, not without, however, an increase in the costs associated with each iteration. With these outer iteration acceleration techniques, together with the need of only a fixed number of inner iterations per outer, the explicit scattering source calculation in the outer loop could win out over the implicit treatment of scattering within the response matrices themselves.

In two-dimensional geometries, two angles are needed to describe the angular neutron distribution. In this work, a rectangular grid of μ and Φ is used to discretize the angular variables. For the 44 angular grid used for most problems, only five distinct angular coordinate pairs serve as finite element support points, but 16 pairs are involved in the calculations. The discrepancy exist for two reasons: (1) double support points are required at angles where discontinuities are allowed, and (2) at the poles of the unit angular sphere ($\mu=\pm1$) all of the support points in Φ degenerate to one point--the pole itself. A systematic treatment of the degenerate poles would reduce the storage and computational requirements dramatically. Low-order spherical harmonics are possible alternatives to the use to Lagrange polynomials as basis functions.

The obvious extensions of the method to time-dependent problems, multi-group formulations, and curvilinear geome-

tries must be mentioned. The most straight forward multi-group approach would be to find response matrices for each group and calculate the group-to-group transfer via in-scattering explicitly in the outer iteration loop.

Finally, a word about implementation of the method on multi-processor or vector computers. It is not difficult to see how one would utilize a multi-processing environment. During the response matrix generation phase, each processor could be dedicated to calculating the response matrices for a unique region. Processor-to-processor communication would be necessary, however, during the global solution iteration phase. The method could be easily and efficiently converted to take advantage of a vector machine architecture. In fact, during the early stages of this investigation, the codes were run on the CRAY-1. All of the response matrix generation codes are easily vectorized if care is taken with the do-loops. The global iteration scheme is also easily vectorized if a Jacobi iteration is used. For the Gauss-Seidel and SOR iteration schemes, vectorization is a bit more complicated. A row-by-row or, alternatively, a red-black scheme would be necessary.

REFERENCES

[Abr70] M. Abramowitz and I. A. Stegun, Handbook of Mathematical Functions, National Bureau of Standards, Washington (1970).

[Alc79] R. E. Alcouffe, E. W. Larsen, W. F. Miller, and B. R. Wienke, "Computational Efficiency of Numerical Methods for the Multi-Group, Discrete Ordinates Neutron Transport Equation: The Slab Geometry Case", Nucl. Sci. Eng., 71, 111 (1979).

[And73] M. M. Anderson and H. C. Honeck, "An Interface Current Technique for Two-Dimensional Cell Calculations", Proc. Conf. Mathematical Models and Computational Techniques for Analysis of Nuclear Systems, Ann Arbor, MI, CONF-730414, Part 1, p. I-53 (1973).

[Aok65] K. Aoki and A. Shimizu, "Applications of the Response Matrix Method to Criticality Calculations of Two-Dimensional Reactors", J. Nucl. Sci. Technol., 2, 149 (1965).

[Aro67] R. Aronson, "One-Velocity Neutron Transport Problem by the Transfer Matrix Method", Nucl. Sci. Eng., 27, 271 (1967).

[Aro73] R. Aronson, "One-Velocity Neutron Transport Problem--Part I: Exact Transfer Matrix Formulation", Nucl. Sci. Eng., 51, 157 (1973).

[Bri75] L. L. Briggs, W. F. Miller, and E. E. Lewis, "Ray-Effect Mitigation in Discrete Ordinate-Like Angular Finite Element Approximations in Neutron Transport", Nucl. Sci. Eng., 57, 205 (1975).

[Bri77] L. L. Briggs and E. E. Lewis, "A Comparison of Constrained Finite Elements and Response Matrices as One-Dimensional Transport Approximations", Nucl. Sci. Eng., 63, 225 (1977).

[Bri80] L. L. Briggs and E. E. Lewis, "A Two-Dimensional Constrained Finite Element Method for Nonuniform Lattice Problems", Nucl. Sci. Eng., 75, 76 (1980).

[Che71] M. S. Cheng, C. T. McDaniel, and A. Leonard, "A Nodal Integral Transport Method for Calculation of Two-Dimensional Power Distributions in Non-Uniform Lattices", Proc. Conf. New Developments in Reactor Mathematics and Applications, Idaho Falls, ID, CONF-710312, Part 2, p. 655 (1971).

[Dah74] G. Dahlquist and A. Björck, Numerical Methods, Prentice-Hall, Englewood Cliffs, N.J. (1974).

[Dud79] J. J. Duderstadt and W. R. Martin, Transport Theory, Wiley, New York (1979).

[Fil73] W. L. Filippone, "Two-Dimensional Neutron Transport Calculations Using the Response Matrix Method", Nucl. Sci. Eng., 52, 23 (1973).

[Jon75] A. Jonsson, R. Goldstein, and A. Mockel, "Integral Transport Theory with Cell Coupling Involving Arbitrarily Distributed Currents", Trans. Am. Nucl. Soc., 21, 231 (1975).

[Kap74] H. G. Kaper, A. J. Lindeman, and G. K. Leaf, "Benchmark Values for the Slab and Sphere Criticality Problem in One-Group Neutron Transport Theory", Nucl. Sci. Eng., 54, 94 (1974).

[Law76] R. D. Lawrence and J. J. Dorning, "A Nodal Green's Function Method for Multidimensional Neutron Diffusion Calculations", Nucl. Sci. Eng., 76, 218 (1980).

[Law80] R. D. Lawrence and J. J. Dorning, "A Discrete Nodal Integral Transport Theory Method for Multidimensional Reactor Physics and Shielding Calculations", Proc. Conf. Advances in Reactor Physics and Shielding, Sun Valley, ID, p. 840 (1980).

[Leo71] A. Leonard, C. T. McDaniel, and W. P. Petrick, "A Modified Collision Probability Method for Non-Uniform Lattices", Proc. Conf. New Developments in Reactor Mathematics and Applications, Idaho Falls, ID, CONF-710312, Part 2, p. 644 (1971).

[Leo76] A. Leonard, "Collision Probabilities and Response Matrices: An Overview", Proc. Conf. Computational Methods in Nuclear Engineering, Charleston, SC, CONF-750413, Vol. II, p. III-15 (1976).

[Lew77] E. E. Lewis, "Progress in Multidimensional Neutron Transport Computation", Nucl. Sci. Eng., 64, 279 (1977).

[Lor79] L. Lorence and W. R. Martin, "Response Matrix Finite Element Solution of the Neutron Transport Equation", Trans. Am. Nucl. Soc., 32, 305 (1979).

[Lor84] L. J. Lorence, "An Explicitly-Interfaced Finite Element Solution of the Neutron Transport Equation", Ph. D. Dissertation, The University of Michigan, Department of Nuclear Engineering, Ann Arbor, MI (1984).

[Mar77] W. R. Martin and J. J. Duderstadt, "Finite Element Solution of the Neutron Transport Equation with Applications to Strong Heterogeneities", Nucl. Sci. Eng., 62, 371 (1977).

[Mar81] W. R. Martin, C. E. Yehnert, L. Lorence, and J. J. Duderstadt, "Phase-Space Finite Element Methods Applied to the First-Order Form of the Transport Equation", Ann. Nucl. Energy, 8, 633 (1981).

[Mil73a] W. F. Miller, E. E. Lewis, and E. C. Rossow, "The Application of Phase-Space Finite Elements to the One-Dimensional Neutron Transport Equation", Nucl. Sci. Eng., 51, 148 (1973).

[Mil73b] W. F. Miller, E. E. Lewis, and E. C. Rossow, "The Application of Phase-Space Finite Elements to the Two-Dimensional Neutron Transport Equation in X-Y Geometry", Nucl. Sci. Eng., 52, 12 (1973).

[Mue72] A. Mueller and M. R. Wagner, "Use of Collisional Probability Methods for Multidimensional Neutron Flux Calculations", Trans. Am. Nucl. Soc., 15, 280 (1972).

[Nak83] H. Nakata and W. R. Martin, "The Finite Element Response Matrix Method", Nucl. Sci. Eng., 85, 289 (1983).

[Pfe69] W. Pfeiffer and J. L. Shapiro, "Reflection and Transmission Functions in Reactor Physics", Nucl. Sci. Eng., 38, 253 (1969).

[Ple76] E. F. Plechaty and J. R. Kimlinger, "TARTNP: A coupled neutron-photon Monte Carlo transport code", UCRL-50400, Vol. 14, Lawrence Livermore Laboratory (1976).

[Pry73] R. J. Pryor and W. E. Graves, "Response Matrix Method for Treating Reactor Calculations", Proc. Conf. Mathematical Models and Computational Techniques for Analysis of Nuclear Systems, Ann Arbor, MI, CONF-730414, Part 2, p. VII-179 (1973).

[Ree71] W. H. Reed, "New Difference Schemes for the Neutron Transport Equation", Nucl. Sci. Eng., 46, 309 (1971).

[Saj81] E. Saji, S. Sakurai, and T. Takeda, "Application of the Response Matrix Method to BWR Lattice Analysis", Ann. Nucl. Energy, 8, 155 (1981).

[San77] R. Sanchez, "Approximate Solution of the Two-Dimensional Integral Transport Equation by Collision Probability Methods", Nucl. Sci. Eng., 64, 384 (1977).

[Shi63a] A. Shimizu, "Response Matrix Method", J. Atom. Energy Soc. Japan, 5, 359 (1963).

[Shi63b] A. Shimizu, K. Monta, and T. Miyamota, "Application of the Response Matrix Method to Criticality Calculations of One-Dimensional Reactors", J. Atom. Energy Soc. Japan, 5, 369 (1963).

[Uka72] S. Ukai, "Solution of Multi-Dimensional Neutron Transport Equation by Finite Element Method", J. Nucl. Sci. Technol., 9(5), 336 (1972).

[Wei72] Z. Weiss, "Nodal Equations Derived from Invariant Imbedding Theory", Nucl. Sci. Eng., 48, 235 (1972).

[Wei75] Z. Weiss and S. O. Lindahl, "Higher-Order Response Matrix Equations in Two-Dimensional Geometry", Nucl. Sci. Eng., 58, 166 (1975).

[Wei77] Z. Weiss, "Some Basic Properties of the Response Matrix Equations", Nucl. Sci. Eng., 63, 457 (1977).

[Win62] Wing, An Introduction to Transport Theory, Wiley, New York (1962).

[Yeh78] C. E. Yehnert, "Finite Element Solution of the Two-Dimensional Neutron Transport Equation", Ph. D. Dissertation, The University of Michigan, Department of Nuclear Engineering, Ann Arbor, MI (1978).